UNIVERSITY OF CALIFORNIA,
IRVINE

Mammalian histones facilitate antimicrobial synergy by disrupting the bacterial proton gradient and rearranging the chromosome

DISSERTATION

submitted in partial satisfaction of the requirements
for the degree of

DOCTOR OF PHILOSOPHY

in Biological Sciences

by

Tory Jacklyn Vizenor

Dissertation Committee:
Professor Steven P. Gross, Chair
Assistant Professor Albert Siryaporn
Associate Professor Debra Mauzy-Melitz

2019

DEDICATION

To my high school biology teacher, Mr. Jeff Caplan, who fostered my love for biology and wrote colorful adjectives on my exams and quizzes such as “stupendous!” and “extraordinary!” When you get to graduate school, nobody tells you that you are doing a stupendous job anymore, and I miss that.

TABLE OF CONTENTS

LIST OF FIGURES vi

LIST OF TABLES xi

ACKNOWLEDGMENTS xii

CURRICULUM VITAE xiii

ABSTRACT OF THE DISSERTATION xv

CHAPTER 1: Introduction and Background 1
- 1.1 The Current State of Antibiotic Resistance 1
- 1.2 The Structure and Function of Histones 3
- 1.3 Innate Immune Responses for Combating Bacterial Infections 6
- 1.4 Possible Side Effects of Histones and How the Host Modulates These Side Effects 9
- 1.5 Biochemical Properties of Antimicrobial Peptides (AMPs) 12
- 1.6 The Role of Histones and Histone Fragments as Antimicrobial Agents 18
  - 1.6.1 Full-length histones are antimicrobial 18
  - 1.6.2 Histone-derived peptide fragments are also antimicrobial 19
    - 1.6.2.1 Histone H1 homologs 20
    - 1.6.2.2 Histone H2A and H2B homologs 20
    - 1.6.2.3 Histone H3 and H4 homologs 24
- 1.7 Insights into the Mechanism of Histone-Mediated Killing of Bacteria 25
- 1.8 Conclusion 28
- 1.9 References 30

CHAPTER 2: Materials and Methods 40
- 2.1 Bacterial Strains 40
- 2.2 Growth Conditions 41
- 2.3 Antimicrobial Peptides, Proteins, and Antibiotics 41
- 2.4 Agar Plate Assay 41
- 2.5 Growth Curves 42
- 2.6 Fluorescence and Phase Contrast Microscopy 43
- 2.7 Propidium Iodide Staining 44
- 2.8 PhoQ Expression Measurements 44
- 2.9 SEM Imaging 45
- 2.10 Cell Aggregate and Size Analysis 45
- 2.11 Fluorescent Histone Labeling 46
- 2.12 Fluorescent Histone and Fluorescent LL-37 Uptake 46

2.13 Fluorescent Histone and Fluorescent LL-37 Uptake in Low Ionic Conditions 47
2.14 PROPS Fluorescence Analysis 47
2.15 Timelapse of *E. coli* Recovery 47
2.16 Time Course of Membrane Healing 48
2.17 Electroporation of Electrocompetent *E. coli* 48
2.18 Bacterial DNA Purification 49
2.19 Non-Denaturing Nucleic Acid PAGE 49
2.20 Chromosomal Organization in *E. coli* 50
2.21 *In vivo* Transcription Assay 50
2.22 RNA Sequencing 51
2.23 Validation of RNA Sequencing 51
2.24 Derivation of the Histone-AMP positive feedback model 52
2.25 Statistical Analysis 53
2.26 References 54

CHAPTER 3: Histone H2A Kills Gram-negative and Gram-positive Bacteria in Low Ionic Environments, but Not Physiological Environments 55
3.1 Histone H2A Kills Gram-negative and Gram-positive Bacteria in Low Magnesium Environments 58
3.2 Histone H2A Enhances Membrane Permeabilization in Low Ionic Environments 65
3.3 The PhoPQ System Improves Survival of *E. coli* Challenged with Histone H2A 68
3.4 Conclusion 73
3.5 References 75

CHAPTER 4: Histone H2A Synergizes with Membrane-Permeabilizing Agents to Kill Bacteria at Physiological Ionic Concentrations 77
4.1 Histone H2A Synergizes with the Antimicrobial Peptide (AMP) LL-37 80
4.2 Histone H2A Does Not Synergize with the Antibiotics Kanamycin or Chloramphenicol 87
4.3 Histone H2A Synergizes with the Antimicrobial Peptide (AMP) LL-37 to Kill Mid-Exponential Phase Bacteria 90
4.4 Histone H2A Synergizes with the Antibiotic Polymyxin B 101
4.5 Histone H2A Synergizes with the Antimicrobial Peptide (AMP) Magainin-2 107
4.6 The Synergistic Combination of Histone H2A and LL-37 Induces Extensive Cellular Damage Not Observed in Individual Treatments 113
4.7 Conclusions 124
4.8 References 126

CHAPTER 5: Histone H2A and AMPs Have Distinct Activities that Increase the Intracellular Concentration of the Other Molecule and Induce Persistent Membrane Damage 129
5.1 Membrane-Permeabilizing Agents Promote Uptake of Histone H2A 130
5.2 Histone-Induced Membrane Permeabilization of *E. coli* Increases Intracellular Concentrations of Histones 142
5.3 Histones Depolarize the Membrane and Disrupt the Proton Motive Force (PMF) 150
5.4 Histones Impair Bacterial Recovery 153
5.5 Histones Have an Intracellular Target 168
5.6 Conclusion 171
5.7 References 173

CHAPTER 6: Histone H2A Disrupts Bacterial Chromosomal DNA Organization and Suppresses Transcription 174
6.1 Histone H2A Interacts with Microbial DNA *in vitro*, Inhibiting DNA Migration 176
6.2 Histone H2A Disrupts Bacterial Chromosomal DNA Organization 180
6.3 Histone H2A Suppresses Bacterial Transcription 183
6.4 Histone H2A Selectively Upregulates Membrane Biogenesis Components 189
6.5 Conclusion 205
6.6 References 207

CHAPTER 7: Conclusions and Future Directions 211
7.1 Histone H2A Provides Multiple Modes of Assault Against Bacteria 211
7.2 Histones and AMPs Form a Positive Feedback Loop 215
7.3 The Effect of Citrullination on the Antimicrobial Activity of Histones in NETs 223
7.4 The Usage of Histones and Histone-Derived Fragments as Future Therapeutic Agents 228
7.5 References 231

APPENDIX A: Effect Size and Power Analyses for ANOVA Tests 234

APPENDIX B: Effect Size and Power Analyses for Welsh t-tests 236

LIST OF FIGURES

		Page
Figure 1.1	Structure of the core histone H2A, the linker histone H1, and the antimicrobial peptide cathelicidin LL-37.	5
Figure 1.2	Sequence alignment of Histone H2A and Histone H2A-derived peptides.	21
Figure 1.3	Potential mechanisms of bacterial killing by histones.	26
Figure 3.1	Differences in the membranes of Gram-negative and Gram-positive bacteria.	57
Figure 3.2	Histones decrease the number of colony forming units (CFUs) of *E. coli* and *S. aureus* in low ionic environments.	60
Figure 3.3	Histones kill stationary phase Gram-negative *E. coli* in a low ionic strength condition but not in a physiological condition.	62
Figure 3.4	Histones kill stationary phase Gram-positive *S. aureus* in a low ionic strength condition but not in a physiological condition.	63
Figure 3.5	Histones increase membrane permeabilization in stationary phase *E. coli* in a low ionic strength condition, but not in a physiological condition.	67
Figure 3.6	The PhoPQ system increases E. coli survival when treated with histones.	70
Figure 3.7	H2A suppresses *phoQ* expression in E. coli growing in low ionic strength conditions.	72
Figure 4.1	Schematic representation of antagonistic, synergistic, and additive drug combinations.	79
Figure 4.2	Solution NMR structure of human LL-37.	82
Figure 4.3	Histone H2A and LL-37 synergize to kill stationary phase *E. coli* and *S. aureus*.	84
Figure 4.4	The combinatorial treatment of H2A and LL-37 decreases the number of colony forming units (CFUs) of *E. coli* in physiological conditions.	86

Figure 4.5	Histone H2A and Kanamycin have no synergistic killing effects on stationary phase *E. coli*.	88
Figure 4.6	Histone H2A and Chloramphenicol have no synergistic killing effects on stationary phase *E. coli*.	89
Figure 4.7	Histone H2A and LL-37 synergize to kill mid-exponential phase *E. coli* and *S. aureus*.	92
Figure 4.8	Histone H2A and kanamycin do not synergize to kill mid-exponential phase *E. coli*.	94
Figure 4.9	Histone H2A and chloramphenicol do not synergize to kill mid-exponential phase *E. coli*.	95
Figure 4.10	Histone H2A and LL-37 synergize to kill mid-exponential phase *E. coli*.	97
Figure 4.11	Histones and LL-37 increase membrane permeabilization.	100
Figure 4.12	Structure of Polymyxin B Sulfate.	102
Figure 4.13	Histone H2A and polymyxin B synergize to kill *E. coli.*	104
Figure 4.14	Histones and polymyxin B increase membrane permeabilization.	106
Figure 4.15	Solution NMR structure of *Xenopus laevis* magainin-2.	108
Figure 4.16	Histone H2A and magainin-2 synergize to kill *E. coli*.	110
Figure 4.17	Histones and magainin-2 increase membrane permeabilization.	112
Figure 4.18	*E. coli* treatment with LL-37 and H2A causes extensive cellular damage.	115
Figure 4.19	*E. coli* treatment with LL-37 and H2A causes membrane blebbing.	116
Figure 4.20	Histone H2A induces bacterial aggregation.	119
Figure 4.21	LL-37 reduces bacterial cell size.	121
Figure 4.22	Dual treatment of H2A and LL-37 dramatically decreases cell size.	123
Figure 5.1	Fluorescently-labeled H2A (AF-H2A) synergizes with	132

LL-37 to kill *E. coli*.

Figure 5.2 Fluorescence and phase contrast images of *E. coli* treated with fluorescently-labeled H2A (AF-H2A) alone or in combination with LL-37 or PMB. 134

Figure 5.3 Intracellular fluorescence intensities of *E. coli* or *S. aureus* treated with AF-H2A and chloramphenicol, kanamycin, LL-37, or polymyxin B. 135

Figure 5.4 Fluorescence and phase contrast images of *E. coli* treated with fluorescently-labeled H2A (AF-H2A) alone or in combination with magainin-2. 137

Figure 5.5 Intracellular fluorescence intensities of *E. coli* treated with AF-H2A and magainin-2. 138

Figure 5.6 Fluorescence and phase contrast images of *E. coli* treated with fluorescently-labeled LL-37 (5-FAM-LL-37) alone or in combination with H2A. 140

Figure 5.7 Intracellular fluorescence intensities of *E. coli* or *S. aureus* treated with H2A and 5-FAM-LL-37. 141

Figure 5.8 Low concentrations of histones kill exponential phase *E. coli* diluted in a low ionic strength condition, but not in a physiological condition. 144

Figure 5.9 Histones increase membrane permeabilization in exponential phase *E. coli* diluted in a low ionic strength condition, but not in a physiological condition. 146

Figure 5.10 Intracellular fluorescence intensity of fluorescently-labeled H2A (AF-H2A) increases in low ionic environments, but not physiological ionic environments. 148

Figure 5.11 Increased membrane permeabilization facilitates histone entry into *E. coli*. 149

Figure 5.12 Histones depolarize the bacterial membrane and disrupt the proton motive force (PMF). 152

Figure 5.13 Histone H2A inhibits membrane recovery by stabilizing LL-37-induced pore formation. 154

Figure 5.14 H2A induces persistent cellular damage when combined with LL-37. 156

Figure 5.15	H2A induces persistent cellular damage when combined with magainin-2.	158
Figure 5.16	H2A induces persistent membrane damage when combined with LL-37.	160
Figure 5.17	H2A induces persistent membrane damage when combined with magainin-2.	162
Figure 5.18	*E. coli* recover from cellular damage in the absence of AMPs.	165
Figure 5.19	*E. coli* can recovery from H2A-induced membrane damage in the absence of AMPs.	167
Figure 5.20	Histones kills bacteria intracellularly.	170
Figure 6.1	Histone H2A inhibits bacterial DNA migration.	177
Figure 6.2	LL-37 weakly inhibits bacterial DNA migration.	179
Figure 6.3	Histone H2A induces a webbed pattern in the bacterial chromosome.	182
Figure 6.4	Histone H2A suppresses bacterial transcription.	184
Figure 6.5	Histone H2A decreases RNA yields.	187
Figure 6.6	High concentrations of Histone H2A kill *E. coli.*	188
Figure 6.7	Histone H2A upregulates membrane biogenesis components.	191
Figure 6.8	Histone H2A upregulates the Rcs phosphorelay pathway.	201
Figure 6.9	Membrane-permeabilized *E. coli* upregulate the Rcs phosphorelay pathway.	202
Figure 6.10	The Rcs phosphorelay pathway improves *E. coli* survival under dual treatment with H2A and LL-37.	204
Figure 7.1	Histones and AMPs form a positive feedback loop that facilitates the uptake of antimicrobials into the cell.	216
Figure 7.2	Low concentrations of AMPs and H2A trigger an exponential uptake of H2A and AMPs.	219

Figure 7.3	A positive feedback loop results in the exponential uptake of H2A and AMPs.	220
Figure 7.4	Dual-treated bacterial populations contain a bimodal distribution of uptake phenotypes.	222
Figure 7.5	Histone H3 and LL-37 synergize to kill *E. coli*.	224
Figure 7.6	Citrullination of Histone H3 eliminates synergy with LL-37.	226

LIST OF TABLES

		Page
Table 1.1	Comparison of the biochemical properties of histones and AMPs.	13
Table 6.1	Fold-change in mRNA transcripts in the top 100 genes upregulated in *E. coli* following a 30-minute treatment with H2A.	192

ACKNOWLEDGMENTS

I would like to express gratitude and appreciation to my research advisors, Dr. Steven Gross and Dr. Albert Siryaporn. You have both been a constant source of support and guidance throughout my Ph.D. research. You have challenged me to be a better scientist and I am truly grateful for your ideas and enthusiasm, which helped my project advance from an abstract idea to a developed story. Thank you for everything!

I would also like to extend my sincere appreciation to Dr. Debra Mauzy-Melitz for sitting on my dissertation committee, leading the GAANN program, and conveying an excitement for teaching. With your guidance, support, and advice I have gained a great appreciation and love for scientific communication and teaching undergraduate students the importance of proper data analysis.

To all the graduate students, postdocs, and undergraduate students – past and present – with whom I have had the pleasure to work with during my graduate studies, thank you!

The research presented herein was partially supported by the GAANN fellowship.

Last but not least, I would like to express my deepest gratitude to my family and friends for their love and support:

To my parents and siblings for always supporting me, loving me, and believing in me.

To the Vizenor clan for always being incredibly supportive of Tor-Tor.

To my puppy, Bieksa, for sleeping besides me while I wrote this dissertation. I love you, you little goober.

To all my friends for being a constant source of love and encouragement. Thank you for always being there for me! This adventure in grad school would not have been possible without all the chats over coffee and dinner.

To the Game Night crew, I love you all and I miss you. Thank you for being the perfect weekly outlet to balance out the stress of grad school. I am very excited to join you guys on the other side.

To Dr. John Kelly for being my favorite third wheel.

And finally, to my husband Nick Vizenor: thank you for loving me, thank you for being there. I truly cannot image having gone through grad school without your love, support, and encouragement. I love you and I cannot wait to start a new adventure with you in a couple weeks.

CURRICULUM VITAE

Tory Jacklyn Vizenor (née Doolin)

EDUCATION

University of California – Irvine **October 2019**
Ph.D – Biological Sciences *Irvine, CA*

- Dissertation Title: "Mammalian histones facilitate antimicrobial synergy by disrupting the bacterial proton gradient and chromosome"
- GAANN Teaching Fellow, four-time Teaching Assistant (TA) for a Scientific Writing course

University of California – Irvine **December 2018**
M.S. – Biological Sciences *Irvine, CA*

University of California – Irvine **June 2015**
B.S. – Biological Sciences *Irvine, CA*

- *Cum* Laude with Honors
- Excellence in Research
- Chancellor's Award of Distinction
- Phi Beta Kappa

RESEARCH EXPERIENCE

University of California - Irvine **October 2016 – October 2019**
Graduate Researcher *Irvine, CA*

- Designed, conducted, and analyzed microbiology and molecular biology experiments focused on elucidating the mechanism of histone-mediated killing of bacteria (manuscript and patent application in submission)
- Trained and supervised two undergraduate students.
- Mentored three first year graduate students.
- Gave numerous seminar and departmental talks.
- Assisted with R01 grant submission.
- Authored review chapter.

Minority Sciences Programs (MSP) Lab **April 2015 – May 2016**
Junior Specialist/Microbiology Lab Manager *Irvine, CA*

- Designed and conducted experiments on antibiotic resistance in the environment.
- Oversaw the collection and characterization of thousands of antibiotic resistant bacterial

isolates using MALDI-TOF, disk diffusion assays, and plasmid isolation and analysis.
- Responsible for overall lab maintenance, including maintaining appropriate levels of reagents, coordinating laboratory duties, overseeing inventory, streamlining expenses and expenditures, handling service calls, optimized protocols and assays, overseeing equipment usage, and lab safety compliance with EH&S regulations.
- Responsible for the training and supervision of over 30 undergraduate students. Optimized protocols.
- Awarded UCI Staff Ally of the Year.

UC Irvine Medical Center **August 2013 – June 2015**
Undergraduate Researcher *Orange, CA*

- Collaborated on a clinical research study focusing on the relationship between air pollution and oxidative stress.
- Designed an independent research project, conducted experiments, and analyzed data for a senior thesis.

Institute for Memory Impairments and Neurological Disorders (UCI MIND) **October 2011 – May 2015**
Clinical Research Assistant *Irvine, CA*

- Prepared for memory and neurological testing visits for a longitudinal study cohort of over 500 individuals.
- Managed informed consent documentation, prepared mailings and reports, organized and maintained charts, performed data entry and quality assurance, drafted data for grant proposals, and trained four new employees.

PUBLICATIONS

- Doolin, T. et al. Mammalian histones facilitate antimicrobial synergy by disrupting the bacterial proton gradient and chromosome. *Nature Communications*. In review (2019).

- Doolin, T. et al. Physical Mechanisms of Bacterial Killing by Histones. *Physical Microbiology.* Springer. In review (2019).

- Reddy, B. J. N. et al. Heterogeneity in kinesin function. Traffic 18, 658–671 (2017).

ABSTRACT OF THE DISSERTATION

Mammalian histones facilitate antimicrobial synergy by disrupting the bacterial proton gradient and rearranging the chromosome

By

Tory Jacklyn Vizenor

Doctor of Philosophy in Biological Sciences

University of California, Irvine, 2019

Professor Steven P. Gross, Chair

Antibiotic resistance is a global epidemic, becoming increasingly pressing due to its rapid spread. Thus, there is a critical need to develop new therapeutic approaches. In addition to searching for new antibiotics, gaining additional insight into existing natural host defense mechanisms may enable researchers to improve existing defenses, and to develop effective, synthetic drugs guided by natural principles. Histone proteins were originally proposed to function as antimicrobial agents, and were later recognized for their role in condensing mammalian chromosomes. More recently, the antimicrobial activity of histones has been reported in innate immune responses, including neutrophil extracellular traps and lipid droplets. However, histones exhibit weak antimicrobial activity *in vitro*. Whether and how histones kill bacteria *in vivo* has remained elusive. This weak antimicrobial activity *in vitro* may be attributed to the fact that histone activity has not been considered in the context of other immune mechanisms. The co-localization of histones with antimicrobial peptides (AMPs) in immune cells suggests that histones function as part of a larger antimicrobial mechanism *in vivo*. I have discovered that the mammalian histone H2A is taken up into the Gram-negative *Escherichia coli* and the Gram-positive bacteria *Staphylococcus aureus* through membrane pores that are formed by the human AMP LL-37 or the

Xenopus laevis AMP magainin-2. Without this crucial first step, whereby AMPs form pores and enable histone entry into the bacteria, mammalian histones have little antimicrobial activity. H2A stabilizes the AMP-induced membrane pores; this depolarizes the bacterial membrane potential. Inside, H2A reorganizes bacterial chromosomal DNA, and inhibits global transcription. I show that while bacteria can recover from the pore-forming effects of AMPs alone, the effects of H2A are irrecoverable. Together, these results suggest that AMPs and histones, which are found ubiquitously in the innate immunity system, synergize as a natural host defense mechanism to kill bacteria. The membrane-permeabilizing activity of AMPs and the DNA-perturbing and proton gradient-altering effects of H2A constitute a positive feedback loop that exponentially amplifies their antimicrobial activities, thus creating a condition of antimicrobial synergy that could be incorporated into antimicrobial design.

Chapter 1: Introduction and Background

1.1 The Current State of Antibiotic Resistance

The rise of antibiotic resistance is a global epidemic that is becoming increasingly pressing due to the ability of antibiotic resistance to spread easily and quickly. Organizations including the Centers for Disease Control (CDC) and the World Health Organization (WHO) argue that this rapid rise in antibiotic resistance is ushering the world into an era without effective antibiotics[1–3]. As such, a growing number of deaths due to bacterial infections are expected.

Bacterial strains that are resistant to nearly all antibiotics have emerged in healthcare settings, and at the present time, multi-drug resistant *Staphylococcus aureus* (MRSA) kills more Americans than HIV/AIDS, emphysema, Parkinson's disease, and homicide combined[1,4–6]. Based on conservative estimates, in the United States alone, at least 2 million people are infected with resistant bacteria every year, and at least 1 out of 100 of those individual dies as a direct result[7]. Additionally, many other individuals die due to other conditions that are complicated by antibiotic-resistant infections. If no effort is made to curb antimicrobial resistance, the death toll could reach one person every three seconds by 2050, with upwards of 300,000 annual deaths in the United States alone[8]. Yearly death tolls in Asia and Africa are predicted to exceed four million deaths across each continent.

Usage of antibiotics is the single greatest contributor to the growing problem of antibiotic resistance. Both an over-usage of antibiotics, stemming from the over-prescription of antibiotics and their widespread usage in agriculture, and an under-usage of antibiotics, from patients failing to properly follow through with completing their full course of antibiotics, heavily contribute to this crisis. Antibiotic-resistant bacterial infections contribute to costlier treatments, extended

hospital stays, additional healthcare visits, and higher disability and death rates, yet the United States healthcare system is poorly equipped to deal with this growing public health epidemic. In addition to the loss of effective treatments for bacterial infections, widespread antibiotic resistance may affect treatment of bacterial complications in alternate diseases, including chemotherapy, surgeries, and organ and bone marrow transplants.

The CDC has assigned threats of urgent, serious, and concerning levels to various pathogens and has issued recommendations for prevention and proper treatment of those afflicted[7]. The largest concern is treating Gram-negative bacteria, including pathogenic *Enterobactericeae*, *Pseudomonas aeruginosa*, and *Acinetobacter*, which are acquiring resistance to nearly all antibiotics that could be prescribed as treatment. Compounding the problem, nearly all new antibiotics that are being developed are members of existing classes of antibiotics. Thus, these antibiotics use mechanisms of action that bacteria have encountered before, leading to rapid cross-resistance and contributing to the lack of effective antibiotics available to treat Gram-negative pathogens[9].

Clearly there is a pressing need to develop new therapeutic approaches to combat the rapid rise of antibiotic resistance. In addition to searching for new antibiotics that may help combat bacterial infections, looking into the mechanisms of natural host defense pathways may enable researchers to improve existing host defense mechanisms and develop effective, synthetic drugs that are guided by the principles of nature.

1.2 The Structure and Function of Histones

In 1922, Alexander Fleming discovered lysozyme from nasal mucus[10]. This was the first human antimicrobial protein to be reported; however, the discovery of penicillin in 1928[11] overshadowed this finding, and ushered the world into the "Golden Age" of antibiotics. Recently, the rise of antibiotic resistance, combined with the stagnation in discovering new, viable antimicrobial agents, has sparked renewed interest in natural host defenses.

The antimicrobial activity of histones was first reported in 1942[12] and *in vitro* histone killing of bacteria was further characterized in 1958 using *Escherichia coli*[13]. It was originally proposed that the size and charge of histones may enable them to act as bactericidal cationic detergents through adsorption to the cell surface, leading to osmotic barrier damage. It was also noted that increased salt concentrations in growth media may relate to ionic strength and impact histone adsorption onto bacterial membranes. The bactericidal effect of histones was antagonized by the basic substances, including protamine and spermine, and acid polysaccharides, including heparin, nucleic acid, and bacterial lipopolysaccharides.

However, despite originally being proposed to function as antimicrobial agents, the role of histones in condensing eukaryotic DNA became seen as their primary function and little is known about their antimicrobial role and the possible mechanisms by which they kill bacteria *in vivo*. The discovery that histones have a central role in innate immune responses[14] has renewed interest into understanding their antimicrobial functions.

Eukaryotic organisms possess a cell nucleus and other organelles enclosed within a membrane. Their nuclei contain genetic material, typically encoded in DNA, within a nuclear envelope. Within the nucleus, small, alkaline histone proteins are used to package the DNA into 5 nm nucleosomes that condense chromatin, the chromosomal material in eukaryotic cells that is

composed protein, DNA, and a small amount of RNA. The basic structural unit of chromatin is made up of 146 DNA base pairs, wrapped roughly 1.5 times around a histone core. This histone core structure is made up of eight histone components: two H2A-H2B dimers and a H3-H4 tetramer[15]. Histones contain the positively charged amino acids lysine and arginine, which facilitate their interactions with negatively charged DNA. Histones are grouped into two classes: lysine-rich (H1, H2A, H2B) and arginine-rich (H3, H4)[16]. These core histones are highly conserved through evolution, containing the 'helix turn helix turn helix' central motif, named the histone fold, and an unstructured amino-terminal tail[16]. The structure of H2A, which is representative of the structure of the four core histones, is shown in Figure 1.1A.

The nucleosome complex, which contains the segment of DNA wrapped around the histone core, forms the repeating units of chromatin, facilitates higher order chromatin structure, and is necessary for eukaryotic survival. Histone H1 functions as a linker that binds to 20 base pairs of DNA, forming a chromatosome[17]. The structure of H1, with a long C-terminal tail, a short N-terminal tail, and a central globular domain with a winged helix domain[18], is shown in Figure 1.1B. Linker DNA from one chromatosome binds to linker DNA from another chromatosome, further condensing the DNA into 30 nm chromatin fiber.

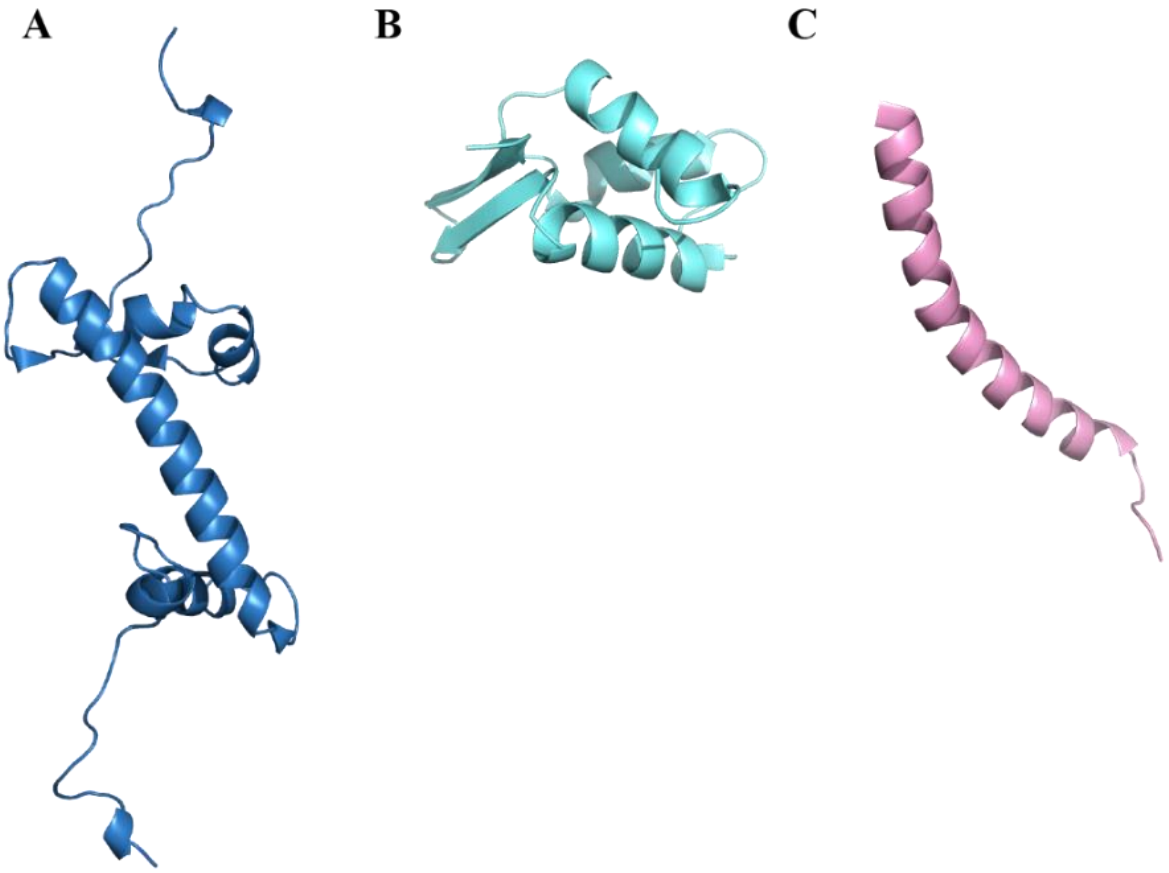

Figure 1.1. Structure of the core histone H2A, the linker histone H1, and the antimicrobial peptide cathelicidin LL-37. (A) The core histone H2A contains a 'helix turn helix turn helix' central motif, named the histone fold, and an unstructured amino-terminal tail (PDB ID: 1AOI)[15]. (B) The linker histone H1 contains a long C-terminal tail, a short N-terminal tail, and a central globular domain with a winged helix domain (PDB ID: 1GHC)[19]. (C) The antimicrobial peptide cathelicidin LL-37 is a linear peptide folded into an amphipathic α-helix (PDB ID: 2K6O)[20].

1.3 Innate Immune Responses for Combating Bacterial Infections

When histones were believed to be localized solely in the nucleus, it was hard to imagine how they might play an antimicrobial role. More recently, the observation of histones localizing outside of the cell nucleus, across multiple species, allows one to speculate that they may have roles in addition to chromosome condensation[14,21]. For instance, histones are observed inside cytoplasmic granules in human neutrophils[22]. Further, they are likely functional: H2A and H2B purified from the fetal membranes of the human placenta show dose-dependent inhibition of LPS endotoxin activity, by binding the core and lipid A portions of LPS[23]. These histones are secreted from placenta epithelial cells into the amniotic fluid, contributing to fetal host defenses. Finally, in the Asian toad *Bufo gargarizans*, H2A is synthesized in excess of the amount required for DNA packaging, and unacetylated H2A accumulates within cytoplasmic secretory granules[24]. Histones are also reported to localize to the plasma membrane, possibly for both signaling and targeted release[25].

Neutrophil extracellular traps (NETs)[14] are one of the best explored examples of histones playing a central role in combating bacterial infections. Neutrophils are the immune system's first line of defense against bacterial infections, and their prototypical function involves engulfing bacteria and other pathogens. The engulfed pathogens are subsequently killed through the fusion of the phagosome with antimicrobial, cytoplasmic granules. These granules contain an array of components that kill bacteria, including myeloperoxidase, defensins, lysozyme, proteinases (cathepsin G, elastase, and proteinase 3), bactericidal/permeability-increasing protein (BPI), NADPH oxidase, cathelicidin LL-37, lactoferrin[26], and of course, the above-mentioned histones[22]. However, neutrophils also have a less canonical, alternate killing pathway. The presence of virulent microorganisms[27], such as *Pseudomonas aeruginosa*[28,29], *Escherichia coli*[30,31], and

Staphylococcus aureus[32], stimulates a neutrophil immune response known as NETosis[14]. Additionally, conditions that interfere with phagosomal killing[33], such as virulent bacterial aggregation[27] or fungal hyphae[34], stimulate NETosis. The process of NETosis occurs over a period of three to eight hours and includes the decondensation of nuclear chromatin, the mixing of DNA with cytoplasmic and granule components, and the release of these NETs into the extracellular space[35]. During this process, histones are citrullinated by peptidylarginine deiminase 4 (PAD4), an enzyme essential for chromatin decondensation[36]. This enzyme converts arginine residues, which are positively charged, into neutral citrulline residues, resulting in a more open chromatin structure. Studies involving histone-derived antimicrobial peptides with varying arginine content concluded that antibacterial activity increases as arginine concentration increases, either by increasing permeabilization or improving translocation, depending on the specific mechanism of the AMP[37].

As expected, PAD4-mediated citrullination of histones during NET formation decreases the potency of histones[38]. PAD4 activity appears to be tightly regulated, presumably to minimize toxic effects to the host and maximize antimicrobial activity by controlling the potency of the histones within NETs[39]. Given that NETs induce inflammation and are damaging to surrounding host tissue, there is a delicate balance that needs to be met in order to fight pathogen microbes without inducing high levels of damage to the host[40].

The process of NETosis concludes with the release of NETs, which are fibrous networks that contain cation-chelating mitochondrial and nuclear DNA and antimicrobial granular proteins[14,33,35,41–44]. NETs kill and suppress the proliferation of microorganisms, though the mechanism of NET-mediated killing remains poorly understood[33]. PAD4 knockout mice have increased susceptibility to bacterial infection due to an inability to form NETs; however, these

neutrophils retain the ability to kill bacteria in other ways and mice exposed to septic conditions had comparable survival to wild-type mice[38,45].

Arguments have been made for DNA playing a vital role in the antimicrobial activity of NETs. DNA has previously been shown to have antimicrobial activity, by chelating cations that stabilize the LPS and outer membrane of bacteria, causing cell lysis and release of cytoplasmic contents and genomic DNA[46]. DNases efficiently disintegrate NETs, reducing their bactericidal activity[14]. Quenching or degrading the ability of the phosphodiester backbone of DNA to chelate cations in a contact-dependent manner protected microbes from NETs[44].

Histones constitute a large fraction of the proteins in NETs[14]. However, initially the role of histones in NETs was unclear, as histones might simply be remnant features of the neutrophils. Nonetheless, the co-localization of histones in the NET scaffold, including with the human antimicrobial peptide cathelicidin LL-37[47,48] and HNP alpha-defensins[49], suggest that histones could have a role as an antimicrobial agent here[50,51]. However, the individual and combined roles of these molecules and how they contribute to the antimicrobial activity of NETs has not been determined[50,51]. Importantly, antibodies against H2A and H2B eliminate NET-mediated killing of bacteria[14]. Furthermore, purified Histone H2A kill *S. flexneri*, *S. typhimurium*, and *S. aureus* bacterial cultures in 30 minutes with concentrations as low as 2 μg/mL[14]. Combined, these findings suggest that histones likely to play an important anti-bacterial role.

While all four core histones (H2A, H2B, H3, and H4) are present in NETs, the presence of the linker histone H1 in NETs remains unclear. Their presence was reported in the first report of NET formation[14]; however, other studies have found that H1 is degraded during NET formation[14,52]. Supporting the degradation of H1 during NET formation, immunofluorescence experiments have shown the presence of all core histones, but not the linker histone H1[53].

1.4 Possible Side Effects of Histones and How the Host Modulates These Side Effects

The role of histone citrullination in NET antimicrobial activity is unclear. Antibacterial activity in antimicrobial peptides (AMPs) correlates with increasing arginine content[37], either by increasing permeabilization or improving translocation, depending on the mechanism of the AMP. PAD4-mediated citrullination of histones, which decreases the arginine content, may decrease the antimicrobial potency of histones[38]. PAD4 is tightly regulated, possibly to minimize the toxic effects of free histones in the host and to maximize antimicrobial activity, by controlling the potency of the histones within NETs[39]. Given that NETs induce inflammation and are damaging to surrounding host tissue, there is a delicate balance that needs to be met in order to fight pathogen microbes without inducing high levels of damage to the host[40].

Extracellular histone release, which can elicit toxic effects on pathogenic bacteria, can have negative side effects. Due to their ability to interact with biological membranes, extracellular histones can act as proinflammatory signals, triggering inflammatory responses and injury in the host. The presence of extracellular histones elicits the production of antibodies against histones and contributes to autoimmune and inflammatory responses in patients with systemic lupus erythematosus, neuropsychiatric lupus, and lupus nephritis[54]. Histones have a pro-inflammatory role in several diseases, including sepsis, trauma, thrombosis, stroke, atherogenesis, and systemic lupus. Histones are suspected to be mediators of mortality in sepsis, contributing to endothelial dysfunction, organ failure, and death during sepsis[55]. Extracellular histones are elevated following traumatic tissue injury and the ongoing rise of histone levels are predictive of mortality, suggesting the role of histones in the sterile inflammatory response following trauma may parallel the role of histones in sepsis[56]. Elevated levels of circulating extracellular histones in trauma-associated lung injuries are associated with endothelial damage and coagulation activation[57].

Extracellular histones contribute as a damage-associated molecular pattern (DAMP), inducing cytotoxicity and pro-inflammatory signaling through toll-like receptors (TLR) TLR2 and TLR4[58]. Extracellular histones promote thrombin generation, which triggers thrombosis[59]. Histones bind to platelets, inducing calcium influx and platelet aggregation, causing thrombocytopenia in mice within minutes[60]. Histones promote chemotaxis of human polymorphonuclear leukocytes, suggesting histones may modulate leukocyte activation[61]. Inflammation frequently causes cellular death, leading to the release of cellular components, such as chromatin components, potentially exacerbating the toxic effects of histones by causing the release of additional histones.

NETs and concentrations of H2A higher than 50 μg/mL induce the death of endothelial and lung epithelial cells[62]. While digestion of extracellular DNA decreases the ability of NETs to kill bacteria, DNA digestion does not have any effect on mediating cytotoxicity on epithelial and endothelial cells[62]. Thus, the controlled storage and release of histones upon bacterial infection appears critical. It is plausible that citrullination of histones decreases histone potency in NETs and provides a mechanism that balances antimicrobial activity and toxicity to the host.

In addition to playing an essential role in NET-mediated killing of microbes, histones have been shown to localize to cytoplasmic lipid droplets. Lipid droplets are lipid-rich organelles, found in all eukaryotic organisms, which dynamically regulate the storage and breakdown of lipids. Originally thought to serve solely as fat reservoirs, proteomic analyses have uncovered the presence various proteins, including histones[63]. In early *Drosophila melanogaster* embryos, excess H2A, H2B, and H2Av histones, a variant of H2A, are recruited and bound to lipid droplets, perhaps as a means of temporary storage to avoid toxic effects introduced by free histones[64]. In the presence of bacterial lipopolysaccharide (LPS) or lipoteichoic acid (LTA), these lipid droplet-bound histones are released from the lipid droplets and kill bacteria *in vivo*[21]. Histones bound to lipid

droplets protect cells against bacteria without causing any of the harm normally associated with the presence of free histones. Purified *Drosophila* embryos lacking lipid droplet-bound histones also showed decreased survival when assaulted with bacterial species[21].

1.5 Biochemical Properties of Antimicrobial Peptides (AMPs)

Histones possess antimicrobial activity and play a critical role in the innate immune system. Histones share many biochemical similarities with AMPs, as summarized in Table 1.1. Like AMPs, histones are cationic, contain a high proportion of hydrophobic amino acids, and possess the ability to form alpha helices[65,66]. AMPs and individual histone proteins are comparable in size, averaging 18 kDa and 14 kDa respectively[67,68]. Additionally, both are present in NETs[49,51]. Despite similarities between histones and AMPs, AMPs are not known to serve as proinflammatory signals for the host. The similar biochemical properties between AMPs, such as LL-37, and histone proteins have led to the conclusion that the molecules serve redundant functions in their antimicrobial activities[42]. Whether AMPs and histones have redundant or independent functions has not been fully explored. Below is a review of the biochemical properties of AMPs and insights into their antimicrobial activity. However, unlike AMPs, far less is known about the antimicrobial and biochemical properties of histones.

Table 1.1. Comparison of the biochemical properties of histones and AMPs.

Property		**Histones**				**AMPs**
	H1	**H2A**	**H2B**	**H3**	**H4**	
Molecular Weight (kDa)	22[69]	14[70]	14[70]	15[70]	11[70]	18[67]
Charge	Positive due to abundance of lysine residues	Positive due to abundance of lysine residues		Positive, due to arginine residues		Positively-charged, due to lysine and arginine residues
Structural Motifs	Winged helix motif in the globular domain, short N-terminal tail, long C-terminal tail	Histone fold domain: three α-helices connected by two loops				α-helical, β-sheet, loop, or extended
Amino Acid Composition	High proportion of positively-charged amino acids and hydrophobic amino acids	High proportion of positively-charged amino acids and hydrophobic amino acids				High proportion of positively-charged amino acids and hydrophobic amino acids
Defining Feature	Linker histone, stabilizing the chromatin fiber	Component of the histone octomer, which binds and condenses DNA				Associates with and permeabilize membranes
Sequence Diversity Among Species	Largely conserved, but less conserved than core histones	Largely conserved				Prominent sequence diversity

In the first line of defense against pathogenic microbes, surface epithelial cells have a crucial role in mediating the host's innate immune response by secreting AMPs[71–73]. In addition to surface epithelial cells, these peptides are secreted by submucosal glands[74,75] and neutrophils[76,77]. AMPs are widely evolutionarily conserved and are found throughout all classes of life, including bacteria[78], plants[79], fungi[80], insects[81], aquatic species[82], birds[83], and mammals[84–86]. AMPs exhibit activity against several classes of microorganisms, including bacteria[84,87–89], fungi[80,90,91], viruses[92–94], protozoa[95], and cancerous cells[96]. In addition to their role as antimicrobial agents, AMPs direct multiple cellular processes in immune defense including cytokine release, chemotaxis, antigen presentation, angiogenesis, and wound healing[97]. These peptides have been proposed as alternative therapeutics due to their rapid-killing, high potency, and broad-spectrum of activity[66]. Furthermore, because these AMPs primarily target the bacterial membrane, they do not lead to prominent levels resistance in bacteria[98].

AMPs tend to be small, typically less than 100 amino acids[99,100]. AMPs are classified into broad groups based on secondary structure, including α-helical, β-sheet, loop, or extended[101]. An example structure of an α-helical AMP, cathelicidin LL-37, is shown in Figure 1.1C. Most of these small peptides are cationic at physiological pH, stemming from the high proportion of the positively-charged amino acids arginine and lysine[102,103]. Despite arginine and lysine having identical charges, arginine occurs more frequently in AMPs, indicating that guanidinium groups may be more beneficial for AMP activity than amine groups[104]. This may be attributed to the ability of arginine to form multiple electrostatic interactions and hydrogen bonds with lipid heads in the membrane, which may cause membrane deformation. AMP sequences also contain a high proportion of hydrophobic residues, lending to an amphipathic structure. Both the cationic and amphipathic characteristics of these AMPs allows for interactions with the anionic lipid bilayers

of bacteria. Many AMPs are unstructured in free solution and fold upon insertion into a biological membrane[105]. The ability to associate with biological membranes is a defining feature of AMPs[105,106].

The mechanism of antimicrobial action for many AMPs involves permeabilization or disruption of the microbial membrane; however, many AMPs also target DNA and protein synthesis, disrupt protein folding, or inhibit cell wall synthesis[107–109]. A proposed global mechanism of action for this class of peptides is the Shai-Matsuzaki-Huang model of spontaneous translocation[110–113]. The cationic and amphipathic properties of AMPs enable their binding to the surface of the bacterial membrane. Bacteria insert themselves into bacterial membranes, breaking lipid chain interactions and displacing cations that stabilize the membrane, such as Mg^{2+}. This alters membrane structure, causing membrane thinning and increasing membrane destabilization, in addition to increasing surface tension. At AMP concentrations above a threshold, the high level of surface tension causes permeabilization of the membrane by the formation of transient pores. This permeabilization enables additional peptides to enter the interior of the cell. If the AMP concentration is below that which will cause the membrane to fully collapse, overall membrane integrity is preserved. Virtually all AMPs, apart from insect apidaecin-type peptides, have high membrane affinity and induce a certain level of membrane perturbation[114]. An alternate mechanism for proline-rich groups of AMPs is to exploit the inner membrane protein SbmA to penetrate *E. coli*[115].

Despite similarities in the cationic and amphipathic nature across AMPs, there is prominent sequence diversity, allowing for some AMPs to interact with intracellular targets or affect key cellular processes, either in addition to, or instead of, membrane permeabilization. Because of their strong positive charge, most AMPs permeabilize the membrane at concentrations above the

minimum inhibitory concentration (MIC) *in vitro*, indicating that membrane permeabilization is a secondary effect of most AMPs[116,117]. Peptide concentrations well above the MIC or high peptide:lipid ratios can falsely indicate a membrane lytic mechanism and mask true intracellular effects. For instance, pleurocidin-derived AMPs inhibit RNA and protein synthesis at the MIC without affecting membrane integrity; however, at ten times the MIC, cells depolarize and membranes are disrupted[116]. Under conditions that support bacterial killing, human neutrophil peptide defensin [HNP]-1 penetrates the outer and inner membranes of *E. coli*[118]. Upon penetration, bacterial synthesis of DNA, RNA, and protein stops. Inhibition of cytokinesis has been seen with the alpha helical peptide cathelin-related AMP (CRAMP), the mouse ortholog of cathelicidin LL-37. CRAMP impairs *Salmonella typhimurium* cell division *in vitro* and in macrophage-phagocytized bacteria, resulting in long, filamentous structures[119]. Given the negative charge of DNA and RNA, it is not surprising that positively charged AMPs bind to nucleic acid polymers *in vitro*[109,120,121]. Other AMPs have been shown to affect protein folding, cell wall synthesis, cell wall integrity, and protein translation. In order to identify these potential intracellular targets, it is vitally important to keep the concentration of AMPs used in research aimed at elucidating the mechanism of bacterial killing via AMPs at an appropriate level relative to the MIC.

Mechanisms of cell death via AMPs can be elucidated by measuring the delay between cell death, measured by an inhibition of colony formation, and membrane permeability changes. AMPs that have a lytic mechanism of action have these two events occur rapidly and concurrently, whereas non-lytic mechanisms of cell death are characterized by a delay between cell death and changes in membrane permeability. Increases in permeability as a secondary effect after bacterial death has been observed with some classic antibiotics, including ceftazidime, ciprofloxacin, and

gentamicin[122,123].Various intracellular AMP mechanisms of action have been studied, but the degree to which membrane permeabilization or intracellular mechanisms have a role in cell death are often not investigated.

The similar biochemical properties between AMPs, such as cathelicidin LL-37, and histone proteins have led to the conclusion that the molecules serve redundant functions in their antimicrobial activities[42]. Whether and AMPs have redundant or independent functions has not been fully explored.

1.6 The Role of Histones and Histone Fragments as Antimicrobial Agents

1.6.1 Full-length histones are antimicrobial

Full-length histones from a range of species have antimicrobial activity, including the rainbow trout, shrimp, and Atlantic salmon. Acetylated H2A is found in skin secretions of the rainbow trout *Oncorhynchus mykiss*[124]. Reconstitution of H2A within the membrane perturbs the membrane, without forming ion channels, supporting a non-pore-forming mechanism of action. All core histone proteins, H2A, H2B, H3, and H4, are found in the blood cells of the invertebrate Pacific white shrimp (*Litopenaeus vannamei*)[125]. These proteins have high sequence identity to the histones of other species, and the N-terminus of H2A has sequence identity to the antimicrobial histone-derived peptides buforin I, parasin, and hopposin. Liver, intestine, and stomach extracts from healthy Atlantic salmon (*Salmo salar*) contain an antimicrobial protein identified as H1[126].

Histones from *Gallus gallus* and mice also have antimicrobial activity. Sequences of bactericidal proteins from mice macrophages activated by gamma interferon have similarities to H1 and H2B histone sequences[127]. H2A, H2B.V, and an H2B C-terminal fragment identified in the liver extracts of White Leghorn hens (*Gallus gallus*) and histones from chicken erythrocytes have antimicrobial activity against Gram-negative and Gram-positive bacteria[128]. Additionally, histones from chicken erythrocytes bind to cell wall components, including lipopolysaccharide (LPS) and lipoteichoic acid (LTA)[129].

Numerous reports indicate antimicrobial activity of histones in humans. H1 and its fragments are present in human terminal ileal mucosal samples and the cytoplasm of villus epithelial cells and showed antimicrobial activity against *Salmonella typhimurium*. *In vitro* culturing of villus epithelial cells from the basement membrane releases antimicrobial H1 proteins while the cells undergo programmed cell death[130]. A shotgun proteomics approach revealed the presence of core

histones (H2A, H2B, H3, H4) and linker histones (H1) in human hair shafts and extracts of partially-purified histones killed *E. coli* in a radial diffusion assay[131]. The antimicrobial action of sebocytes from the SEB-1 cell line against *S. aureus* has been attributed to histone H4. Here, synergy between histones and free fatty acids in human sebum are responsible for the antimicrobial effects. As cells in the sebaceous gland secrete their cellular contents into the sebum through holocrine secretion, a secretion mode involving plasma membrane rupture and cellular death, sebocytes use histones as antimicrobial agents released as a sebum component. Analysis of the antimicrobial activity and polypeptide composition of meconium identified histones H2 and H4[132].

1.6.2 Histone-derived peptide fragments are also antimicrobial

Peptides that have antimicrobial activity are formed from the N-terminus cleavage of full-length histones, although this cleavage is not known to occur in humans. These are considered to be AMPs and have been extensively observed in non-mammalian species. The synthesis of inactive proteins require processing to function properly is a common tactic used to prevent off-target harmful effects to the host. Classic examples in the antimicrobial realm are antimicrobial peptides generated from trypsin-mediated cleavage of lactoferrin and neutrophil elastase-mediated cleavage of thrombin[133,134]. Endogenous proteases are implicated in the production of AMPs from lysine-rich histones. Following cleavage, AMP antimicrobial activity can be attributed to the amphipathic secondary structure with net positive charge, allowing for membrane binding, membrane permeabilization, and binding to nucleic acids[65]. Below is a summary of AMPs that have sequence similarity to the N-terminus of the different histones.

1.6.2.1 Histone H1 homologs

AMPs with sequence similarity to H1 are present in Atlantic salmon, rainbow trout, and Coho salmon. In *Salmo salar*, the Atlantic salmon, a 30-residue N-terminally acetylated peptide derived from H1 is present in the skin mucus and has activity against both Gram-negative and Gram-positive bacteria. Isomerization of the proline peptide bond is crucial for activity, leading to increased structure, condensation, and rigidity of the peptide[135]. A potent antimicrobial peptide in *O. mykiss*[136] with sequence identity to the H1 induces destabilization of planar lipid bilayers. Blood and mucus antimicrobial fractions of Coho salmon (*Oncorhynchus kisutch*) has sequence identity with the N-terminus of H1. Synthetic peptides showed no antimicrobial effects, but showed synergy with the flounder peptide pleurocidin and lysozyme[137].

1.6.2.2 Histone H2A and H2B homologs

There are several known AMPs that have sequence similarity with histone H2A. A schematic depicting the sequence alignment of histone H2A-derived peptides is shown in Figure 1.2**.** Parasin I is a 19-amino acid antimicrobial peptide secreted into the epithelial mucosal layer by the catfish *Parasilurus asotus* in response to epidermal injury[138]. The AMP shows high homology to the N-terminal region of H2A and is thought to be produced by cathepsin D-directed H2A proteolysis upon injury[139]. The basic N-terminal residue is essential for membrane-binding, and the α-helical structure is necessary for membrane permeabilization[140].

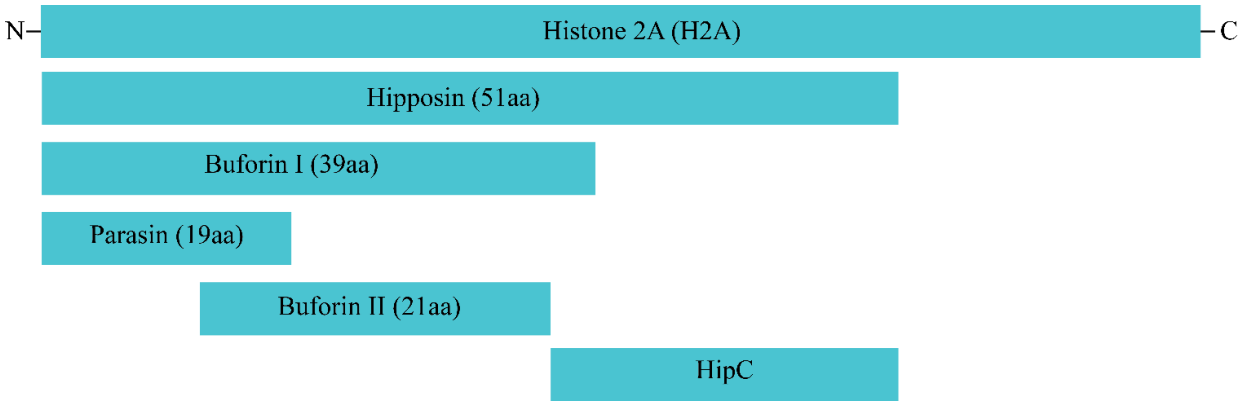

Figure 1.2. Sequence alignment of Histone H2A and Histone H2A-derived peptides. The histone-derived antimicrobial peptides (AMPs) hipposin, buforin I, and parasin align with the N-terminus of Histone H2A. The histone-derived AMPs buforin II and HipC also align with Histone H2A.

Buforin I is a 39-amino acid AMP isolated from the Asian toad *Bufo bufo gargarizans*, composed of the N-terminal parasin and buforin II. Upon pepsin-mediated proteolysis of the Tyr^{39}-Ala^{40} H2A bond in the cytoplasm of gastric gland cells, buforin I is secreted into the gastric lumen where it adheres to the stomach mucosal surface and forms a protective antimicrobial coating[24]. In contrast, unacetylated H2A is located in the cytoplasm of gastric gland cells, suggesting a portion of cytoplasmic unacetylated H2A is secreted into the lumen and undergoes pepsin processing, while another portion of H2A is acetylated and targeted for nuclear translocation.

Buforin II (BF2) is a 21-amino acid peptide derived from endoproteinase Lys-C treatment of buforin I, which displays increased antimicrobial activity compared to buforin I and adopts a helix-hinge-helix structure in 50% trifluoroenthanol[141,142]. Both buforin I and buforin II share sequence identity to the N-terminus of H2A[143]. Circular dichroism measurements of equipotent Trp-substituted peptides indicate that BF2 binds selectively to liposomes composed of acidic phospholipids and has weak membrane permeabilization activity when compared to magainin-2, a membrane-permeabilizing *Xenopus laevis* antimicrobial peptide[144]. Instead, BF2 is efficiently translocated across lipid bilayers, supporting an intracellular mechanism of bacterial death by nucleic acid binding. The Pro^{11} residue is structurally responsible for introducing a kink in the α helix and disturbing the helical structure[145]. To translocate the lipid bilayer, BF2 forms a toroidal pore that is destabilized by the electrostatic repulsion that accompanies five basic amino acids in close proximity. In membranes, amidated BF2 adopts a poorly helical structure in membranes, mimicking the composition of *E. coli*, and binds to duplex DNA causing condensation[146].

The α-helical structure, which directs cell-penetration, has been shown to be critical in determining antimicrobial efficacy[147]. The helix-hinge-helix domain enables BF2 to enter bacterial cells without inducing membrane disruption, where the AMP binds to intracellular nucleic acids

and inhibit cellular functioning[120]. Although *in vitro* binding of BF2 to nucleic acid has been shown, it is unknown whether this interaction is directed, or if it is a result of opposite charged interactions. Further characterization of the nucleic acid binding property of BF2 indicates that the R^2 and R^{20} side chains of BF2 form interactions with DNA that are stronger than non-specific electrostatic interactions, and that the substitution of the basic residues with alanine decreases the antimicrobial activity of BF2[148].

A combination of molecular dynamics (MD) simulations and DNA binding affinity experiments provide support for BF2 forming specific interactions with DNA[148]. Additionally, through the use of BF2 variants, the affinity of the peptide for DNA has been correlated with increased antimicrobial activity. Additional MD simulations, along with electrostatic analysis and nucleic acid binding experiments, on BF2 and DesHDAP1, a designed histone-derived AMP thought to share a similar structure and mechanism of action with BF2, support a sequence-independent method of AMP binding to DNA[121]. Instead of peptide binding with sequence specificity, peptide-phosphate interactions are thought to be the predominant basis of AMP binding to DNA. As such, arginine residues are shown to have greater antimicrobial activity than lysine residues, possibly due to increases interactions with DNA; however, higher arginine composition could also influence AMP-membrane interactions.

Hipposin is a potent 51-residue antimicrobial peptide isolated from the skin mucus of Atlantic halibut *Hippoglossus hippoglossus L*[149]. This AMP has 98% sequence similarity to the N-terminal of histone 2A from rainbow trout, and has sequence similarities to both parasin and BF2. The AMP has been shown to kill bacteria through membrane permeabilization, as evidenced by increased propidium iodide fluorescence intracellularly following peptide exposure and localization of fluorescently-labeled AlexaFluor conjugates around the cellular membrane[150]. The localization of

fluorescence around the cell membrane, with low fluorescence intracellularly, is similar to the fluorescence pattern depicted by parasin, another histone-derived peptide that causes permeabilization[140]. The N-terminal parasin domain of hipposin is necessary for membrane permeabilization, as peptides lacking the parasin domain show translocation of the membrane, without permeabilization. The C-terminal domain of hipposin, HipC, is cell-penetrating, but shows no measurable antimicrobial activity.

Skin extracts from Schlegel's green tree frog, *Rhacophorus schlegelii*, contained a protein, with homogeneity to H2B, that inhibited the growth of *E. coli*[151].

1.6.2.3 Histone H3 and H4 homologs

No known natural fragments with similarity to H3 have been identified. Histograninn, a slightly modified C-terminal 15 amino acid fragment showing similarities to the C-terminal end of H4 has been identified from bovine adrenal medulla[152]. The fragment, which is synthesized from a separate mRNA variant, is an antagonist of N-methyl-D-aspartate (NMDA) receptor activity. Histograninn has antimicrobial activity against Gram-negative and Gram-positive bacteria and is thought to function through inhibition of ATP-dependent DNA gyrase, a mechanism similar to quinolone antibiotics[153].

1.7 Insights into the Mechanism of Histone-Mediated Killing of Bacteria

The findings from histone-derived AMPs suggest that part of the antimicrobial activity of histones is achieved through membrane permeabilization, as depicted in Figure 1.3. The linker histone H1 and four core histones from calf thymus bind to LPS present on the outer bacterial membrane. All histones except H4 have affinities for LPS that are greater than that of the antibiotic polymyxin B[154]. The strong affinity of histones for phosphodiester bonds enables histone binding to DNA and facilitates proper chromatin structure formation. However, this affinity may extend to the phosphodiester bonds in phospholipids, facilitating the off-target integration of histones into host membranes. The strong positive charge of histones from *Plasmodium falciparum*, a unicellular protozoan parasite that causes malaria in humans, increases membrane permeability in human endothelial cells and induces IL-8 production at concentrations higher than 50 μg/mL[155]. The negatively-charged glycoaminoglycans (GAGs) heparan sulfate and hyaluronan protect CHO cells from histone-induced cytotoxicity, supporting the notion that glycocalyx, the negatively-charged polysaccharide network that protects cells from bacteria, may further mitigate the effects of histones by preventing membrane insertion[156]. Thus, the strong positive charge of histones may induce permeability in membranes across of a broad range of organisms including bacteria. Divalent cations, such as Mg^{2+}, function as cationic bridges between adjacent phosphates on LPS. Histones may compete with divalent cations, compromising LPS cross-bridges, and destroying the outer membrane integrity.

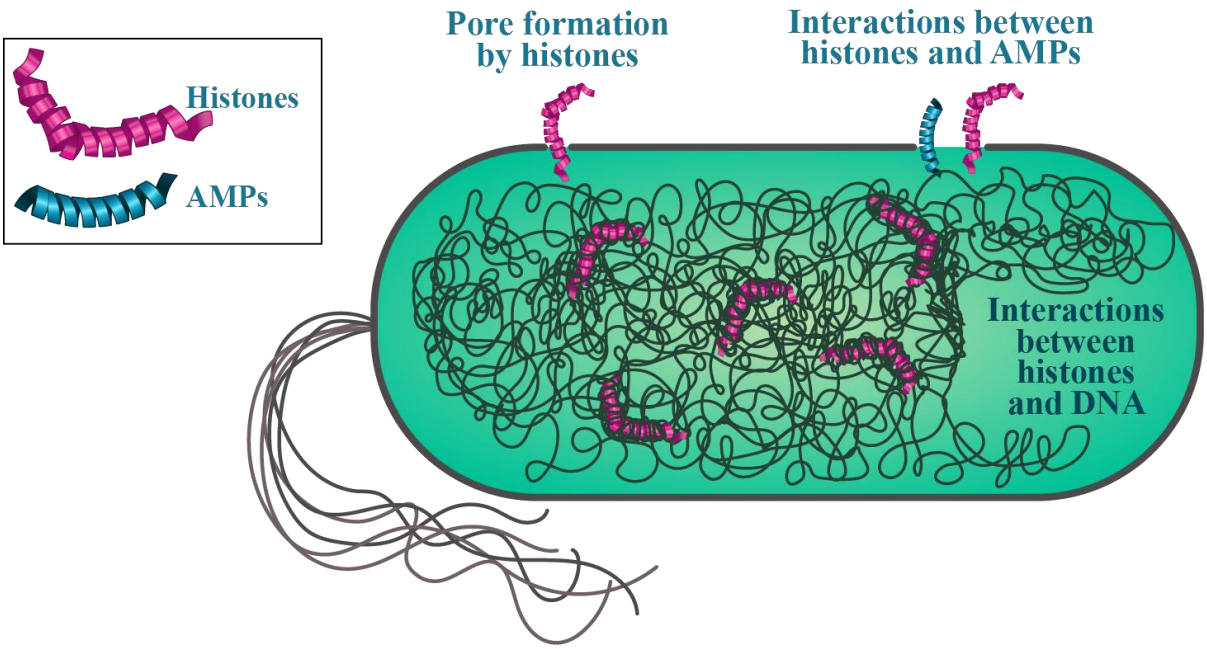

Figure 1.3. Potential mechanisms of bacterial killing by histones. Histones have high affinity for LPS and LTA and histone-derived peptides induce membrane permeabilization. Full-length histones thus may bind to bacterial membranes, disrupting the membrane and forming pores. The high affinity of histones for phosphodiester bonds, which enables histones to bind and condense DNA, suggests that part of the antimicrobial activity of histones may involve interactions between histones and microbial DNA. Since histones alone show weak antimicrobial activity *in vivo*, the antimicrobial activity of histones may be dependent upon interactions with AMPs or other antimicrobial agents. Schematic created by Robert Gant.

Other work suggests that the antimicrobial mechanism of histones occurs following entry into the bacterium and that the target is cytoplasmic (Figure 1.3). An active fragment of H2B from *R. schlegelli* is thought to be generated via digestion by the bacterial outer membrane protease T (OmpT)[127]. This fragment of H2B can penetrate the cell membrane of OmpT-expressing *E. coli*, but not *ompT*-deleted *E. coli*, accumulate in the cytoplasm, and inhibit cell function, presumably by binding to nucleic acids. In the absence of OmpT, H2B is unable to penetrate the membrane, and remains localized on the exterior of the bacteria[157]. Consistent with requirement for H2B translocation into the cell, the MIC values for H2B, H3, and H4 are significantly increase in the absence of OmpT[158]. The antimicrobial effects observed at higher concentrations of histones may be due to the secondary effect of histones increasing membrane permeability, and not the primary mechanism by which lysine-rich histones kill bacteria. In addition, lysine-rich (H1, H2A, H2B) and arginine-rich (H3, H4) histones likely kill bacteria using distinct mechanisms. While H2B penetrates *E. coli* membranes and enters the cytoplasmic space, H3 and H4 remain localized on the cell surface, causing membrane blebbing[158].

1.8 Conclusion

Despite being originally proposed to function as antimicrobial agents [159,160], and having an essential role in mammalian innate immune responses[14], little is known about how histones function as antimicrobial agents. Complicating matters, that studies on the antimicrobial activity of histones typically utilize low-ionic solutions and buffers that are not physiologically relevant[14,21,53,63,157,158,161–170]. In physiologically relevant conditions, histones are far less effective at killing bacteria[21,66], and require high, unphysiological concentrations of histones (120 μg/mL) [21,158,171]. This reduced efficacy of histone killing in physiologically relevant concentrations has raised questions regarding their utility as antimicrobial agents. Furthermore, some studies use concentrations of histones well above the MIC[158,171]. As noted above, peptide concentrations in excess of the MIC may render bacteria susceptible to the secondary mechanisms of histones through membrane permeabilization[116,117].

It is plausible that since that histones show weak antimicrobial activity *in vivo*, the antimicrobial activity of histones is dependent upon interactions with other immune system mechanisms or components (Figure 1.3)[172]. Synergies are common between AMPs, with three-AMP combinations showing stronger levels of synergy than two-AMP combinations[173]. Synergy between antibacterial peptides released from activated neutrophils has been reported previously. In the absence of salt, defensins show antibacterial activity in a dose-dependent manner; however, antimicrobial activity is lost in the presence of salt[174]. Defensins exhibit synergy with cathelicidins in the killing of *E. coli* and *S. aureus*[174]. There have also been reports of histone H1 fragments having synergistic antimicrobial effects with lysozyme, lysozyme-containing extracts from *O. kisutch*, and pleurocidin against *Vibrio anguillarum* and *Aeromonas salmonicida*[137].

These above findings prompted this research on the mechanistic details of histone-mediated killing of bacteria, considering their role in the context of the immune system as a whole, not as a sole antimicrobial agent. I considered that the weak antimicrobial activity of histones in physiological conditions may be attributed to the fact that histone activity has not been considered in the context of other immune mechanisms. In immune cells, histones are co-localized with antimicrobial peptides (AMPs), suggesting that histones function as part of a larger antimicrobial mechanism *in vivo* and may synergize with other antimicrobial agents.

1.9 References

1. Ventola, C. L. The antibiotic resistance crisis: part 1: causes and threats. *P T* **40**, 277–283 (2015).
2. Bush, K. *et al.* Tackling antibiotic resistance. *Nature Reviews Microbiology* **9**, 894–896 (2011).
3. Bald, D. & Koul, A. Advances and strategies in discovery of new antibacterials for combating metabolically resting bacteria. *Drug Discovery Today* **18**, 250–255 (2013).
4. Golkar, Z., Bagasra, O. & Pace, D. G. Bacteriophage therapy: a potential solution for the antibiotic resistance crisis. *J Infect Dev Ctries* **8**, 129–136 (2014).
5. Klevens, R. M. Invasive Methicillin-Resistant Staphylococcus aureus Infections in the United States. *JAMA* **298**, 1763 (2007).
6. Rossolini, G. M., Arena, F., Pecile, P. & Pollini, S. Update on the antibiotic resistance crisis. *Current Opinion in Pharmacology* **18**, 56–60 (2014).
7. Centers for Disease Control and Prevention. *Antibiotic Resistance Threats in the United States, 2013*. (2013).
8. O'Neill, J. *Tackling Drug-Resistant Infections Globally: Final Report and Recommendations*. (2016).
9. Coates, A. R. M., Halls, G. & Hu, Y. Novel classes of antibiotics or more of the same? *Br. J. Pharmacol.* **163**, 184–194 (2011).
10. Fleming, A. On a Remarkable Bacteriolytic Element Found in Tissues and Secretions. *Proceedings of the Royal Society B: Biological Sciences* **93**, 306–317 (1922).
11. Fleming, A. Classics in infectious diseases: on the antibacterial action of cultures of a penicillium, with special reference to their use in the isolation of B. influenzae by Alexander Fleming, Reprinted from the British Journal of Experimental Pathology 10:226-236, 1929. *Rev. Infect. Dis.* **2**, 129–139 (1980).
12. Miller, B. F., Abrams, R., Dorfman, A. & Klein, M. ANTIBACTERIAL PROPERTIES OF PROTAMINE AND HISTONE. *Science* **96**, 428–430 (1942).
13. Hirsch, J. G. BACTERICIDAL ACTION OF HISTONE. *Journal of Experimental Medicine* **108**, 925–944 (1958).
14. Brinkmann, V. Neutrophil Extracellular Traps Kill Bacteria. *Science* **303**, 1532–1535 (2004).
15. Luger, K., Mäder, A. W., Richmond, R. K., Sargent, D. F. & Richmond, T. J. Crystal structure of the nucleosome core particle at 2.8 Å resolution. *Nature* **389**, 251–260 (1997).
16. DeLange, R. J. & Smith, E. L. Histones: Structure and Function. *Annual Review of Biochemistry* **40**, 279–314 (1971).
17. Allan, J., Hartman, P. G., Crane-Robinson, C. & Aviles, F. X. The structure of histone H1 and its location in chromatin. *Nature* **288**, 675–679 (1980).
18. Zhou, B.-R. *et al.* Structural insights into the histone H1-nucleosome complex. *Proceedings of the National Academy of Sciences* **110**, 19390–19395 (2013).
19. Cerf, C. *et al.* Homo- and Heteronuclear Two-Dimensional NMR Studies of the Globular Domain of Histone H1: Full Assignment, Tertiary Structure, and Comparison with the Globular Domain of Histone H5. *Biochemistry* **33**, 11079–11086 (1994).
20. Wang, G. Structures of Human Host Defense Cathelicidin LL-37 and Its Smallest Antimicrobial Peptide KR-12 in Lipid Micelles. *J. Biol. Chem.* **283**, 32637–32643 (2008).

21. Anand, P. *et al.* A novel role for lipid droplets in the organismal antibacterial response. *eLife* **1**, (2012).
22. Lominadze, G. *et al.* Proteomic Analysis of Human Neutrophil Granules. *Molecular & Cellular Proteomics* **4**, 1503–1521 (2005).
23. Kim, H. S. *et al.* Endotoxin-Neutralizing Antimicrobial Proteins of the Human Placenta. *The Journal of Immunology* **168**, 2356–2364 (2002).
24. Kim, H. S. *et al.* Pepsin-Mediated Processing of the Cytoplasmic Histone H2A to Strong Antimicrobial Peptide Buforin I. *The Journal of Immunology* **165**, 3268–3274 (2000).
25. Watson, K. *et al.* Extra-nuclear location of histones in activated human peripheral blood lymphocytes and cultured T-cells. *Biochem. Pharmacol.* **50**, 299–309 (1995).
26. Segal, A. W. HOW NEUTROPHILS KILL MICROBES. *Annual Review of Immunology* **23**, 197–223 (2005).
27. Delgado-Rizo, V. *et al.* Neutrophil Extracellular Traps and Its Implications in Inflammation: An Overview. *Frontiers in Immunology* **8**, (2017).
28. Dwyer, M. *et al.* Cystic Fibrosis Sputum DNA Has NETosis Characteristics and Neutrophil Extracellular Trap Release Is Regulated by Macrophage Migration-Inhibitory Factor. *Journal of Innate Immunity* **6**, 765–779 (2014).
29. Floyd, M. *et al.* Swimming Motility Mediates the Formation of Neutrophil Extracellular Traps Induced by Flagellated Pseudomonas aeruginosa. *PLOS Pathogens* **12**, e1005987 (2016).
30. Kambas, K. *et al.* Autophagy Mediates the Delivery of Thrombogenic Tissue Factor to Neutrophil Extracellular Traps in Human Sepsis. *PLoS ONE* **7**, e45427 (2012).
31. Yu, Y. *et al.* Characterization of Early-Phase Neutrophil Extracellular Traps in Urinary Tract Infections. *PLOS Pathogens* **13**, e1006151 (2017).
32. Pilsczek, F. H. *et al.* A novel mechanism of rapid nuclear neutrophil extracellular trap formation in response to Staphylococcus aureus. *J. Immunol.* **185**, 7413–7425 (2010).
33. Papayannopoulos, V. Neutrophil extracellular traps in immunity and disease. *Nature Reviews Immunology* **18**, 134–147 (2017).
34. Branzk, N. *et al.* Neutrophils sense microbe size and selectively release neutrophil extracellular traps in response to large pathogens. *Nature Immunology* **15**, 1017–1025 (2014).
35. Fuchs, T. A. *et al.* Novel cell death program leads to neutrophil extracellular traps. *J. Cell Biol.* **176**, 231–241 (2007).
36. Lewis, H. D. *et al.* Inhibition of PAD4 activity is sufficient to disrupt mouse and human NET formation. *Nat. Chem. Biol.* **11**, 189–191 (2015).
37. Cutrona, K. J., Kaufman, B. A., Figueroa, D. M. & Elmore, D. E. Role of arginine and lysine in the antimicrobial mechanism of histone-derived antimicrobial peptides. *FEBS Letters* **589**, 3915–3920 (2015).
38. Li, P. *et al.* PAD4 is essential for antibacterial innate immunity mediated by neutrophil extracellular traps. *J. Exp. Med.* **207**, 1853–1862 (2010).
39. Neeli, I. & Radic, M. Opposition between PKC isoforms regulates histone deimination and neutrophil extracellular chromatin release. *Front Immunol* **4**, 38 (2013).
40. Cheng, O. Z. & Palaniyar, N. NET balancing: a problem in inflammatory lung diseases. *Front Immunol* **4**, 1 (2013).
41. Keshari, R. S. *et al.* Cytokines induced neutrophil extracellular traps formation: implication for the inflammatory disease condition. *PLoS ONE* **7**, e48111 (2012).

42. Brinkmann, V. & Zychlinsky, A. Neutrophil extracellular traps: Is immunity the second function of chromatin? *The Journal of Cell Biology* **198**, 773–783 (2012).
43. Yipp, B. G. *et al.* Infection-induced NETosis is a dynamic process involving neutrophil multitasking in vivo. *Nat. Med.* **18**, 1386–1393 (2012).
44. Halverson, T. W. R., Wilton, M., Poon, K. K. H., Petri, B. & Lewenza, S. DNA Is an Antimicrobial Component of Neutrophil Extracellular Traps. *PLOS Pathogens* **11**, e1004593 (2015).
45. Martinod, K. *et al.* PAD4-deficiency does not affect bacteremia in polymicrobial sepsis and ameliorates endotoxemic shock. *Blood* **125**, 1948–1956 (2015).
46. Mulcahy, H., Charron-Mazenod, L. & Lewenza, S. Extracellular DNA Chelates Cations and Induces Antibiotic Resistance in Pseudomonas aeruginosa Biofilms. *PLoS Pathogens* **4**, e1000213 (2008).
47. von Kockritz-Blickwede, M. *et al.* Phagocytosis-independent antimicrobial activity of mast cells by means of extracellular trap formation. *Blood* **111**, 3070–3080 (2008).
48. Chow, O. A. *et al.* Statins Enhance Formation of Phagocyte Extracellular Traps. *Cell Host & Microbe* **8**, 445–454 (2010).
49. Ganz, T. Defensins: antimicrobial peptides of innate immunity. *Nature Reviews Immunology* **3**, 710–720 (2003).
50. Brinkmann, V. & Zychlinsky, A. Beneficial suicide: why neutrophils die to make NETs. *Nature Reviews Microbiology* **5**, 577–582 (2007).
51. Kawasaki, H. & Iwamuro, S. Potential roles of histones in host defense as antimicrobial agents. *Infect Disord Drug Targets* **8**, 195–205 (2008).
52. Papayannopoulos, V., Metzler, K. D., Hakkim, A. & Zychlinsky, A. Neutrophil elastase and myeloperoxidase regulate the formation of neutrophil extracellular traps. *The Journal of Cell Biology* **191**, 677–691 (2010).
53. Urban, C. F. *et al.* Neutrophil Extracellular Traps Contain Calprotectin, a Cytosolic Protein Complex Involved in Host Defense against Candida albicans. *PLoS Pathogens* **5**, e1000639 (2009).
54. Sun, X., Shi, J., Han, L., Su, Y. & Li, Z. Anti-histones antibodies in systemic lupus erythematosus: prevalence and frequency in neuropsychiatric lupus. *Journal of Clinical Laboratory Analysis* **22**, 271–277 (2008).
55. Xu, J. *et al.* Extracellular histones are major mediators of death in sepsis. *Nat. Med.* **15**, 1318–1321 (2009).
56. Kutcher, M. E. *et al.* Extracellular histone release in response to traumatic injury: implications for a compensatory role of activated protein C. *J Trauma Acute Care Surg* **73**, 1389–1394 (2012).
57. Abrams, S. T. *et al.* Circulating Histones Are Mediators of Trauma-associated Lung Injury. *American Journal of Respiratory and Critical Care Medicine* **187**, 160–169 (2013).
58. Xu, J., Zhang, X., Monestier, M., Esmon, N. L. & Esmon, C. T. Extracellular Histones Are Mediators of Death through TLR2 and TLR4 in Mouse Fatal Liver Injury. *The Journal of Immunology* **187**, 2626–2631 (2011).
59. Semeraro, F. *et al.* Extracellular histones promote thrombin generation through platelet-dependent mechanisms: involvement of platelet TLR2 and TLR4. *Blood* **118**, 1952–1961 (2011).
60. Fuchs, T. A., Bhandari, A. A. & Wagner, D. D. Histones induce rapid and profound thrombocytopenia in mice. *Blood* **118**, 3708–3714 (2011).

61. Nowak, D., Piasecka, G. & Hrabec, E. Chemotactic activity of histones for human polymorphonuclear leukocytes. *Experimental Pathology* **40**, 111–116 (1990).
62. Saffarzadeh, M. *et al.* Neutrophil extracellular traps directly induce epithelial and endothelial cell death: a predominant role of histones. *PLoS ONE* **7**, e32366 (2012).
63. Cermelli, S., Guo, Y., Gross, S. P. & Welte, M. A. The Lipid-Droplet Proteome Reveals that Droplets Are a Protein-Storage Depot. *Current Biology* **16**, 1783–1795 (2006).
64. Li, Z. *et al.* Lipid Droplets Control the Maternal Histone Supply of Drosophila Embryos. *Current Biology* **22**, 2104–2113 (2012).
65. Hancock, R. E. W. & Lehrer, R. Cationic peptides: a new source of antibiotics. *Trends in Biotechnology* **16**, 82–88 (1998).
66. Hancock, R. E. W. & Sahl, H.-G. Antimicrobial and host-defense peptides as new anti-infective therapeutic strategies. *Nat. Biotechnol.* **24**, 1551–1557 (2006).
67. Dürr, U. H. N., Sudheendra, U. S. & Ramamoorthy, A. LL-37, the only human member of the cathelicidin family of antimicrobial peptides. *Biochimica et Biophysica Acta (BBA) - Biomembranes* **1758**, 1408–1425 (2006).
68. Chua, E. Y. D. *et al.* 3.9 Å structure of the nucleosome core particle determined by phase-plate cryo-EM. *Nucleic Acids Res.* **44**, 8013–8019 (2016).
69. Bäuerle, M., Doenecke, D. & Albig, W. The Requirement of H1 Histones for a Heterodimeric Nuclear Import Receptor. *J. Biol. Chem.* **277**, 32480–32489 (2002).
70. Haas, A. L., Bright, P. M. & Jackson, V. E. Functional diversity among putative E2 isozymes in the mechanism of ubiquitin-histone ligation. *J. Biol. Chem.* **263**, 13268–13275 (1988).
71. Bals, R. Epithelial antimicrobial peptides in host defense against infection. *Respiratory Research* **1**, 5 (2000).
72. Agerberth, B. *et al.* Antibacterial Components in Bronchoalveolar Lavage Fluid from Healthy Individuals and Sarcoidosis Patients. *American Journal of Respiratory and Critical Care Medicine* **160**, 283–290 (1999).
73. Bals, R., Wang, X., Zasloff, M. & Wilson, J. M. The peptide antibiotic LL-37/hCAP-18 is expressed in epithelia of the human lung where it has broad antimicrobial activity at the airway surface. *Proc. Natl. Acad. Sci. U.S.A.* **95**, 9541–9546 (1998).
74. Dajani, R. *et al.* Lysozyme Secretion by Submucosal Glands Protects the Airway from Bacterial Infection. *American Journal of Respiratory Cell and Molecular Biology* **32**, 548–552 (2005).
75. Chen, P.-H. & Fang, S.-Y. The Expression of Human Antimicrobial Peptide LL-37 in the Human Nasal Mucosa. *American Journal of Rhinology* **18**, 381–385 (2004).
76. Wiesner, J. & Vilcinskas, A. Antimicrobial peptides: The ancient arm of the human immune system. *Virulence* **1**, 440–464 (2010).
77. Jann, N. J. *et al.* Neutrophil antimicrobial defense against *Staphylococcus aureus* is mediated by phagolysosomal but not extracellular trap-associated cathelicidin. *Journal of Leukocyte Biology* **86**, 1159–1169 (2009).
78. Hassan, M., Kjos, M., Nes, I. F., Diep, D. B. & Lotfipour, F. Natural antimicrobial peptides from bacteria: characteristics and potential applications to fight against antibiotic resistance. *Journal of Applied Microbiology* **113**, 723–736 (2012).
79. Castro, M. S. & Fontes, W. Plant defense and antimicrobial peptides. *Protein Pept. Lett.* **12**, 13–18 (2005).
80. Hegedüs, N. & Marx, F. Antifungal proteins: More than antimicrobials? *Fungal Biology Reviews* **26**, 132–145 (2013).

81. Lemaitre, B. & Hoffmann, J. The Host Defense of *Drosophila melanogaster*. *Annual Review of Immunology* **25**, 697–743 (2007).
82. Cole, A. M., Weis, P. & Diamond, G. Isolation and characterization of pleurocidin, an antimicrobial peptide in the skin secretions of winter flounder. *J. Biol. Chem.* **272**, 12008–12013 (1997).
83. van Dijk, A., Veldhuizen, E. J. A. & Haagsman, H. P. Avian defensins. *Vet. Immunol. Immunopathol.* **124**, 1–18 (2008).
84. Hancock, R. E. W. & Diamond, G. The role of cationic antimicrobial peptides in innate host defences. *Trends in Microbiology* **8**, 402–410 (2000).
85. Selsted, M. E. & Ouellette, A. J. Mammalian defensins in the antimicrobial immune response. *Nature Immunology* **6**, 551–557 (2005).
86. Zanetti, M. Cathelicidins, multifunctional peptides of the innate immunity. *Journal of Leukocyte Biology* **75**, 39–48 (2004).
87. Mahlapuu, M., Håkansson, J., Ringstad, L. & Björn, C. Antimicrobial Peptides: An Emerging Category of Therapeutic Agents. *Frontiers in Cellular and Infection Microbiology* **6**, (2016).
88. Reddy, K. V. R., Yedery, R. D. & Aranha, C. Antimicrobial peptides: premises and promises. *International Journal of Antimicrobial Agents* **24**, 536–547 (2004).
89. Marr, A., Gooderham, W. & Hancock, R. Antibacterial peptides for therapeutic use: obstacles and realistic outlook. *Current Opinion in Pharmacology* **6**, 468–472 (2006).
90. Cheng, S.-C., Joosten, L. A. B., Kullberg, B.-J. & Netea, M. G. Interplay between Candida albicans and the Mammalian Innate Host Defense. *Infection and Immunity* **80**, 1304–1313 (2012).
91. De Lucca, A. J. & Walsh, T. J. Antifungal Peptides: Novel Therapeutic Compounds against Emerging Pathogens. *Antimicrobial Agents and Chemotherapy* **43**, 1–11 (1999).
92. Hsieh, I.-N. & Hartshorn, K. The Role of Antimicrobial Peptides in Influenza Virus Infection and Their Potential as Antiviral and Immunomodulatory Therapy. *Pharmaceuticals* **9**, 53 (2016).
93. Bastian, A. & Schäfer, H. Human alpha-defensin 1 (HNP-1) inhibits adenoviral infection in vitro. *Regul. Pept.* **101**, 157–161 (2001).
94. Horne, W. S. *et al.* Antiviral cyclic d,l-α-peptides: Targeting a general biochemical pathway in virus infections. *Bioorganic & Medicinal Chemistry* **13**, 5145–5153 (2005).
95. Torrent, M., Pulido, D., Rivas, L. & Andreu, D. Antimicrobial peptide action on parasites. *Curr Drug Targets* **13**, 1138–1147 (2012).
96. Deslouches, B. & Di, Y. P. Antimicrobial peptides with selective antitumor mechanisms: prospect for anticancer applications. *Oncotarget* **8**, (2017).
97. Lai, Y. & Gallo, R. L. AMPed up immunity: how antimicrobial peptides have multiple roles in immune defense. *Trends in Immunology* **30**, 131–141 (2009).
98. Zasloff, M. Antimicrobial peptides of multicellular organisms. *Nature* **415**, 389–395 (2002).
99. Jenssen, H., Hamill, P. & Hancock, R. E. W. Peptide Antimicrobial Agents. *Clinical Microbiology Reviews* **19**, 491–511 (2006).
100. Sang, Y. & Blecha, F. Antimicrobial peptides and bacteriocins: alternatives to traditional antibiotics. *Anim. Health. Res. Rev.* **9**, 227–235 (2008).
101. Bahar, A. & Ren, D. Antimicrobial Peptides. *Pharmaceuticals* **6**, 1543–1575 (2013).
102. Epand, R. M. & Vogel, H. J. Diversity of antimicrobial peptides and their mechanisms of action. *Biochim. Biophys. Acta* **1462**, 11–28 (1999).

103. Lehrer, R. I. & Ganz, T. Antimicrobial peptides in mammalian and insect host defence. *Curr. Opin. Immunol.* **11**, 23–27 (1999).
104. Hristova, K. & Wimley, W. C. A look at arginine in membranes. *J. Membr. Biol.* **239**, 49–56 (2011).
105. Yeaman, M. R. & Yount, N. Y. Mechanisms of antimicrobial peptide action and resistance. *Pharmacol. Rev.* **55**, 27–55 (2003).
106. Pasupuleti, M., Schmidtchen, A. & Malmsten, M. Antimicrobial peptides: key components of the innate immune system. *Critical Reviews in Biotechnology* **32**, 143–171 (2012).
107. Kumar, P., Kizhakkedathu, J. & Straus, S. Antimicrobial Peptides: Diversity, Mechanism of Action and Strategies to Improve the Activity and Biocompatibility In Vivo. *Biomolecules* **8**, 4 (2018).
108. Scocchi, M., Mardirossian, M., Runti, G. & Benincasa, M. Non-Membrane Permeabilizing Modes of Action of Antimicrobial Peptides on Bacteria. *Curr Top Med Chem* **16**, 76–88 (2016).
109. Le, C.-F., Fang, C.-M. & Sekaran, S. D. Intracellular Targeting Mechanisms by Antimicrobial Peptides. *Antimicrob. Agents Chemother.* **61**, e02340-16, /aac/61/4/e02340-16.atom (2017).
110. Shai, Y. Mechanism of the binding, insertion and destabilization of phospholipid bilayer membranes by alpha-helical antimicrobial and cell non-selective membrane-lytic peptides. *Biochim. Biophys. Acta* **1462**, 55–70 (1999).
111. Shai, Y. Mode of action of membrane active antimicrobial peptides. *Biopolymers* **66**, 236–248 (2002).
112. Matsuzaki, K. Magainins as paradigm for the mode of action of pore forming polypeptides. *Biochim. Biophys. Acta* **1376**, 391–400 (1998).
113. Huang, H. W. Action of Antimicrobial Peptides: Two-State Model †. *Biochemistry* **39**, 8347–8352 (2000).
114. Casteels, P. & Tempst, P. Apidaecin-type peptide antibiotics function through a non-poreforming mechanism involving stereospecificity. *Biochem. Biophys. Res. Commun.* **199**, 339–345 (1994).
115. Mattiuzzo, M. *et al.* Role of the Escherichia coli SbmA in the antimicrobial activity of proline-rich peptides. *Mol. Microbiol.* **66**, 151–163 (2007).
116. Patrzykat, A., Friedrich, C. L., Zhang, L., Mendoza, V. & Hancock, R. E. W. Sublethal concentrations of pleurocidin-derived antimicrobial peptides inhibit macromolecular synthesis in Escherichia coli. *Antimicrob. Agents Chemother.* **46**, 605–614 (2002).
117. Podda, E. *et al.* Dual mode of action of Bac7, a proline-rich antibacterial peptide. *Biochim. Biophys. Acta* **1760**, 1732–1740 (2006).
118. Lehrer, R. I. *et al.* Interaction of human defensins with Escherichia coli. Mechanism of bactericidal activity. *Journal of Clinical Investigation* **84**, 553–561 (1989).
119. Rosenberger, C. M., Gallo, R. L. & Finlay, B. B. Interplay between antibacterial effectors: a macrophage antimicrobial peptide impairs intracellular Salmonella replication. *Proc. Natl. Acad. Sci. U.S.A.* **101**, 2422–2427 (2004).
120. Park, C. B., Kim, H. S. & Kim, S. C. Mechanism of Action of the Antimicrobial Peptide Buforin II: Buforin II Kills Microorganisms by Penetrating the Cell Membrane and Inhibiting Cellular Functions. *Biochemical and Biophysical Research Communications* **244**, 253–257 (1998).

121. Sim, S. *et al.* Investigating the nucleic acid interactions of histone-derived antimicrobial peptides. *FEBS Letters* **591**, 706–717 (2017).
122. Walberg, M., Gaustad, P. & Steen, H. B. Rapid assessment of ceftazidime, ciprofloxacin, and gentamicin susceptibility in exponentially-growing E. coli cells by means of flow cytometry. *Cytometry* **27**, 169–178 (1997).
123. Wickens, H. J., Pinney, R. J., Mason, D. J. & Gant, V. A. Flow cytometric investigation of filamentation, membrane patency, and membrane potential in Escherichia coli following ciprofloxacin exposure. *Antimicrob. Agents Chemother.* **44**, 682–687 (2000).
124. Fernandes, J. M. O., Kemp, G. D., Molle, M. G. & Smith, V. J. Anti-microbial properties of histone H2A from skin secretions of rainbow trout, Oncorhynchus mykiss. *Biochemical Journal* **368**, 611–620 (2002).
125. Patat, S. A. *et al.* Antimicrobial activity of histones from hemocytes of the Pacific white shrimp. *European Journal of Biochemistry* **271**, 4825–4833 (2004).
126. Richards, R. C., O'Neil, D. B., Thibault, P. & Ewart, K. V. Histone H1: An Antimicrobial Protein of Atlantic Salmon (Salmo salar). *Biochemical and Biophysical Research Communications* **284**, 549–555 (2001).
127. Kawasaki, H., Koyama, T., Conlon, J. M., Yamakura, F. & Iwamuro, S. Antimicrobial action of histone H2B in Escherichia coli: Evidence for membrane translocation and DNA-binding of a histone H2B fragment after proteolytic cleavage by outer membrane proteinase T. *Biochimie* **90**, 1693–1702 (2008).
128. Li, G.-H., Mine, Y., Hincke, M. T. & Nys, Y. Isolation and characterization of antimicrobial proteins and peptide from chicken liver. *Journal of Peptide Science* **13**, 368–378 (2007).
129. Rose-Martel, M. & Hincke, M. T. Antimicrobial histones from chicken erythrocytes bind bacterial cell wall lipopolysaccharides and lipoteichoic acids. *International Journal of Antimicrobial Agents* **44**, 470–472 (2014).
130. Rose, F. R. *et al.* Potential role of epithelial cell-derived histone H1 proteins in innate antimicrobial defense in the human gastrointestinal tract. *Infect. Immun.* **66**, 3255–3263 (1998).
131. Adav, S. S. *et al.* Studies on the Proteome of Human Hair - Identification of Histones and Deamidated Keratins. *Scientific Reports* **8**, (2018).
132. Kai-Larsen, Y. *et al.* Antimicrobial Components of the Neonatal Gut Affected Upon Colonization. *Pediatric Research* **61**, 530–536 (2007).
133. Kuwata, H., Yip, T.-T., Yip, C. L., Tomita, M. & Hutchens, T. W. Bactericidal Domain of Lactoferrin: Detection, Quantitation, and Characterization of Lactoferricin in Serum by SELDI Affinity Mass Spectrometry. *Biochemical and Biophysical Research Communications* **245**, 764–773 (1998).
134. Papareddy, P. *et al.* Proteolysis of Human Thrombin Generates Novel Host Defense Peptides. *PLoS Pathogens* **6**, e1000857 (2010).
135. Luders, T., Birkemo, G. A., Nissen-Meyer, J., Andersen, O. & Nes, I. F. Proline Conformation-Dependent Antimicrobial Activity of a Proline-Rich Histone H1 N-Terminal Peptide Fragment Isolated from the Skin Mucus of Atlantic Salmon. *Antimicrobial Agents and Chemotherapy* **49**, 2399–2406 (2005).
136. Fernandes, J. Isolation and characterisation of oncorhyncin II, a histone H1-derived antimicrobial peptide from skin secretions of rainbow trout, Oncorhynchus mykiss. *Developmental & Comparative Immunology* **28**, 127–138 (2004).

137. Patrzykat, A., Zhang, L., Mendoza, V., Iwama, G. K. & Hancock, R. E. W. Synergy of Histone-Derived Peptides of Coho Salmon with Lysozyme and Flounder Pleurocidin. *Antimicrobial Agents and Chemotherapy* **45**, 1337–1342 (2001).
138. Park, I. Y., Park, C. B., Kim, M. S. & Kim, S. C. Parasin I, an antimicrobial peptide derived from histone H2A in the catfish, *Parasilurus asotus*. *FEBS Letters* **437**, 258–262 (1998).
139. Cho, J. H. *et al.* Cathepsin D produces antimicrobial peptide parasin I from histone H2A in the skin mucosa of fish. *The FASEB Journal* **16**, 429–431 (2002).
140. Koo, Y. S. *et al.* Structure–activity relations of parasin I, a histone H2A-derived antimicrobial peptide. *Peptides* **29**, 1102–1108 (2008).
141. Park, C. B., Kim, M. S. & Kim, S. C. A Novel Antimicrobial Peptide fromBufo bufo gargarizans. *Biochemical and Biophysical Research Communications* **218**, 408–413 (1996).
142. Yi, G.-S., Park, C. B., Kim, S. C. & Cheong, C. Solution structure of an antimicrobial peptide buforin II. *FEBS Letters* **398**, 87–90 (1996).
143. Kim, H. S., Park, C. B., Kim, M. S. & Kim, S. C. cDNA Cloning and Characterization of Buforin I, an Antimicrobial Peptide: A Cleavage Product of Histone H2A. *Biochemical and Biophysical Research Communications* **229**, 381–387 (1996).
144. Kobayashi, S., Takeshima, K., Park, C. B., Kim, S. C. & Matsuzaki, K. Interactions of the Novel Antimicrobial Peptide Buforin 2 with Lipid Bilayers: Proline as a Translocation Promoting Factor †. *Biochemistry* **39**, 8648–8654 (2000).
145. Kobayashi, S. *et al.* Membrane Translocation Mechanism of the Antimicrobial Peptide Buforin 2 †. *Biochemistry* **43**, 15610–15616 (2004).
146. Lan, Y. *et al.* Structural contributions to the intracellular targeting strategies of antimicrobial peptides. *Biochimica et Biophysica Acta (BBA) - Biomembranes* **1798**, 1934–1943 (2010).
147. Park, C. B., Yi, K.-S., Matsuzaki, K., Kim, M. S. & Kim, S. C. Structure-activity analysis of buforin II, a histone H2A-derived antimicrobial peptide: The proline hinge is responsible for the cell-penetrating ability of buforin II. *Proceedings of the National Academy of Sciences* **97**, 8245–8250 (2000).
148. Uyterhoeven, E. T., Butler, C. H., Ko, D. & Elmore, D. E. Investigating the nucleic acid interactions and antimicrobial mechanism of buforin II. *FEBS Letters* **582**, 1715–1718 (2008).
149. Birkemo, G. A., Lüders, T., Andersen, Ø., Nes, I. F. & Nissen-Meyer, J. Hipposin, a histone-derived antimicrobial peptide in Atlantic halibut (Hippoglossus hippoglossus L.). *Biochimica et Biophysica Acta (BBA) - Proteins and Proteomics* **1646**, 207–215 (2003).
150. Bustillo, M. E. *et al.* Modular analysis of hipposin, a histone-derived antimicrobial peptide consisting of membrane translocating and membrane permeabilizing fragments. *Biochimica et Biophysica Acta (BBA) - Biomembranes* **1838**, 2228–2233 (2014).
151. Kawasaki, H., Isaacson, T., Iwamuro, S. & Conlon, J. M. A protein with antimicrobial activity in the skin of Schlegel's green tree frog Rhacophorus schlegelii (Rhacophoridae) identified as histone H2B. *Biochemical and Biophysical Research Communications* **312**, 1082–1086 (2003).
152. Lemaire, S. *et al.* Isolation and characterization of histogranin, a natural peptide with NMDA receptor antagonist activity. *Eur. J. Pharmacol.* **245**, 247–256 (1993).
153. Lemaire, S. *et al.* Antimicrobial effects of H4-(86-100), histogranin and related compounds--possible involvement of DNA gyrase. *FEBS J.* **275**, 5286–5297 (2008).
154. Augusto, L. A. *et al.* Histones: A Novel Class of Lipopolysaccharide-Binding Molecules †. *Biochemistry* **42**, 3929–3938 (2003).

155. Gillrie, M. R. *et al.* Plasmodium falciparum Histones Induce Endothelial Proinflammatory Response and Barrier Dysfunction. *The American Journal of Pathology* **180**, 1028–1039 (2012).
156. Chaaban, H. *et al.* Inter- inhibitor protein and its associated glycosaminoglycans protect against histone-induced injury. *Blood* **125**, 2286–2296 (2015).
157. Kawasaki, H., Koyama, T., Conlon, J. M., Yamakura, F. & Iwamuro, S. Antimicrobial action of histone H2B in Escherichia coli: Evidence for membrane translocation and DNA-binding of a histone H2B fragment after proteolytic cleavage by outer membrane proteinase T. *Biochimie* **90**, 1693–1702 (2008).
158. Tagai, C., Morita, S., Shiraishi, T., Miyaji, K. & Iwamuro, S. Antimicrobial properties of arginine- and lysine-rich histones and involvement of bacterial outer membrane protease T in their differential mode of actions. *Peptides* **32**, 2003–2009 (2011).
159. Miller, B. F., Abrams, R., Dorfman, A. & Klein, M. ANTIBACTERIAL PROPERTIES OF PROTAMINE AND HISTONE. *Science* **96**, 428–430 (1942).
160. Hirsch, J. G. BACTERICIDAL ACTION OF HISTONE. *Journal of Experimental Medicine* **108**, 925–944 (1958).
161. Brinkmann, V. *et al.* Neutrophil extracellular traps kill bacteria. *Science* **303**, 1532–1535 (2004).
162. Kahlenberg, J. M., Carmona-Rivera, C., Smith, C. K. & Kaplan, M. J. Neutrophil Extracellular Trap-Associated Protein Activation of the NLRP3 Inflammasome Is Enhanced in Lupus Macrophages. *The Journal of Immunology* **190**, 1217–1226 (2013).
163. Park, I. Y., Park, C. B., Kim, M. S. & Kim, S. C. Parasin I, an antimicrobial peptide derived from histone H2A in the catfish, *Parasilurus asotus*. *FEBS Letters* **437**, 258–262 (1998).
164. Birkemo, G. A., Lüders, T., Andersen, Ø., Nes, I. F. & Nissen-Meyer, J. Hipposin, a histone-derived antimicrobial peptide in Atlantic halibut (Hippoglossus hippoglossus L.). *Biochimica et Biophysica Acta (BBA) - Proteins and Proteomics* **1646**, 207–215 (2003).
165. Patat, S. A. *et al.* Antimicrobial activity of histones from hemocytes of the Pacific white shrimp. *European Journal of Biochemistry* **271**, 4825–4833 (2004).
166. Luders, T., Birkemo, G. A., Nissen-Meyer, J., Andersen, O. & Nes, I. F. Proline Conformation-Dependent Antimicrobial Activity of a Proline-Rich Histone H1 N-Terminal Peptide Fragment Isolated from the Skin Mucus of Atlantic Salmon. *Antimicrobial Agents and Chemotherapy* **49**, 2399–2406 (2005).
167. Cho, J. H., Sung, B. H. & Kim, S. C. Buforins: Histone H2A-derived antimicrobial peptides from toad stomach. *Biochimica et Biophysica Acta (BBA) - Biomembranes* **1788**, 1564–1569 (2009).
168. Dorrington, T., Villamil, L. & Gómez-chiarri, M. Upregulation in response to infection and antibacterial activity of oyster histone H4. *Fish & Shellfish Immunology* **30**, 94–101 (2011).
169. Morita, S., Tagai, C., Shiraishi, T., Miyaji, K. & Iwamuro, S. Differential mode of antimicrobial actions of arginine-rich and lysine-rich histones against Gram-positive Staphylococcus aureus. *Peptides* **48**, 75–82 (2013).
170. Hancock, R. E. W. & Sahl, H.-G. Antimicrobial and host-defense peptides as new anti-infective therapeutic strategies. *Nat. Biotechnol.* **24**, 1551–1557 (2006).
171. Morita, S., Tagai, C., Shiraishi, T., Miyaji, K. & Iwamuro, S. Differential mode of antimicrobial actions of arginine-rich and lysine-rich histones against Gram-positive Staphylococcus aureus. *Peptides* **48**, 75–82 (2013).

172. Elsbach, P., Weiss, J. & Levy, O. Integration of antimicrobial host defenses: role of the bactericidal/permeability-increasing protein. *Trends Microbiol.* **2**, 324–328 (1994).
173. Yu, G., Baeder, D. Y., Regoes, R. R. & Rolff, J. Combination Effects of Antimicrobial Peptides. *Antimicrob. Agents Chemother.* **60**, 1717–1724 (2016).
174. Nagaoka, I., Hirota, S., Yomogida, S., Ohwada, A. & Hirata, M. Synergistic actions of antibacterial neutrophil defensins and cathelicidins. *Inflamm. Res.* **49**, 73–79 (2000).

Chapter 2: Materials and Methods

2.1 Bacterial Strains

Experiments were performed using the *E. coli* strain MG1655 (seq), which is devoid of the bacteriophage lambda and F plasmid, and approximates wild-type *E. coli*[1]. The *S. aureus* strain RN4220, which was originally derived from NCTC8325-4 was used for experiments involving Gram-positive bacteria[2].

The PhoPQ reporter strain (*PmgrB-yfp PtetA-cfp (kanR, camR)*) contains a PhoP-regulated *mgrB* reporter driving YFP expression and a constitutive promoter expressing CFP, allowing for controlled reporting of expression and intensity levels. *D(phoP) D(phoQ) PmgrB-yfp PtetA-cfp (kanR, camR)* is an equivalent PhoQ mutant strain.

The proton gradient was measured using pJMK001 in the *E. coli* strain XL1 Blue (Addagene, Watertown, MA), which expresses the proteorhodopsin optical proton sensor (PROPS) protein under the control of the arabinose promoter[3]. MAL204 (MG1655 f(*ompA-cfp*) attl::[P_{rcsA}-*yfp*]), constructed by Melissa Lasaro and Mark Goulian, unpublished) contains YFP fused to the promoter of *rcsA*, integrated at the lambda attachment site and constitutively expresses a transcriptional fusion of CFP to *ompA*. Chromosomal reorganization experiments were performed with a a strain of *E. coli* containing fluorescent HupA (*hupA-mRuby2-FRT-cat-FRT*)[4]. MAL190 (MG1655 attl::[*cat tetR* f(*tetA-mCherry)*], constructed by Melissa Lasaro and Mark Goulian, unpublished) contains the *tetR* and *tetA* genes integrated at the phage lambda attachment site and a transcriptional fusion of mCherry to the 3′ end of *tetA*. The *rcsA* mutant strain was constructed by P1 transduction of the D(*rcsA*)::kan allele from the Keio collection[5] strain JW1935 (Yale Genetic Stock Center, New Haven, CT), yielded AT14A.

2.2 Growth Conditions

Strains were streaked onto LB-Miller (BD Biosciences, Franklin Lakes, NJ) petri dishes containing 2% Bacto agar (BD Biosciences), incubated at 37 ºC to obtain single colonies, and inoculated into MinA minimal media[6] with 1 mM $MgSO_4$ and supplemented with 0.1% casamino acids. In summary, MinA minimal media contains per 1L Milli-Q water: 4.5 g KH_2PO_4, 10.5 g K_2HPO_4 1 g $(NH_4)_2SO_4$, 0.5 g sodium citrate • $2H_20$, 0.2% glucose, 0.1% casamino acids, and 1 mM $MgSO_4$. Cultures were grown to stationary phase at 37°C in a shaking incubator at 225 rpm overnight, sub-cultured, and grown to mid-exponential phase (OD_{600} 0.2). In low ionic conditions, liquid cultures growing in MinA media containing 1 mM $MgSO_4$ were diluted into MinA media containing 1 μM $MgSO_4$.

2.3 Antimicrobial Peptides, Proteins, and Antibiotics

Experiments involving histone treatments used calf thymus histone H2A (Sigma, St. Louis, MO), calf thymus histone H3 (Sigma, St. Louis, MO), human histone H3 (Cayman Chemical, Ann Arbor, MI), or citrullinated human histone H3 (Cayman Chemical, Ann Arbor, MI). Experiments involving antimicrobial peptide treatment used the human cathelicidin LL-37 (Anaspec, Fremont, CA), FAM-LC-LL-37 (Anaspec, Fremont, CA), or magainin-2 (Anaspec, Fremont, CA). Experiments involving antibiotic treatments used kanamycin sulfate (Sigma), chloramphenicol (Sigma), or polymyxin B sulfate salt (Sigma).

2.4 Agar Plate Assay

To quantify the effects of histone treatment in low ionic conditions, overnight cultures of stationary phase *E. coli* or *S. aureus* were diluted 1:1000 into MinA medium with 1 μM or 1 mM

$MgSO_4$ and cultured with or without 10 μg/mL histone H2A. Bacteria were incubated for 1 hour at 37°C in a shaking incubator at 225 rpm. Bacterial suspensions were diluted 1:1000 into fresh MinA media with either 1 μM or 1 mM $MgSO_4$ and 25 μL of diluted bacterial suspension was plated on LB-Miller agar plates. Plates were incubated for 18 hours at 37°C before colony forming units (CFU) were counted.

To quantify the effects of synergy treatments on CFU counts, overnight cultures of stationary phase *E. coli* were diluted 1:1000 in MinA with 1 mM $MgSO_4$ and cultured with 10 μg/mL H2A, 2 μM LL-37, or both H2A and LL-37 for 1 hour. After treatment, bacterial suspensions were diluted 1:1000 into fresh MinA media with 1 mM $MgSO_4$ and 25 μL of diluted bacterial suspension was plated on LB-Miller agar plates. Plates were incubated for 18 hours at 37°C before colony forming units (CFU) were counted.

2.5 Growth Curves

Growth curve experiments were performed using a Synergy HTX multi-mode plate reader and sterile, tissue-culture treated, clear bottom, black polystyrene 96-well microplates (Corning). The temperature setpoint was 37°C, preheated before beginning measurements. Each well contained 200 μL of total bacterial solution.

For experiments performed with stationary phase bacteria, overnight cultures of bacteria were grown overnight to saturation, diluted 1:1000 into MinA media with 1 μM or 1 mM $MgSO_4$, and supplemented with H2A, LL-37, kanamycin, chloramphenicol, or polymyxin B. For experiments performed with exponential phase bacteria, overnight cultures of bacteria were subcultured in fresh MinA media containing 1 mM $MgSO_4$ and grown to OD_{600} 0.2. Exponential phase bacteria were diluted 1:20 into fresh MinA media with 1 μM or 1 mM $MgSO_4$, and supplemented with H2A, LL-

37, magainin-2, kanamycin, chloramphenicol, or polymyxin B. After adding antimicrobial agents, bacterial cultures were immediately added to the 96-well microplates for growth measurements.

Growth curves were constructed by taking optical density at 600 nm (OD_{600}) measurements every 15 minutes for up to 48 hours. Shaking was set to continuous orbital, with a frequency of 282 cpm (3 mm). The read speed was normal, with a 100 msec delay, and 8 measurements per data points.

2.6 Fluorescence and Phase Contrast Microscopy

Microscopy images were obtained by visualizing fluorescence with a Nikon Eclipse Ti-E microscope (Nikon, Melville, NY) containing a Nikon 100X Plan Apo (1.45 N.A.) objective, a Sola light engine (Lumencor, Beaverton, OR), an LED-DA/FI/TX filter set (Semrock, Rochester, NY) for visualizing the GFP and mCherry fluorescence spectrum containing a 409/493/596 dichroic and 474/27 nm and 575/25 nm filters for excitation and 525/45 nm and 641/75 nm filters for emission, an LED-CFP/YFP/MCHERRY filter set (Semrock) for visualizing CFP and YFP fluorescence containing a 459/526/596 dichroic and 438/24 nm and 509/22 nm filters for excitation and 482/25 nm and 544/24 nm filters for emission, a Cy5 filter set (Chroma) for imaging PROPS fluorescence containing a 640/30 nm filter for excitation, a 690/50 nm filter for emission, and a 660 nm long pass dichroic, and a Hamamatsu Orca Flash 4.0 V2 camera (Hamamatsu, Bridgewater, NJ). Images were acquired using Nikon NIS-Elements and analyzed using custom built software written previously [7] in Matlab (Mathworks, Natick, MA). After treating bacteria with antimicrobial agents, 5µl of culture was plated on 1% agarose-MinA pads and imaged immediately, as described previously [8]. Approximately 100 cells were imaged and analyzed in each experiment.

2.7 Propidium Iodide Staining

To visualize membrane lysis of stationary phase *E. coli* in low and physiological magnesium concentrations, overnight cultures of MG1655 were grown overnight to saturation and diluted 1:1000 into MinA media with 1 μM or 1 mM $MgSO_4$, with or without 10 μg/mL H2A. 30 μM propidium iodide was co-incubated with the solution of bacteria for one hour at 37°C in a shaking incubator at 225 rpm before plating on 1% agarose-MinA pads. Data was collected using the mCherry filter.

To visualize membrane lysis of mid-exponential phase *E. coli*, overnight cultures of MG1655 were grown overnight to saturation, subcultured in fresh MinA media containing 1 mM $MgSO_4$ and grown to OD_{600} 0.2. Exponential phase bacteria were diluted 1:20 into fresh MinA media with 1 μM or 1 mM $MgSO_4$, and supplemented with H2A, LL-37, magainin-2, kanamycin, chloramphenicol, or polymyxin B. Bacteria were cultured at least one hour at 37°C in a shaking incubator at 225 rpm before plating on 1% agarose-MinA pads. 30 μM propidium iodide was co-incubated with the solution of bacteria for at least 15 minutes before imaging. Data was collected using the mCherry filter.

2.8 PhoQ Expression Measurements

A PhoPQ reporter strain (*PmgrB-yfp PtetA-cfp (kanR, camR)*), containing a PhoP-regulated *mgrB* reporter driving YFP expression and a constitutive promoter expressing CFP, was used to measure PhoQ expression in 1 μM or 1 mM $MgSO_4$, with or without the addition of 10 μg/mL H2A. Stationary phase *E. coli* were diluted 1:1000 into fresh MinA media with or without 10 μg/mL H2A and incubated for three hours at 37°C in a shaking incubator at 225 rpm before plating on 1% agarose-MinA pads. Data was collected using the YFP and CFP filters.

2.9 SEM Imaging

E. coli were grown to an OD_{600} of 0.2, diluted 1:20, and supplemented with 10 μg/mL H2A, 1 μM LL-37, or the dual combination of 10 μg/mL H2A and 1 μM LL-37 Cells were treated for 1 hour at 37℃ in a shaking incubator at 225 rpm. Bacterial cultures were then added to a glass bottomed petri dish for 15 minutes. Due to lower levels of adhesion, control cells were not diluted 1:20 and were allowed to sit in the glass-bottomed petri dish for 45 minutes after the one-hour incubation period. Media was removed and 4% paraformaldehyde (PFA) was added for 20 minutes to fix bacteria. Dehydration was performed with serial ethanol dilutions. The fixed and dehydrated sampled were coated with 10 nm of iridium using an ACE600 sputter coater (Leica Microsystems, Buffalo Grove, IL). Bacteria and surfaces were then characterized using a FEI Magellan 400 XHR Scanning Electron Microscope (FEI Company, Hillsboro, OR) at a 45° tilt angle with an acceleration voltage of 3kV.

2.10 Cell Aggregate and Size Analysis

E. coli were cultured to an OD_{600} of 0.2 in MinA media, diluted 1:20 into fresh MinA media, treated with increasing concentrations of H2A, increasing concentrations of LL-37, or the synergy treatment conditions. Concentrations of H2A used were 0-100 μg/mL H2A. Concentrations of LL-37 used were 0-4 μM LL-37. Synergy conditions were 10 μg/mL H2A, 2 μM LL-37, and the dual combination of 10 μg/mL H2A and 2 μM LL-37. Bacteria were treated with H2A and/or LL-37 and incubated for 1 hour. Cells were immobilized on an agarose pad using, imaged using phase contrast microscopy, and analyzed using Canny edge detection using image analysis tools developed previously[9] that were modified in Matlab (Version R2017b; Mathworks, Natick, MA).

2.11 Fluorescent Histone Labeling

Histone H2A was fluorescently labeled with Alexa Fluor 488 NHS Ester (Invitrogen). Briefly, 10 mg of H2A was dissolved in 1 mL of 0.1 M sodium bicarbonate buffer. 50 μL Alexa Fluor dye dissolved in DMSO (10 mg/mL) was added, and the solution continuously stirred at room temperature for 1 hour. A PD MidiTrap G-25 column (GE Healthcare Life Sciences, Pittsburgh, PA) was equilibrated with Milli-Q water and used to remove unreacted Alexa Fluor. The fluorescent solution was frozen at -20°C until used.

2.12 Fluorescent Histone and Fluorescent LL-37 Uptake

E. coli or *S. aureus* was grown to OD_{600} of 0.2, and diluted 1:20 into fresh MinA media, containing 1 mM $MgSO_4$. H2A uptake in *E. coli* was measured by adding 10 μg/mL AF-H2A (1% Alexa Fluor-labeled H2A mixed with 99% unlabeled H2A) and 10 μg/mL Cam, 50 μg/mL Kan, 2 μM LL-37, 1 μg/mL PMB, or 10 μM MAG2, incubating for 1 hour, and analyzing using fluorescence microscopy. H2A uptake in *S. aureus* was measured using same concentrations of AF-H2A and LL-37.

LL-37 uptake in both bacteria was measured by adding 1 μM fluorescently-labeled LL-37 (1% 5-FAM-LC-LL-37 (Anaspec) mixed with 99% unlabeled LL-37) and 10 μg/mL unlabeled H2A, incubating for 1 hour, and analyzing using fluorescence microscopy. In all experiments, untreated cells were used to measure background fluorescence levels and values below the average background were excluded from the analysis to exclude lysed cells.

2.13 Fluorescent Histone and Fluorescent LL-37 Uptake in Low Ionic Conditions

E. coli was grown to OD_{600} of 0.2 in MinA media containing 1 mM $MgSO_4$, and diluted 1:20 into fresh MinA media, containing 1 μM or 1 mM $MgSO_4$. H2A uptake in *E. coli* was measured by adding 10 μg/mL AF-H2A (1% Alexa Fluor-labeled H2A mixed with 99% unlabeled H2A), incubating for 3 hours, and analyzing using fluorescence microscopy. Untreated cells were used to measure background fluorescence levels and values below the average background were excluded from the analysis to exclude lysed cells.

2.14 PROPS Fluorescence Analysis

The *E. coli* strain containing the PROPS plasmid pJMK001 were grown in LB in a shaking incubator at 33° C, induced with arabinose and 5 μM retinal, and incubated in darkness for 3.5 hours. The culture was spun down and resuspended in M9. *E. coli* were back-diluted into fresh MinA, cultured to an OD_{600} of 0.2, diluted 1:20 into fresh MinA media, treated with 10 μg/mL H2A, 1 μM LL-37, both 10 μg/mL H2A and 1 μM LL-37, 1 μg/mL PMB, or both 10 μg/mL H2A and 1 μg/mL PMB, and incubated for 1 hour. Cells were immobilized on a 1% agarose pad and and Cy5 fluorescence was analyzed using fluorescence microscopy.

2.15 Timelapse of *E. coli* Recovery

To quantify the time-course of recovery in *E. coli* treated with LL-37 alone or with the synergistic combination of LL-37 and H2A, we grew MAL204 to mid-exponential phase, added 10 μg/mL H2A, 1 μM LL-37, or 1 μM LL-37 with 10 μg/mL H2A, and incubated for 1 hour. The solution was filtered through a 0.22 μm filter to remove excess LL-37 and H2A and cells were

resuspended in fresh MinA medium. Cells were immobilized on a 1% agarose pad and imaged over an hour time period.

2.16 Time Course of Membrane Healing

To quantify the time-course of membrane repair in bacteria treated with H2A alone, AMPs alone, or the synergistic combination of AMPs and H2A, MAL204 was grown to mid-exponential phase, diluted 1:20 with 10 μg/mL H2A, 1 μM LL-37, 1 μM LL-37 with 10 μg/mL H2A, 10 μM MAG2, or 1 μM MAG2 with 10 μg/mL H2A, and incubated for 1 hour. The solution was filtered through a 0.22 μm filter to remove excess LL-37 and H2A and cells were resuspended in fresh MinA medium. Cells were allowed to recover for 0, 30, 60 minutes before the addition of 30 μM propidium iodide for 15 minutes prior to performing fluorescence microscopy. Intracellular propidium iodide fluorescence and CFP fluorescence were quantified.

To quantify the time-course of membrane repair in bacteria treated with H2A in low and physiological environments, MAL204 was grown to mid-exponential phase, diluted 1:20 into MinA media with 1 μM or 1 mM $MgSO_4$, with or without 10 μg/mL H2A, and incubated for 3 hours. The solution was filtered through a 0.22 μm filter to remove excess H2A and cells were resuspended in fresh MinA medium. Cells were allowed to recover for up to 60 minutes before the addition of 30 μM propidium iodide for 15 minutes prior to performing fluorescence microscopy. Intracellular propidium iodide fluorescence and CFP fluorescence were quantified.

2.17 Electroporation of Electrocompetent *E. coli*

To prepare electrocompetent cells, *E. coli* was cultured in SOB to an OD_{600} of 0.5. The bacterial cultures were placed on ice for 30 minutes and spun down at 6000 rpm for 15 minutes at 4°C.

Supernatant was removed and bacteria were resuspended in ice cold sterile 10% glycerol. Bacteria were centrifuged at 6000 rpm for 3.5 minutes at 4°C, supernatant was removed, and bacteria were resuspended in ice cold sterile 10% glycerol. Wash cycles were repeated four times. The pellet was resuspended to a final concentration of OD of 0.2 in ice cold 10% glycerol.

50 uL of OD 0.2 electrocompetent *E. coli* were added to a 1 mm cuvette, with or without 50 μg/mL H2A. Electroporation was performed using the "Ec1" setting on a Bio-Rad micropulser. Cold SOC media was added to a final volume of 1 mL. Electrocompetent cells were diluted 1:20 into cold SOC, with or without 50 μg/mL H2A as a control. These control cells were not electroporated.

2.18 Bacterial DNA Purification

Overnight *E. coli* cultures were grown to saturation in MinA. DNA purification was performed using a Miniprep kit (Qiagen, Germantown, MD). A three-second sonication step was performed after lysis to isolate genomic DNA.

2.19 Non-Denaturing Nucleic Acid PAGE

E. coli DNA was purified from MG1655 using a Miniprep kit (Qiagen), with a three-second sonication step to ensure bacterial lysis. 10 μL mixtures containing 1 μg purified DNA from *E. coli* were incubated with 0-1.4 μg Histone H2A or LL-37 for 25 minutes at 25ºC. Gel loading sample buffer (5x, Bio-Rad, Hercules, CA) was added to a final concentration of 1x and the products were separated by native PAGE on a 5% TBE gel (Bio-Rad, Hercules, CA) at 100 V for 60 minutes. The gel was stained with 1x SYBR safe (Invitrogen, Carlsbad, CA) in TBE buffer[10] for 30 minutes before visualization.

2.20 Chromosomal Organization in *E. coli*

E. coli cultures were grown at OD_{600} of 0.2, diluted 1:20 into fresh MinA media, treated with 2 μM LL-37 or both LL-37 and 10 μg/mL H2A for 30 minutes and stained with 3 μM SYTOX Green nucleic acid stain (ThermoFisher, Waltham, MA) for 10 minutes. Cells were immobilized on agarose pads containing 2 μM LL-37 alone or in combination with 10 μg/mL H2A, and 5 μM SYTOX Green and remained on the pad for 3 hours before imaging using the fluorescence microscopy. Raw images were analyzed through principal component analysis using image analysis tools developed previously [11] and modified in Matlab (Version R2017b; Mathworks, Natick, MA). Individual cells were identified in phase contrast images using canny edge detection. Images of LL-37-treated cells and of cells treated with both LL-37 and H2A were pooled together, rotated such that the major axis of the cell was parallel to the x-axis and resized to 30x100 pixels. The covariances between corresponding pixels of different cells were computed using the 16 bit intensity values from the rotated and resized fluorescence images and for the same images rotated by an additional 180 degrees. The orientation that gave the lower covariance was used for the analysis. Principal components for the covariance matrix was computed using approximately 100 cells and the principal components that gave the two largest eigenvalues were identified.

2.21 *In vivo* Transcription Assay

To determine how histone entry into the bacterial cell impacts transcription, MAL190 was cultured to mid-log, diluted 1:20 in MinA medium, treated with 10 μg/mL Histone H2A and/or 2 μM LL-37, incubated for one hour, and induced for transcription using 50 ng/mL of anhydrotetracycline (aTc). The fluorescence of mCherry was measured after one hour using single-cell fluorescence microscopy.

2.22 RNA Sequencing

E. coli cultures were grown to saturation overnight in MinA media, diluted 1:1000 into the same media, cultured to an OD_{600} of 0.2, diluted 1:20 in pre-warmed media, and supplemented with 10 μg/mL H2A, 1 μM LL-37, or both. 10 mL of culture was harvested at 0, 30, and 60 minutes, filtered through a 0.8 μm filter, washed with 2 mL H_2O, and resuspended in 600 uL Total Lysis Solution (TE 8.0 (10 mM Tris-HCl, 1 mM EDTA), 0.5 mg/mL lysozyme (Sigma), and 1% SDS). Samples were incubated for 3 minutes at room temperature before freezing in liquid N_2. Samples were kept in -80 °C until nucleic acid extraction with a hot phenol-chloroform extraction and ethanol precipitation[12]. RNA yield was measured using a Nanodrop 2000 (Thermo Fisher, Waltham, MA). Samples were DNase digested (Ambion, Waltham, MA) and treated with RiboZero (Illumina, San Diego, CA). A NEBNext Ultra Directional Library kit (NEB, Ipswich, MA) was used to construct a cDNA library which was sequenced by the Princeton University Genomics Core Facility. Experiments were performed in triplicate and each experiment was sequenced with a depth of at least 10 M reads. Sequencing data was analyzed using our own software written in Python and using R (The R Foundation, Vienna, Austria). Sequences were aligned to the MG1655 genome (U00096.3) using Bowtie2 (Langmead and Salzberg, 2012). Sequencing data (accession pending) is available in the NCBI GEO database.

2.23 Validation of RNA Sequencing

E. coli containing YFP fused to the promoter of *rcsA*, integrated at the lambda attachment site, and constitutively expressing a transcriptional fusion of CFP to *ompA* was grown to mid-exponential phase. Bacteria were diluted into warmed MinA media with increasing concentrations of H2A. In addition, 30 μM PI was added to the culture to specifically measure fluorescence

intensities in membrane-permeabilized cells. After a 30-minute incubation period, cells were immobilized on a 1% agarose pad and and YFP, CFP, and PI fluorescence was analyzed using fluorescence microscopy.

2.24 Derivation of the Histone-AMP positive feedback model

We developed a mathematical model to describe the dynamics of histone and AMP uptake into bacterial cells. Histones and AMPs enter passively using simple diffusion: $\frac{d[His_{in}]}{dt} = k_{His}[His_{out}]$ and $\frac{d[AMP_{in}]}{dt} = k_{AMP}[AMP_{out}]$ where [*His*$_{in}$] and [*His*$_{out}$] represent the concentrations of histones inside and outside of the cell, respectively, [*AMP*$_{in}$] and [*AMP*$_{out}$] represent the concentrations of AMP inside and outside of the cell, respectively, and $k_{Hisentry}$ and $k_{AMPentry}$ are the rate constants associated with the passive entry of histones and AMPs into the cell, respectively. Molecules of histones and AMPs can leave the cell through a number of ways including cell division, shedding of cell components, and transport through drug efflux pumps. We describe these combined effects on histones and AMPs using the rate constants $k_{Hisexit}$ and $k_{AMPexit}$, respectively. To encode the behaviors that histones increases the intracellular AMP concentration and that AMPs increase intracellular histone concentrations, potentially through pore-stabilization, we defined the rate constants $k_{Hisstab}$ and $k_{AMPstab}$, arriving at the equations:

$$\frac{d[His_{in}]}{dt} = k_{Hisentry}[His_{out}] \quad k_{Hisexit}[His_{in}] + k_{Hisstab}[AMP_{in}] \quad (1)$$

$$\frac{d[AMP_{in}]}{dt} = k_{AMPentry}[AMP_{out}] \quad k_{AMPexit}[AMP_{in}] + k_{AMPstab}[His_{in}] \quad (2)$$

In our simulations, we set the initial histones and AMP concentrations inside the cell to 0. The concentration of histones and AMPs outside the cell remained constant, which describes an environment in which there is an excess of histones and AMPs. We set the permeation rates of

$k_{Hisentry}$ and $k_{AMPentry}$ to 0.004 s^{1} based on permeation measurements of the charged antibiotic tetracycline into bacterial cells[13]. The rate constants $k_{Hisexit}$ and $k_{AMPexit}$ were set to correspond to a doubling time of 30 minutes, which is a conservative estimate of the rate of histone and AMP removal from the cell that does not require the existence of an export mechanism. We simulated the synergy condition by setting $k_{Hisstab}$ and $k_{AMPstab}$ to 0.1 s^{1} and simulated the non-synergistic condition by setting these rate constants to 0 s^{1}. For the uptake dynamics figure, we set the concentrations of histones and AMP outside of the cell to 1 and computed the total intracellular concentration of these molecules as a function of time. Density plots were constructed by computing the total intracellular concentration of histones and AMPs following 60 minutes of exposure to a range of histones and AMPs concentrations outside of the cell.

2.25 Statistical Analysis

Statistical analysis was performed by running Welsh t-tests or one- or two-way ANOVA and Tukey's post-hoc tests using R 3.4.3 (Kite Eating Tree). Data and image analysis was performed using Image J (v1.51k), or custom-written MATLAB scripts from the Siryaporn lab.

2.26 References

1. Blattner, F. R. *et al.* The complete genome sequence of Escherichia coli K-12. *Science* **277**, 1453–1462 (1997).
2. Kreiswirth, B. N. *et al.* The toxic shock syndrome exotoxin structural gene is not detectably transmitted by a prophage. *Nature* **305**, 709–712 (1983).
3. Kralj, J. M., Hochbaum, D. R., Douglass, A. D. & Cohen, A. E. Electrical spiking in Escherichia coli probed with a fluorescent voltage-indicating protein. *Science* **333**, 345–348 (2011).
4. Snoussi, M. *et al.* Heterogeneous absorption of antimicrobial peptide LL37 in Escherichia coli cells enhances population survivability. *eLife* **7**, (2018).
5. Baba, T. *et al.* Construction of Escherichia coli K-12 in-frame, single-gene knockout mutants: the Keio collection. *Molecular Systems Biology* **2**, (2006).
6. Miller, J. H. *A short course in bacterial genetics: a laboratory manual and handbook for Escherichia coli and related bacteria*. (Cold Spring Harbor Laboratory Press, 1992).
7. Siryaporn, A., Kuchma, S. L., O'Toole, G. A. & Gitai, Z. Surface attachment induces *Pseudomonas aeruginosa* virulence. *Proceedings of the National Academy of Sciences* **111**, 16860–16865 (2014).
8. Siryaporn, A., Perchuk, B. S., Laub, M. T. & Goulian, M. Evolving a robust signal transduction pathway from weak cross-talk. *Molecular Systems Biology* **6**, (2010).
9. Cowles, K. N. *et al.* The putative Poc complex controls two distinct *Pseudomonas aeruginosa* polar motility mechanisms: *tonB / exbB / exbD* homologues regulate polar motility. *Molecular Microbiology* **90**, 923–938 (2013).
10. TBE buffer. *Cold Spring Harbor Protocols* **2006**, pdb.rec8458 (2006).
11. Cowles, K. N. *et al.* The putative Poc complex controls two distinct *Pseudomonas aeruginosa* polar motility mechanisms: *tonB / exbB / exbD* homologues regulate polar motility. *Molecular Microbiology* **90**, 923–938 (2013).
12. Siryaporn, A., Kuchma, S. L., O'Toole, G. A. & Gitai, Z. Surface attachment induces *Pseudomonas aeruginosa* virulence. *Proceedings of the National Academy of Sciences* **111**, 16860–16865 (2014).
13. Sigler, A., Schubert, P., Hillen, W. & Niederweis, M. Permeation of tetracyclines through membranes of liposomes and Escherichia coli. *Eur. J. Biochem.* **267**, 527–534 (2000).

Chapter 3: Histone H2A Kills Gram-negative and Gram-positive Bacteria in Low Ionic Environments, but Not Physiological Environments

The first initial report of the antimicrobial activity of histones appeared in 1942[1]. An in-depth analysis of the factors that affected *in vitro* killing of *E. coli* followed in 1958[2]. Although some of the claims made were inaccurate, such as the conclusion that only the arginine-rich fraction of calf thymus histones showed antimicrobial activity, the effects of ionic strength, osmolarity, and salt concentration on histones were characterized. Histones were documented to have reduced bactericidal activity at salt concentrations greater than 0.15 - 0.2 M NaCl, and this was proposed to be due to an effect on ionic strength affecting adsorption of the histone, rather than osmolarity.

The outer membrane of Gram-negative bacteria, including *E. coli*, contains an outer leaflet primarily composed of lipopolysaccharides (LPS). LPS molecules are composed of lipid A, a core oligosaccharide, and an O antigen[3]. Lipid A, a phosphorylated glucosamine disaccharide with multiple hydrophobic fatty acyl chains, anchors LPS to the outer membrane[3]. The highly diverse core oligosaccharide component is a short chain of sugar residues, attached directly to lipid A[4]. The core oligosaccharide may also contain non-carbohydrate components, such as amino acids and phosphate[5]. O antigen, a repetitive polymer, is attached to the core oligosaccharide. The polymer makes up the outermost portion of the LPS molecule. The O antigen varies between bacterial strains and serves as a host antibody target[6]. Additionally, there is considerable variety in the O antigen within a given species. For example, there are approximately 170 O antigen serotypes produced by *E. coli*[3]. The presence of full-length O antigen makes LPS smooth, whereas a reduced amount of O antigen, or the absence of O antigen altogether, makes LPS rough[7]. As

rough LPS is more hydrophobic, bacteria with rough LPS are more susceptible to hydrophobic antibiotics[8].

As the main component of the outer layer of the bacterium, LPS contributes heavily to the structural integrity of the membrane. LPS molecules are polyanionic, stemming from multiple phosphate groups in the lipid A and oligosaccharide regions. The presence of divalent cations, such as magnesium (Mg^{2+}) and calcium (Ca^{2+}), are integral to neutralizing the negative charges and stabilizing the bacterial outer membrane[9]. Chelation of divalent cations by EDTA is well-documented as a cell-permeabilizing technique, indicating the importance of these cations in preserving the integrity of the LPS and stabilizing the bacterial outer membrane[10]. By binding the anionic phosphate groups in the LPS, divalent cations electrostatically link LPS molecules together and contribute to bacterial resistance against hydrophobic antimicrobial peptides[11,12]. Several antimicrobial agents, such as cationic antibiotics and EDTA, are known to function by outer membrane permeabilization due to the disruption of electrostatic LPS linkages[13].

Similar to LPS in the membranes of Gram-negative bacteria, Gram-positive bacteria, such as *Staphylococcus aureus*, have teichoic acids within their cell walls. These anionic glycopolymers to provide rigidity by binding cations such as magnesium and sodium[14–16]. Teichoic acids include both wall teichoic acids (WTAs), covalently linked to peptidoglycan, and lipoteichoic acids (LTAs), anchored in the bacterial membrane by a glycolipid. Teichoic acids are thought to play a key role in antibiotic resistance in Gram-positive microorganisms[17].

A schematic image of the major differences between Gram-positive and Gram-negative bacterial membranes, and how they facilitate binding to divalent cations, is illustrated in Figure 3.1.

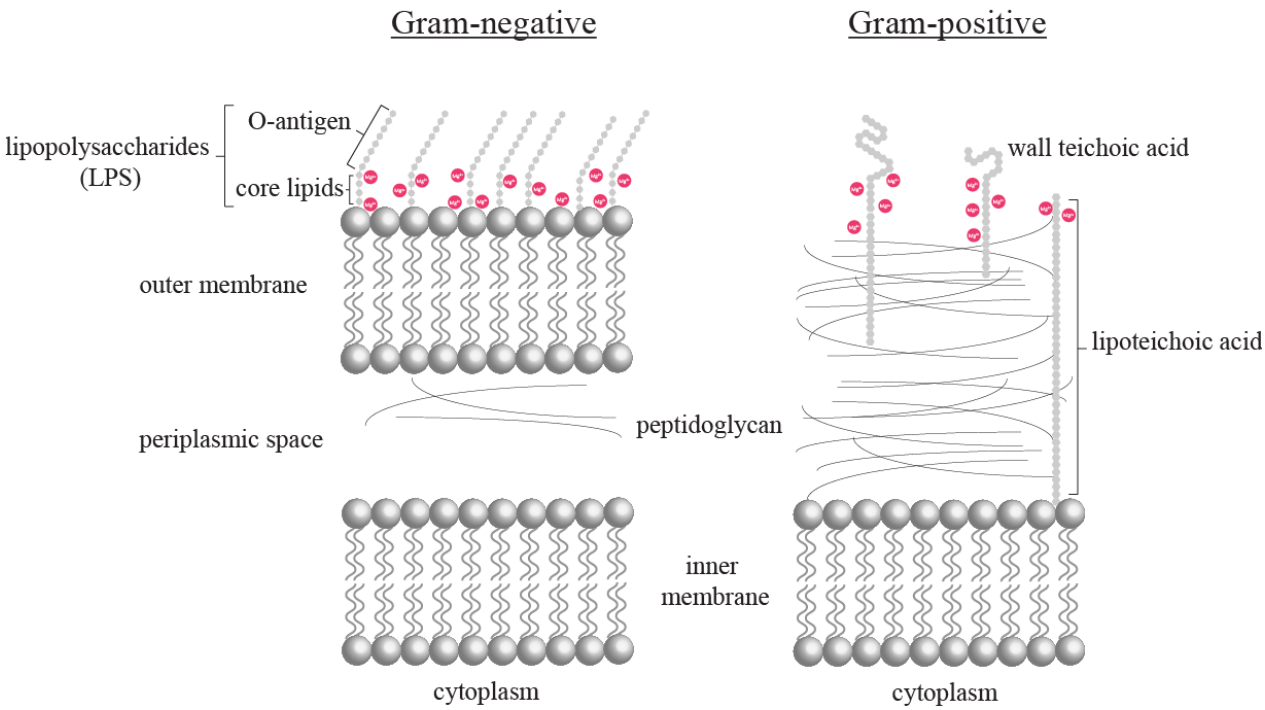

Figure 3.1. Differences in the membranes of Gram-negative and Gram-positive bacteria. Gram-negative bacteria have a thin peptidoglycan layer between an inner cytoplasmic cell membrane and an outer membrane that binds lipopolysaccharides (LPS). Gram-positive bacteria are characterized by a cytoplasmic cell membrane surrounded by a thick peptidoglycan layer that contains lipoteichoic acid and wall teichoic acid. The LPS and teichoic acid are both negatively charged, and bind to divalent cations, like magnesium (represented as pink circles). Membrane proteins have been omitted for simplification purposes.

3.1 Histone H2A Kills Gram-negative and Gram-positive Bacteria in Low Magnesium Environments

Since cations, like calcium and magnesium, stabilize the bacterial membranes of both Gram-negative and Gram-positive bacteria, and previous experiments reported the antimicrobial activity of histones is only observed in low ionic solutions and buffers that are not physiologically relevant[18–20] (see Chapter 1.8), the antimicrobial activity of histones was initially investigated in a low ionic environment. Low ionic environments, as defined by a reduction in the concentration of divalent cations, disrupt electrostatic LPS interactions, compromising the integrity of the membrane and increasing membrane permeability. I hypothesized that in low ionic environments, where a reduction in divalent cations disrupts electrostatic interactions, positively charged histones may further disrupt the outer membrane of bacteria, resulting in increased antimicrobial activity.

The concentration of magnesium in the plasma and extracellular fluid is between 1.2 – 1.4 mM, with approximately one-third of that bound by proteins or moieties[21]. Based on the levels of free magnesium in the plasma and extracellular fluid, initial bacterial killing experiments were performed using two concentrations of magnesium: 1 mM $MgSO_4$ (physiological concentration) and 1 μM $MgSO_4$ (low magnesium, cation-chelating conditions). Antimicrobial activity was assayed using 10 μg/mL H2A, based on the report that 15 μg/mL of H3 are detected in blood plasma of baboons after *E. coli* challenge[22]. Experiments were predominantly performed using only Histone H2A since antibodies against H2A and H2B eliminated NET-mediated killing of bacteria[18].

To test whether magnesium concentration had an effect on histone killing, traditional plate assays were performed. Overnight cultures of stationary phase *E. coli* or *S. aureus* were diluted 1:1000 in minimal media (MinA) containing 1 μM or 1 mM $MgSO_4$, and cultured with or without

10 μg/mL H2A for 1 hour. After treatment, bacterial suspensions were diluted 1:1000 into fresh MinA media with either 1 μM or 1 mM $MgSO_4$ and 25 μL of diluted bacterial suspension was plated on LB-Miller agar plates without H2A. Plates were grown for 18 hours before CFU counts were obtained. The addition of H2A to bacteria in the low ionic environment decreased the CFU count for both Gram-negative *E. coli* and Gram-positive *S. aureus*. However, the addition of H2A to bacteria in the physiological environment had no effect on *E. coli* or *S. aureus.* The low ionic environment without the addition of H2A did not reduce CFU counts for either strain (Figure 3.2).

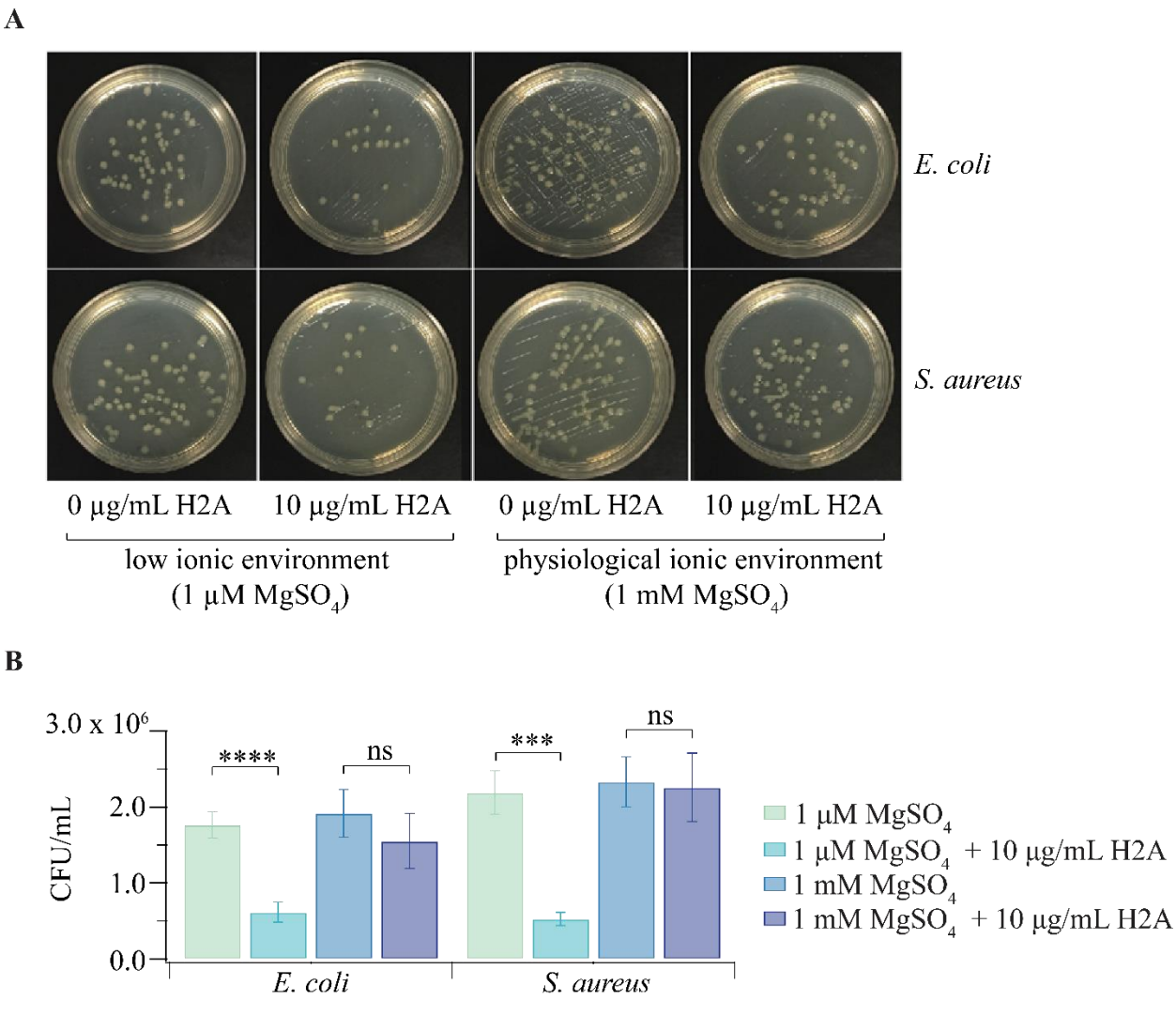

Figure 3.2. Histones decrease the number of colony forming units (CFUs) of *E. coli* and *S. aureus* in low ionic environments. (A) H2A decreases the number of colony forming units (CFUs) of *E. coli* and *S. aureus* growing in low concentrations of magnesium, but not in physiological conditions. Overnight cultures of stationary phase *E. coli* or *S. aureus* were diluted 1:1000 in MinA with 1 µM or 1 mM $MgSO_4$ and cultured with or without 10 µg/mL H2A for 1 hour. After treatment, bacterial suspensions were diluted 1:1000 into fresh MinA media with either 1 µM or 1 mM $MgSO_4$ and 25 µL of diluted bacterial suspension was plated on LB-Miller agar plates without histones. Plates were grown for 18 hours before imaging. Representative plates are shown for each condition. (B) Data shown as mean ± SEM and are representative of at least three independent experiments (n=3). **** $p \leq 0.0001$, *** $p \leq 0.001$, ns > 0.05.

Complementary growth curves were constructed using a plate reader. Overnight cultures of stationary phase *E. coli* or *S. aureus* were diluted 1:1000 in MinA containing either 1 μM or 1 mM $MgSO_4$ and cultured with or without 10 μg/mL H2A. Optical density (OD_{600}) was measured across a 24-hour growth period to construct growth curves. In liquid cultures, low magnesium decreased bacterial growth for both *E. coli* (Figure 3.3A) and *S. aureus* (Figure 3.4A), consistent with previous reports[23,24]. In low magnesium conditions, the addition of 10 μg/mL H2A extended the lag time and slowed the growth rate of *E. coli*. Furthermore, *E. coli* treated with H2A reached a lower OD_{600} after a 24-hour growth period (Figure 3.3A). The addition of 10 μg/mL H2A to *S. aureus* growing in low magnesium did not allow any bacterial growth over a 24-hour time period (Figure 3.4A). This complete inhibition of bacterial growth may be due to *S. aureus*-specific physiology. It is possible that Gram-positive bacteria may be more sensitive to histones in low magnesium environments. Together, the plate killing assay and the growth curves showed that the addition of H2A inhibited bacterial growth at low magnesium in liquid culture for both *E. coli* (Figure 3.3A) and *S. aureus* (Figure 3.4A).

The growth profiles of *E. coli* and *S. aureus* grown in physiological magnesium conditions, with and without 10 μg/mL H2A, showed similar lag times, comparable exponential growth rates, and equivalent OD_{600} after a 24-hour growth period (Figure 3.3B, 3.4B). Thus, the addition of H2A had no effect on bacterial growth at physiological magnesium for *E. coli* (Figure 3.3B) or *S. aureus* (Figure 3.4B). Together, these growth profiles further support the plate killing assay, indicating that H2A kills Gram-negative and Gram-positive bacteria in a low ionic condition, but not in a physiological condition.

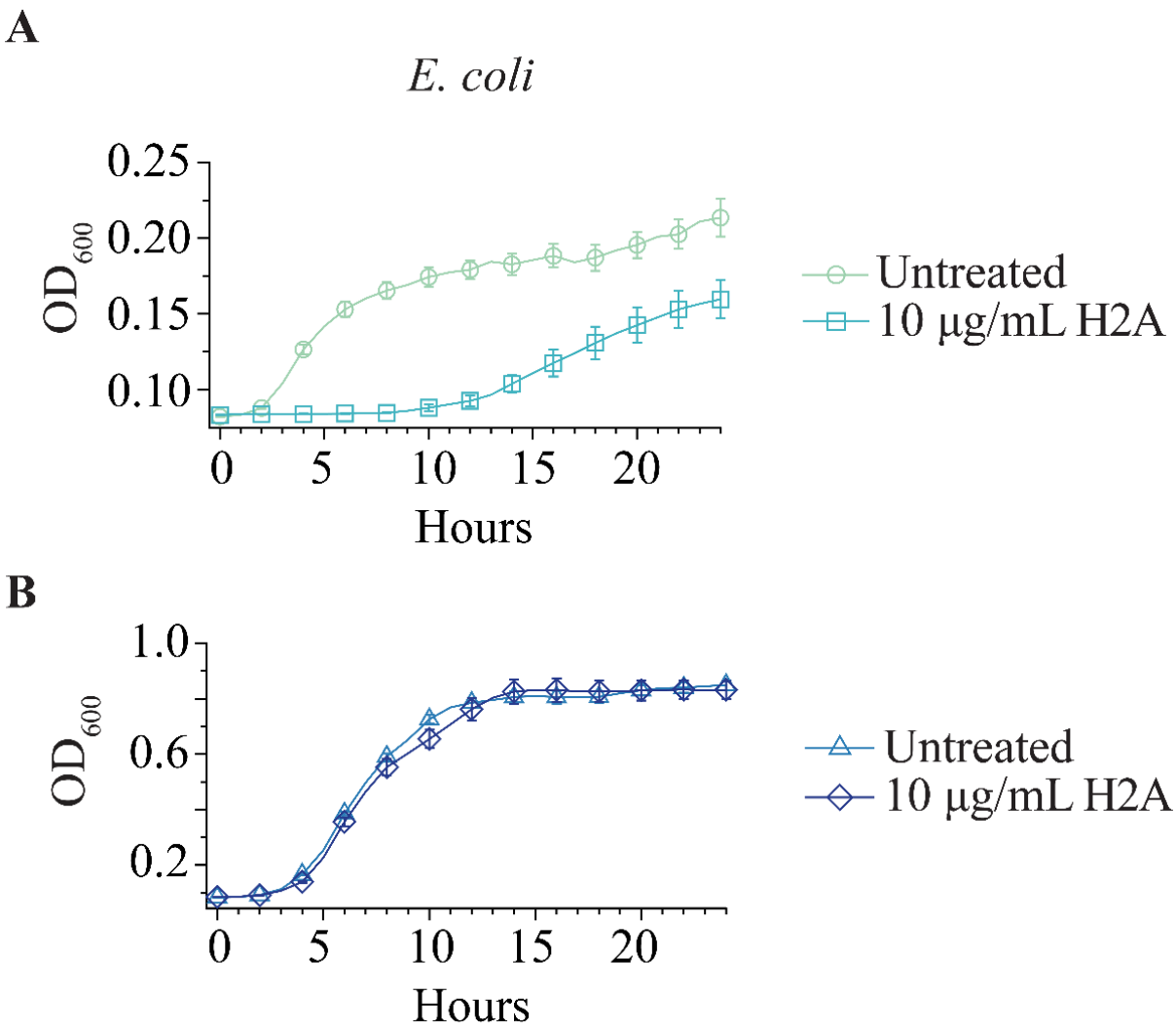

Figure 3.3. Histones kill stationary phase Gram-negative *E. coli* in a low ionic strength condition but not in a physiological condition. Growth profiles of stationary phase *E. coli* treated with 10 µg/mL H2A in MinA media containing (A) low (1 µM) magnesium and (B) physiological (1 mM) magnesium. The addition of H2A had no effect on *E. coli* growth in the physiological concentration of magnesium. In low ionic conditions, the addition of H2A inhibited bacterial growth. Points in (A) and (B) are the average of at least ten independent experiments. Error bars indicate standard error of the mean (SEM).

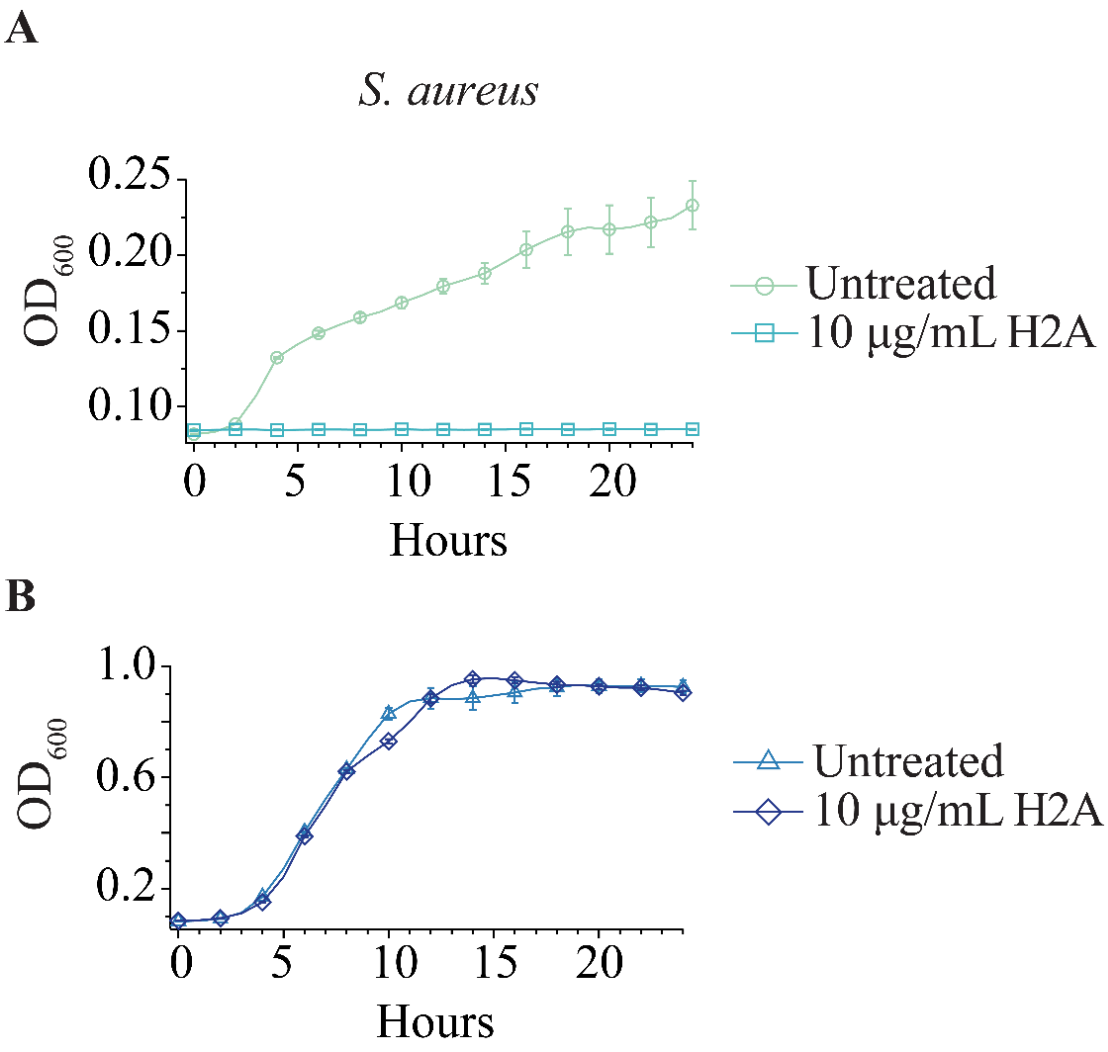

Figure 3.4. Histones kill stationary phase Gram-positive *S. aureus* in a low ionic strength condition but not in a physiological condition. Growth profiles of stationary phase *S. aureus* treated with 10 µg/mL H2A in MinA media containing (A) low (1 µM) magnesium and (B) physiological (1 mM) magnesium. The addition of H2A had no effect on *S. aureus* growth in the physiological concentration of magnesium. In low ionic conditions, the addition of H2A inhibited bacterial growth. Points in (A) and (B) are the average of at least ten independent experiments. Error bars indicate standard error of the mean (SEM).

As seen in the growth profiles of *E. coli* and *S. aureus* in physiological ionic conditions, 10 μg/mL H2A had no effect on growth of either bacterial strain. This was unsurprising, as previous studies reported that histones are far less effective at killing bacteria in physiologically relevant conditions[25,26]. Additionally, prior reports concluded that bacterial killing requires high, unphysiological concentrations of histones[19,25,27]. However, as discussed in Chapter 1, peptide concentrations in excess of the MIC may render bacteria susceptible to secondary mechanisms of histones through membrane permeabilization[28,29]. To address questions regarding the utility of histones as antimicrobial agents and the mechanism of histone-mediated killing of bacteria under physiological conditions, a concentration of 10 μg/mL H2A was used for all subsequent experiments, regardless of whether bacteria were cultured in low magnesium conditions or physiological magnesium conditions.

3.2 Histone H2A Enhances Membrane Permeabilization in Low Ionic Environments

Since H2A is cationic and amphipathic, and many known antimicrobial agents function by inducing perturbations in the bacterial membrane, I investigated whether H2A inhibits growth through disruption of the microbial membrane. Cells were treated with propidium iodide (PI), a bacterial fluorescence stain commonly used in microbial viability assays. This ethidium bromide analog fluoresces upon binding nucleic acids and does not permeate the outer membranes of viable bacteria. When membrane integrity is compromised, PI can pass through the bacterial membrane, bind to DNA, and emit mCherry fluorescence.

To visualize whether H2A induces membrane lysis in *E. coli* in low ionic conditions, stationary phase *E. coli* was diluted 1:1000 into fresh MinA media, with or without 10 μg/mL H2A, and incubated with 30 μM propidium iodide for one hour. Bacteria were plated on 1% agarose-MinA pads and mCherry fluorescence was imaged and quantified. The addition of 10 μg/mL H2A induced PI fluorescence in *E. coli* cultured in low magnesium (Figure 3.5), a condition that inhibited growth on agar plates and in liquid culture (Figure 3.2, 3.3), suggesting that H2A inhibits growth in low magnesium by enhancing membrane permeabilization. No increase in PI fluorescence was observed for *E. coli* in low ionic conditions without the addition of H2A, indicating low magnesium conditions alone are not sufficient to induce membrane permeabilization. No PI fluorescence occurred with the addition of 10 μg/mL H2A at physiological magnesium (Figure 3.5A, 3.5B), indicating that this concentration of histones does not permeabilize the *E. coli* membrane under physiological ionic conditions.

Thus, histone-mediated bacterial growth inhibition is accompanied by increased membrane permeabilization in low ionic environments, supporting a mechanism by which the histones disrupt the microbial membrane to kill bacteria in low ionic conditions. Additionally, the permeabilization

of the bacterial membrane may function to facilitate histone entry into the bacterial cell, where histones may have intracellular targets.

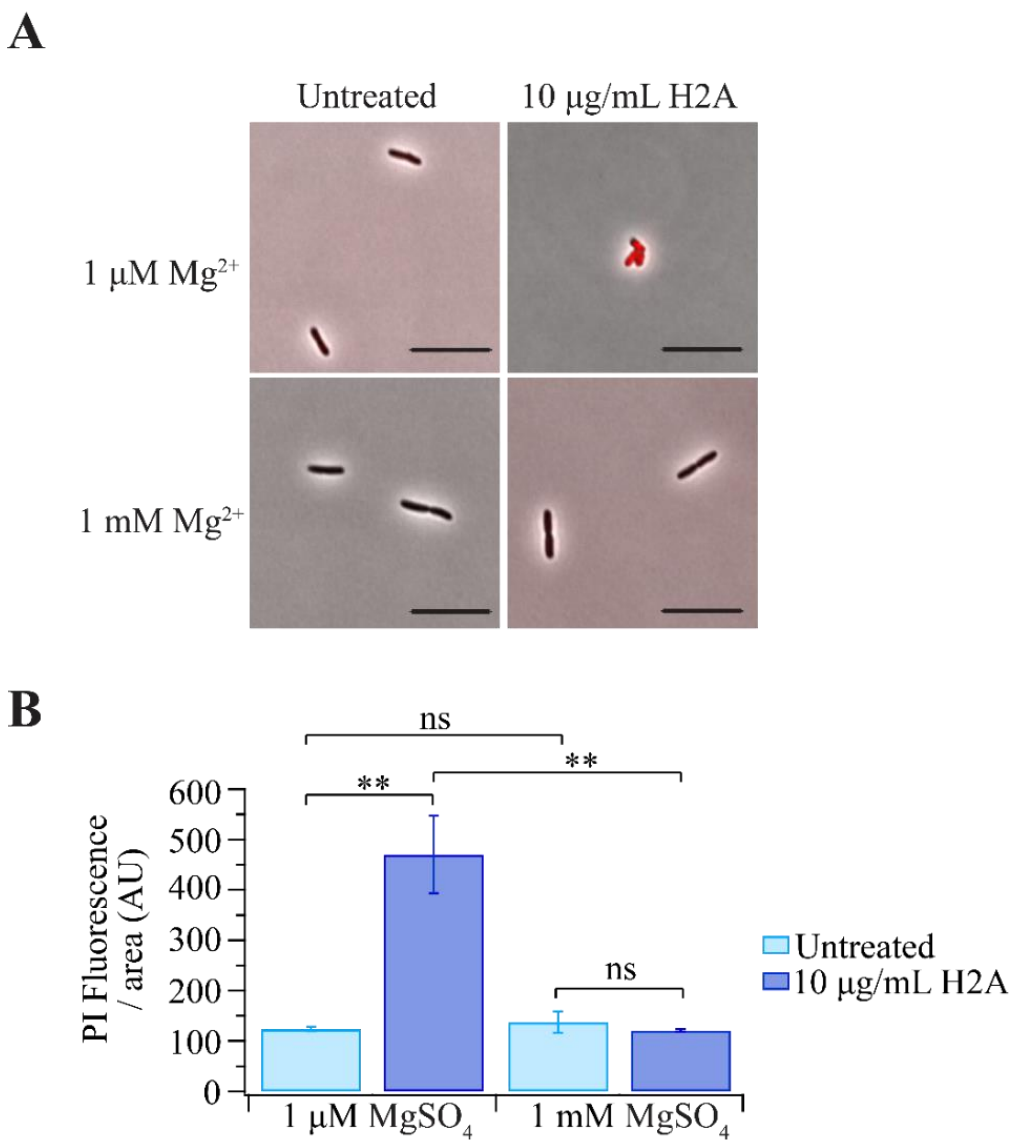

Figure 3.5. Histones increase membrane permeabilization in stationary phase *E. coli* in a low ionic strength condition, but not in a physiological condition. Propidium iodide (PI) fluorescence of H2A-treated *E. coli* increased in bacteria cultured in low concentrations of magnesium, but not physiological concentrations. (A) Representative images are shown for each condition. (B) Quantification of the average PI fluorescence/area (AU) for each condition indicates low magnesium conditions alone are not sufficient to induce membrane permeabilization. 10 µg/mL H2A significantly increased PI fluorescence in conditions of low magnesium, whereas the addition of 10 µg/mL H2A to *E. coli* in physiological concentrations of magnesium had no effect. Data shown as mean ± SEM and are representative of three independent experiments (n=3). ** indicates a p-value ≤ 0.01, and ns indicates a p-value > 0.05. Scale bars represent 10 µm.

3.3 The PhoPQ System Improves Survival of *E. coli* Challenged with Histone H2A

To explain histone-mediated killing in low ionic conditions that promote bacterial membrane instability, the potential involvement of the PhoPQ system was considered. The PhoPQ system is a two-component system, which senses the presence of extracellular magnesium and responds to low levels by upregulating magnesium transport and inducing PmrAB-dependent lipid A modifications to promote stability[30]. In this system, the membrane-bound histidine kinase PhoQ senses low magnesium concentrations, likely by direct binding of divalent cations at an acidic cluster of residues (EDDDDAE). PhoQ undergoes autophosphorylation, transferring a phosphoryl group from ATP to a histidine residue[31]. The response regulator PhoP catalyzes the transfer of the phosphoryl group to an aspartate residue within the regulatory response domain, triggering a conformational change and producing downstream cellular responses. In addition, the PhoPQ system is thought to be involved in the direct binding of anti-microbial peptides[32]. It is thought that the competition between divalent ions and host antimicrobial peptides for PhoQ binding serves as a signal for the bacteria, allowing it to determine its subcellular environment and upregulate transcription of virulence factors accordingly[33]. Furthermore, the addition of sub-inhibitory concentrations of DNA has been shown to create a cation-limited environment that induced PhoPQ- and PmrAB-regulated AMP resistance in *P. aeruginosa*[34].

To investigate the potential role of this system in histone-mediated killing, 10 μg/mL H2A was added to a PhoQ-null strain of *E. coli* at both low and physiological levels of magnesium. Growth curves were constructed over a 24-hour growth period for the PhoQ-null strain (*D(phoP) D(phoQ) PmgrB-yfp PtetA-cfp (kanR, camR)*) and an equivalent reporter strain (*PmgrB-yfp PtetA-cfp (kanR, camR)*), which approximates wild-type (WT) *E. coli*. Overnight cultures of

stationary phase WT or PhoQ-null *E. coli* were diluted 1:1000 in MinA with 1 μM or 1 mM $MgSO_4$ and cultured with or without 10 μg/mL H2A.

As expected, since the PhoQ-null strain cannot appropriately respond to conditions of low ionic strength, the PhoQ-null strain shows an extended lag phase and slower exponential growth in conditions of low ionic strength (Figure 3.6A). However, after 24 hours, the PhoQ mutant strain reached a comparable OD_{600} to wild-type *E. coli*. The addition of 10 μg/mL H2A to the PhoQ-null strain in low magnesium eliminated bacterial growth entirely over a 24-hour growth period. As previously observed, the addition of 10 μg/mL H2A to wild-type *E. coli* culture in a low ionic environment slowed the growth rate, caused an extended lag time, and led to a lower OD_{600} after a 24-hour growth period when compared to untreated, wild-type *E. coli* (Figure 3.6A).

In physiological ionic conditions, wild-type *E. coli* and PhoQ-null *E. coli* showed similar lag times and exponential growth rates, and reached comparable OD_{600} measurements after 24 hours of growth (Figure 3.6B). As expected, the addition of 10 μg/mL H2A had no effect on wild-type *E. coli* growing in physiological concentrations of magnesium. However, the addition of 10 μg/mL H2A extended the lag time of the PhoQ-null strain, indicating that the absence of a functional PhoPQ system induces sensitivity to histones at physiological levels of magnesium (Figure 3.6B). The PhoQ-null *E. coli* strain showed increased sensitivity to histones in both ionic conditions, indicating that the absence of a functional PhoPQ system increases sensitivity to histones.

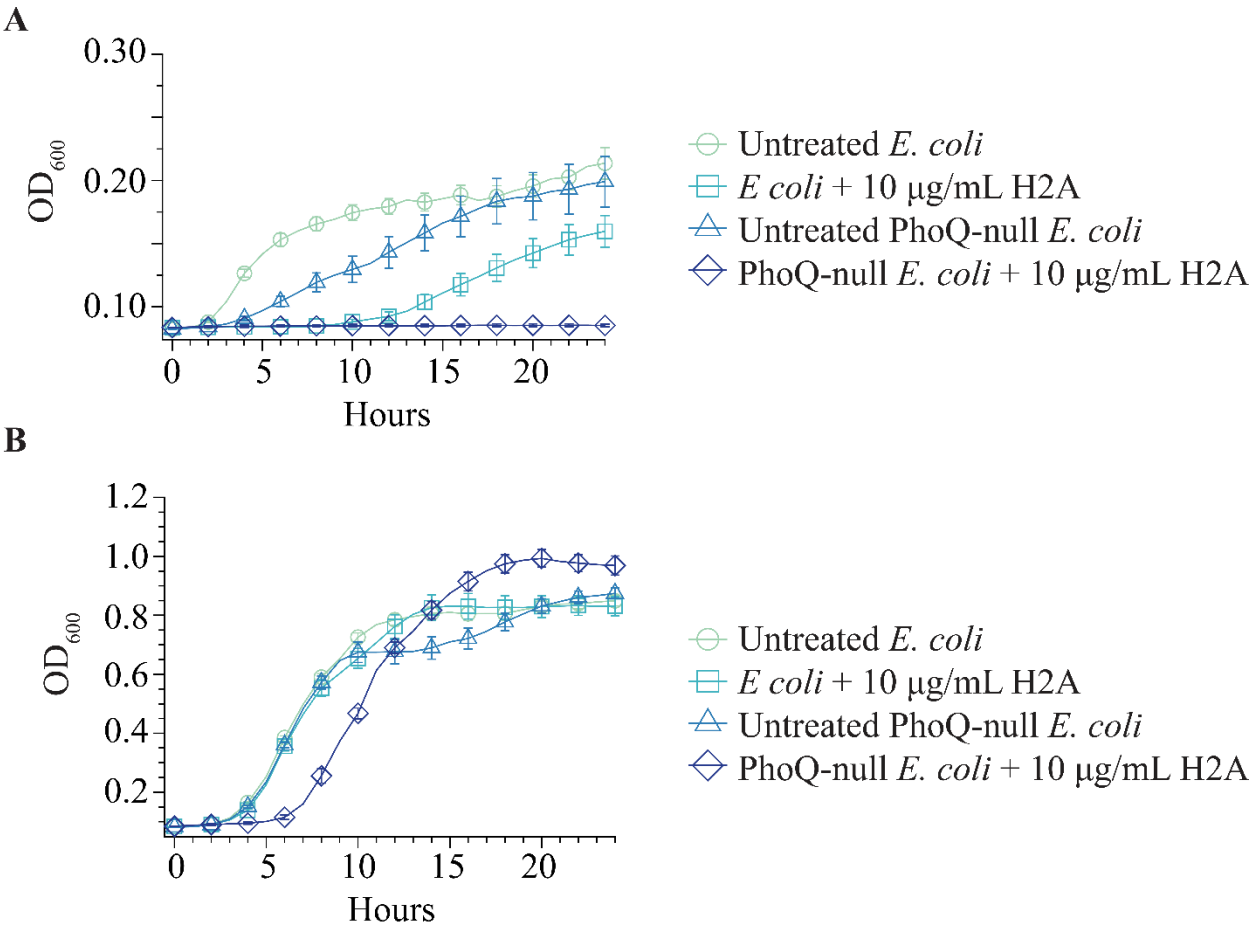

Figure 3.6. The PhoPQ system increases *E. coli* survival when treated with histones. Growth profiles of wild-type *E. coli* and an equivalent PhoQ-null *E. coli* strain in media containing low (1 µM) magnesium (A) and physiological (1 mM) magnesium (B). The PhoQ-null *E. coli* strain showed increased sensitivity to histones in both ionic conditions, indicating that the absence of a functional PhoPQ system increases sensitivity to histones. Points in (A) and (B) are the average of four independent experiments. Error bars indicate standard error of the mean (SEM).

The PhoPQ reporter strain used to approximate WT *E. coli* in growth profiles (Figure 3.6) is an engineered strain of wild-type *E. coli* with a PhoP-regulated *mgrB* reporter driving YFP expression and a constitutive promoter expressing CFP, allowing for controlled reporting of expression and intensity levels. This strain was used to further investigate expression of the PhoPQ system in response to histone treatment in low and physiological magnesium conditions. Stationary phase *E. coli* were diluted 1:1000 into fresh MinA with 1 μM or 1 mM $MgSO_4$ and cultured with or without 10 μg/mL H2A. Bacteria were incubated for three hours. Bacteria were plated on 1% agarose-MinA pads and *phoQ-yfp* and *tetA-cfp* were imaged and quantified. To compare conditions, the ratio of *phoQ-yfp* to *tetA-cfp* was calculated.

The *phoQ-yfp* to *tetA-cfp* ratio increased for *E. coli* cultured in a low ionic environment, compared to *E. coli* cultured in physiological ionic environments, confirming that low magnesium environments increase expression of the PhoPQ system in this strain (Figure 3.7). The addition of 10 μg/mL histones to *E. coli* cultured in physiological ionic environments had no effect on the *phoQ-yfp* to *tetA-cfp* ratio compared to untreated *E.coli* in the same ionic environment. However, the addition of 10 μg/mL histones to *E. coli* cultured in low ionic environments decreased the ratio of *phoQ-yfp* to *tetA-cfp* compared to untreated *E. coli*, indicating H2A suppresses transcription of the phoQ gene in low ionic environments (Figure 3.7).

It is plausible that the downregulation of the PhoPQ two-component system when *E. coli* are exposed to H2A in conditions of low magnesium prevents the bacteria from upregulating downstream genes associated with increased membrane stability. By circumventing this pathway, the presence of histones may keep the bacteria in a state of increased membrane instability. In theory, this membrane instability may lead to increased concentrations of histones entering the bacterial cell, where they can interact with nucleic acids or alter metabolic pathways further.

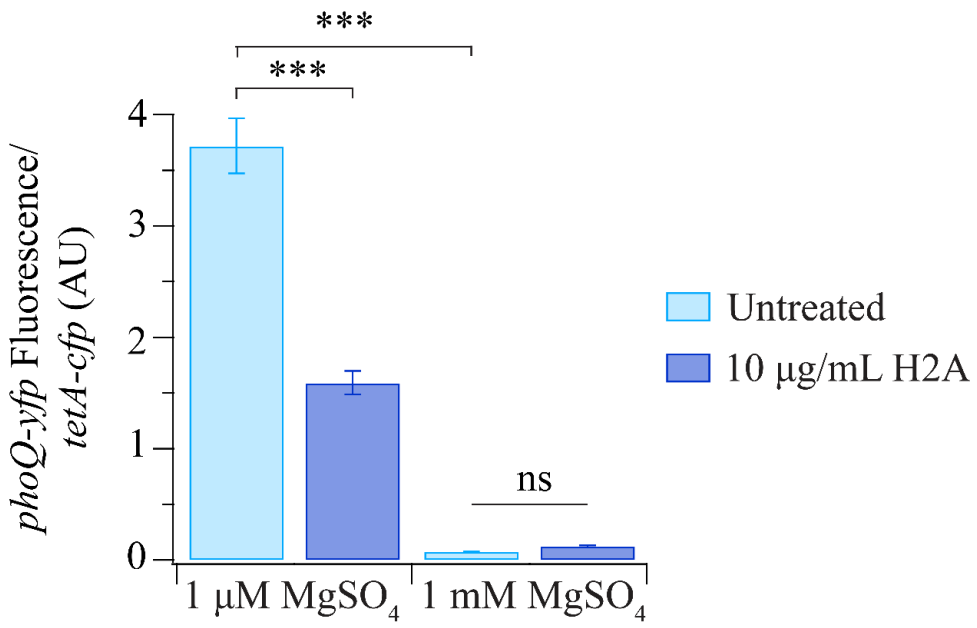

Figure 3.7. H2A suppresses *phoQ* expression in *E. coli* growing in low ionic strength conditions. The ratios of *phoQ-yfp* to the constitutively-expressed *tetA-cfp* gene in an engineered strain of wild-type *E. coli* with a PhoP-regulated *mgrB* reporter driving YFP expression and a constitutive promoter expressing CFP. Stationary phase *E. coli* were diluted 1:1000 into fresh MinA with 1 µM or 1 mM $MgSO_4$ and cultured with or without 10 µg/mL H2A. Bacteria were incubated for three hours before imaging *phoQ-yfp* and *tetA-cfp*. The addition of H2A to *E. coli* cultured in a low magnesium environment decreased the *phoQ-yfp* to *tetA-cfp* ratio compared to untreated *E. coli* cultured in a low magnesium environment, indicating H2A suppresses transcription of the *phoQ* gene. Data are shown as the mean ± SEM and are representative of three independent experiments (n=3). *** $p \leq 0.001$, ns > 0.05.

3.4 Conclusion

Magnesium cations stabilize the bacterial membranes of Gram-negative and Gram-positive bacteria. As such, decreased concentrations of magnesium cations disrupt electrostatic LPS interactions and compromise the integrity of the membrane. In conditions of low ionic strength, positively charged histones further disrupted the outer membrane of bacteria, resulting in increased antimicrobial activity in the Gram-positive *S. aureus* and the Gram-negative *E. coli*. In contrast, the addition of H2A had no effect on *E. coli* or *S. aureus* growing in physiological concentrations of magnesium.

Since many known AMPs function by inducing membrane perturbations, propidium iodide (PI) staining was used to determine if the mechanism of histone-mediated bacterial killing in low ionic environments relied on histones compromising the integrity of the bacterial membrane. PI fluorescence of H2A-treated *E. coli* increased in bacteria cultured in low concentrations of magnesium, but not physiological concentrations, suggesting that H2A inhibits growth in low magnesium by increasing membrane permeabilization. Low magnesium conditions alone were not sufficient to induce membrane permeabilization. Additionally, little to no PI fluorescence was seen in physiological magnesium conditions, with or without the addition of H2A. This supports a mechanism by which the histones increasingly disrupt the microbial membrane to kill bacteria in low ionic environments. Additionally, this permeabilization of the bacterial membrane may function to facilitate histone entry into the bacterial cell, where histones may have intracellular targets.

Because the addition of H2A compromised membrane integrity at low ionic conditions, the potential role of the PhoPQ system was investigated. The potential role of PhoPQ system, a two-component system that responds to low levels of extracellular magnesium, was investigated using

a PhoQ-null strain of *E. coli*. In conditions that promote membrane instability, the addition of H2A completely prevented growth of a PhoQ-mutant strain of *E. coli* over a 24-hour period. Additionally, the absence of a functional PhoPQ system induced sensitivity to H2A at physiological concentrations of magnesium. Furthermore, the addition of H2A to cultures growing in low ionic strength decreased expression of *phoQ*, indicating H2A suppresses transcription of the phoQ gene in low ionic environments.

3.5 References

1. Miller, B. F., Abrams, R., Dorfman, A. & Klein, M. ANTIBACTERIAL PROPERTIES OF PROTAMINE AND HISTONE. *Science* **96**, 428–430 (1942).
2. Hirsch, J. G. BACTERICIDAL ACTION OF HISTONE. *J. Exp. Med.* **108**, 925–944 (1958).
3. Raetz, C. R. H. & Whitfield, C. Lipopolysaccharide Endotoxins. *Annu. Rev. Biochem.* **71**, 635–700 (2002).
4. Heinrichs, D. E., Yethon, J. A. & Whitfield, C. Molecular basis for structural diversity in the core regions of the lipopolysaccharides of *Escherichia coli* and *Salmonella enterica*. *Mol. Microbiol.* **30**, 221–232 (1998).
5. Silipo, A. & Molinaro, A. The Diversity of the Core Oligosaccharide in Lipopolysaccharides. in *Endotoxins: Structure, Function and Recognition* (eds. Wang, X. & Quinn, P. J.) vol. 53 69–99 (Springer Netherlands, 2010).
6. Wang, L., Wang, Q. & Reeves, P. R. The Variation of O Antigens in Gram-Negative Bacteria. in *Endotoxins: Structure, Function and Recognition* (eds. Wang, X. & Quinn, P. J.) vol. 53 123–152 (Springer Netherlands, 2010).
7. Rittig, M. G. *et al.* Smooth and rough lipopolysaccharide phenotypes of *Brucella* induce different intracellular trafficking and cytokine/chemokine release in human monocytes. *J. Leukoc. Biol.* **74**, 1045–1055 (2003).
8. Tsujimoto, H., Gotoh, N. & Nishino, T. Diffusion of macrolide antibiotics through the outer membrane of Moraxella catarrhalis. *J. Infect. Chemother.* **5**, 196–200 (1999).
9. Clifton, L. A. *et al.* Effect of Divalent Cation Removal on the Structure of Gram-Negative Bacterial Outer Membrane Models. *Langmuir* **31**, 404–412 (2015).
10. Leive, L. Release of lipopolysaccharide by EDTA treatment of E., coli. *Biochem. Biophys. Res. Commun.* **21**, 290–296 (1965).
11. Hansen, L. T., Austin, J. W. & Gill, T. A. Antibacterial effect of protamine in combination with EDTA and refrigeration. *Int. J. Food Microbiol.* **66**, 149–161 (2001).
12. Brock, T. D. THE EFFECT OF SALMINE ON BACTERIA. *Can. J. Microbiol.* **4**, 65–71 (1958).
13. Vaara, M. Agents that increase the permeability of the outer membrane. *Microbiol. Rev.* **56**, 395–411 (1992).
14. Neuhaus, F. C. & Baddiley, J. A Continuum of Anionic Charge: Structures and Functions of D-Alanyl-Teichoic Acids in Gram-Positive Bacteria. *Microbiol. Mol. Biol. Rev.* **67**, 686–723 (2003).
15. Archibald, A. R., Armstrong, J. J., Baddiley, J. & Hay, J. B. Teichoic Acids and the Structure of Bacterial Walls. *Nature* **191**, 570–572 (1961).
16. Heptinstall, S., Archibald, A. R. & Baddiley, J. Teichoic Acids and Membrane Function in Bacteria. *Nature* **225**, 519–521 (1970).
17. Brown, S., Santa Maria, J. P. & Walker, S. Wall Teichoic Acids of Gram-Positive Bacteria. *Annu. Rev. Microbiol.* **67**, 313–336 (2013).
18. Brinkmann, V. Neutrophil Extracellular Traps Kill Bacteria. *Science* **303**, 1532–1535 (2004).
19. Tagai, C., Morita, S., Shiraishi, T., Miyaji, K. & Iwamuro, S. Antimicrobial properties of arginine- and lysine-rich histones and involvement of bacterial outer membrane protease T in their differential mode of actions. *Peptides* **32**, 2003–2009 (2011).

20. Morita, S., Tagai, C., Shiraishi, T., Miyaji, K. & Iwamuro, S. Differential mode of antimicrobial actions of arginine-rich and lysine-rich histones against Gram-positive Staphylococcus aureus. *Peptides* **48**, 75–82 (2013).
21. Romani, A. M. P. Cellular magnesium homeostasis. *Arch. Biochem. Biophys.* **512**, 1–23 (2011).
22. Xu, J. *et al.* Extracellular histones are major mediators of death in sepsis. *Nat. Med.* **15**, 1318–1321 (2009).
23. Lusk, J. E., Williams, R. J. & Kennedy, E. P. Magnesium and the growth of Escherichia coli. *J. Biol. Chem.* **243**, 2618–2624 (1968).
24. Bhat, K. G., Joseph, K. M. & Shivananda, P. G. Effect of magnesium on the physiology of Staphylococcus aureus. *Indian J. Exp. Biol.* **32**, 274–276 (1994).
25. Anand, P. *et al.* A novel role for lipid droplets in the organismal antibacterial response. *eLife* **1**, (2012).
26. Hancock, R. E. W. & Sahl, H.-G. Antimicrobial and host-defense peptides as new anti-infective therapeutic strategies. *Nat. Biotechnol.* **24**, 1551–1557 (2006).
27. Morita, S., Tagai, C., Shiraishi, T., Miyaji, K. & Iwamuro, S. Differential mode of antimicrobial actions of arginine-rich and lysine-rich histones against Gram-positive Staphylococcus aureus. *Peptides* **48**, 75–82 (2013).
28. Patrzykat, A., Friedrich, C. L., Zhang, L., Mendoza, V. & Hancock, R. E. W. Sublethal concentrations of pleurocidin-derived antimicrobial peptides inhibit macromolecular synthesis in Escherichia coli. *Antimicrob. Agents Chemother.* **46**, 605–614 (2002).
29. Podda, E. *et al.* Dual mode of action of Bac7, a proline-rich antibacterial peptide. *Biochim. Biophys. Acta* **1760**, 1732–1740 (2006).
30. Herrera, C. M., Hankins, J. V. & Trent, M. S. Activation of PmrA inhibits LpxT-dependent phosphorylation of lipid A promoting resistance to antimicrobial peptides: Phosphorylation of lipid A inhibits pEtN addition. *Mol. Microbiol.* **76**, 1444–1460 (2010).
31. Cheung, J., Bingman, C. A., Reyngold, M., Hendrickson, W. A. & Waldburger, C. D. Crystal Structure of a Functional Dimer of the PhoQ Sensor Domain. *J. Biol. Chem.* **283**, 13762–13770 (2008).
32. Bader, M. W. *et al.* Recognition of antimicrobial peptides by a bacterial sensor kinase. *Cell* **122**, 461–472 (2005).
33. Zwir, I. *et al.* Dissecting the PhoP regulatory network of Escherichia coli and Salmonella enterica. *Proc. Natl. Acad. Sci.* **102**, 2862–2867 (2005).
34. Mulcahy, H., Charron-Mazenod, L. & Lewenza, S. Extracellular DNA Chelates Cations and Induces Antibiotic Resistance in Pseudomonas aeruginosa Biofilms. *PLoS Pathog.* **4**, e1000213 (2008).

Chapter 4: Histone H2A Synergizes with Membrane-Permeabilizing Agents to Kill Bacteria at Physiological Ionic Concentrations

Growth in low magnesium conditions or treatment with histone H2A alone in physiological conditions were insufficient to permeabilize the bacterial membrane; however, the combined effects of low ionic conditions and histone treatment increased histone-mediated killing of bacteria by facilitating increased membrane disruption. In contrast, the addition of 10 μg/mL H2A to bacteria in physiological ionic conditions had minimal effects on bacterial growth profiles or membrane permeability. This correlates well with previous studies that report histones are ineffective at killing bacteria in physiologically relevant conditions[1,2] and prior studies reporting histone-mediated killing requires high, unphysiological concentrations of histones. These concentrations are well above the MIC[1,3,4], which may render bacteria susceptible to secondary mechanisms of histones through membrane permeabilization[5,6]. The reduction of histone-mediated killing of bacteria in physiologically relevant conditions *in vitro* has raised questions about the potential therapeutic usage of histones as antimicrobial agents.

However, given reports of the antimicrobial activity of histones in innate immune responses, including neutrophil extracellular traps (NETs) and lipid droplets (LDs) (Chapter 1.3 and 1.4), this weak antimicrobial activity of histones *in vitro* may be attributed to the fact that histone activity has not been considered in the context of other immune mechanisms. In particular, NETs and LDs both contain co-localized histones and antimicrobial peptides (AMPs), suggesting histones may function as part of a larger antimicrobial mechanism to kill bacteria *in vivo*.

In conditions of low ionic strength, positively charged histones disrupted the already destabilized bacterial membrane, resulting in increased antimicrobial activity in Gram-negative

and Gram-positive bacterial species. In principle, histones could synergize with membrane-permeabilizing AMPs in physiological conditions to increase histone-mediated killing. In order to measure potential synergies between AMPs and histones, growth profiles of bacteria were constructed in physiological ionic conditions. Identical concentrations of histones were used (10 μg/mL H2A), along with AMP concentrations below the MIC.

Synergy between antibacterial peptides released from activated neutrophils has been reported previously. Synergies are common between AMPs, two and three-AMP combinations showing strong levels of synergy[7]. For example, defensins synergize with cathelicidins, killing *E. coli* and *S. aureus*, and increasing *E. coli* membrane permeabilization. Additionally, histone H1 antimicrobial peptide fragments synergize with lysozyme, lysozyme-containing extracts from *O. kisutch*, and pleurocidin against *Vibrio anguillarum* and *Aeromonas salmonicida*[8].

In cases where multiple antimicrobial agents, or drugs, are added, there are three potential interactions: no effect on one another (no interaction), a greater effect than the sum of their individual effects (synergy), or a lesser effect than the sum of their individual effects (antagonism). Loewe additivity assumes no interaction between two drugs if the combined effect is equal to the effect that is expected from a linear interpolation from the two individual effects[9]. Synergistic drug combinations have a stronger than additive effect. Schematic representations of antagonistic, synergistic, and additive drug combinations are shown in Figure 4.1.

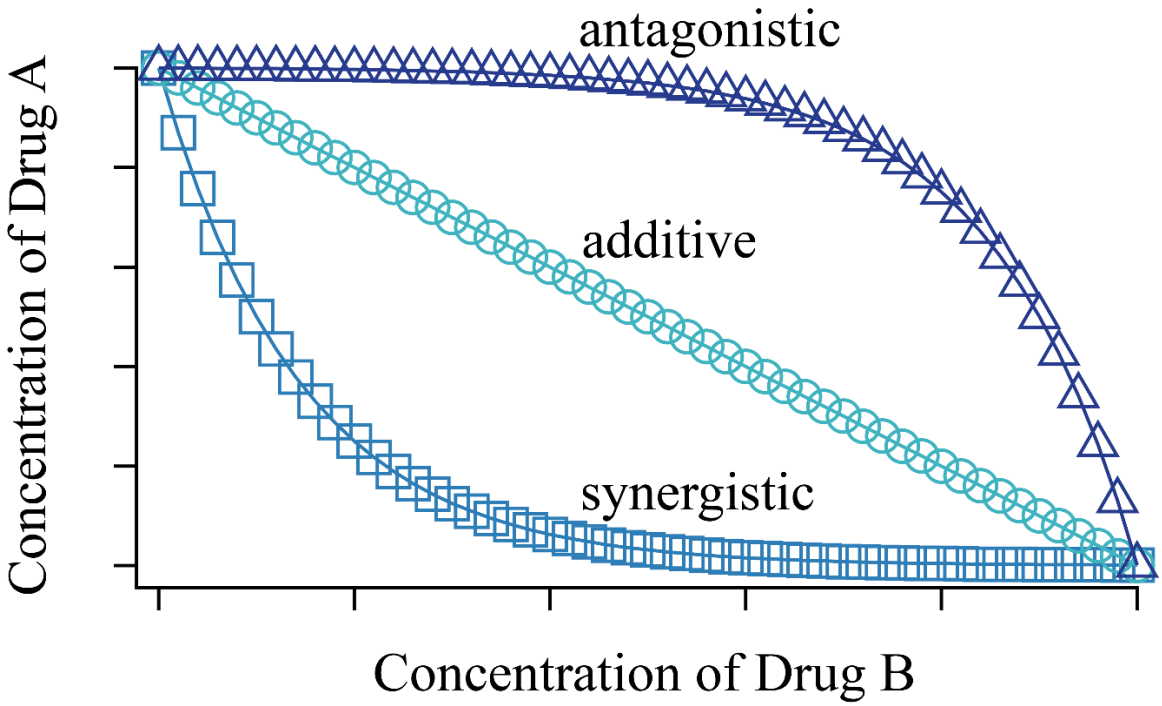

Figure 4.1. Schematic representation of antagonistic, synergistic, and additive drug combinations. Model lines of equal effect of drug combination and bacterial growth rate for additivity (light blue circles), antagonism (dark blue triangles), and synergism (blue squares) for Drug A and Drug B. Additivity assumes that two drugs do not interact if the combined effect is equal to what is expected from a linear interpolation of the two individual effects. Antagonistic drug combinations have a lesser effect than the sum of their individual effects. Individual drug effects lie along their respective axes.

4.1 Histone H2A Synergizes with the Antimicrobial Peptide (AMP) LL-37

The human cathelicidin, hCAP18, is cleaved by proteinase 3 to form the antimicrobial peptide LL-37[10], an AMP that is co-localized with histones in NETs[11]. The precursor of LL-37, hCAP-18, is present in neutrophil granules for targeted release[12]. Plasma concentrations of hCAP18 were found to be 1.18 μg/mL, and this full length protein binds to lipoprotein, perhaps as a means of preventing off-target damage[13,14]. Upon proteolytic cleavage, the active C-terminus 37 amino acid AMP LL-37 (LLGDFFRKSKEKIGKEFKRIVQRIKDFLRNLVPRTES) is released. This AMP disrupts lipid bilayers through the formation of toroidal pores[15] and exhibits broad-spectrum microbial activity[16]. Fluorescence microscopy experiments on *E. coli* revealed that 8 μM LL-37 is sufficient to saturate the bacterial outer membrane within 1 minute[17]. Translocation across the outer membrane and into the periplasmic space occurs 5-25 minutes later and corresponds to stalling of growth.

AMPs, like LL-37, have a critical role in the mammalian innate immune system. They are synthesized in elevated levels in tissues that are exposed to microbes, such as skin and mucosal epithelia, for rapid defense against microbial infections[18]. On unstimulated mucosal surfaces, LL-37 is found at concentrations around 2 μg/mL; however concentrations in excess of 50 μg/mL are found in inflamed epithelium[19]. LL-37 killing has been shown to be sensitive to NaCl concentration, and LL-37 synergizes with lactoferrin and lysozyme[19], defensins[20], and the antibiotics rifampicin and polymyxin B[21].

LL-37 is a curved peptide with 37 amino acid residues, 54% of which are hydrophilic. LL-37 has a net positive charge of +6 at physiological pH. In aqueous solution, circular dichroism spectrums reveal that LL-37 has a disordered structure; however, in lipophilic environments, intramolecular hydrogen bonds facilitate peptide folding into an amphipathic α helix, with a helix-

bend-helix motif, as visualized through solution NMR spectroscopy in Figure 4.2[22]. The extent of α-helicity correlates with antimicrobial activity against Gram-positive and Gram-negative microbes[23].

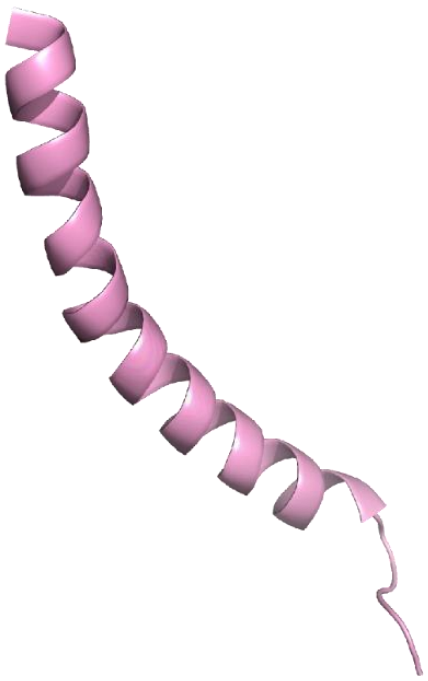

Figure 4.2. Solution NMR structure of human LL-37. The structure of ^{13}C, ^{15}N-labeled LL-37 was determined by 3D triple resonance NMR spectroscopy[22]. The structure reveals a curved amphipathic helix-bend-helix motif, with a helical bend between Gly-14 and Glu-16, followed by a disordered C-terminal tail. Image adapted from Protein Data Base (PDB: 2K6O).

Previous experiments with histones alone showed PI fluorescence of histone-treated *E. coli* increased in bacteria cultured in low concentrations of magnesium, but not physiological concentrations, suggesting that H2A inhibits growth in low magnesium by increasing membrane permeabilization. Since histone-mediated bacterial growth inhibition in low ionic environments was associated with compromised membrane integrity, I hypothesized that LL-37 may disrupt the bacterial membrane by inducing pore formation, allowing increased levels of histone H2A to enter the cell and increasing histone-mediated killing. In principle, histones could synergize with LL-37 to disrupt the microbial membrane, causing microbial death. LL-37-formed pores could also permeabilize the bacterial membrane, facilitating histones entry into the bacterial cell, where histones may have intracellular targets. To determine whether histones and LL-37 synergize to kill bacteria, *E. coli* and *S. aureus* were treated with combinatorial treatments of LL-37 and histone H2A in physiological ionic conditions (1 mM $MgSO_4$) to avoid membrane stress from low ionic conditions.

Treatment of stationary phase *E. coli* with human LL-37 at 2 μM, a concentration reported to be the bulk MIC of *E. coli* after 12 hours[17] and a concentration below that found in inflamed epithelial cells[19], decreased the growth rate and slightly extended the lag time (Figure 4.3 A). As previously seen, the addition of histone H2A alone had no effect on *E. coli* growth. However, cultures treated with both histone H2A and LL-37 had significantly decreased growth rates and extended lag times compared to untreated or LL-37-treated samples. This synergistic killing effect was also seen with *S. aureus* (Figure 4.3 B), suggesting that treatment of bacteria with the pore-forming AMP LL-37 enhances the antimicrobial activity of histone H2A.

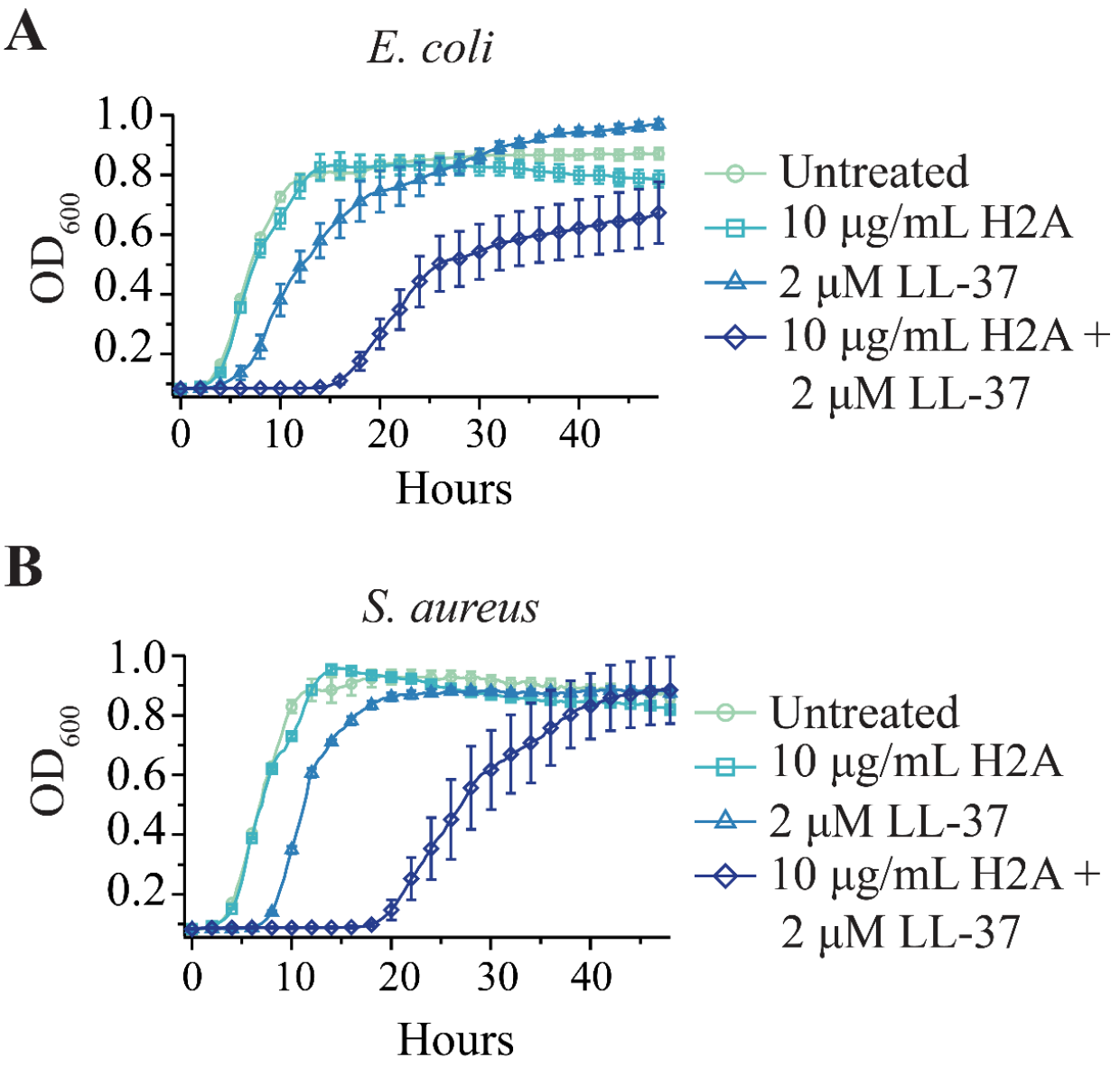

Figure 4.3. Histone H2A and LL-37 synergize to kill stationary phase *E. coli* and *S. aureus*. Growth profiles of stationary phase *E. coli* (A) and *S. aureus* (B) treated with 10 µg/mL H2A and 2 µM LL-37 in media containing physiological (1 mM) magnesium over a 48-hour growth period. The addition of H2A has no effect on *E. coli* or *S. aureus* growth in physiological concentrations of magnesium. The addition of LL-37 extends the lag phase and slows exponential growth. Histones and LL-37 synergize to kill *E. coli* and *S. aureus*, significantly decreasing growth rates and extending lag times compared to untreated or LL-37-treated samples. Points in (A) and (B) are the average of at least four independent experiments (n = 4) and error bars indicate SEM.

As discussed above, synergy is defined as a combination that gives rise to an effect that is greater than the sum of each of the constituents. The antimicrobial activities of LL-37 and H2A are synergistic – the combined treatment inhibited growth to a larger degree than the two individual effects combined.

To quantify the number of viable *E. coli* following the dual treatment of histones and LL-37, a traditional plate assay was performed. Overnight cultures of stationary phase *E. coli* were diluted 1:1000 in MinA with 1 mM $MgSO_4$ and cultured with 10 μg/mL H2A, 2 μM LL-37, or both H2A and LL-37 for 1 hour. After treatment, bacterial suspensions were diluted 1:1000 into fresh MinA media with 1 mM $MgSO_4$ and 25 μL of diluted bacterial suspension was plated on LB-Miller agar plates without histones or LL-37. Plates were grown for 18 hours before CFU counts were obtained. As previously seen (Figure 3.2 A, B), H2A had no effect on the number of colony forming units (CFUs) of *E. coli* in physiological conditions (Figure 4.4). Additionally, treatment with 2 μM LL-37 had no effect on the CFU count of *E. coli*. However, the combinatorial treatment of H2A and LL-37 significantly decreased the CFU count, indicating the combinatorial treatment is synergistic and bactericidal (Figure 4.4).

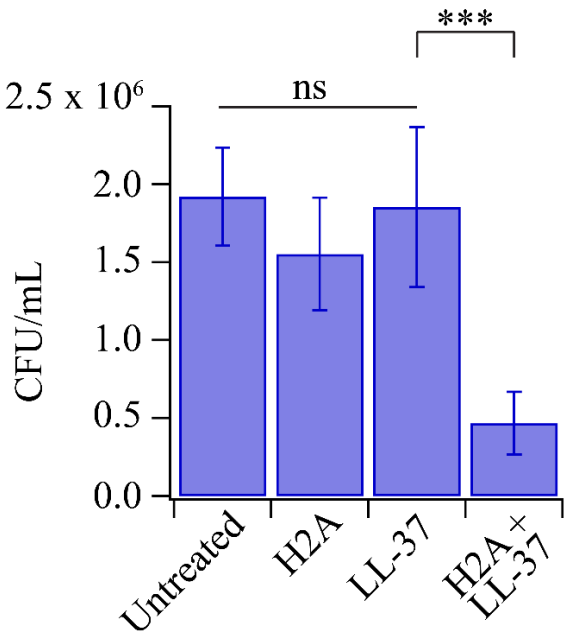

Figure 4.4. The combinatorial treatment of H2A and LL-37 decreases the number of colony forming units (CFUs) of *E. coli* in physiological conditions. The addition of H2A to *E. coli* treated with LL-37 decreased the number of colony forming units (CFUs) of *E. coli* growing in physiological concentrations of magnesium. Overnight cultures of stationary phase *E. coli* were diluted 1:1000 in MinA with 1 mM $MgSO_4$ and cultured with 10 μg/mL H2A, 2 μM LL-37, or both H2A and LL-37 for 1 hour. After treatment, bacterial suspensions were diluted 1:1000 into fresh MinA media with 1 mM $MgSO_4$ and 25 μL of diluted bacterial suspension was plated on LB-Miller agar plates without histones or LL-37. Plates were grown for 18 hours before imaging. Data shown as mean ± SEM and are representative of three independent experiments. *** $p \leq 0.001$, ns > 0.05.

4.2 Histone H2A Does Not Synergize with the Antibiotics Kanamycin or Chloramphenicol

To address whether the growth inhibition seen in combinatorial treatments of H2A with LL-37 reflects a trivial effect of overwhelming the bacteria with multiple antimicrobial agents, or if it was truly a mechanism dependent upon membrane permeabilization, I combined histone H2A with the aminoglycoside kanamycin, a bactericidal antibiotic that interacts with the 30S subunit of prokaryotic ribosomes, or the amphenicol chloramphenicol, a bacteriostatic antibiotic that binds to residues in the 50S ribosomal subunit of prokaryotic ribosomes. These antibiotics inhibit translation and do not affect membrane permeability[24]. However, some reports have noted that aminoglycosides, like kanamycin, cause membrane disruption through mistranslation of proteins[25–27].

Treatment of *E. coli* with kanamycin (Figure 4.5) or chloramphenicol (Figure 4.6) alone extended the lag time when compared to untreated *E. coli*. The combinatorial treatment of H2A with kanamycin, at concentrations close to MIC (Figure 4.5A) or concentrations well above MIC, had no effect on bacterial growth compared to kanamycin treatment alone. Similarly, chloramphenicol showed no synergies with H2A (Figure 4.6), suggesting that synergistic killing of bacteria with histones and other antimicrobial agents requires membrane permeabilization.

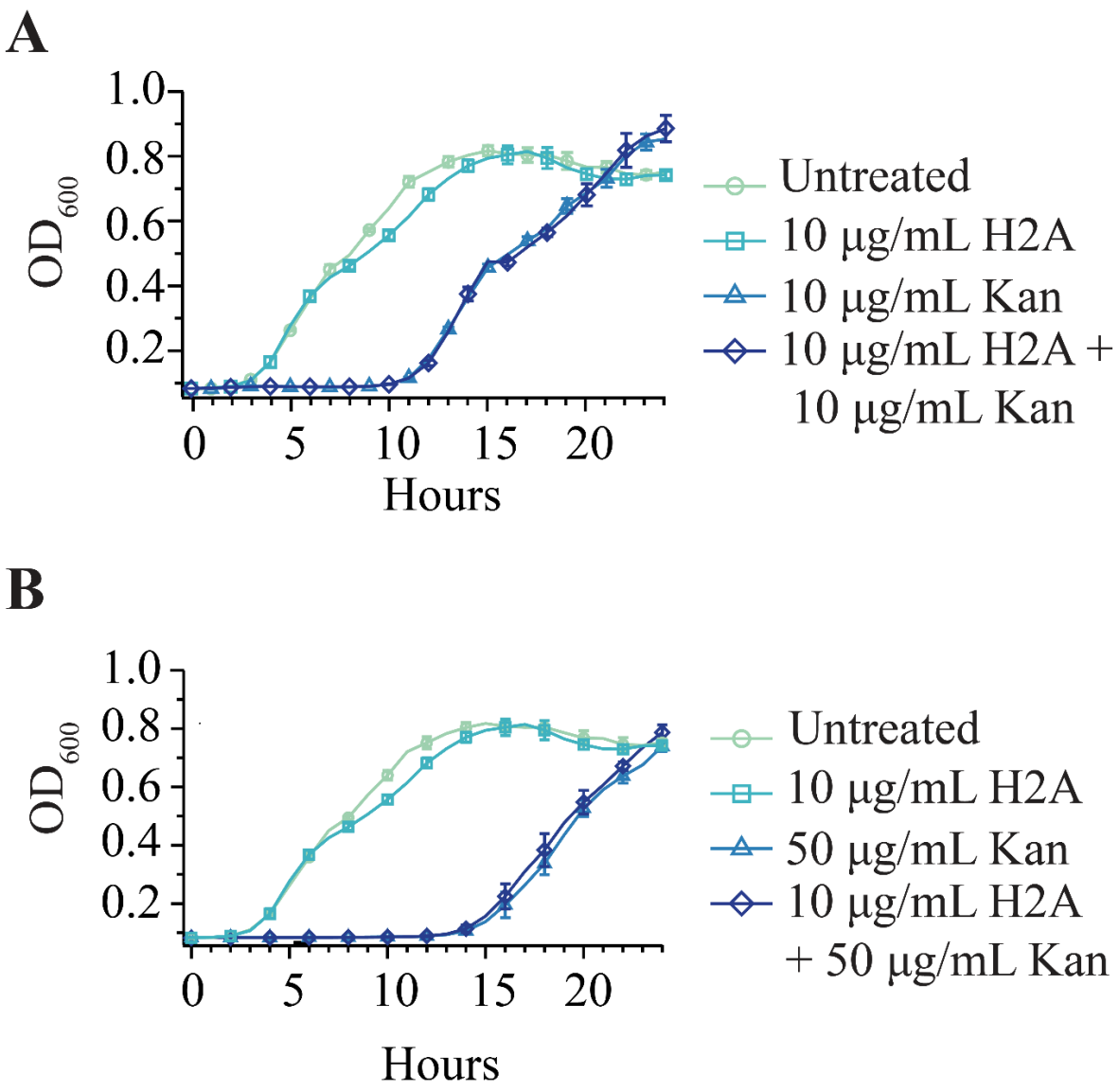

Figure 4.5. Histone H2A and Kanamycin have no synergistic killing effects on stationary phase *E. coli*. Growth profiles of stationary phase *E. coli* treated with 10 μg/mL H2A, 10 μg/mL kanamycin (Kan), or both 10 μg/mL H2A and 10 μg/mL Kan in media containing physiological (1 mM) magnesium over a 24-hour growth period. This concentration of Kan, a concentration near the MIC, does not synergize with H2A (A). Similarly, 50 μg/mL, a concentration of Kan well above the MIC does not synergize with H2A. Kanamycin, a bactericidal antibiotic that interacts with the 30S subunit of prokaryotic ribosomes and does not affect membrane permeability, does not synergize with histones at either concentration. Data points are the average of four independent experiments (n = 4) and error bars indicate SEM.

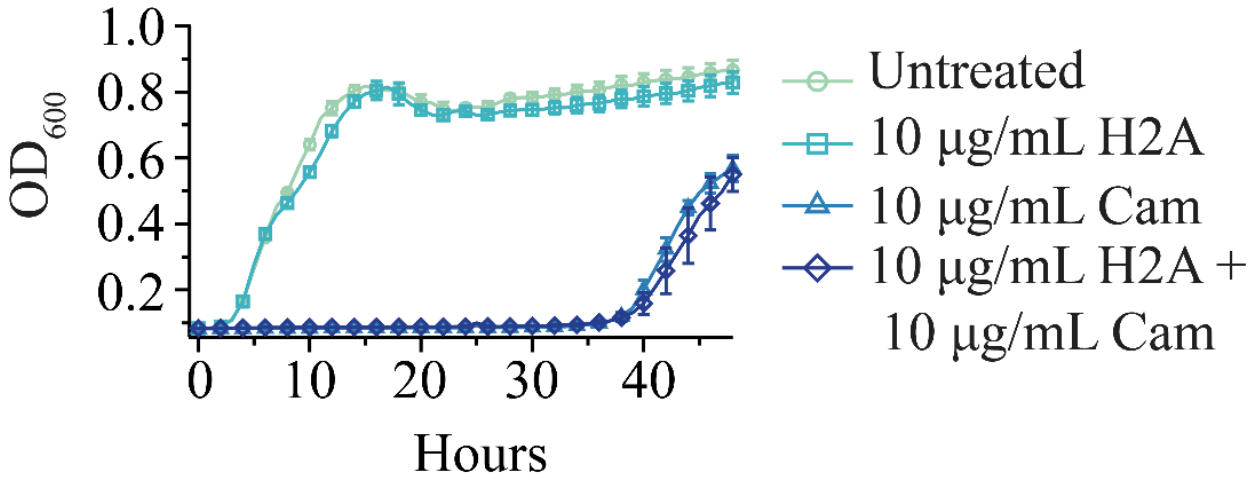

Figure 4.6. Histone H2A and Chloramphenicol have no synergistic killing effects on stationary phase *E. coli*. Growth profiles of stationary phase *E. coli* treated with 10 µg/mL H2A, 10 µg/mL chloramphenicol (Cam), or both 10 µg/mL H2A and 10 µg/mL Cam in media containing physiological (1 mM) magnesium over a 48-hour growth period. Chloramphenicol, a bacteriostatic antibiotic that binds to residues in the 50S ribosomal subunit of prokaryotic ribosomes and does not affect membrane permeability, does not synergize with histones. Data points are the average of four independent experiments (n = 4) and error bars indicate SEM.

4.3 Histone H2A Synergizes with the Antimicrobial Peptide (AMP) LL-37 to Kill Mid-Exponential Phase Bacteria

Bacterial growth curves typically have five phases of growth: lag phase, exponential phase, stationary phase, death phase, and long-term stationary phase[28]. In addition to differences in growth patterns in the different phases, genetic expression is vastly different between the phases. During stationary phase, *E. coli* undergoes changes in DNA topography and structure and alters transcriptional regulation, enabling the bacterium to survive in adverse conditions, such as low nutrient levels, harsh environmental conditions, and high concentrations of toxic waste[28]. Environmental bacteria are typically in the stationary phase. Although stationary phase bacteria are growth-arrested, stationary phase bacteria have been reported to have constant protein production activity[29]. However, stationary phase *E. coli* has been reported to be more resistant to membrane permeabilization by AMPs than exponentially growing bacteria[30].

The growth curves (Figure 4.3) and the complementary plate killing assay (Figure 4.4) were performed with overnight cultures of stationary bacteria, which have a different physiology than bacteria in the exponential phase of growth, during which cell division is occurring at a consistent rate. To identify the effect of growth phase on histone-mediated killing of bacteria, growth curves were constructed using exponentially growing bacteria. Stationary phase *E. coli* were back-diluted into fresh MinA media and were grown to exponential phase (OD_{600} 0.2). Bacteria were diluted 1:20 into fresh MinA media and treated with the dual combination of 10 μg/mL H2A and 2 μM LL-37 (Figure 4.7).

As previously observed using stationary phase bacteria, the addition of 10 μg/mL H2A alone had no effect on *E. coli* or *S. aureus* growth. Similarly, *E. coli* cultures treated with both histone H2A and LL-37 had significantly decreased growth rates and extended lag times compared to

untreated or LL-37-treated samples (Figure 4.7A). This synergistic killing effect was also seen with *S. aureus* (Figure 4.7B), suggesting that treatment of bacteria with the pore-forming AMP LL-37 enhances the antimicrobial activity of H2A against mid-exponential phase bacteria.

Given that synergy was seen using low concentrations of LL-37 and H2A with stationary phase and mid-exponential phase *E. coli* and *S. aureus*, mid-exponential phase bacteria were used in subsequent experiments, in an effort to increase reproducibility[31]. All subsequent experiments were conducted using mid-exponential phase bacteria grown to OD_{600} 0.2.

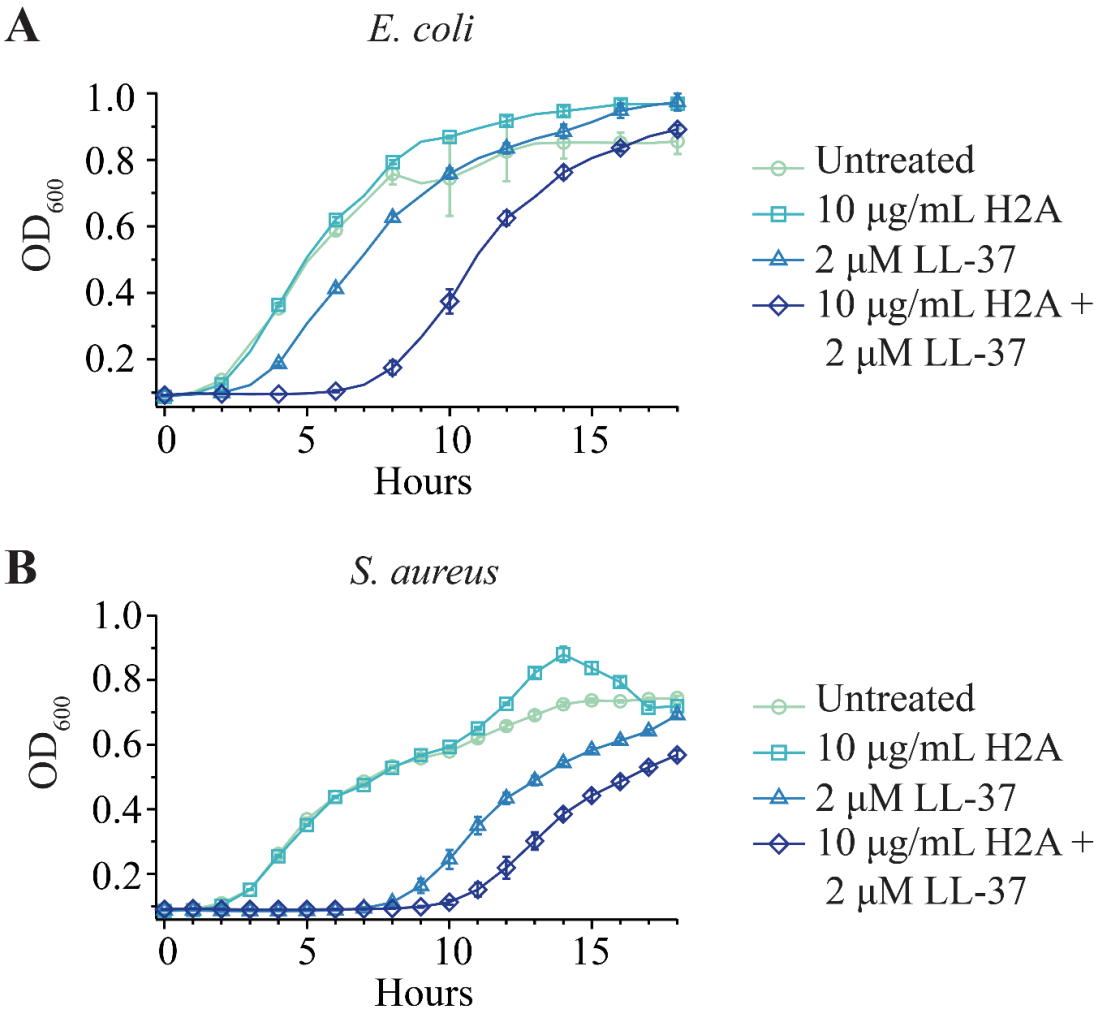

Figure 4.7. Histone H2A and LL-37 synergize to kill mid-exponential phase *E. coli* and *S. aureus*. Growth profiles of mid-exponential phase *E. coli* (A) and *S. aureus* (B) treated with 10 µg/mL H2A, 2 µM LL-37, or both 10 µg/mL H2A and 2 µM LL-37 in media containing physiological (1 mM) magnesium over an 18-hour growth period. The addition of H2A has no effect on *E. coli* growth in the physiological concentration of magnesium. The addition of LL-37 extended the lag phase and slowed exponential growth for both *E. coli* and *S. aureus*. Histones and LL-37 synergized to kill *E. coli* and *S. aureus*, significantly decreasing growth rates and extending lag times compared to untreated or LL-37-treated samples. Data points are the average of four independent experiments (n = 4) and error bars indicate SEM.

Overnight cultures of stationary phase bacteria were used to conclude that histones do not synergize with antibiotics that inhibit translation and do not affect membrane permeability (Figure 4.5, 4.6). To identify whether the growth phase affects potential synergy between histones and antibiotics that do not permeabilize the membrane, growth curves were constructed using mid-exponential phase bacteria. Similar to synergy experiments with mid-exponential phase bacteria, stationary phase *E. coli* were back-diluted into fresh MinA media and grown to exponential phase (OD_{600} 0.2). Bacteria were diluted 1:20 into fresh MinA media and treated with the dual combination of 10 μg/mL H2A and 10 μg/mL kanamycin (Figure 4.8).

The addition of 10 μg/mL H2A alone had no effect on *E. coli* growth. Treatment of *E. coli* with 10 μg/mL kanamycin alone extended the lag time and delayed exponential growth when compared to untreated *E. coli*. However, the combinatorial treatment of histone H2A with kanamycin had no effect on bacterial growth (Figure 4.8). Similar results were observed with chloramphenicol. Treatment of *E. coli* with 10 μg/mL chloramphenicol significantly slowed exponential growth; however there were low levels of growth across the 24-hour time period. The dual treatment of H2A and chloramphenicol had no effect on bacterial growth compared to *E. coli* treated with only chloramphenicol (Figure 4.9). Together, these findings suggest that synergistic killing of bacteria with histones requires membrane permeabilization, regardless of the growth phase of the bacteria.

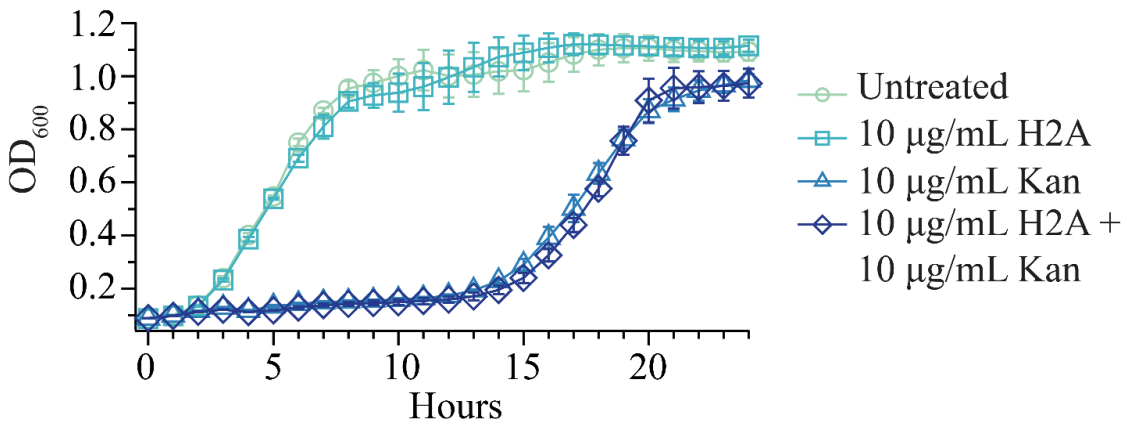

Figure 4.8. Histone H2A and kanamycin do not synergize to kill mid-exponential phase *E. coli*. Growth profiles of mid-exponential phase *E. coli* treated with 10 µg/mL H2A, 10 µg/mL kanamycin (Kan), or both 10 µg/mL H2A and 10 µg/mL Kan in media containing physiological (1 mM) magnesium over a 24-hour growth period. Kanamycin, a bactericidal antibiotic that interacts with the 30S subunit of prokaryotic ribosomes and does not affect membrane permeability, does not synergize with histones. Data points are the average of four independent experiments (n = 4) and error bars indicate SEM.

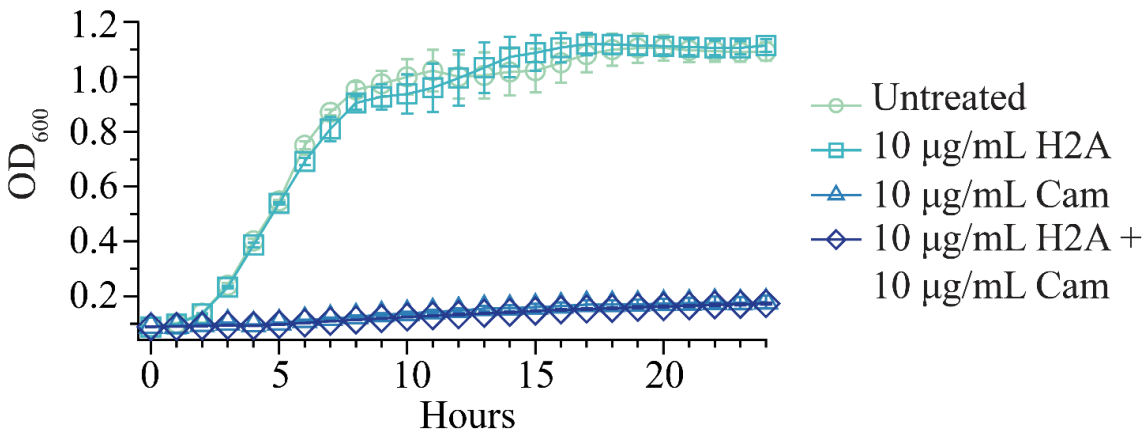

Figure 4.9. Histone H2A and chloramphenicol do not synergize to kill mid-exponential phase *E. coli*. Growth profiles of mid-exponential phase *E. coli* treated with 10 µg/mL H2A, 10 µg/mL chloramphenicol (Cam), or both 10 µg/mL H2A and 10 µg/mL Cam in media containing physiological (1 mM) magnesium over a 24-hour growth period. Chloramphenicol, a bacteriostatic antibiotic that binds to residues in the 50S ribosomal subunit of prokaryotic ribosomes and does not affect membrane permeability, does not synergize with histones. Data points are the average of four independent experiments (n = 4) and error bars indicate SEM.

Since the positively-charged AMP LL-37 disrupts lipid bilayers through the formation of toroidal pores[15], I investigated whether the synergistic bacterial growth inhibition observed upon histone and LL-37 treatment was truly dependent upon perturbing the bacterial membrane. *E. coli* were grown to mid-exponential phase (OD_{600} 0.2). Bacteria were diluted 1:20 into fresh MinA media and treated with 10 μg/mL H2A, 10 μg/mL kanamycin, the dual combination of H2A and kanamycin, 1 μM LL-37, 2 μM LL-37, or the dual combination of H2A with 1 μM or 2 μM LL-37, The addition of 2 μM LL-37 caused a notable decrease in the number of cells for imaging. Thus, to maximize the number of cells available for statistical analysis, PI analysis was performed using 1 μM LL-37, in addition to 2 μM LL-37, to observe trends related to PI staining in the presence of LL-37. 1 μM LL-37 showed synergies with 10 μg/mL H2A against *E. coli* (Figure 4.10); however, the delay in growth was minimized compared to the higher 2 μM concentration of LL-37 used previously (Figure 4.7).

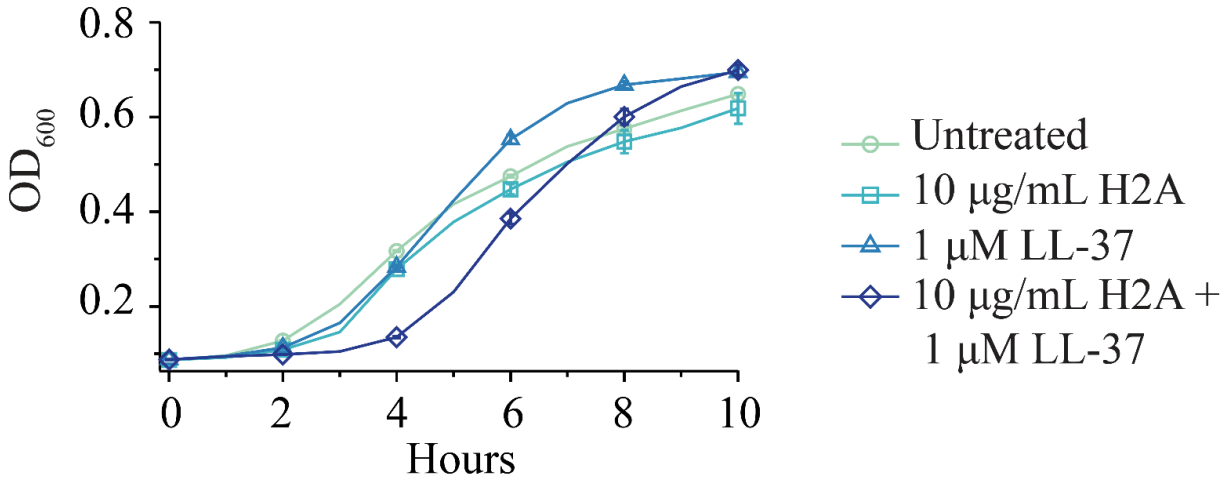

Figure 4.10. Histone H2A and LL-37 synergize to kill mid-exponential phase *E. coli*. Growth profiles of mid-exponential *E. coli* treated with 10 μg/mL H2A, 1 μM LL-37, or both in media containing physiological (1 mM) magnesium over a 10-hour growth period. The addition of H2A and LL-37 alone have minimal effects on *E. coli* growth in the physiological concentration of magnesium. Histones and LL-37 synergize to kill *E. coli*, decreasing growth rates and extending lag times compared to untreated or LL-37-treated samples. Data points are the average of four independent experiments (n = 4) and error bars indicate SEM.

Bacteria were cultured with the antimicrobial agents, along with 30 μM propidium iodide (PI), for one hour. Bacteria were plated on 1% agarose-MinA pads and mCherry fluorescence was imaged and quantified (Figure 4.11).

No increase in PI fluorescence was observed for *E. coli* in physiological ionic conditions with low levels of histones, LL-37, or kanamycin alone, indicating that these concentrations of antimicrobials alone are not sufficient to induce significant membrane permeabilization. Additionally, the dual combination of histones and kanamycin, a treatment that did not induce synergistic killing of *E. coli* (Figure 4.8), did not induce membrane permeabilization. Although aminoglycosides, like kanamycin, have been reported to cause membrane disruption through mistranslation of proteins[25–27], this mechanism did not appear to form pores large enough for PI to enter the cell. Presumably, since no synergy was seen at kanamycin concentrations of 10 μg/mL (near MIC) or 50 μg/mL (well above MIC), it is unlikely that this mechanism forms pores that are large enough for histones to enter the cell. This lack of histone uptake is shown later in Chapter 5, where treatment with kanamycin did not induce uptake of fluorescently labeled H2A, consistent with the lack of membrane permeabilization observed in PI fluorescence measurements (Figure 4.10) and absence of synergy with histones in growth profiles (Figure 4.5, 4.8).

With both concentrations of LL-37, the synergistic combination of LL-37 and H2A induced PI fluorescence in *E. coli*, a condition that inhibited growth in liquid culture (Figure 4.7, 4.10), indicating membrane permeabilization accompanies the enhanced antimicrobial activity of H2A. Since the bacterial growth inhibition seen upon bacterial treatment with the synergistic combination of LL-37 and H2A was accompanied by increased membrane permeabilization in physiological ionic environments, these results support a mechanism by which disruption of the microbial membrane is required for histone-mediated killing of bacteria. Since the addition of

histone to LL-37-treated *E. coli* did not significantly increase PI fluorescence, the complete inhibition of growth in dual treated cells (Figure 4.7, 4.10) may be explained by a secondary mechanism, such as an intracellular target for histones. As such, permeabilization of the bacterial membrane by LL-37 may function to facilitate histone entry into the bacterial cell.

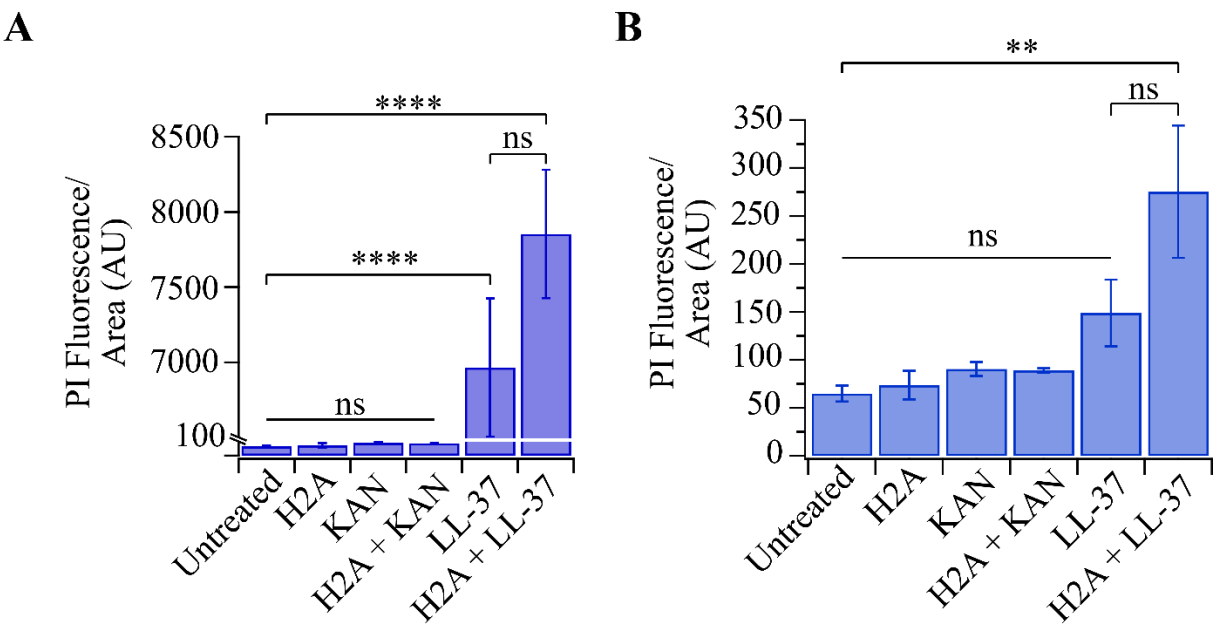

Figure 4.11. Histones and LL-37 increase membrane permeabilization. Intracellular propidium iodide (PI) fluorescence intensities of mid-exponential phase *E. coli* treated with H2A, LL-37, H2A and LL-37, Kan, or H2A and Kan in medium containing 1 mM magnesium. The concentrations used were 10 μg/mL H2A, 10 μg/mL Kan, along with 2 μM LL-37 (A) or 1 μM LL-37 (B). Experiments with kanamycin and LL-37 were conducted separately and PI fluorescence was normalized to H2A-treated cells for comparison purposes. With both concentrations of LL-37, the combinatorial treatment of H2A and LL-37 significantly increased PI fluorescence compared to untreated *E. coli*. Data is from three separate experiments (n=3). Data shown is the mean ± SE. **** indicates a p-value ≤ 0.0001, ** indicates a p-value ≤ 0.01, and ns indicates a p-value > 0.05.

4.4 Histone H2A Synergizes with the Antibiotic Polymyxin B

To identify whether the synergies observed between LL-37 and histones represented a more global mechanism whereby histones may synergize with any membrane-permeabilizing agent, I further explored synergy between histone H2A and polymyxin B (PMB), a pentabasic (net charge of +5) peptide antibiotic containing a cycloheptapeptide ring with a C-8 fatty acid attached through an amide bond[32] (Figure 4.12). This cationic antibiotic is produced by *Bacillus polymyxa,* a Gram-positive, nitrogen-fixing bacterium that is found in soil and plant roots[33]. PMB binds to LPS and lipid A sites and displaces cations from LPS. Since cationic peptides, including PMB, have affinities for LPS that at least three orders of magnitude greater than those of Ca^{2+} or Mg^{2+}, these cationic peptides displace the cations and permeabilize the membrane, enabling uptake of the peptide itself, a pathway known as the self-promoted uptake pathway[34]. Once PMB passes through the outer membrane, its amphipathic nature allows it to insert itself into the negatively-charged cytoplasmic membrane, further compromising membrane integrity[16], a mechanism sharing similarities with LL-37.

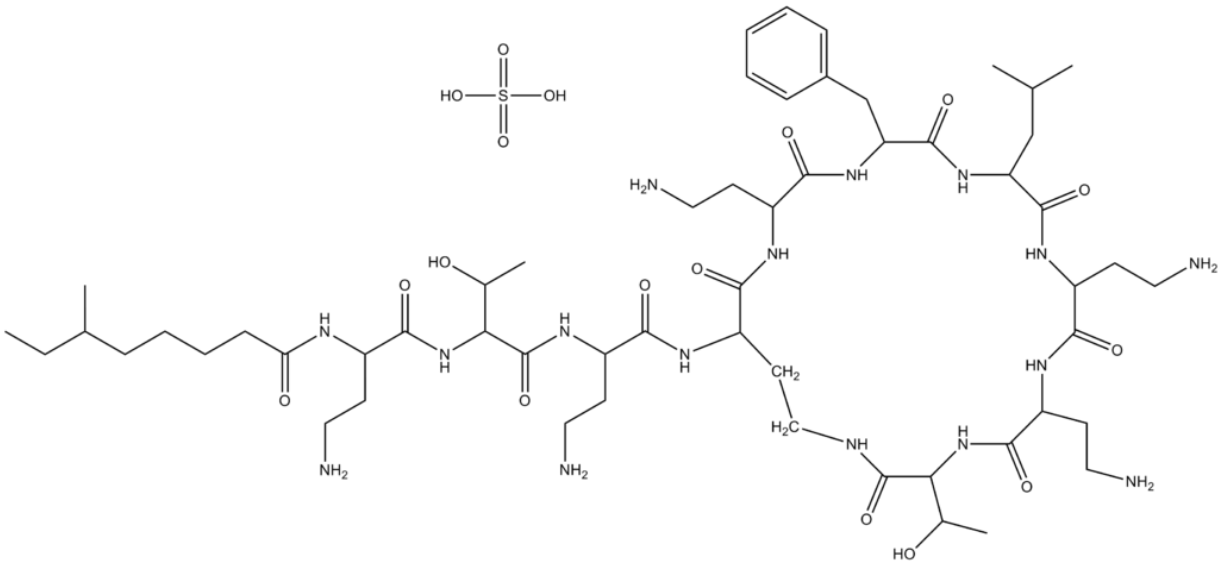

Figure 4.12. Structure of Polymyxin B Sulfate. Polymyxin B (PMB) contains a cycloheptapeptide ring with a C-8 fatty acid attached through an amide bond. Its structure permits it to bind to negatively charged sites in the LPS layer of Gram-negative bacteria via electrostatic interactions between the negatively charged LPS and the positively charged amino groups in the cyclic peptide portion of antibiotic, altering membrane structure and increasing membrane permeability.

To identify whether histones synergize with the membrane-permeabilizing antibiotic PMB to kill bacteria, growth curves were constructed using exponentially growing bacteria treated with the dual combination of histones and PMB. Stationary phase *E. coli* were back-diluted into fresh MinA media and grown to exponential phase (OD_{600} 0.2). Bacteria were diluted 1:20 into fresh MinA media and treated with 10 μg/mL H2A, 1 μg/mL PMB, or the dual combination of H2A and PMB.

The addition of 10 μg/mL H2A alone had no effect on *E. coli* growth, whereas the addition of 1 μg/mL PMB decreased the growth rate slightly and minimally extended the lag time compared to untreated *E. coli* (Figure 4.13). Consistent with a synergistic mechanism of killing, treatment with both histone H2A and PMB completely prevented bacterial growth over a 24-hour period. Given that histones synergize with the pore-forming antibiotic PMB and the pore-forming AMP LL-37, this suggests that histones synergize with any membrane permeabilizing agents to kill bacteria, and that this mechanism is not specific to histones and LL-37.

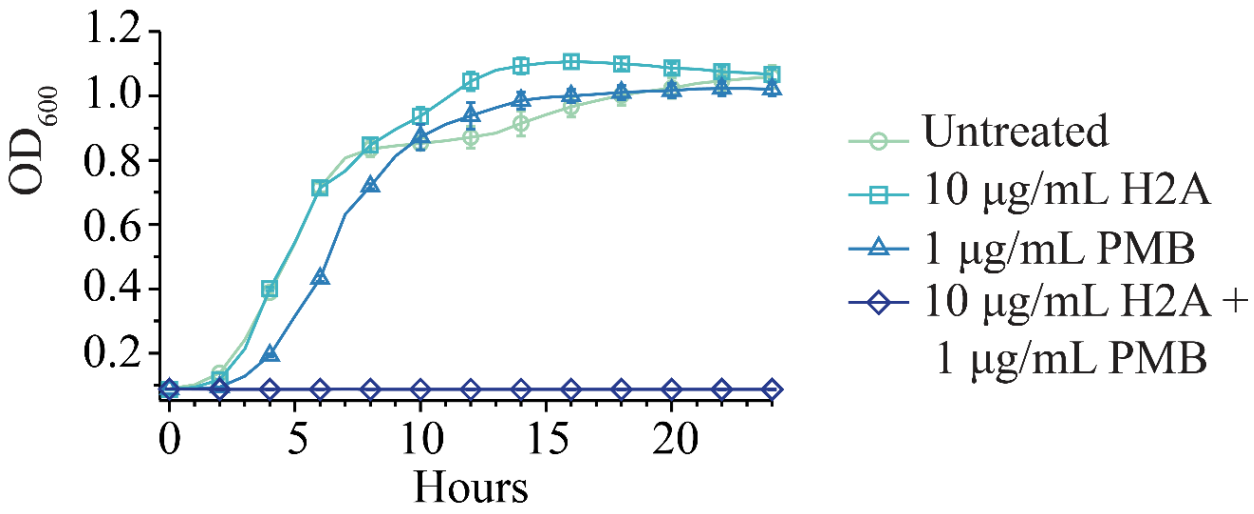

Figure 4.13. Histone H2A and polymyxin B synergize to kill *E. coli*. Growth profiles of mid-exponential phase *E. coli* treated with 10 μg/mL H2A, 1 μg/mL polymyxin B (PMB), or the dual combination of H2A and PMB in media containing physiological (1 mM) magnesium over a 24-hour growth period. The addition of H2A has no effect on *E. coli* growth in the physiological concentration of magnesium. The addition of polymyxin B decreased the growth rate slightly and minimally extended the lag time. Histones and polymyxin B synergize to kill *E. coli*, completely preventing *E. coli* growth. Data points are the average of at four independent experiments (n = 4) and error bars indicate SEM.

To identify whether the synergistic killing effect observed upon histone and PMB treatment was dependent upon perturbing the bacterial membrane, *E. coli* were grown to mid-exponential phase (OD_{600} 0.2), diluted 1:20 into fresh MinA media, and treated with 10 μg/mL H2A, 1 μg/mL PMB, or a combination of H2A and PMB. Bacteria were cultured with histones and/or PMB, along with 30 μM propidium iodide (PI), for one hour. Bacteria were plated on 1% agarose-MinA pads and mCherry fluorescence was imaged and quantified (Figure 4.14).

As previously observed, no increase in PI fluorescence was observed for *E. coli* in physiological ionic conditions with low levels of histones. However, treatment with PMB alone or PMB and histones, treatments which inhibited growth in liquid culture (Figure 4.13), induced PI fluorescence in *E. coli*, suggesting growth inhibition by histones is dependent upon disruption of the bacterial membrane. Since the addition of histone to PMB-treated *E. coli* did not significantly increase PI fluorescence, the complete inhibition of growth in dual treated cells (Figure 4.13) may be explained by a secondary mechanism, such as an intracellular target for histones.

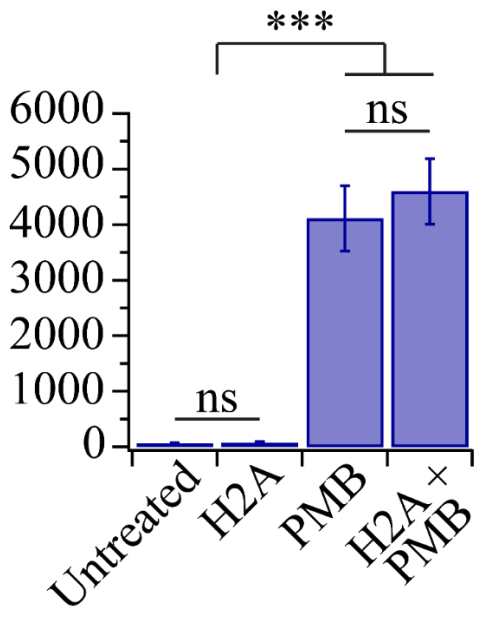

Figure 4.14. Histones and polymyxin B increase membrane permeabilization. Intracellular propidium iodide (PI) fluorescence intensities of mid-exponential phase *E. coli* treated with 10 μg/mL H2A, 1 μg/mL PMB, or a combination of H2A and PMB in medium containing 1 mM magnesium. The combinatorial treatment of H2A and PMB significantly increased PI fluorescence compared to untreated *E. coli*; however, there were no significant difference in PI fluorescence between PMB-treated *E. coli* and dual-treated *E. coli*. Data is from three separate experiments (n=3). Data shown is the mean ± SE. *** indicates a p-value ≤ 0.001, and ns indicates a p-value > 0.05.

4.5 Histone H2A Synergizes with the Antimicrobial Peptide (AMP) Magainin-2

Magainin-2 (MAG2), an α-helical peptide belonging to a class of antimicrobial peptides from the African claw frog (*Xenopus laevis*)[36], shares several characteristics with LL-37, including a cationic nature and a tendency to form amphipathic, α-helical structures in membranes[37]. The 23-amino acid AMP (GIGKFLHSAKKFGKAFVGEIMNS), as visualized in Figure 4.15, is thought to form a 2-3 nm toroidal pore, disrupting the ion gradient[38] and inducing lipid flip-flop, peptide translocation, and membrane permeabilization[39–41].

Figure 4.15. Solution NMR structure of *Xenopus laevis* magainin-2. The structure of magainin-2 (MAG2) was determined by two-dimensional 1H NMR spectroscopy in dodecylphosphocholine micelles, sodium dodecylsulfate micelles, and a trifluoroethanol/water solution.[38]. The structure reveals an alpha-helical peptide structure, with a helical bend between Phe-12 and Gly-13. Image adapted from Protein Data Base (PDB: 2MAG).

To identify whether histones synergize with the membrane-permeabilizing African claw frog AMP MAG2 to kill bacteria, growth curves were constructed using exponentially growing bacteria treated with the dual combination of histones and MAG2. Stationary phase *E. coli* were back-diluted into fresh MinA media and grown to exponential phase (OD_{600} 0.2). Bacteria were diluted 1:20 into fresh MinA media and treated with 10 μg/mL H2A, 10 μM MAG2, or the dual combination of H2A and MAG2.

Treatment of exponential phase *E. coli* with 10 μg/mL histone H2A or 10 μM MAG2, a concentration below the MIC for *E. coli*[42], minimally affected *E. coli* growth (Figure 4.16). However, consistent with a synergistic mechanism of killing, treatment of *E. coli* with both H2A and MAG2 inhibited growth and increased the lag time. This further suggests that histones synergize with membrane-permeabilizing agents to kill bacteria. Since histones synergize with LL-37, PMB, and MAG2, this mechanism is not specific to an individual pore-forming agent. Additionally, these synergistic interactions between histones and pore-forming AMPs are not specific to only mammalian AMPs, such as LL-37. Since *X. laevis* contain MAG2 and histones[43], the synergistic killing of bacteria by histones and pore-forming AMPs may represent a mechanism of the innate immune system which spans across multiple species.

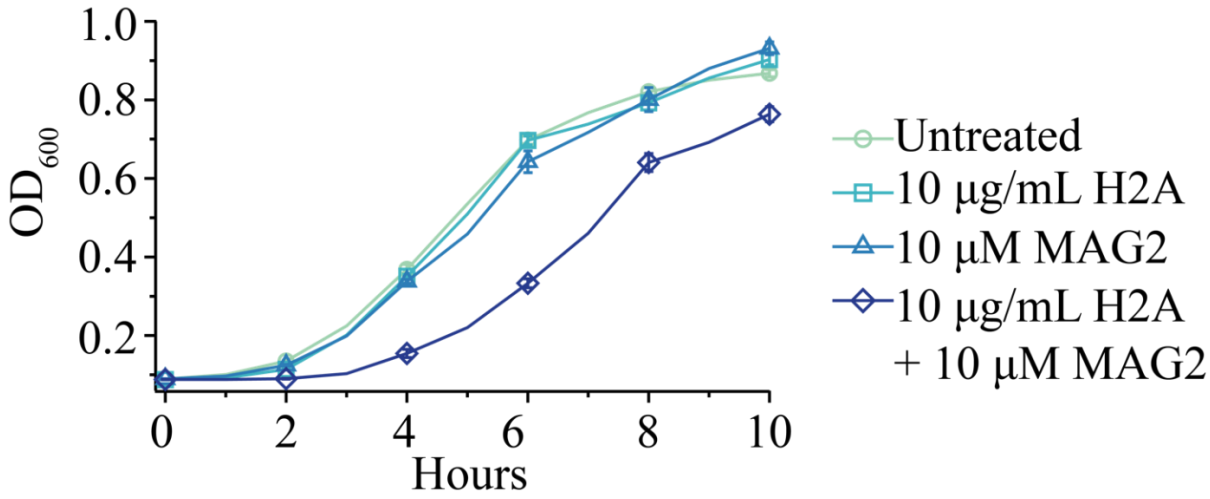

Figure 4.16. Histone H2A and magainin-2 synergize to kill *E. coli*. Growth profiles of mid-exponential phase *E. coli* treated with 10 µg/mL H2A, 10 µM magainin-2 (MAG2), or the dual combination of H2A and MAG2 in media containing physiological (1 mM) magnesium over a 10-hour growth period. The addition of H2A or magainin-2 alone had no effect on *E. coli* growth in physiological concentrations of magnesium. Histones and MAG2 synergize to kill *E. coli*, extending the lag phase and slowing bacterial growth. Growth curves are presented for the first ten hours of growth to better visualize the effect of the dual treatment. Data points are the average of four independent experiments (n = 4) and error bars indicate SEM.

Since the cationic AMP MAG2 disrupts the ion gradient through the formation of toroidal pores[38–41], I investigated whether the synergistic bacterial growth inhibition observed upon histone and MAG2 treatment was truly dependent upon perturbing the bacterial membrane. *E. coli* were grown to mid-exponential phase (OD_{600} 0.2). Bacteria were diluted 1:20 into fresh MinA media and treated with 10 μg/mL H2A, 10 μM MAG2, or the dual combination of H2A and MAG2. Bacteria were cultured with the antimicrobial agents, along with 30 μM propidium iodide (PI), for one hour. Bacteria were plated on 1% agarose-MinA pads and mCherry fluorescence was imaged and quantified (Figure 4.17).

Low levels of PI fluorescence were observed for *E. coli* in physiological ionic conditions with low concentrations of histones or MAG2 alone, indicating that these concentrations of antimicrobials alone are not sufficient to induce significant membrane permeabilization. However, the synergistic combination of MAG2 and H2A, a condition that inhibited growth in liquid culture (Figure 4.16), induced PI fluorescence in *E. coli*, indicating membrane permeabilization accompanies the enhanced antimicrobial activity of H2A upon MAG2 treatment. This membrane permeabilization supports a mechanism by which treatment with histones and AMPs disrupts the microbial membrane to kill bacteria. Further, this increased permeabilization of the bacterial membrane may enable increased amounts of histones to enter the bacterial cell.

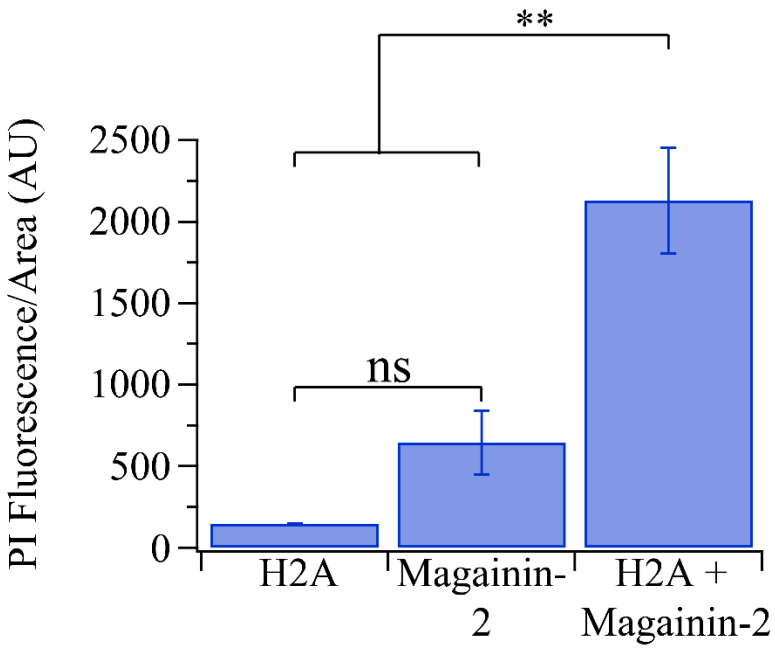

Figure 4.17. Histones and magainin-2 increase membrane permeabilization. Propidium iodide (PI) fluorescence of *E. coli* treated with 10 μg/mL histone H2A, 10 μM magainin-2 or both H2A and maganin-2 after a 1-hour treatment period. Quantification of the average PI fluorescence/area (AU) for each condition indicates this concentration of magainin-2 alone was not sufficient to induce significant membrane permeabilization. The combinatorial treatment of H2A and MAG2 significantly increased PI fluorescence. Data is from three separate experiments (n=3). Data shown is the mean ± SE. ** indicates a p-value ≤ 0.01, and ns indicates a p-value > 0.05.

4.6 The Synergistic Combination of Histone H2A and LL-37 Induces Extensive Cellular Damage Not Observed in Individual Treatments

The observation that histones synergize with a range of membrane-permeabilizing agents, including the human AMP LL-37, the antibiotic PMB, and the African claw frog AMP MAG2, and the finding that these synergies are accompanied by increased membrane permeabilization, support a global mechanism by which histones and AMPs increasingly disrupt the microbial membrane to kill bacteria. Since individual treatments had minimal effects on the growth profiles of bacteria, scanning electron microscopy (SEM) imaging was employed to visualize the effects of the individual treatments and the synergistic combination of histones and AMPs.

E. coli were grown to an OD_{600} of 0.2, diluted 1:20, and supplemented with 10 μg/mL H2A, 1 μM LL-37, or a combination of H2A and LL-37. Cells were treated for 1 hour and added to a glass bottomed petri dish for 15 minutes. Due to lower levels of adhesion, untreated, control cells were not diluted 1:20 and were allowed to sit in the glass-bottomed petri dish for 45 minutes. Media was removed and 4% paraformaldehyde (PFA) was added for 20 minutes to fix bacteria. Dehydration was performed with serial ethanol dilutions. The fixed and dehydrated sampled were coated with 10 nm of iridium using an ACE600 sputter coater before characterization using a FEI Magellan 400 XHR Scanning Electron Microscope at a 45° tilt angle with an acceleration voltage of 3kV.

The synergistic effects of Histone H2A and LL-37 were clearly apparent through SEM (Figure 4.18, 4.19). Treatment with LL-37 or H2A alone for 1 hour induced few cell morphology differences from untreated cells. *E. coli* treated with H2A alone showed some extracellular matrix on the exterior of the cells and linkage at the bacterial poles, while *E. coli* treated with LL-37 alone

were reduced in size compared to untreated cells. However, the combined treatment of LL-37 and H2A caused extensive cellular damage, including membrane permeabilization, cell linkage and aggregation, and the extensive production of insoluble components to the outer surface of the membrane and to the surrounding surfaces. In some cells treated with LL-37 and H2A, the formation of membrane blebs was observed. Since these membrane blebs are transient events, they were not observed in all cells (Figure 4.19).

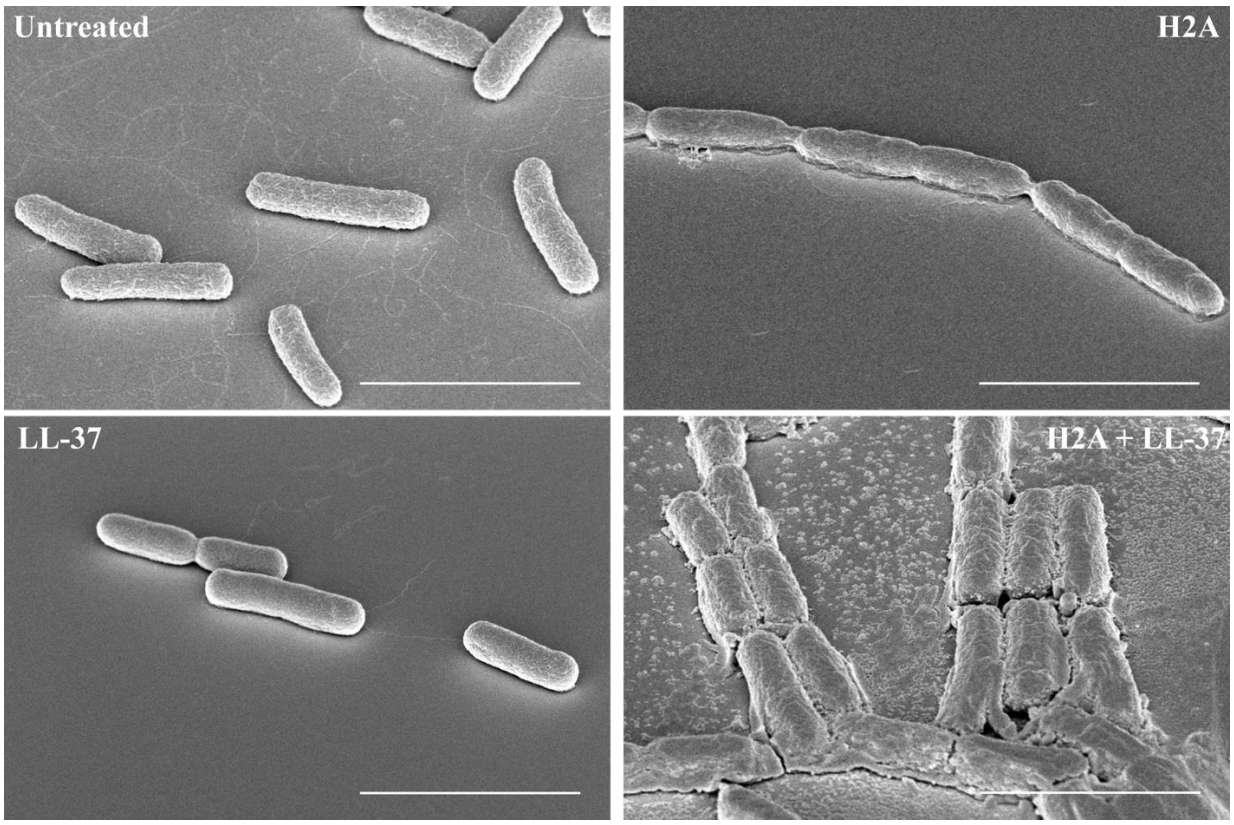

Figure 4.18. *E. coli* treatment with LL-37 and H2A causes extensive cellular damage. Scanning electron microscopy (SEM) images of *E. coli* treated with 10 μg/mL H2A, 1 μM LL-37, or both in medium containing 1 mM magnesium. Mid-exponential phase *E. coli* were grown, diluted 1:20, and supplemented with 10 μg/mL H2A, 1 μM LL-37, or both. Cells were treated for 1 hour and added to a glass bottomed petri dish for 15 minutes. Untreated cells were not diluted 1:20 and were allowed to sit in the glass-bottomed petri dish for 45 minutes due to lower adhesion levels. Following adhesion to the glass bottomed petri dish, media was removed and 4% paraformaldehyde (PFA) was added for 20 minutes to fix bacteria. Dehydration was performed with serial ethanol dilutions. The fixed and dehydrated sampled were coated with 10 nm of iridium using an ACE600 sputter coater before characterization using a FEI Magellan 400 XHR Scanning Electron Microscope at a 45° tilt angle with an acceleration voltage of 3kV. Representative images are shown for each condition. Scale bars represent 3 μm. Imaging assistance was provided by Rachel Rosenzweig.

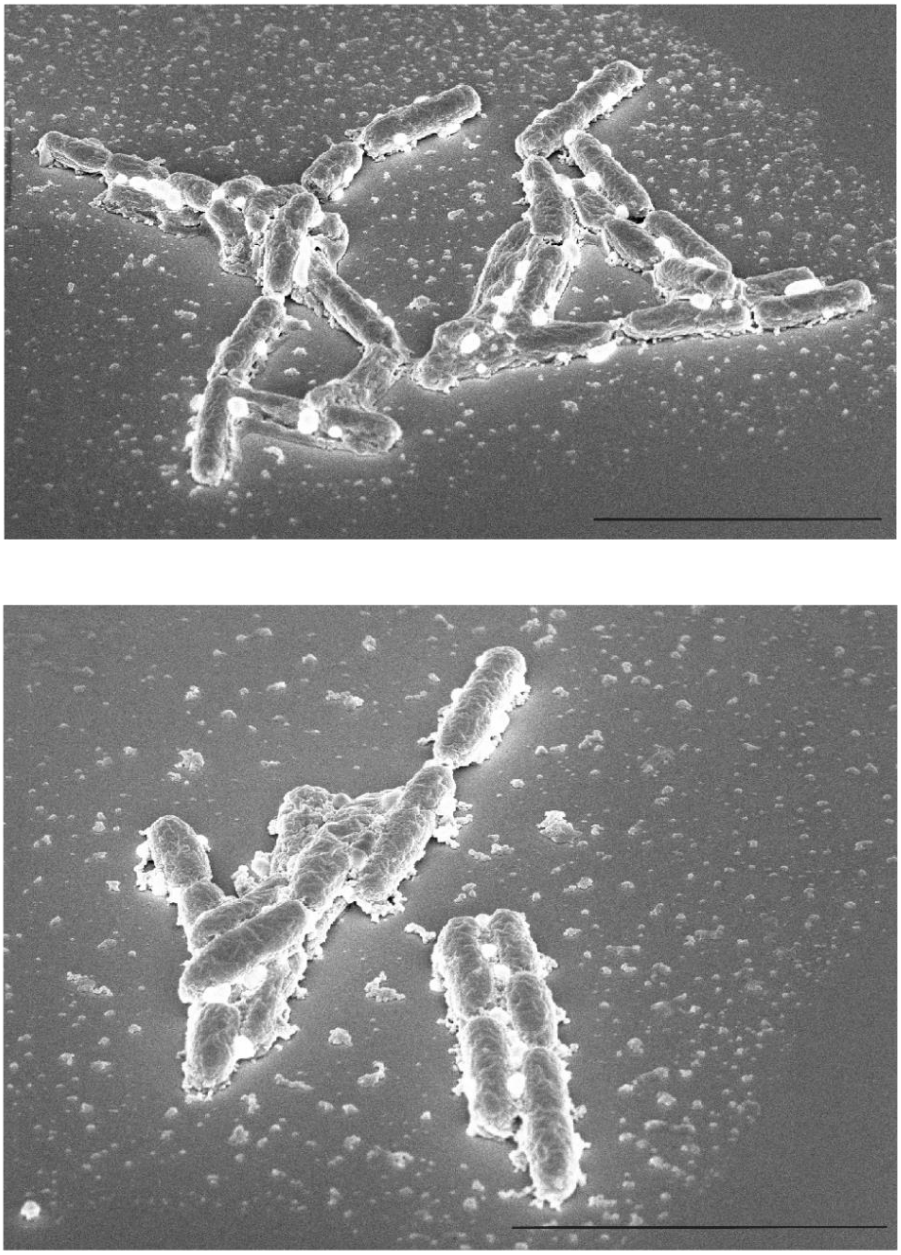

Figure 4.19. *E. coli* treatment with LL-37 and H2A causes membrane blebbing. Scanning electron microscopy (SEM) images of *E. coli* treated with 10 μg/mL H2A and 1 μM LL-37 in medium containing 1 mM magnesium. Mid-exponential phase *E. coli* were grown, diluted 1:20, and supplemented with 10 μg/mL H2A and 1 μM LL-37. Cells were treated for 1 hour and added to a glass bottomed petri dish for 15 minutes. Following adhesion to the glass bottomed petri dish, media was removed and 4% paraformaldehyde (PFA) was added for 20 minutes to fix bacteria. Dehydration was performed with serial ethanol dilutions. The fixed and dehydrated sampled were coated with 10 nm of iridium using an ACE600 sputter coater before characterization using a FEI Magellan 400 XHR Scanning Electron Microscope at a 45° tilt angle with an acceleration voltage of 3kV. Scale bars represent 5 μm. Imaging assistance was provided by Rachel Rosenzweig.

The individual effects of histones were observed using increasing histone concentrations. Mid-exponential phase *E. coli* were diluted 1:20 into fresh MinA media, treated with 0-100 μg/mL H2A, and incubated for 1 hour before immobilization on a 1% agarose pad and imaging using phase contrast microscopy. Although the range of histone concentrations used included higher concentrations than utilized in other experiments, including 50 and 100 μg/mL H2A, these increasing concentrations revealed general trends in the physiological effects of histones. Additionally, it is feasible that similar or higher concentrations of histones may occur locally in NETs or upon release from lipid droplets.

Increasing concentrations of H2A caused bacterial aggregation, frequently by fusing the poles of the cells together (Figure 4.20). Minimal aggregation was seen with the addition of 10 μg/mL H2A; however, the addition of 25 μg/mL or 50 μg/mL induced significant bacterial aggregation. This phenomenon is not due to inhibition of cell division, as aggregates contain many more cells linked together than can be grown in 1 hour in minimal medium (Figure 4.20). This could potentially result from a charge interaction at the poles. Previous reports have noted that positively charged molecules accumulate at the bacterial cell poles, where the Gaussian curvature is highest[44,45].The bacterial aggregation here may be explained by large positive charge accumulation on the outside of the cells at the poles.

This pattern is consistent with the observation of bacterial aggregation at chronic wound sites[46] and could be related to the mechanism underlying host-induced bacterial aggregation. Whether this serves to promote bacterial survival remains to be fully understood. Previous reports have noted that *Klebsiella pneumoniae* can form small clumps of antibiotic-resistant bacteria within a two-hour time period in moving liquid[47]. Alternatively, clumping has been shown to be beneficial

from a host standpoint: by mediating cross-linking of dividing bacteria, IgA accelerates clearance from the gut lumen and protects against infection[48].

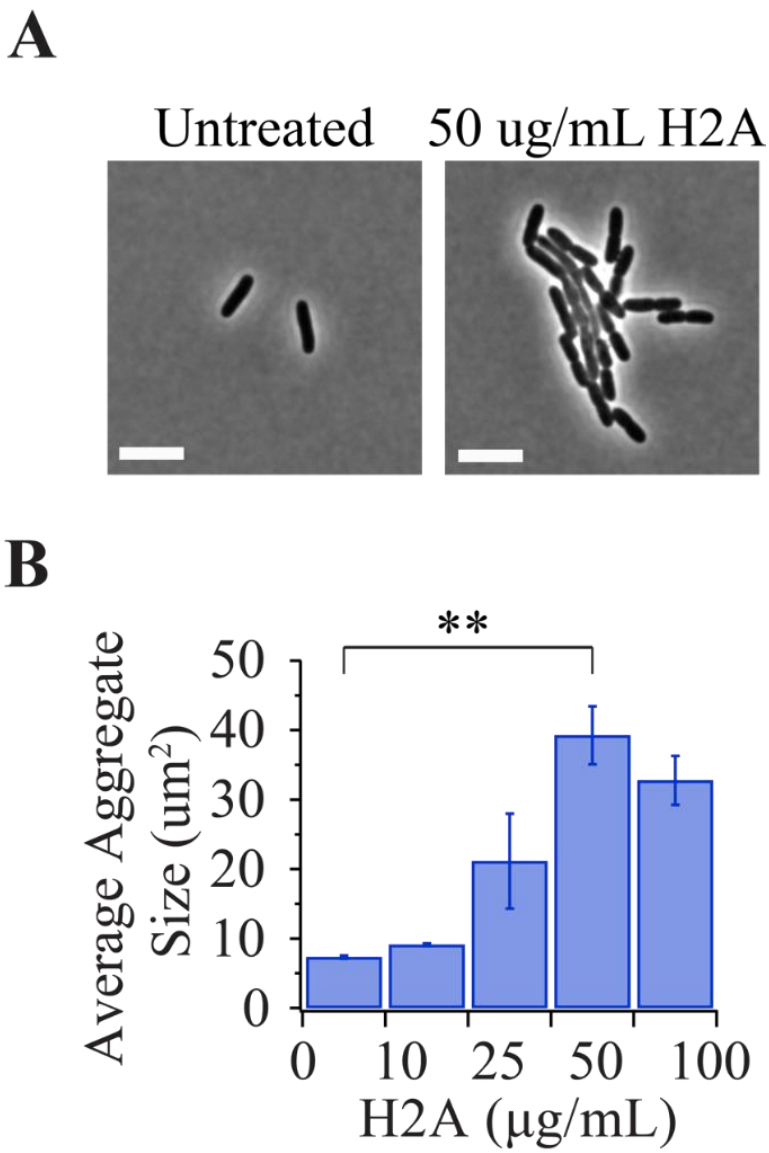

Figure 4.20. Histone H2A induces bacterial aggregation. Mid-exponential phase *E. coli* were diluted 1:20 into fresh MinA media, treated with 0-100 µg/mL H2A, and incubated for 1 hour before immobilization on an agarose pad. Histone-induced cell aggregation was observed by phase contrast microscopy (A) and measured through an image analysis (B). Cell size was converted from pixels to μm^2 by multiplying the pixel value by a factor of 0.004225. Representative images are shown for untreated (0 µg/mL H2A) and 50 µg/mL H2A-treated *E. coli*. Bars indicate mean ± SEM for three independent experiments. ** $p \leq 0.01$. Scale bars represent 3 µm.

Similarly, the individual effects of LL-37 were observed using increasing LL-37 concentrations. Mid-exponential phase *E. coli* were diluted 1:20 into fresh MinA media, treated with 0-4 μM LL-37, and incubated for 1 hour before immobilization on a 1% agarose pad and imaging using phase contrast microscopy. 0.5 μM LL-37 is roughly equivalent to the concentration of LL-37 found on unstimulated mucosal surfaces, whereas 4 μM LL-37 is approximately one-third of the concentration of LL-37 found in inflamed epithelium[19]. Treatment with LL-37 alone did not induce bacterial aggregation. Instead, concentrations in excess of 0.5 μM LL-37 induced a significant reduction in cell size, consistent with permeabilization of the inner and outer bacterial membrane (Figure 4.21).

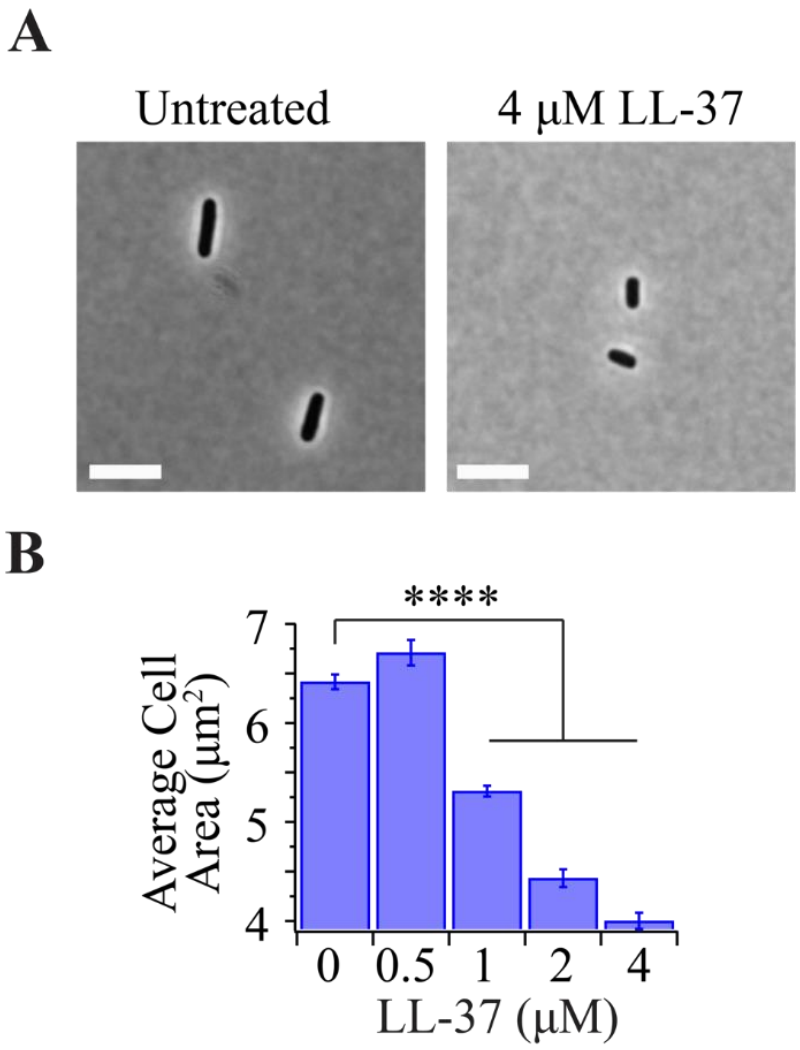

Figure 4.21. LL-37 reduces bacterial cell size. Mid-exponential phase *E. coli* were diluted 1:20 into fresh MinA media, treated with 0-4 μM LL-37, and incubated for 1 hour before immobilization on an agarose pad. Cell size following LL-37 treatment was observed by phase contrast microscopy (A) and measured through an image analysis (B). Cell size was converted from pixels to μm^2 by multiplying the pixel value by a factor of 0.004225. Representative images are shown for untreated (0 μM LL-37) and 4 μM LL-37-treated *E. coli*. Bars indicate mean ± SEM for three independent experiments. **** $p \leq 0.0001$. Scale bars represent 3 μm.

The dual effects of LL-37 and H2A on bacterial cell size were observed using the concentrations used in growth profile experiments (Figure 4.7A). Mid-exponential phase *E. coli* were diluted 1:20 into fresh MinA media, treated with 10 μg/mL H2A, 2 μM LL-37, or the combination of 10 μg/mL H2A and 2 μM LL-37, and incubated for 1 hour before immobilization on a 1% agarose pad and imaging using phase contrast microscopy.

The H2A/LL-37 dual treatment caused a dramatic reduction in cell size compared to untreated *E. coli* (Figure 4.20). This decrease in cell size is consistent with a model in which LL-37 and H2A increasingly disrupt the bacterial membrane, enabling the efflux of cytoplasmic components out of the cell, as observed in the dual-treated SEM images (Figure 4.22).

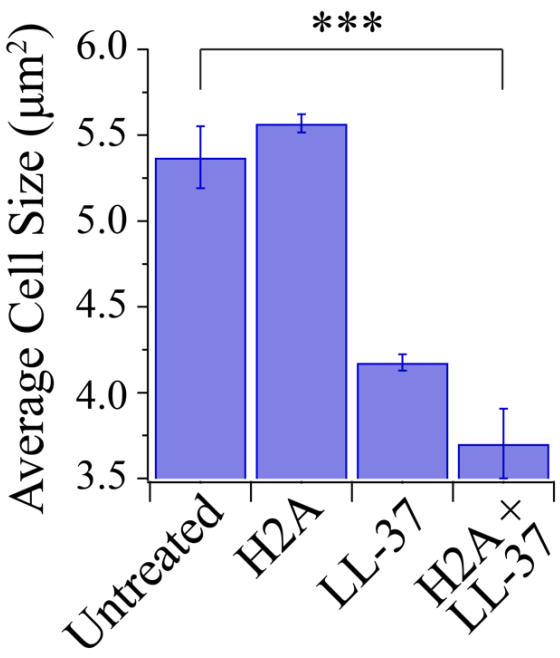

Figure 4.22. Dual treatment of H2A and LL-37 dramatically decreases cell size. Mid-exponential phase *E. coli* were diluted 1:20 into fresh MinA media, treated with 10 μg/mL H2A, 2 μM LL-37, or the combination of 10 μg/mL H2A and 2 μM LL-37, and incubated for 1 hour before immobilization on an agarose pad. Cell size was converted from pixels to μm^2 by multiplying the pixel value by a factor of 0.004225. Bars indicate mean ± SEM for three independent experiments. *** $p \leq 0.001$.

4.7 Conclusion

In physiological ionic conditions, H2A synergizes with the AMP LL-37 to kill Gram-negative *E. coli* and Gram-positive *S. aureus*, regardless of the phase of the bacteria. Since LL-37 disrupts lipid bilayers through the formation of toroidal pores, synergies between LL-37 and H2A support a mechanism by which low levels of LL-37 disrupt the microbial membrane by inducing pore formation, increasing histone-mediated killing of bacteria. This increased membrane permeabilization may enable increased amounts of histones to enter the bacterial cell, where histones may have an intracellular target. Alternatively, histones may interact with AMP-formed pores to kill bacteria.

Synergy was also observed between H2A and the pentabasic peptide antibiotic polymyxin B, which permeabilizes the bacterial membrane and promotes self-uptake, and H2A and the African claw frog AMP magainin-2, which forms 2-3 nm toroidal pores in the bacterial membrane. These synergies between polymyxin B and H2A and magainin-2 and H2A further support a mechanism where a membrane-permeabilizing agent induces pore formation and enables uptake of histones, increasing histone-mediated killing of bacteria.

Since histones synergize with numerous pore-forming agents, including LL-37, PMB, and MAG2, this mechanism appears to be general in nature. Additionally, since histones synergize with MAG2, this mechanism is not limited to mammalian AMPs. The synergistic killing of bacteria by histones and pore-forming AMPs may represent a mechanism of the innate immune system which spans across multiple species.

Individual treatments revealed LL-37 and H2A have distinct physiological effects on *E. coli*. Increasing concentrations of H2A induced aggregation of cells, often by fusing the poles of cells together. Treatment with increasing concentrations of LL-37 did not induce bacterial aggregation

and instead induced a significant reduction in cell size. Low levels of H2A and LL-37 induced striking physiological effects on *E. coli* at the sub-cellular level. SEM imaging revealed the combined treatment of LL-37 and H2A caused extensive cellular damage, including membrane permeabilization, cell aggregation, and the extensive production of insoluble components to the outer surface of the membrane and to the surrounding surfaces. This H2A/LL-37 dual treatment is accompanied by a dramatic decrease in cell size, consistent with a mechanism by which H2A and LL-37 induce membrane permeabilization, enabling the efflux of cytoplasmic components out of the cell.

4.8 References

1. Anand, P. *et al.* A novel role for lipid droplets in the organismal antibacterial response. *eLife* **1**, (2012).
2. Hancock, R. E. W. & Sahl, H.-G. Antimicrobial and host-defense peptides as new anti-infective therapeutic strategies. *Nat. Biotechnol.* **24**, 1551–1557 (2006).
3. Tagai, C., Morita, S., Shiraishi, T., Miyaji, K. & Iwamuro, S. Antimicrobial properties of arginine- and lysine-rich histones and involvement of bacterial outer membrane protease T in their differential mode of actions. *Peptides* **32**, 2003–2009 (2011).
4. Morita, S., Tagai, C., Shiraishi, T., Miyaji, K. & Iwamuro, S. Differential mode of antimicrobial actions of arginine-rich and lysine-rich histones against Gram-positive Staphylococcus aureus. *Peptides* **48**, 75–82 (2013).
5. Patrzykat, A., Friedrich, C. L., Zhang, L., Mendoza, V. & Hancock, R. E. W. Sublethal concentrations of pleurocidin-derived antimicrobial peptides inhibit macromolecular synthesis in Escherichia coli. *Antimicrob. Agents Chemother.* **46**, 605–614 (2002).
6. Podda, E. *et al.* Dual mode of action of Bac7, a proline-rich antibacterial peptide. *Biochim. Biophys. Acta* **1760**, 1732–1740 (2006).
7. Yu, G., Baeder, D. Y., Regoes, R. R. & Rolff, J. Combination Effects of Antimicrobial Peptides. *Antimicrob. Agents Chemother.* **60**, 1717–1724 (2016).
8. Patrzykat, A., Zhang, L., Mendoza, V., Iwama, G. K. & Hancock, R. E. W. Synergy of Histone-Derived Peptides of Coho Salmon with Lysozyme and Flounder Pleurocidin. *Antimicrobial Agents and Chemotherapy* **45**, 1337–1342 (2001).
9. Loewe, S. The problem of synergism and antagonism of combined drugs. *Arzneimittelforschung* **3**, 285–290 (1953).
10. Sørensen, O. E. *et al.* Human cathelicidin, hCAP-18, is processed to the antimicrobial peptide LL-37 by extracellular cleavage with proteinase 3. *Blood* **97**, 3951–3959 (2001).
11. Kahlenberg, J. M., Carmona-Rivera, C., Smith, C. K. & Kaplan, M. J. Neutrophil Extracellular Trap-Associated Protein Activation of the NLRP3 Inflammasome Is Enhanced in Lupus Macrophages. *The Journal of Immunology* **190**, 1217–1226 (2013).
12. Cowland, J. B., Johnsen, A. H. & Borregaard, N. hCAP-18, a cathelin/pro-bactenecin-like protein of human neutrophil specific granules. *FEBS Lett.* **368**, 173–176 (1995).
13. Sørensen, O., Cowland, J. B., Askaa, J. & Borregaard, N. An ELISA for hCAP-18, the cathelicidin present in human neutrophils and plasma. *Journal of Immunological Methods* **206**, 53–59 (1997).
14. Sørensen, O., Bratt, T., Johnsen, A. H., Madsen, M. T. & Borregaard, N. The human antibacterial cathelicidin, hCAP-18, is bound to lipoproteins in plasma. *J. Biol. Chem.* **274**, 22445–22451 (1999).
15. Henzler Wildman, K. A., Lee, D.-K. & Ramamoorthy, A. Mechanism of Lipid Bilayer Disruption by the Human Antimicrobial Peptide, LL-37. *Biochemistry* **42**, 6545–6558 (2003).
16. Turner, J., Cho, Y., Dinh, N. N., Waring, A. J. & Lehrer, R. I. Activities of LL-37, a cathelin-associated antimicrobial peptide of human neutrophils. *Antimicrob. Agents Chemother.* **42**, 2206–2214 (1998).
17. Sochacki, K. A., Barns, K. J., Bucki, R. & Weisshaar, J. C. Real-time attack on single Escherichia coli cells by the human antimicrobial peptide LL-37. *Proceedings of the National Academy of Sciences* **108**, E77–E81 (2011).

18. Zanetti, M. Cathelicidins, multifunctional peptides of the innate immunity. *Journal of Leukocyte Biology* **75**, 39–48 (2004).
19. Bals, R., Wang, X., Zasloff, M. & Wilson, J. M. The peptide antibiotic LL-37/hCAP-18 is expressed in epithelia of the human lung where it has broad antimicrobial activity at the airway surface. *Proc. Natl. Acad. Sci. U.S.A.* **95**, 9541–9546 (1998).
20. Nagaoka, I., Hirota, S., Yomogida, S., Ohwada, A. & Hirata, M. Synergistic actions of antibacterial neutrophil defensins and cathelicidins. *Inflamm. Res.* **49**, 73–79 (2000).
21. Gupta, K., Singh, S. & van Hoek, M. Short, Synthetic Cationic Peptides Have Antibacterial Activity against Mycobacterium smegmatis by Forming Pores in Membrane and Synergizing with Antibiotics. *Antibiotics* **4**, 358–378 (2015).
22. Wang, G. Structures of Human Host Defense Cathelicidin LL-37 and Its Smallest Antimicrobial Peptide KR-12 in Lipid Micelles. *Journal of Biological Chemistry* **283**, 32637–32643 (2008).
23. Johansson, J., Gudmundsson, G. H., Rottenberg, M. E., Berndt, K. D. & Agerberth, B. Conformation-dependent Antibacterial Activity of the Naturally Occurring Human Peptide LL-37. *Journal of Biological Chemistry* **273**, 3718–3724 (1998).
24. Kohanski, M. A., Dwyer, D. J. & Collins, J. J. How antibiotics kill bacteria: from targets to networks. *Nature Reviews Microbiology* **8**, 423–435 (2010).
25. Kohanski, M. A., Dwyer, D. J., Wierzbowski, J., Cottarel, G. & Collins, J. J. Mistranslation of Membrane Proteins and Two-Component System Activation Trigger Antibiotic-Mediated Cell Death. *Cell* **135**, 679–690 (2008).
26. Hancock, R. E., Farmer, S. W., Li, Z. S. & Poole, K. Interaction of aminoglycosides with the outer membranes and purified lipopolysaccharide and OmpF porin of Escherichia coli. *Antimicrobial Agents and Chemotherapy* **35**, 1309–1314 (1991).
27. John, T. *et al.* How kanamycin A interacts with bacterial and mammalian mimetic membranes. *Biochimica et Biophysica Acta (BBA) - Biomembranes* **1859**, 2242–2252 (2017).
28. Pletnev, P., Osterman, I., Sergiev, P., Bogdanov, A. & Dontsova, O. Survival guide: Escherichia coli in the stationary phase. *Acta Naturae* **7**, 22–33 (2015).
29. Gefen, O., Fridman, O., Ronin, I. & Balaban, N. Q. Direct observation of single stationary-phase bacteria reveals a surprisingly long period of constant protein production activity. *Proceedings of the National Academy of Sciences* **111**, 556–561 (2014).
30. Agrawal, A., Rangarajan, N. & Weisshaar, J. C. Resistance of early stationary phase E. coli to membrane permeabilization by the antimicrobial peptide Cecropin A. *Biochimica et Biophysica Acta (BBA) - Biomembranes* **1861**, 182990 (2019).
31. Neidhardt, F. C. Apples, oranges and unknown fruit. *Nat Rev Microbiol* **4**, 876–876 (2006).
32. Storm, D. R., Rosenthal, K. S. & Swanson, P. E. Polymyxin and Related Peptide Antibiotics. *Annual Review of Biochemistry* **46**, 723–763 (1977).
33. Shaheen, M., Li, J., Ross, A. C., Vederas, J. C. & Jensen, S. E. Paenibacillus polymyxa PKB1 Produces Variants of Polymyxin B-Type Antibiotics. *Chemistry & Biology* **18**, 1640–1648 (2011).
34. Hancock, R. E. Peptide antibiotics. *The Lancet* **349**, 418–422 (1997).
35. Zhang, L., Dhillon, P., Yan, H., Farmer, S. & Hancock, R. E. W. Interactions of Bacterial Cationic Peptide Antibiotics with Outer and Cytoplasmic Membranes of Pseudomonas aeruginosa. *Antimicrobial Agents and Chemotherapy* **44**, 3317–3321 (2000).

36. Zasloff, M. Magainins, a class of antimicrobial peptides from Xenopus skin: isolation, characterization of two active forms, and partial cDNA sequence of a precursor. *Proceedings of the National Academy of Sciences* **84**, 5449–5453 (1987).
37. Michael Conlon, J., Mechkarska, M. & King, J. D. Host-defense peptides in skin secretions of African clawed frogs (Xenopodinae, Pipidae). *General and Comparative Endocrinology* **176**, 513–518 (2012).
38. Gesell, J., Zasloff, M. & Opella, S. J. Two-dimensional 1H NMR experiments show that the 23-residue magainin antibiotic peptide is an alpha-helix in dodecylphosphocholine micelles, sodium dodecylsulfate micelles, and trifluoroethanol/water solution. *J. Biomol. NMR* **9**, 127–135 (1997).
39. Matsuzaki, K. Magainins as paradigm for the mode of action of pore forming polypeptides. *Biochim. Biophys. Acta* **1376**, 391–400 (1998).
40. Huang, H. W. Molecular mechanism of antimicrobial peptides: the origin of cooperativity. *Biochim. Biophys. Acta* **1758**, 1292–1302 (2006).
41. Imura, Y., Choda, N. & Matsuzaki, K. Magainin 2 in Action: Distinct Modes of Membrane Permeabilization in Living Bacterial and Mammalian Cells. *Biophysical Journal* **95**, 5757–5765 (2008).
42. Imura, Y., Nishida, M. & Matsuzaki, K. Action mechanism of PEGylated magainin 2 analogue peptide. *Biochimica et Biophysica Acta (BBA) - Biomembranes* **1768**, 2578–2585 (2007).
43. Moorman, A. P. M., de Laaf, R. T. M., Destrée, O. H. J., Telford, J. & Birnstiel, M. L. Histone genes from Xenopus laevis: molecular cloning and initial characterization. *Gene* **10**, 185–193 (1980).
44. Huang, K. C. & Ramamurthi, K. S. Macromolecules that prefer their membranes curvy: Curvature-dependent localization of macromolecules. *Molecular Microbiology* **76**, 822–832 (2010).
45. Lenarcic, R. *et al.* Localisation of DivIVA by targeting to negatively curved membranes. *EMBO J* **28**, 2272–2282 (2009).
46. Secor, P. R., Michaels, L. A., Ratjen, A., Jennings, L. K. & Singh, P. K. Entropically driven aggregation of bacteria by host polymers promotes antibiotic tolerance in *Pseudomonas aeruginosa*. *Proceedings of the National Academy of Sciences* **115**, 10780–10785 (2018).
47. Thornton, M. M. *et al.* Multicellularity and Antibiotic Resistance in Klebsiella pneumoniae Grown Under Bloodstream-Mimicking Fluid Dynamic Conditions. *The Journal of Infectious Diseases* **206**, 588–595 (2012).
48. Moor, K. *et al.* High-avidity IgA protects the intestine by enchaining growing bacteria. *Nature* **544**, 498–502 (2017).

Chapter 5: Histone H2A and AMPs Have Distinct Activities that Increase the Intracellular Concentration of the Other Molecule and Induce Persistent Membrane Damage

Although the addition of 10 μg/mL histone H2A has no effect on Gram-negative or Gram-positive bacteria growing in physiological concentrations of magnesium, Histone H2A synergizes with low concentrations of the membrane-permeabilizing human AMP LL-37, which disrupts lipid bilayers through the formation of toroidal pores[1]. The synergy between LL-37 and H2A supports a mechanism by which disruption of the bacterial membrane and pore formation increases histone-mediated killing of bacteria. PI staining revealed that increased membrane permeabilization accompanied the bacterial growth inhibition seen upon bacterial treatment with the synergistic combination of LL-37 and H2A in physiological ionic environments. I hypothesized that this synergistic interaction supports a mechanism by which disruption of the bacterial membrane and pore formation increases histone-mediated killing of bacteria, presumably through increased entry of histones into the bacterial cell.

Histone H2A showed additional synergies with the pentabasic peptide antibiotic polymyxin B, which permeabilizes the bacterial membrane and promotes self-uptake, and the African claw frog AMP magainin-2, which forms 2-3 nm toroidal pores in the bacterial membrane. These synergies between H2A and other pore-forming agents further support a mechanism where a membrane-permeabilizing agent induces pore formation and enables uptake of histones and increased histone-mediated killing of bacteria.

5.1 Membrane-Permeabilizing Agents Promote Uptake of Histone H2A

In conditions of low magnesium, LPS interactions are disrupted and the integrity of the bacterial membrane is compromised[2,3]. Under these low ionic conditions, positively charged histones can interact with the bacterial membrane, further compromising membrane integrity (Figure 3.5). Although the antimicrobial activity of histones is seen at concentrations of 10 μg/mL histone H2A in low ionic environments, this concentration of histones has no effect on bacterial growth profiles in a physiological ionic environment. Furthermore, increased PI fluorescence was associated with histone treatment in low ionic environments, but not physiological ionic environments. Additionally, low magnesium conditions alone were not sufficient to induce membrane permeabilization. This supports a mechanism by which histones permeabilize the bacterial membrane under conditions of low ionic concentrations, facilitating the antimicrobial activity of histones.

Similarly, the antimicrobial activity of histones was increased in physiological ionic environments upon addition of membrane-permeabilizing agents, including LL-37, PMB, and MAG2 (Chapter 4). This antimicrobial activity was similarly associated with an increase in membrane permeabilization, suggesting the antimicrobial effects of histones are dependent on membrane permeabilization. I hypothesized that increased membrane permeabilization facilitates histone-mediated killing of bacteria through increased uptake of histones into the cytoplasm of the bacteria.

To track the localization dynamics of H2A, I fluorescently labeled the primary amines of Histone H2A with Alexa Fluor 488 NHS Ester (AF-H2A). Briefly, 10 mg of H2A was dissolved in 1 mL of 0.1 M sodium bicarbonate buffer. 50 μL Alexa Fluor dye, dissolved in DMSO (10 mg/mL), was added, and the solution continuously stirred at room temperature for 1 hour. A PD

MidiTrap G-25 column was equilibrated with Milli-Q water and used to remove unreacted Alexa Fluor.

Before conducting AF-H2A localization experiments, I confirmed the bactericidal activity of AF-H2A using growth inhibition assays. As previously seen with unlabeled H2A, the addition of AF-H2A had minimal effects on *E. coli* growth. The addition of LL-37 extended the lag phase and slowed exponential growth rates, as previously observed. The dual treatment of AF-H2A and LL-37 synergized to kill *E. coli*, significantly decreasing growth rates and extending lag times compared to untreated or LL-37-treated samples (Figure 5.1).

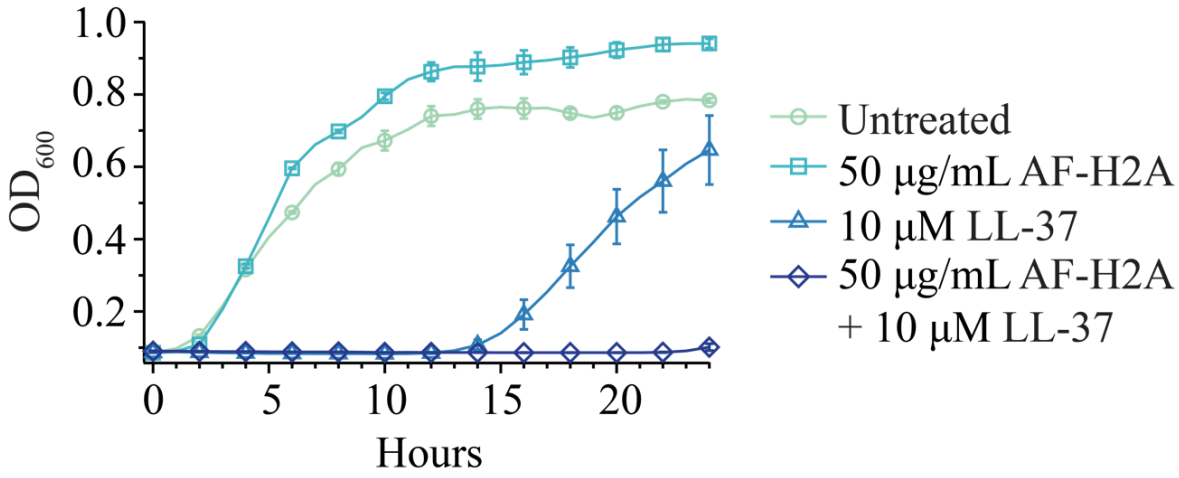

Figure 5.1. Fluorescently-labeled H2A (AF-H2A) synergizes with LL-37 to kill *E. coli*. Growth profiles of mid-exponential phase *E. coli* treated with 50 µg/mL AF-H2A, 10 µM LL-37, or the dual combination of AF-H2A and LL-37 in media containing physiological (1 mM) magnesium over a 24-hour growth period. The addition of AF-H2A has minimal effects on *E. coli* growth in the physiological concentration of magnesium. As previously observed with unlabeled H2A, AF-H2A and LL-37 synergize to kill *E. coli*, significantly decreasing growth rates and extending lag times compared to untreated or LL-37-treated samples. Data points in are the average of four independent experiments (n = 4) and error bars indicate SEM.

To quantify cytoplasmic uptake of histones in the presence of membrane-permeabilizing agents, exponential-phase *E. coli* were diluted into fresh MinA media with 10 μg/mL AF-H2A (1% Alexa Fluor-labeled H2A mixed with 99% unlabeled H2A), in the presence of 2 μM LL-37, 1 μg/mL polymyxin B, 50 μg/mL kanamycin, or 10 μg/mL chloramphenicol. 1% Alexa Fluor-labeled H2A mixed was mixed with 99% unlabeled H2A to decrease GFP fluorescence intensity. After a 1-hour incubation, GFP fluorescence was analyzed using fluorescence microscopy. Experiments were repeated with *S. aureus* using 10 μg/mL AF-H2A, in the presence or absence of 2 μM LL-37.

Treatment of *E. coli* with AF-H2A alone produced little fluorescence following background subtraction (Figure 5.2, 5.3), indicating the lack of incorporation of H2A into the cell. This is consistent with the result that histone concentrations of 10 μg/mL do not induce permeabilization of the membrane in medium containing physiological magnesium (Figure 4.10). Treatment with the antibiotics kanamycin or chloramphenicol did not induce AF-H2A uptake (Figure 5.3), consistent with these lack of membrane permeabilization observed in PI fluorescence measurements (Figure 4.11) and absence of synergy with histones in growth profiles (Figure 4.8, 4.9).

In contrast, membrane permeabilization by LL-37 or polymyxin B (PMB) enhanced AF-H2A uptake (Figure 5.2, 5.3A) in *E. coli*. Similar results were seen with *S. aureus.* Membrane permeabilization by LL-37 enhanced AF-H2A uptake in *S. aureus* (Figure 5.3B). Coupled with the growth dynamics findings visualized in the growth curves (Figure 4.7, 4.12), these results indicate that H2A-mediated growth inhibition via synergy and membrane permeabilization are concomitant with the uptake of H2A into the bacterial cell.

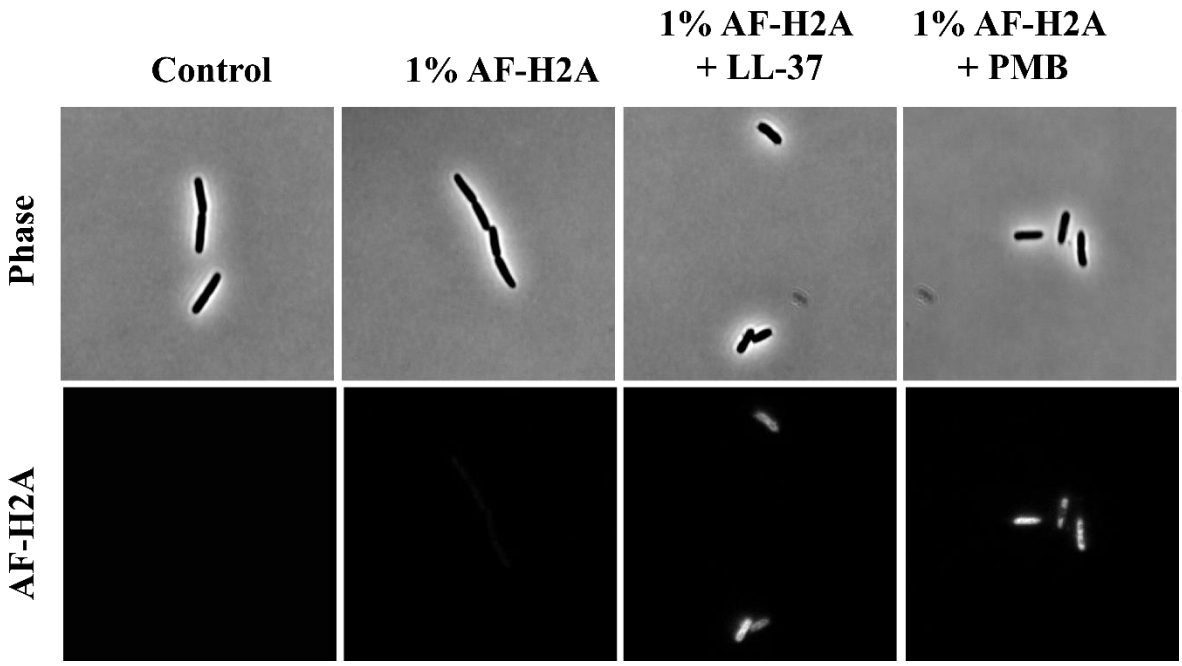

Figure 5.2. Fluorescence and phase contrast images of *E. coli* treated with fluorescently-labeled H2A (AF-H2A) alone or in combination with LL-37 or PMB. Mid-exponential phase *E. coli* were treated with 10 μg/mL H2A alone or with 2 μM LL-37 or 1 μg/mL PMB. AF-H2A was mixed with unlabeled H2A to decrease fluorescence intensity (1% AF-H2A, 99% unlabeled H2A). Phase and GFP images were taken after a 1-hour incubation. Representative images are shown for each condition.

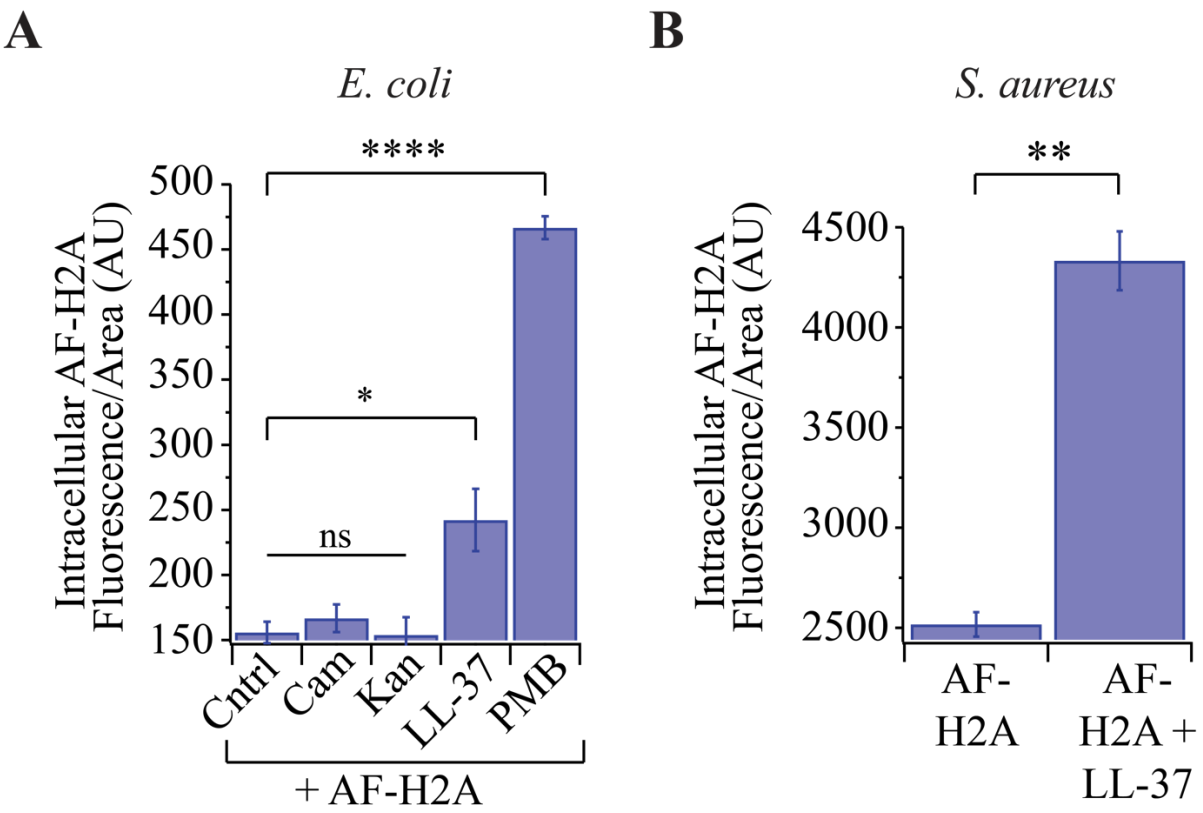

Figure 5.3. Intracellular fluorescence intensities of *E. coli* or *S. aureus* treated with AF-H2A and chloramphenicol, kanamycin, LL-37, or polymyxin B. Mid-exponential phase *E. coli* were treated with 10 μg/mL AF-H2A (1% AF-H2A, 99% unlabeled H2A) alone or with 10 μg/mL chloramphenicol (Cam), 50 μg/mL kanamycin (Kan), 2 μM LL-37, or 1 μg/mL polymyxin B (PMB) (A). Mid-exponential phase *S. aureus* were treated with 10 μg/mL AF-H2A alone or with 2 μM LL-37 (B). GFP fluorescence was measured after 1-hour incubation. Bars indicate background-subtracted mean ± SEM for three independent experiments. **** $p \leq 0.0001$, ** $p \leq 0.01$, * $p \leq 0.05$, ns > 0.05.

Similar results were observed with the combinatorial treatment of 10 μg/mL H2A and 10 μM magainin-2. Exponential-phase *E. coli* were diluted into fresh MinA media with 10 μg/mL AF-H2A, in the presence or absence of 10 μM MAG2, for a 1-hour incubation period. Whereas treatment of *E. coli* with AF-H2A alone produced little fluorescence (Figure 5.4, 5.5), membrane permeabilization by MAG2 enhanced AF-H2A uptake. Together with the decrease in bacterial growth visualized in the growth curves of *E. coli* treated with H2A and MAG2 (Figure 4.16) and the increase in membrane permeabilization upon dual treatment (Figure 4.17), the increased uptake of H2A into the bacterial cell is consistent with a mechanism by which the uptake of histones into the bacterial cytoplasm increases histone-mediated killing of bacteria.

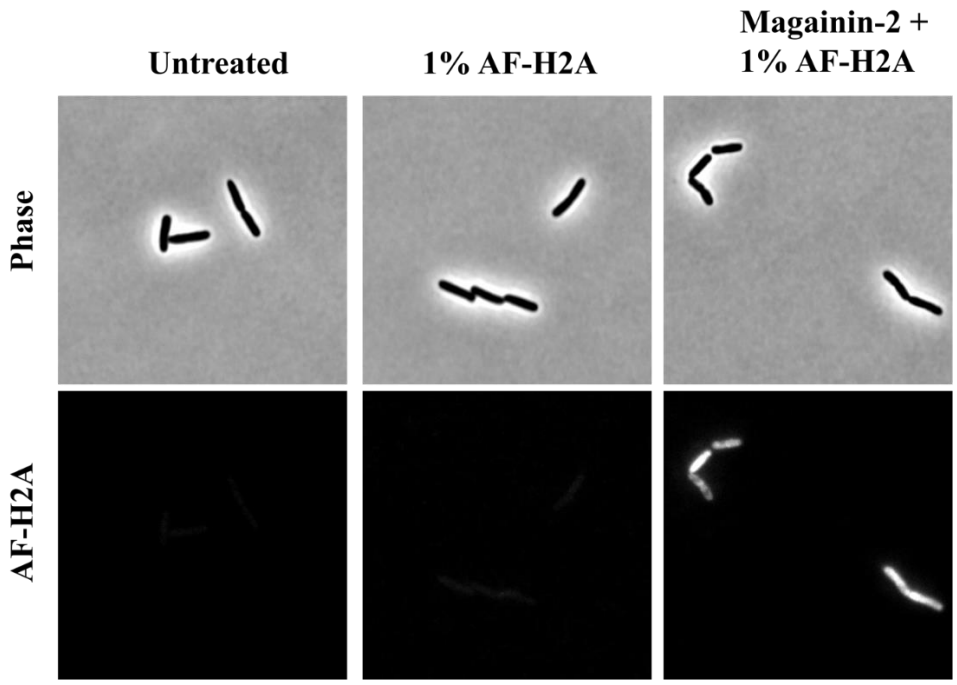

Figure 5.4. Fluorescence and phase contrast images of *E. coli* treated with fluorescently-labeled H2A (AF-H2A) alone or in combination with magainin-2. Mid-exponential phase *E. coli* were treated with 10 μg/mL H2A alone or with 10 μM magainin-2. AF-H2A was mixed with unlabeled H2A to decrease fluorescence intensity (1% AF-H2A, 99% unlabeled H2A). Phase and GFP fluorescence images were taken after a 1-hour incubation. Representative images are shown for each condition.

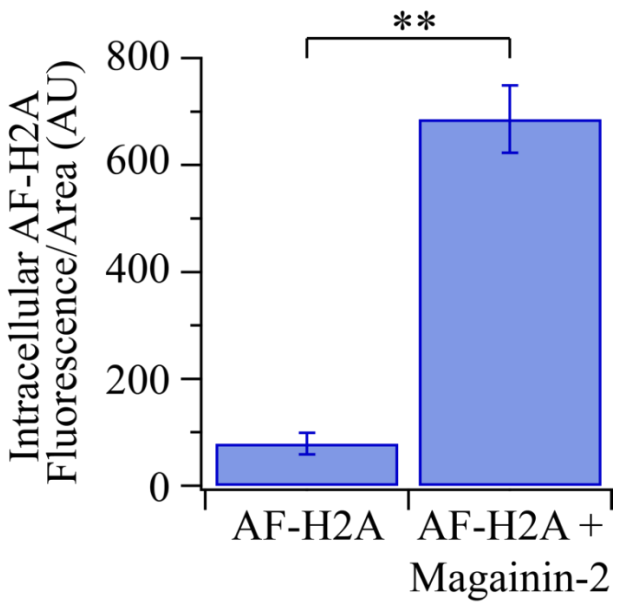

Figure 5.5. Intracellular fluorescence intensities of *E. coli* treated with AF-H2A and magainin-2. Mid-exponential phase *E. coli* were treated with 10 μg/mL AF-H2A (1% AF-H2A, 99% unlabeled H2A) alone or with 10 μM magainin-2. GFP fluorescence was measured after 1-hour incubation. Bars indicate background-subtracted mean ± SEM for at least three independent experiments. ** $p \leq 0.01$.

While treatment of bacteria with 10 μg/mL H2A alone does not induce membrane permeabilization, I hypothesized that H2A could enhance or stabilize membrane pores formed by the membrane-permeabilizing agents, increasing their uptake into the cytoplasm. The effects of H2A on LL-37 uptake into the cytoplasm were quantified using fluorescently-labeled LL-37 (FAM-LL-37).

Exponential-phase *E. coli* or *S. aureus* were diluted into fresh MinA media with 2 μM FAM-LL-37 (1% FAM-LL-37 mixed with 99% unlabeled LL-37), with or without the addition of 10 μg/mL H2A (unlabeled). 1% FAM-LL-37 was mixed with 99% unlabeled LL-37 to decrease GFP fluorescence intensity After a 1-hour incubation period, GFP fluorescence was analyzed using fluorescence microscopy. Treatment of *E. coli* or *S. aureus* with FAM-LL-37 alone produced low levels of fluorescence after background subtraction (Figure 5.6, 5.7). Membrane localization of LL-37 was not observed, consistent with a previous report[4]. As hypothesized, the addition of 10 μg/mL H2A significantly increased uptake of FAM-LL-37 in *E. coli* and *S. aureus*. This is consistent with the result that LL-37 induces membrane permeabilization (Figure 4.11A) and the increased cytoplasmic fluorescence of FAM-LL-37 in the presence of H2A strengthens a mechanism by which H2A enhances or stabilizes membrane pores formed by LL-37.

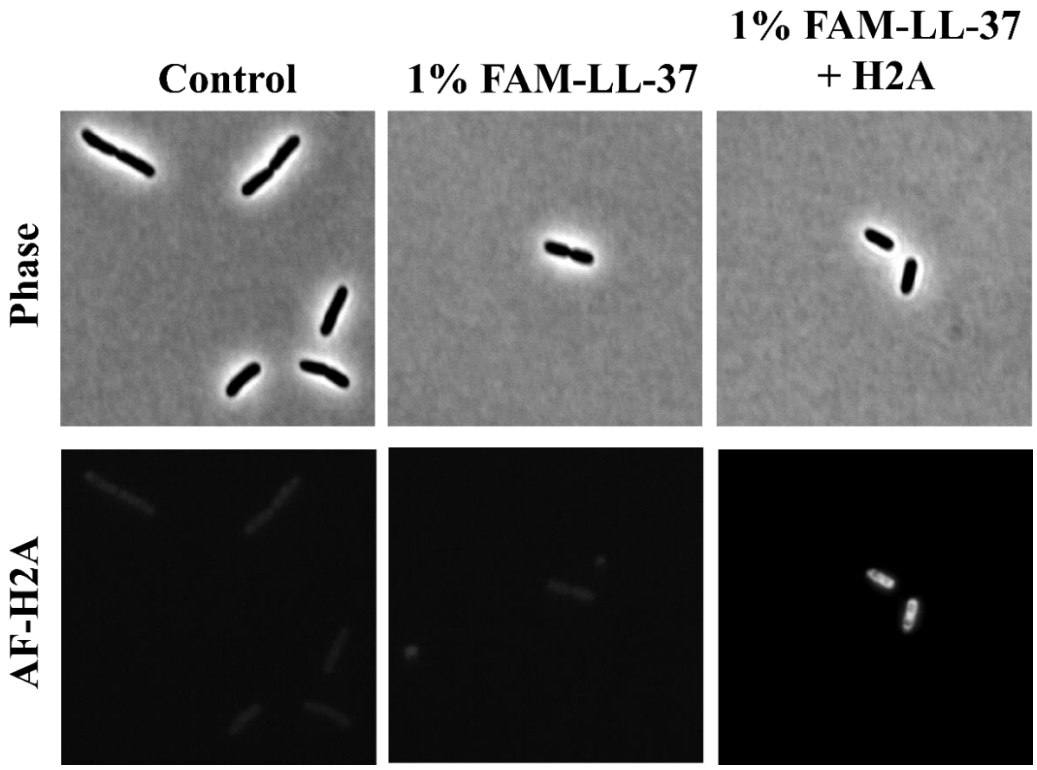

Figure 5.6. Fluorescence and phase contrast images of *E. coli* treated with fluorescently-labeled LL-37 (5-FAM-LL-37) alone or in combination with H2A. Mid-exponential phase *E. coli* were treated with 2 μM FAM-LL-37 alone or with 10 μg/mL H2A. FAM-LL-37 was mixed with unlabeled LL-37 to decrease fluorescence intensity (1% FAM-LL-37, 99% unlabeled LL-37). Phase and GFP fluorescence images were taken after a 1-hour incubation. Representative images are shown for each condition.

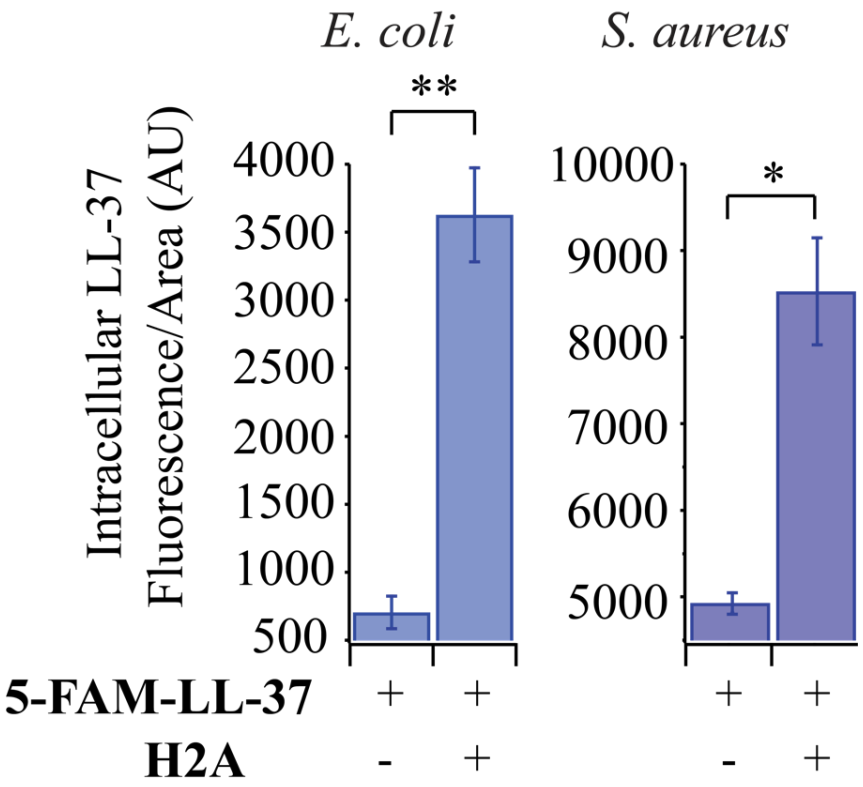

Figure 5.7. Intracellular fluorescence intensities of *E. coli* or *S. aureus* treated with H2A and 5-FAM-LL-37. *E. coli* (A) or *S. aureus* (B) were treated with 2 μM FAM-LL-37 (1% FAM-LL-37, 99% unlabeled LL-37) alone or with 10 μg/mL H2A. GFP fluorescence was measured after a 1-hour incubation period. Bars indicate background-subtracted mean ± SEM for three independent experiments. ** $p \leq 0.01$, * $p \leq 0.05$.

5.2 Histone-Induced Membrane Permeabilization of *E. coli* Increases Intracellular Concentrations of Histones

Since the dual treatment of histones and membrane-permeabilizing agents increased the intracellular concentration of histones, and this increased uptake of H2A into the bacterial cell is concomitant with H2A-mediated growth inhibition via synergy, I hypothesized that increased membrane permeability due to low magnesium similarly facilitates histone entry into the bacterial cell, where the histones may then promote further membrane damage, interact with bacterial DNA, or alter metabolic pathways. Histone treatment in low concentrations of magnesium previously induced membrane instability (Figure 3.5) and low ionic environments were associated with increased histone-mediated killing of stationary-phase *E. coli* (Figure 3.3) and *S. aureus* (Figure 3.4).

Imaging a large enough number of bacteria in the low magnesium conditions became difficult, given an initial 1:1000 dilution of stationary phase bacteria into fresh media in the aforementioned experiments. Thus, I constructed growth curves using exponentially growing *E. coli* (OD_{600} 0.2) diluted 1:20 into MinA media containing 1 μM $MgSO_4$. Stationary phase *E. coli* was first back diluted into MinA media containing physiological concentrations of magnesium and grown to exponential phase. Exponential phase *E. coli* was then diluted 1:20 into MinA media containing physiological concentrations or low concentrations of magnesium, with or without the addition of 10 μg/mL H2A (Figure 3.8). This resulted in a 20-fold difference in magnesium concentration between the physiological (1 mM) magnesium and low (1 μM) magnesium conditions.

E. coli diluted into low magnesium conditions showed similar lag times and comparable exponential growth rates to *E. coli* diluted into physiological magnesium conditions. However, *E. coli* diluted into low magnesium conditions reached stationary phase before *E. coli* diluted into

physiological magnesium conditions and reached a lower OD_{600} after a 24-hour growth period, consistent with previous reports indicating low magnesium conditions decrease bacterial growth[5] and previous experiments performed with stationary phase bacteria (Figure 3.3). As expected, *E. coli* diluted 1:20 in physiological magnesium conditions, with and without 10 μg/mL H2A, showed similar lag times, comparable exponential growth rates, and reached equivalent OD_{600} after a 24-hour growth period. In low magnesium conditions, the addition of 10 μg/mL H2A extended the lag phase and slowed exponential growth rates; however, *E. coli* treated with 10 μg/mL H2A reached an equivalent OD_{600} as untreated *E. coli* diluted into low magnesium conditions after 24 hours (Figure 5.8).

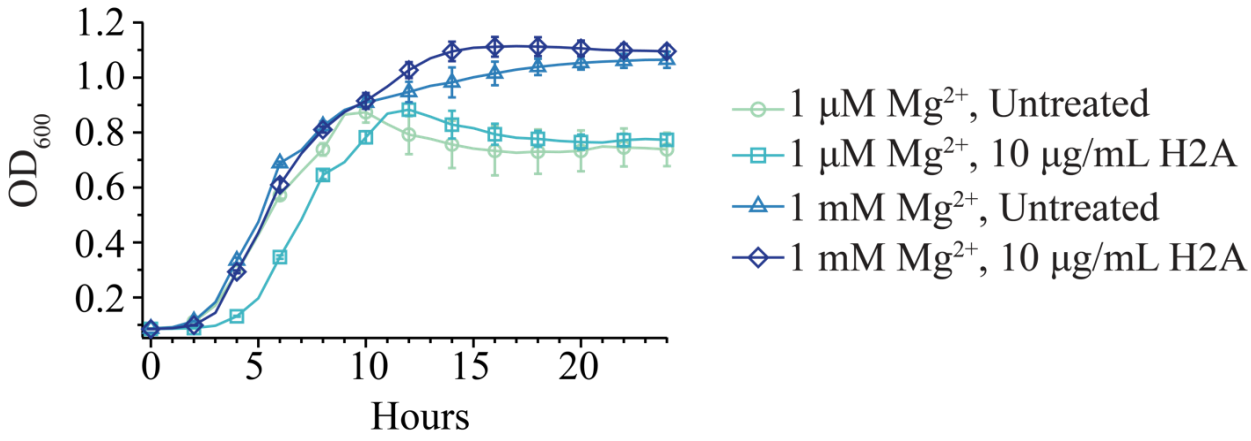

Figure 5.8. Low concentrations of histones kill exponential phase *E. coli* diluted in a low ionic strength condition, but not in a physiological condition. Growth profiles of mid-exponential phase *E. coli* diluted 1:20 into low (1 μM) magnesium and physiological (1 mM) magnesium, with or without 10 μg/mL H2A, over a 24-hour growth period. Histone concentrations of 10 μg/mL H2A extended the lag phase and slowed exponential growth rates for *E. coli* diluted into low magnesium conditions, but not physiological conditions. Bacteria diluted into low magnesium environments reached a lower OD_{600} than bacteria diluted into physiological magnesium environments. Data points are the average of four independent experiments (n=4). Error bars indicate standard error of the mean (SEM).

To identify if histones increased membrane permeabilization under these reduced magnesium conditions, exponential phase *E. coli* were diluted 1:20 into MinA media containing physiological concentrations or low concentrations of magnesium, with or without the addition of 10 μg/mL H2A. Bacteria were cultured with histones for three hours, then incubated with 30 μM propidium iodide (PI) for 15 minutes. Bacteria were plated on 1% agarose-MinA pads and mCherry fluorescence was imaged and quantified (Figure 5.9).

H2A induced PI fluorescence in *E. coli* diluted in low magnesium (Figure 5.9), a condition that inhibited growth in liquid culture (Figure 5.8), suggesting that H2A inhibits growth in this condition by enhancing membrane permeabilization. No PI fluorescence occurred in physiological magnesium environments or in the low magnesium condition without the addition of 10 μg/mL H2A, indicating that these conditions do not induce significant membrane permeabilization (Figure 5.9).

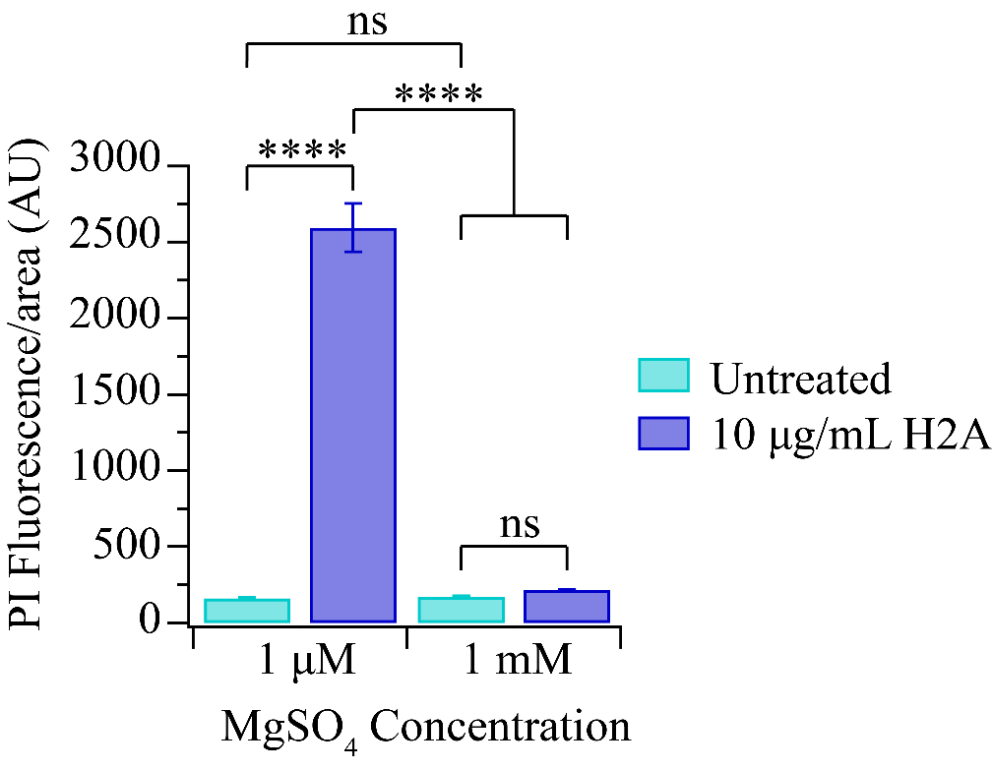

Figure 5.9. Histones increase membrane permeabilization in exponential phase *E. coli* diluted in a low ionic strength condition, but not in a physiological condition. Propidium iodide (PI) fluorescence of H2A-treated *E. coli* increased in bacteria diluted in low concentrations of magnesium, but not physiological concentrations. Quantification of the average PI fluorescence/area (AU) for each condition indicates dilution into low magnesium conditions alone is not sufficient to induce membrane permeabilization. 10 µg/mL H2A significantly increased PI fluorescence in conditions of low magnesium, whereas the addition of 10 µg/mL H2A to *E. coli* in physiological concentrations of magnesium had no effect. Data is from three separate experiments (n=3). Data shown is the mean ± SE. **** indicates a p-value ≤ 0.0001, and ns indicates a p-value > 0.05.

Since the bacterial growth inhibition seen upon histone treatment in low magnesium environments is accompanied by increased membrane permeabilization, this supports a mechanism by which the histones increasingly disrupt the microbial membrane to kill bacteria cultured in low magnesium environments. As previously observed with AMPs, permeabilization of the bacterial membrane functions to facilitate histone entry into the bacterial cell, where histones may have intracellular targets.

To identify if increased membrane permeabilization in exponential phase *E. coli* diluted in a low ionic strength condition facilitates histone entry into the bacterial cell, exponential-phase *E. coli* were diluted into fresh MinA media containing physiological concentrations or low concentrations of magnesium. H2A uptake in *E. coli* was measured by adding 10 μg/mL AF-H2A. Bacteria were incubated for 3 hours, plated on 1% agarose-MinA pads, and analyzed using fluorescence microscopy.

Dilution of *E. coli* into low concentrations of magnesium increased intracellular the uptake of H2A (Figure 5.10A, 5.11), indicating increased membrane permeabilization facilitates histone entry into the bacterial cell. Little AF-H2A fluorescence was observed in *E. coli* diluted into physiological magnesium (Figure 5.10B, 5.11), consistent with the magnesium and histone concentrations used in this experiment failing to induce permeabilization of the bacterial membrane (Figure 5.9).

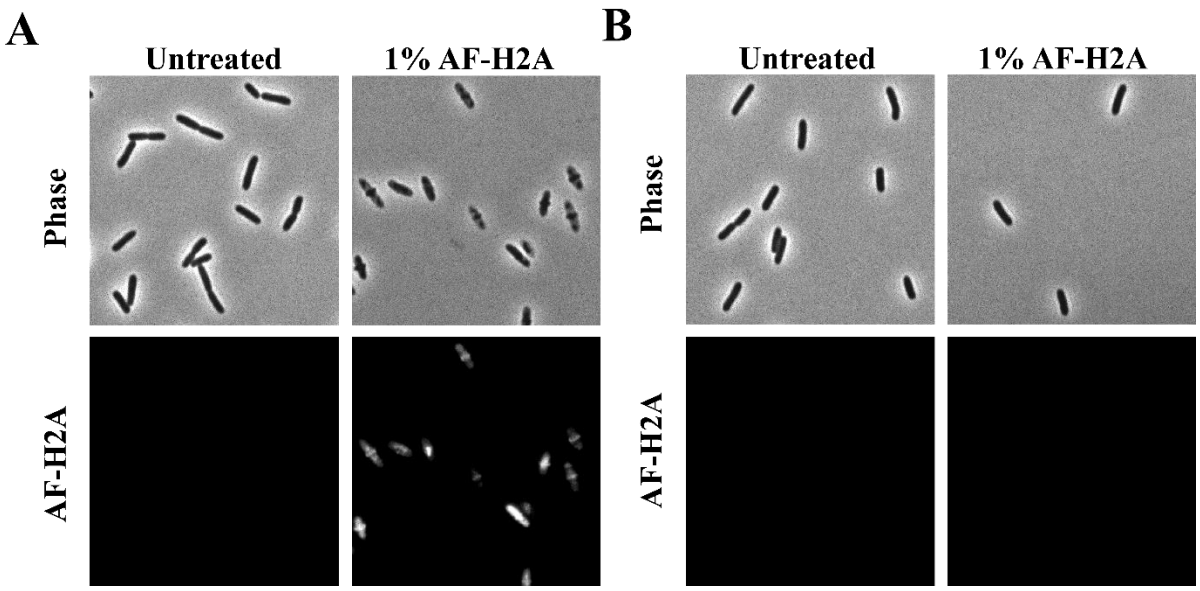

Figure 5.10. Intracellular fluorescence intensity of fluorescently-labeled H2A (AF-H2A) increases in low ionic environments, but not physiological ionic environments. Mid-exponential phase *E. coli* were diluted 1:20 into MinA containing low (1 μM) or physiological concentrations of magnesium (1 mM), with or without the addition of 10 μg/mL H2A. AF-H2A was mixed with unlabeled H2A to decrease fluorescence intensity (1% AF-H2A, 99% unlabeled H2A). Phase and GFP fluorescence images were taken after a 3-hour incubation. The addition of AF-H2A to the low ionic environment (A) increases intracellular the uptake of H2A, whereas little fluorescence is observed in *E. coli* diluted into physiological magnesium (B). Representative images are shown for each condition.

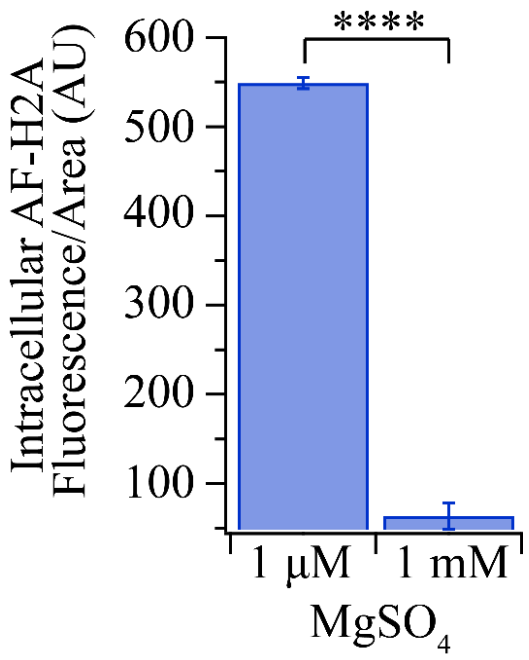

Figure 5.11. Increased membrane permeabilization facilitates histone entry into *E. coli*. Mid-exponential phase *E. coli* were diluted 1:20 into MinA containing low (1 μM) or physiological concentrations of magnesium (1 mM), with or without the addition of 10 μg/mL H2A. AF-H2A was mixed with unlabeled H2A to decrease fluorescence intensity (1% AF-H2A, 99% unlabeled H2A). Quantification of the average intracellular AF-H2A fluorescence/area was performed after a 3 hour incubation. Low ionic environments increased the intracellular concentration of AF-H2A. Data shown as mean ± SEM and are representative of three independent experiments (n=3). **** $p \leq 0.0001$.

5.3 Histones Depolarize the Membrane and Disrupt the Proton Motive Force (PMF)

Given that the presence of pore-forming agents increased uptake of AF-H2A and the presence of H2A increased uptake of FAM-LL-37 in *E. coli* and *S. aureus*, I hypothesized that the formation of membrane pores by membrane-permeabilizing agents, and the stabilization or enhancement of these pores by H2A, could significantly impact ion gradients across the membrane, disrupting ATP production. To investigate this potential effect, I measured the proton motive force (PMF) using using pJMK001 in the *E. coli* strain XL1 Blue (Addagene, Watertown, MA), which expresses the proteorhodopsin optical proton sensor (PROPS) protein under the control of the arabinose promoter[6]. An increase in PROPS fluorescence is associated with a loss in PMF due to electrical depolarization[6].

The *E. coli* strain containing the PROPS plasmid pJMK001 was grown in LB in a shaking incubator at 33° C, induced with arabinose and 5 μM retinal, and incubated in darkness for 3.5 hours. The culture was spun down and resuspended in M9. E. coli were back-diluted into fresh MinA and cultured to an OD_{600} of 0.2. Exponential-phase *E. coli* containing the PROPS plasmid were diluted 1:20 into fresh MinA media, treated with 10 μg/mL H2A, 1 μM LL-37, both 10 μg/mL H2A and 1 μM LL-37, 1 μg/mL PMB, or both 10 μg/mL H2A and 1 μg/mL PMB, and incubated for 1 hour. Cells were immobilized on a 1% agarose pad and Cy5 fluorescence was analyzed using fluorescence microscopy.

Treatment of *E. coli* with 10 μg/mL H2A alone had no effect on the PMF compared to the untreated sample (Figure 5.12), consistent with the lack of membrane permeabilization by H2A (Figure 4.11). Bacteria treated with LL-37 or PMB alone showed moderate levels of PROPS fluorescence, indicating membrane depolarization and disruption of the PMF, consistent with membrane permeabilization seen in *E. coli* treated with 2 μM LL-37 (Figure 4.11A) or 1 μg/mL

PMB (Figure 4.14). However, *E. coli* treated with both H2A and LL-37 or PMB exhibited significantly higher PROPS fluorescence than cells treated with LL-37 or PMB alone (Figure 5.12), indicating that H2A further depolarizes the membrane and disrupts the PMF, likely due to enhancement or stabilization of the pores formed by LL-37 or PMB.

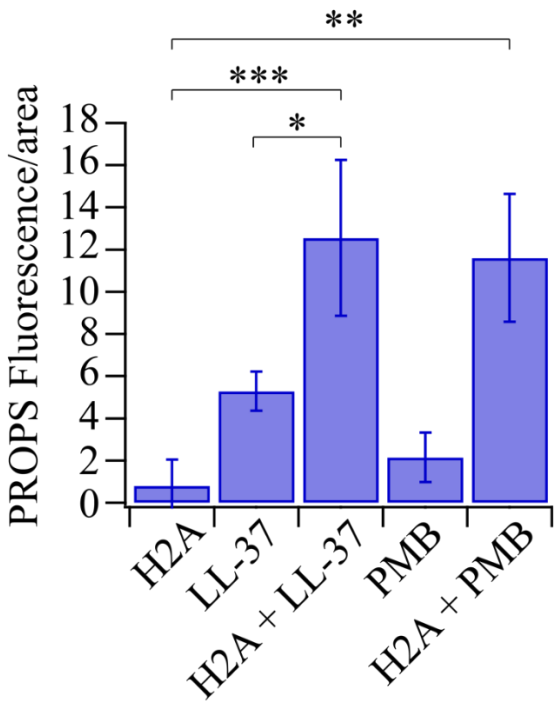

Figure 5.12. Histones depolarize the bacterial membrane and disrupt the proton motive force (PMF). *E. coli* containing the PROPS plasmid pJMK001 were treated with a combination of 10 μg/mL H2A, 2 μM LL-37, or 1 μg/mL PMB. Intracellular Cy5 fluorescence intensity of the proteorhodopsin optical proton sensor (PROPS), which measures membrane potential, was measured after a 1-hour incubation. Bars indicate background-subtracted mean ± SEM for at least three independent experiments. *** $p \leq 0.001$, ** $p \leq 0.01$, * $p \leq 0.05$.

5.4 Histones Impair Bacterial Recovery

Based on the findings that suggest the antimicrobial activity of histones requires membrane permeabilization and histone uptake, and the findings that suggest H2A stabilizes membrane pores and depolarizes the membrane, I hypothesized that these mechanisms would inhibit the ability of bacteria to recover from damage induced by histone assault. To investigate bacterial recovery from damage induced by H2A, I quantified the extent of membrane repair in a strain of *E. coli* that expresses CFP under the control of a constitutively active *ompA* promoter. Exponential phase *E. coli* were treated with 10 μg/mL H2A, 1 μM LL-37, or both and incubated for 1 hour. The bacterial solution was filtered through a 0.22 μm filter to remove excess LL-37 and H2A and cells were resuspended in fresh MinA medium. Bacterial cells were immobilized, and their recovery was analyzed over a 1-hour time period. During this recovery period, *E. coli* treated with H2A showed high levels of CFP fluorescence, increased in cellular size, and began division (Figure 5.13). Similarly, during the 1-hour recovery period, LL-37-treated cells resumed growth and division and retained expression of CFP. In contrast, cells treated with H2A and LL-37 formed membrane blebs at the mid-cell position. Within 10 minutes of the formation of membrane blebs, dual-treated cells lost CFP fluorescence, indicating the rapid leakage of cytoplasmic contents into the surrounding media. This CFP leakage is consistent with a dramatic decrease in cell size in the dual treatment of H2A and LL-37 (Figure 4.22). Furthermore, these results support a mechanism by which H2A-stabilized pores enable the efflux of cytoplasmic components out of the cell, as observed with the debris in the dual-treated SEM images (Figure 4.18, 4.19).

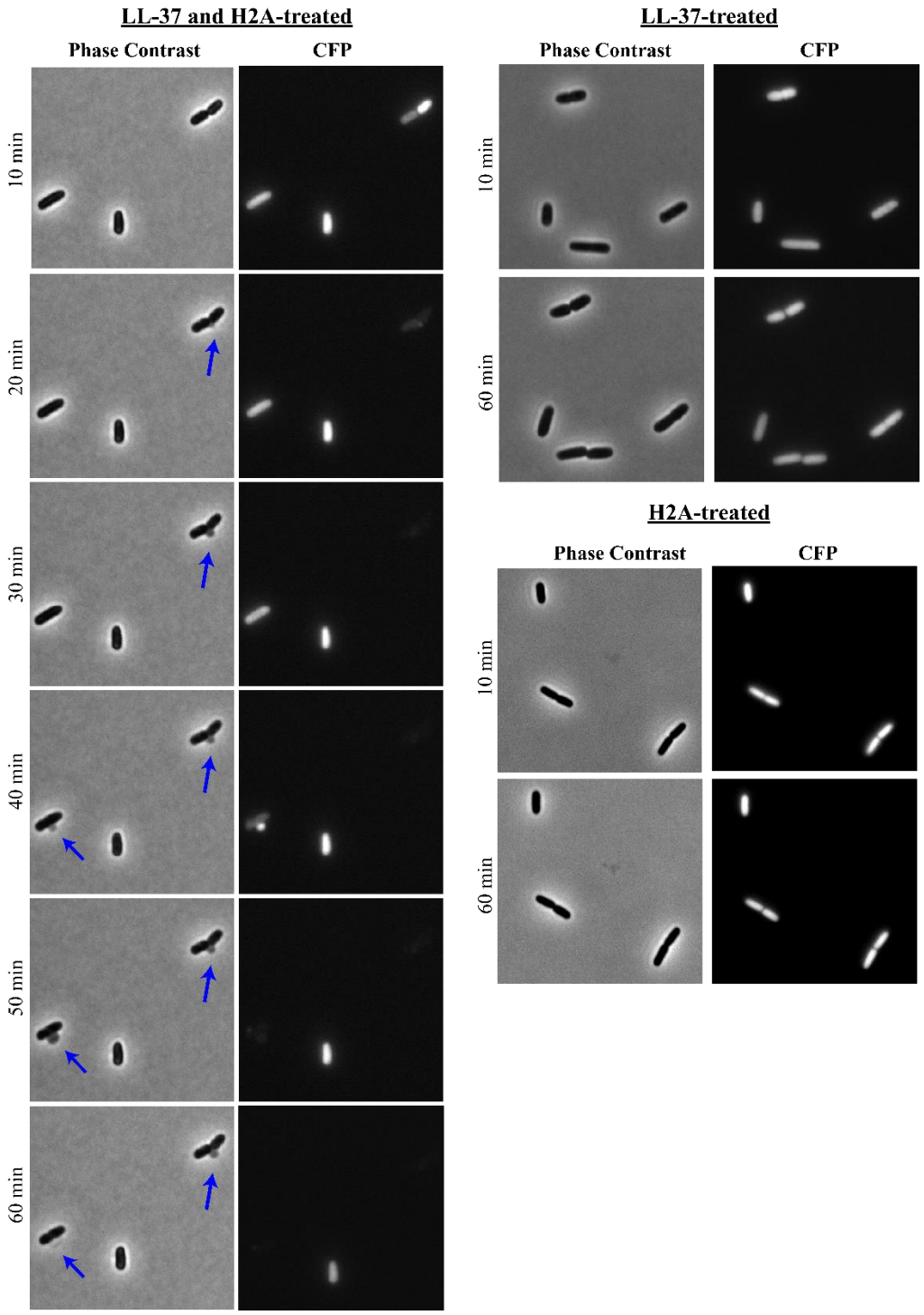

Figure 5.13. Histone H2A inhibits membrane recovery by stabilizing LL-37-induced pore formation. Phase contrast and CFP fluorescence timelapse images of *E. coli* that constitutively express CFP that were initially treated with 10 μg/mL H2A, 1 μM LL-37, or the combination of 10 μg/mL H2A and 1 μM LL-37 and then recovered without the treatments over a 1-hour time period. Arrows indicate the formation of membrane blebs.

To quantify the time-course of membrane repair in bacteria treated with histones, the strain of *E. coli* that expresses CFP under the control of a constitutively active *ompA* promoter was grown to exponential phase and treated with 10 μg/mL H2A, 1 μM LL-37, or both. After a 1-hour incubation period, the bacterial solution was filtered through a 0.22 μm filter to remove excess LL-37 and H2A and cells were resuspended in fresh MinA medium. Cells were allowed to recover for 0, 30, 60 minutes before the addition of 30 μM propidium iodide for 15 minutes prior to performing fluorescence microscopy to quantify CFP and mCherry fluorescence. The addition of PI was to ensure the membrane recovery analysis focused specifically on the ability to recover and did not include existing severe membrane damage. CFP fluorescence in cells treated with H2A alone was consistently high across the recovery period (Figure 5.14), consistent with the lack of membrane permeabilization in the presence of 10 μg/mL H2A alone (Figure 4.11).

CFP fluorescence for *E. coli* treated with LL-37 alone or the dual treatment of LL-37 and histones at 0 minutes was significantly lower than *E. coli* treated with histones alone, consistent with the reduction in cell size seen in these conditions (Figure 4.22) and the increase in PI fluorescence due to pore formation (Figure 4.11). There was no significant difference in CFP fluorescence between LL-37 alone at 0 minutes and the dual treatment at 0 minutes. However, CFP fluorescence increased during the 60-minute recovery period following treatment with LL-37 alone, indicating the ability of cells to recover from LL-37-induced membrane pore formation. In contrast, *E. coli* treated with LL-37 and H2A did not recover over the 60-minute recovery period. CFP fluorescence in the dual-treated cells remained consistently low (Figure 5.14), indicating that the addition of H2A induces persistent cell damage from which the cell cannot recover.

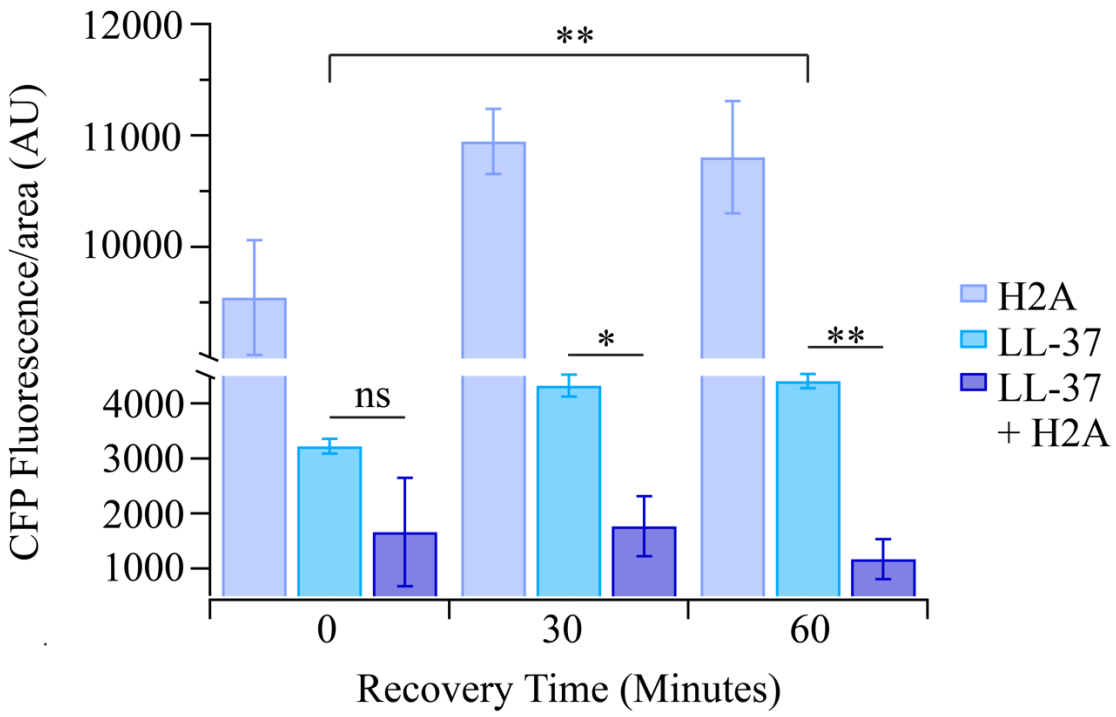

Figure 5.14. H2A induces persistent cellular damage when combined with LL-37. *E. coli* that constitutively express CFP were initially treated with 10 μg/mL H2A, 1 μM LL-37, or the combination of 10 μg/mL H2A and 1 μM LL-37 and then recovered without the treatments over a 1-hour time period. Cells were allowed to recover for 0, 30, 60 minutes before the addition of 30 μM PI for 15 minutes. CFP and mCherry fluorescence intensities were measured after the 15-minute PI treatment. Propidium iodide positive cells were excluded from the analysis. Bars indicate mean ± SEM for three independent experiments. ** $p \leq 0.01$, * $p \leq 0.05$, ns > 0.05.

Similar results were observed with the combinatorial treatment of H2A and magainin-2. *E. coli* treated with H2A or magainin-2 (MAG2) alone had consistently high CFP fluorescence across the recovery period (Figure 5.15). There was no significant difference in CFP fluorescence between H2A-treated *E. coli* and MAG2-treated *E. coli* at 0 or 60 minutes, consistent with the lack of membrane permeabilization in the presence of 10 μg/mL H2A alone or 10 μM MAG2 alone (Figure 4.17). In contrast, the addition of H2A to MAG2-treated cells decreased CFP levels. No recovery of CFP was seen across the 1-hour recovery period. CFP fluorescence in *E. coli* treated with both H2A and MAG2 remained consistently low (Figure 5.15). This low CFP fluorescence in cells treated with both MAG2 and H2A supports a mechanism by which the addition of H2A induces persistent cell damage from which the cell cannot recover. This persistent cell damage requires the addition of a pore-forming agent, such as MAG2, along with histones, since *E. coli* treated with H2A or MAG2 alone showed consistently high CFP fluorescence (Figure 5.15).

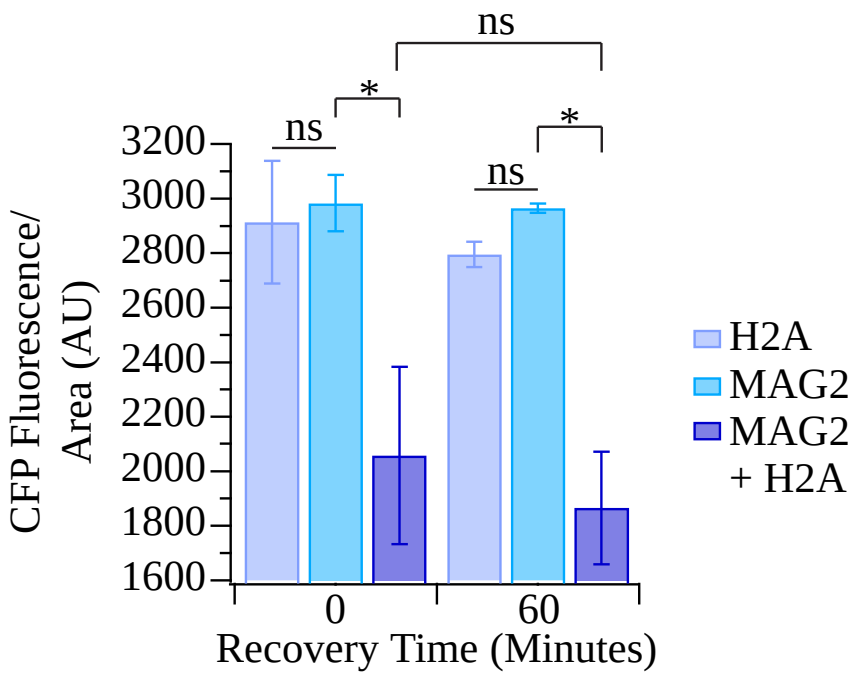

Figure 5.15. H2A induces persistent cellular damage when combined with magainin-2. *E. coli* that constitutively express CFP were initially treated with 10 μg/mL H2A, 10 μM MAG2, or the combination of 10 μg/mL H2A and 10 μM MAG2 and then recovered without the treatments over a 1-hour time period. Cells were allowed to recover for 0 or 60 minutes before the addition of 30 μM PI for 15 minutes. CFP and mCherry fluorescence intensities were measured after the 15-minute PI treatment. Propidium iodide positive cells were excluded from the analysis. Bars indicate mean ± SEM for three independent experiments. * $p \leq 0.05$, ns > 0.05.

The ability of bacteria to recover from histone treatment was further assessed by monitoring membrane permeabilization via PI fluorescence during the recovery period following treatment with histones and LL-37. The same population of *E. coli* used in the quantification of CFP fluorescence (Figure 5.14) was used to measure PI fluorescence. Across the 1-hour recovery period, there was little to no PI fluorescence for *E. coli* treated with H2A alone (Figure 5.16), consistent with a lack of membrane permeabilization at this concentration of histones in medium containing physiological magnesium (Figure 4.11). The addition of LL-37 alone and the combinatorial treatment of LL-37 and H2A induce similar levels of membrane permeabilization after a 1-hour treatment period (Figure 4.11, Figure 5.16). Additionally, after a 30-minute recovery period, PI fluorescence was similar for LL-37 treated *E. coli* and dual-treated *E. coli*. However, after 1 hour of recovery, PI fluorescence in LL-37-treated cells was significantly lower than cells that were treated with H2A and LL-37 (Figure 5.16), indicating AMP-treated cells can repair their bacterial membranes, whereas H2A induces persistent membrane damage.

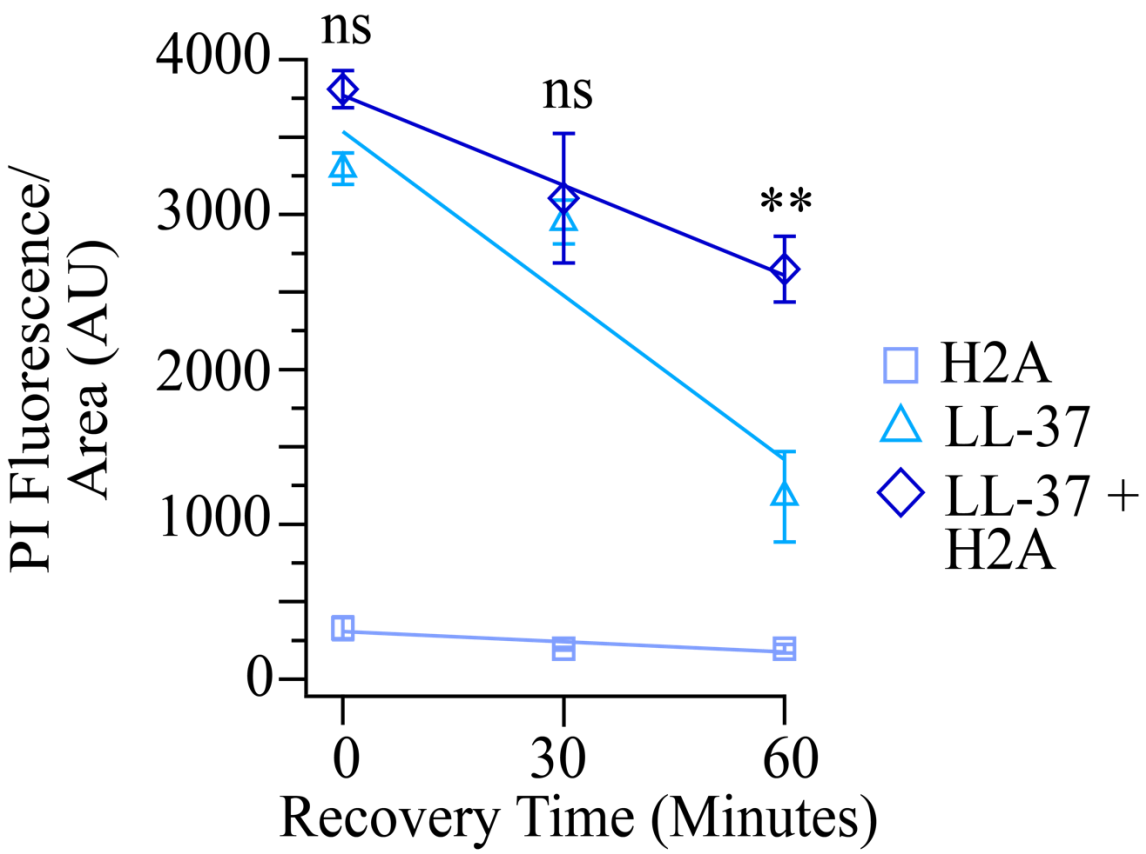

Figure 5.16. H2A induces persistent membrane damage when combined with LL-37. Propidium iodide (PI) fluorescence of *E. coli* across a 1-hour recovery period following treatment with H2A, LL-37, or the combination of H2A and LL-37**.** *E. coli* that constitutively express CFP were initially treated with 10 μg/mL H2A, 1 μM LL-37, or the combination of 10 μg/mL H2A and 1 μM LL-37 and then recovered without the treatments over a 1-hour time period. Cells were allowed to recover for 0, 30, or 60 minutes before the addition of 30 μM PI for 15 minutes. mCherry fluorescence intensities were measured after the 15-minute PI treatment. Bars indicate mean ± SEM for three independent experiments. ** $p \leq 0.01$, ns > 0.05.

Similar trends in PI fluorescence during a recovery period were observed with the combinatorial treatment of H2A and magainin-2. Treatment of 10 μg/mL H2A alone caused little to no membrane permeabilization, as supported by the low levels of PI fluorescence immediately after treatment and across the 1-hour recovery period (Figure 5.17). Similarly, treatment with magainin-2 caused minimal PI fluorescence. There was not a significant difference in PI fluorescence for *E. coli* treated with 10 μg/mL H2A or 10 μM magainin-2 after their respective 1-hour treatments or across the 1-hour recovery period, consistent with the lack of membrane permeabilization previously seen for both individual treatments (Figure 4.17). In contrast, the addition of H2A to MAG-2 treated cells significantly increased PI fluorescence after the 1-hour combinatorial treatment, consistent with previous results (Figure 4.17). PI fluorescence for dual-treated *E. coli* remained consistently higher than MAG2-treated cells and there was no decrease in PI fluorescence for dual-treated cells across the 1-hour recovery period, indicating persistent membrane damage in dual-treated cells (Figure 5.17).

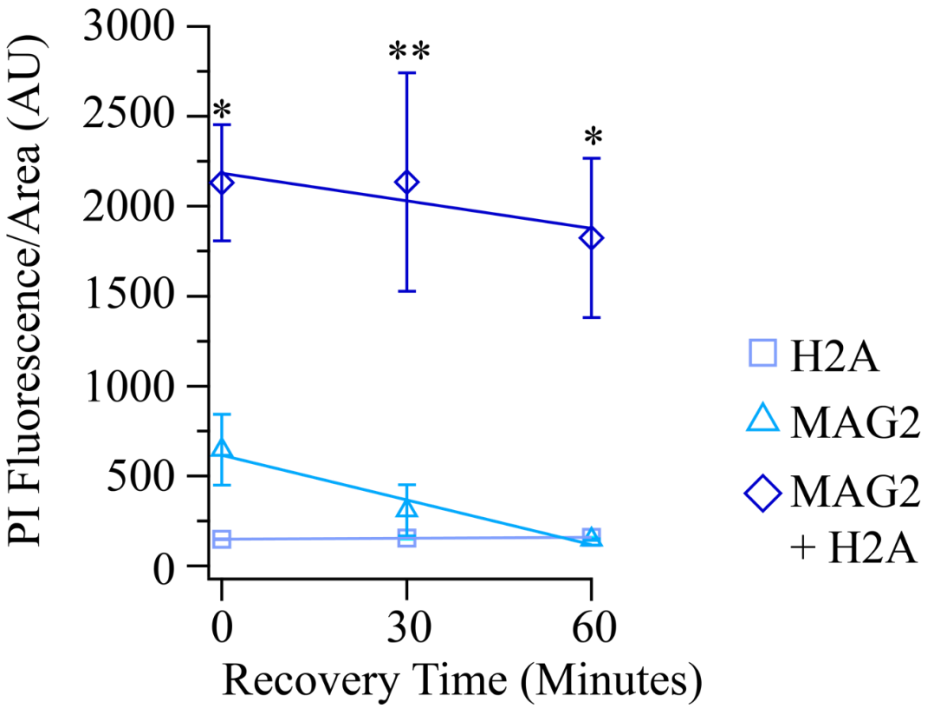

Figure 5.17. H2A induces persistent membrane damage when combined with magainin-2. Propidium iodide (PI) fluorescence of *E. coli* across a 1-hour recovery period following treatment with H2A, MAG2, or the combination of H2A and MAG2**.** *E. coli* that constitutively express CFP were initially treated with 10 μg/mL H2A, 10 μM MAG2, or the combination of 10 μg/mL H2A and 10 μM MAG2 and then recovered without the treatments over a 1-hour time period. Cells were allowed to recover for 0, 30, or 60 minutes before the addition of 30 μM PI for 15 minutes. mCherry fluorescence intensities were measured after the 15-minute PI treatment. Bars indicate mean ± SEM for three independent experiments. ** $p \leq 0.01$, * $p \leq 0.05$.

Together, these time-course experiments measuring CFP fluorescence and PI fluorescence over a 1-hour recovery period help quantify membrane repair in bacteria treated with AMPs alone or the dual treatment of AMPs and histones. The results suggest that bacteria can recover from pore formation induced by LL-37 and that minimal recovery is needed in *E. coli* treated with magainin-2 alone. However, the presence of H2A to AMP-treated cells inhibits membrane repair, which is consistent with H2A stabilizing the pores formed by LL-37 or magainin-2. Since *E. coli* treated with H2A alone showed consistently high CFP fluorescence levels and minimal PI fluorescence, consistent with an absence of membrane permeabilization and cell damage, this suggests the persistent cell damage requires the addition of pore-forming agents, such as the AMPs LL-37 and MAG2.

To identify if the mechanism by which histones impair membrane repair is dependent upon the presence of AMP-formed pores, membrane recovery was measured in bacteria diluted into a low magnesium environment. To quantify the effects of histones alone on membrane repair, in conditions where histones compromise membrane integrity, *E. coli* were treated with 10 μg/mL H2A following dilution into a low ionic environment. Exponential phase *E. coli* were diluted 1:20 into MinA media containing physiological concentrations or low concentrations of magnesium, with or without the addition of 10 μg/mL H2A. In previous experiments, the addition of H2A to this low ionic media decreased extended the lag phase and slowed exponential growth rates (Figure 5.8), increased membrane permeabilization (Figure 5.9), and facilitated AF-H2A entry into the cell (Figure 5.10, 5.11). After a 3-hour incubation period, the bacterial solution was filtered through a 0.22 μm filter to remove excess H2A and cells were resuspended in fresh MinA medium containing 1 mM $MgSO_4$. Cells were allowed to recover for up to 60 minutes before the addition of 30 μM

propidium iodide for 15 minutes prior to performing fluorescence microscopy to quantify CFP and mCherry fluorescence.

CFP fluorescence in cells treated with H2A in physiological ionic environments were consistently high over the 1-hour recovery period, consistent with the lack of membrane permeabilization under these conditions (Figure 5.9). After a 3-hour treatment with 10 μg/mL H2A in a low ionic environment, CFP fluorescence was significantly lower than *E. coli* treated with 10 μg/mL H2A in a physiological ionic environment (Figure 5.18). However, CFP fluorescence increased across the 60-minute recovery period following treatment with histones in the low ionic environment, indicating the ability of cells to recover from histone-induced membrane pore formation. There was no difference in CFP fluorescence after the 1-hour recovery period for *E. coli* treated with 10 μg/mL H2A in a low or physiological ionic environment (Figure 5.18). These results suggest *E. coli* can recover from this concentration of histones alone and is consistent with the persistent cell damage requiring the addition of pore-forming agents, such as AMPs. Furthermore, this supports the proposed mechanism by which histones synergize with AMPs to kill bacteria by stabilizing pores formed by AMPs. Thus, the addition of H2A induces persistent cell damage only in conditions where a pore-forming agent, such as LL-37 or MAG2 is also present.

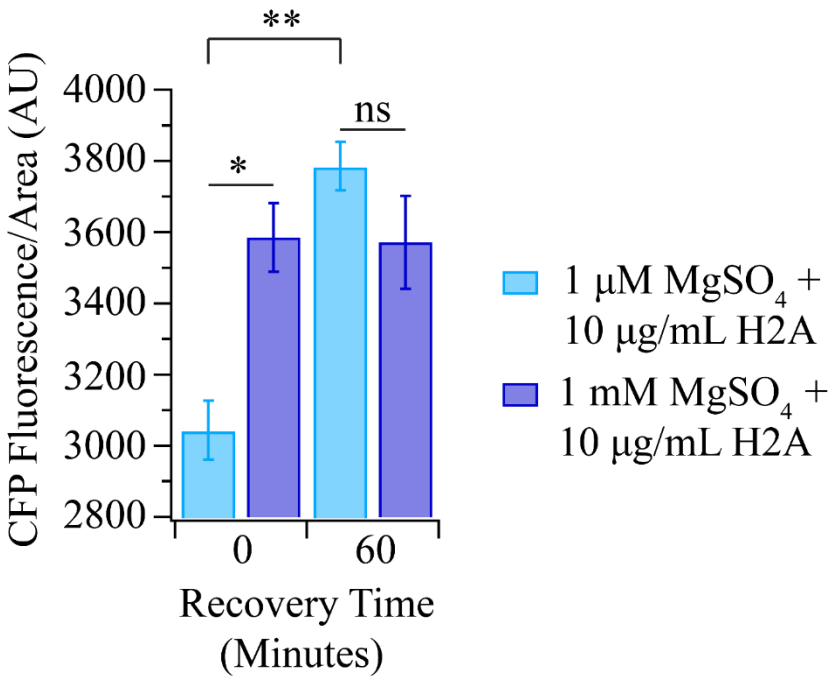

Figure 5.18. *E. coli* recover from cellular damage in the absence of AMPs. *E. coli* that constitutively express CFP were initially treated with 10 μg/mL H2A in media containing low (1 μM) magnesium or physiological (1 mM) magnesium. *E. coli* were cultured for three hours and then recovered without the treatments over a 1-hour time period. CFP and mCherry fluorescence intensities were measured after the 15-minute PI treatment. Propidium iodide positive cells were excluded from the analysis. Bars indicate mean ± SEM for three independent experiments. ** $p \leq 0.01$, * $p \leq 0.05$, ns > 0.05.

Consistent with previous experiments (Figure 5.9), the addition of histones to *E. coli* in low ionic environments increased PI fluorescence after a 3-hour treatment (Figure 5.19). However, after 30 minutes of recovery, PI fluorescence of *E. coli* treated with histones in a low ionic environment decreased to levels comparable to *E. coli* recovering from a low ionic environment without histones or histone treatment in a physiological ionic environment. There was no significant difference in PI fluorescence across the three conditions after a 30-minute or 60-minute recovery period (Figure 5.15), indicating bacteria can recover when assaulted with histones alone, in the absence of AMPs. Since the synergistic treatments of AMPs and H2A show impaired membrane recovery (Figure 5.16, 5.17), these results are consistent with histones stabilizing pores formed by AMPs, contributing to reduced healing.

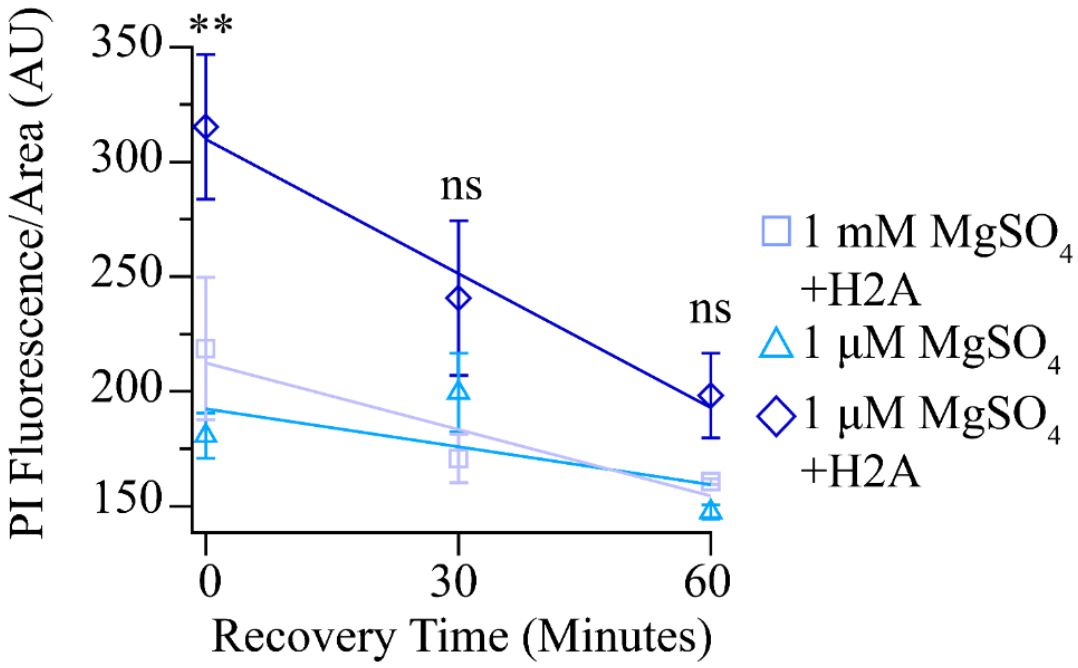

Figure 5.19. *E. coli* can recovery from H2A-induced membrane damage in the absence of AMPs. Propidium iodide (PI) fluorescence of *E. coli* across a 1-hour recovery period following treatment with H2A in media containing low (1 µM) magnesium or physiological (1 mM) magnesium.**.** *E. coli* that constitutively express CFP were diluted into low or physiological media, with or without 10 µg/mL H2A for three hours and then recovered without the treatments over a 1-hour time period. Cells were allowed to recover for 0, 30, or 60 minutes before the addition of 30 µM PI for 15 minutes. mCherry fluorescence intensities were measured after the 15-minute PI treatment. Bars indicate mean ± SEM for three independent experiments. ** $p \leq 0.01$, ns > 0.05.

5.5 Histones Have an Intracellular Target

To identify if pore formation is required for histone-mediated killing of bacteria, I tested whether electroporation of *E. coli* was sufficient to facilitate histone-mediated killing. Electroporation, the application of a high-voltage electrical shocks to bacteria to transiently permeabilize the membrane, is commonly used to introduce DNA or small molecules into cells[7]. Given the increased uptake of histones into the cell in the presence of membrane-permeabilizing AMPs, I hypothesized that histones had an intracellular target. Thus, I predicted that the application of an electrical field would be sufficient to enable uptake of histones into the cell where histones could kill bacteria by acting on intracellular targets.

To prepare electrocompetent cells, *E. coli* was cultured in SOB to an OD_{600} of 0.5. The bacterial cultures were placed on ice for 30 minutes and spun down at 6000 rpm for 15 minutes at 4°C. Supernatant was removed and bacteria were resuspended in ice cold sterile 10% glycerol. Bacteria were centrifuged at 6000 rpm for 3.5 minutes at 4°C, supernatant was removed, and bacteria were resuspended in ice cold sterile 10% glycerol. Wash cycles were repeated four times. The pellet was resuspended to a final concentration of OD_{600} of 0.2 in ice cold 10% glycerol.

50 uL of OD_{600} 0.2 electrocompetent *E. coli* were added to a 1 mm cuvette, in the presence or absence of 50 μg/mL H2A. Electroporation was performed using the "Ec1" setting on a Bio-Rad micropulser. Cold SOC media was added to a final volume of 1 mL. Electrocompetent cells were diluted 1:20 into cold SOC, with or without 50 μg/mL H2A as a control. These control cells were not electroporated.

This electroporation treatment did not affect bacterial growth, nor did the presence of 50 μg/mL H2A in the absence of electroporation, compared to untreated electrocompetent *E. coli* (Figure

5.15). In contrast, electroporation in the presence of 50 μg/mL H2A significantly inhibited bacterial growth. Together, these results indicate that histones kill bacteria intracellularly, suggesting histones have an intracellular target. Furthermore, this finding is consistent with histones stabilizing pores formed by AMPs. In the absence of pores, *E. coli* can recover quickly. However, histones prevent bacterial recovery in pore-forming conditions (Figure 5.14-5.17).

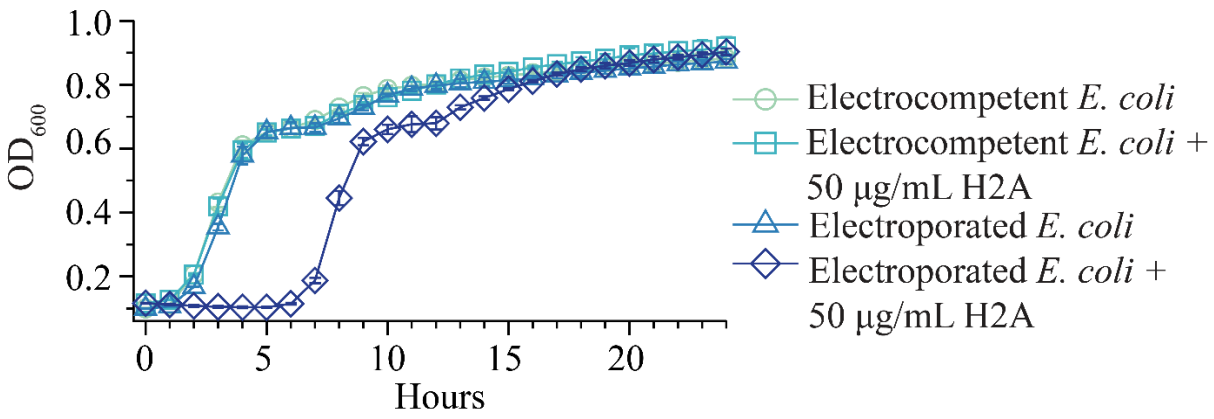

Figure 5.20. Histones kills bacteria intracellularly. Growth profiles of electrocompetent *E. coli* treated with 0 or 50 µg/mL H2A in SOC media over a 24-hour growth period. This concentration of H2A had no effect on bacterial growth. Additionally, electroporation had no effect of electrocompetent *E. coli*. Application of an electric field to transiently permeabilize the membrane inhibited bacterial growth by allowing uptake of histones into the bacterial cell where histones have an intracellular target. Data points are the average of four independent experiments (n = 4) and error bars indicate SEM.

5.6 Conclusion

Histone H2A synergizes with low concentrations of the membrane-permeabilizing agents LL-37, PMB, and MAG2 to kill bacteria. Since PI staining revealed increased membrane permeabilization accompanied the bacterial growth inhibition in synergistic treatments, I hypothesized that membrane disruption facilitated histone uptake into the bacterial cell. Indeed, membrane permeabilization by LL-37, PMB, MAG2 enhanced the uptake of fluorescent histones, whereas antimicrobial agents that do not permeabilize the membrane and do not synergize with histones, such as kanamycin and chloramphenicol, do not promote histone uptake. Although the histone concentrations used do not induce membrane permeabilization, H2A facilitated uptake of fluorescent LL-37 into the bacterial cytoplasm, supporting a mechanism by which histones stabilize LL-37-formed pores. This formation of membrane pores by membrane-permeabilizing agents, and the stabilization or enhancement of these pores by H2A, significantly impacted ion gradients across the bacterial membrane, depolarizing the membrane and likely disrupting ATP production.

AMPs are not required for histone uptake into the cell, as increased membrane permeabilization following histone treatment in low magnesium environments similarly facilitated histone entry into the bacterial cell. This suggests that histones are able to kill bacteria, through histone uptake into the cell, in the absence of AMPs. Furthermore, this indicates a primary role of AMPs in the innate immune system could be permeabilizing the membrane to enable histone uptake.

To further quantify the effects of histones on the bacterial membranes, I investigated bacterial recovery from damage induced by H2A. Persistent cellular and membrane damage were observed in dual treatments with histones and AMPs. In contrast, cells treated with AMPs alone or with

histones alone in conditions of low ionic strength showed significant recovery, suggesting the presence of both pore-forming AMPs and histones are a requirement of impaired membrane recovery. Whether pore stabilization by histones occurs internally or externally remains to be determined. However, given that impaired membrane repair was observed in dual treatments with histones and two distinct AMPs, LL-37 and MAG2, the mechanism of pore stabilization is not due to a specific and direct interaction between histones and AMPs. Rather, AMPs and histones have separate functions, whereby histones impeded repair of pores formed by AMPs.

Given that histone uptake into the bacterial cytoplasm is concomitant with membrane-permeabilization and growth inhibition, I hypothesized that the antimicrobial activity of histones was primarily from interactions with intracellular targets, such as DNA. However, since histones stabilize AMP-formed pores, it was plausible that the primary function of histones was pore stabilization from within the bacterial cell. Thus, electroporation was employed to identify if pore formation was required for histone-mediated killing of bacteria. The application of a high-voltage electrical shocks to transiently permeabilize the membrane in the presence of histones caused significantly inhibition of bacterial growth, indicating that histones have an intracellular target.

5.7 References

1. Henzler Wildman, K. A., Lee, D.-K. & Ramamoorthy, A. Mechanism of Lipid Bilayer Disruption by the Human Antimicrobial Peptide, LL-37. *Biochemistry* **42**, 6545–6558 (2003).
2. Clifton, L. A. *et al.* Effect of Divalent Cation Removal on the Structure of Gram-Negative Bacterial Outer Membrane Models. *Langmuir* **31**, 404–412 (2015).
3. Leive, L. Release of lipopolysaccharide by EDTA treatment of E., coli. *Biochemical and Biophysical Research Communications* **21**, 290–296 (1965).
4. Snoussi, M. *et al.* Heterogeneous absorption of antimicrobial peptide LL37 in Escherichia coli cells enhances population survivability. *eLife* **7**, (2018).
5. Lusk, J. E., Williams, R. J. & Kennedy, E. P. Magnesium and the growth of Escherichia coli. *J. Biol. Chem.* **243**, 2618–2624 (1968).
6. Kralj, J. M., Hochbaum, D. R., Douglass, A. D. & Cohen, A. E. Electrical spiking in Escherichia coli probed with a fluorescent voltage-indicating protein. *Science* **333**, 345–348 (2011).
7. Potter, H. Transfection by Electroporation. in *Current Protocols in Molecular Biology* (eds. Ausubel, F. M. et al.) mb0903s62 (John Wiley & Sons, Inc., 2003). doi:10.1002/0471142727.mb0903s62.

Chapter 6: Histone H2A Disrupts Bacterial Chromosomal DNA Organization and Suppresses Transcription

Given that pore-forming antimicrobial agents, including the AMPs LL-37 and magainin-2, and the antibiotic polymyxin B, synergize with histones to inhibit bacterial growth by facilitating the entry of Histone H2A into the bacterial cell, the role of Histone H2A subsequent to entry into the cytoplasm was explored. Furthermore, histone treatment in conditions of low magnesium similarly inhibited bacterial growth while enabling significant uptake of histones into the cell, indicating that the role of AMPs in histone-mediated killing is facilitating their uptake in physiological environments, where histones have an intracellular role. Additionally, electroporation of *E. coli* in the presence of H2A led to significant inhibition of bacterial growth, further supporting a mechanism where histones have an intracellular target.

Binding to intracellular moieties has been seen with other AMPs. Puroindoline-derived tryptophan-rich AMPs do not appear to disrupt membrane integrity in *E. coli*; instead, the potency of the AMP is correlated with DNA binding[1]. Pseudin-2, an AMP from the South American paradoxical frog *Pseudis paradoxa*, takes on an α-helical structure in the presence of bacterial membranes, forming pores to enter the cytoplasm[2]. Once intracellular, pseudin-2 is thought to binds to RNA, inhibiting protein synthesis. Cfb-14, a synthetic AMP derived from a cathelin-like domain, was shown to cause membrane permeation, in addition to binding DNA and inhibiting gene replication and protein expression[3]. Piscidin 1 and piscidin 3 have an α-helical structure when bound to model membranes, translocate across membranes, and colocalize with bacterial nucleoids. In addition to non-lethal permeabilization, piscidins bind DNA and have a condensing effect[4]. Because H2A is well-characterized as a component of the histone core, it is feasible that

the positively charged histone subunit may complex with negatively charged microbial DNA, thereby perturbing replication and transcription.

6.1 Histone H2A Interacts with Microbial DNA *in vitro*, Inhibiting DNA Migration

Although mammalian histones are well-known for their role in binding and condensing mammalian DNA, binding of mammalian histone subunits to bacterial DNA has not yet been explored. *E. coli* DNA was purified using a Miniprep kit, with a three-second sonication step, to ensure bacterial lysis. To explore whether calf thymus histone H2A binds purified *E. coli* genomic DNA *in vitro*, 1 μg purified DNA from *E. coli* was incubated with a range of histone concentrations from 0-1.4 μg H2A for 25 minutes at 25ºC. DNA products were separated by native nucleic acid polyacrylamide gel electrophoresis (PAGE) on a 5% TBE gel at 100 V for 60 minutes before staining with 1x SYBR Safe in TBE buffer[5] for 30 minutes before visualization.

Since histone proteins have a strong positive charge (PI ~ 10.8), histones should not enter the gel under the native conditions used. Likewise, microbial DNA bound to H2A should not be able to enter the gel, resulting in lower amounts of bacterial DNA migrating through the gel. Indeed, increasing levels of Histone H2A inhibited DNA migration through the gel (Figure 6.1A, 6.1B), indicating significant interactions between histone H2A and *E. coli* DNA *in vitro*.

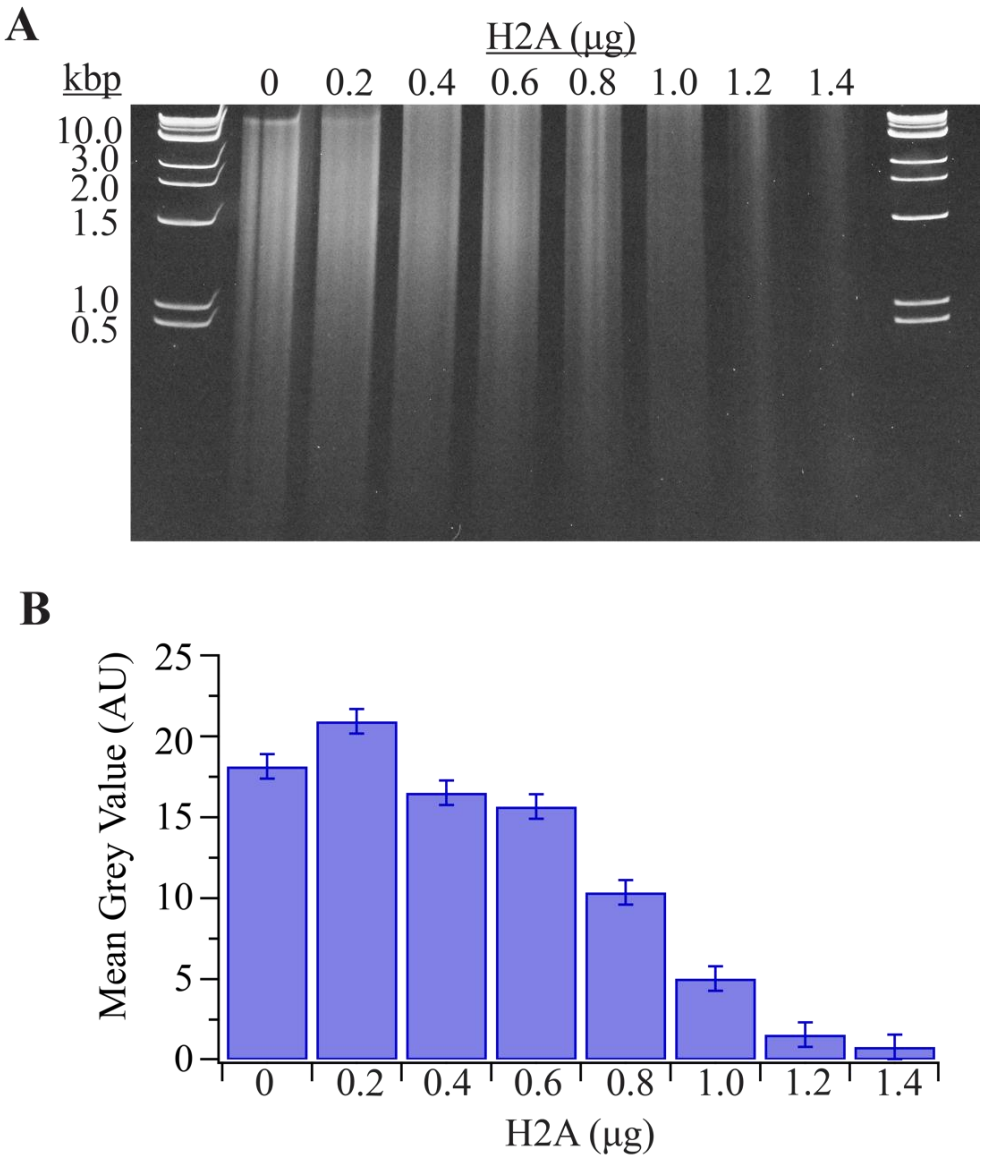

Figure 6.1. Histone H2A inhibits bacterial DNA migration. 1 µg purified *E. coli* DNA was incubated with a range of histone concentrations from 0-1.4 µg H2A for 25 minutes at 25ºC. DNA products were separated by native nucleic acid polyacrylamide gel electrophoresis (PAGE) on a 5% TBE gel at 100 V for 60 minutes before staining with 1x SYBR Safe in TBE buffer for 30 minutes before visualization (A) Associated DNA band intensities were quantified used ImageJ (B). A representative gel is shown. Bars indicate mean ± SEM for three independent experiments.

LL-37 has also been reported to interact with DNA[6,7]. To explore whether LL-37 binds purified *E. coli* genomic DNA *in vitro*, 1 μg purified DNA from *E. coli* was incubated with a range of LL-37 concentrations from 0-1.4 μg H2A for 25 minutes at 25ºC. DNA products were separated by native nucleic acid PAGE as described above (Figure 6.2A). While low levels of nucleic acid binding were evident when higher amounts of LL-37 were added, LL-37 exhibited less retention of bacterial DNA for a comparable range of concentrations (Figure 6.2A, 6.2B). Accounting for the higher molecular weight of histone H2A (14 kDa) compared to LL-37 (4.5 kDa), the addition of equal weights of proteins to microbial DNA resulted in over three times as many LL-37 molecules present compared to Histone H2A molecules. These results help support a mechanism by which the primary role of AMPs in NETs and on lipid droplets is membrane permeabilization and facilitation of histone entry into the bacterial cell.

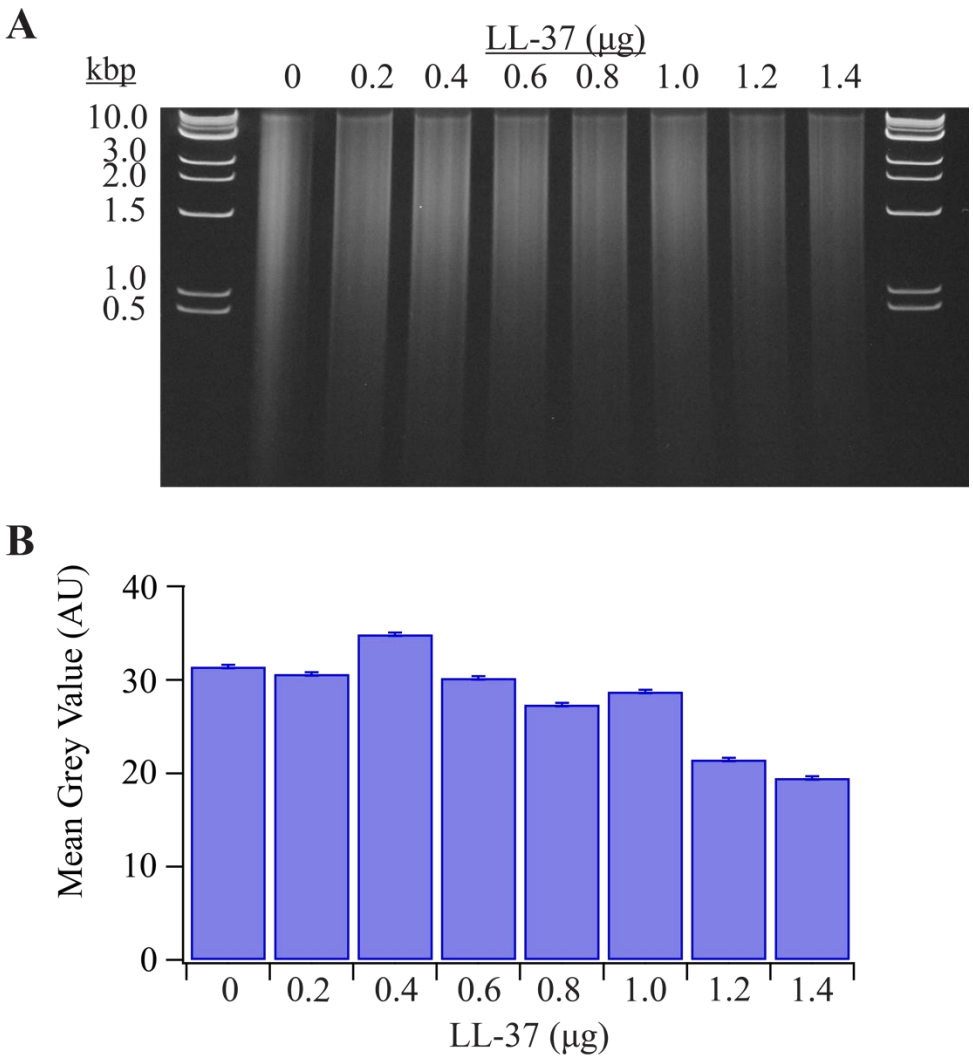

Figure 6.2. LL-37 weakly inhibits bacterial DNA migration. 1 µg purified DNA from *E. coli* was incubated with a range of LL-37 concentrations from 0-1.4 µg H2A for 25 minutes at 25ºC. DNA products were separated by native nucleic acid polyacrylamide gel electrophoresis (PAGE) on a 5% TBE gel at 100 V for 60 minutes before staining with 1x SYBR Safe in TBE buffer for 30 minutes before visualization (A) Associated DNA band intensities were quantified used ImageJ (B). A representative gel is shown. Bars indicate mean ± SEM for three independent experiments.

6.2 Histone H2A Disrupts Bacterial Chromosomal DNA Organization

To supplement the *in vitro* experiments, the effect of H2A on *E. coli* chromosomes was measured in live cells using SYTOX Green, a nucleic acid stain which exhibits green fluorescence upon binding nucleic acids. Mid-exponential *E. coli* were pre-treated for 30 minutes with 2 μM LL-37, with or without the addition of 10 μg/mL H2A. Since LL-37 showed low retention of bacterial DNA *in vitro*, minimal changes in chromosomal organization were expected with the addition of LL-37 alone. Instead, the addition of LL-37 served to increase entry of histone H2A to observe the effects of H2A on chromosomal organization.

After pre-treatment with H2A and LL-37, bacteria were stained with 3 μM SYTOX Green, a concentration which fluoresces upon binding to DNA in live cells but does not inhibit bacterial growth[8], for ten minutes. *E. coli* were added to 1% agarose pads containing identical concentrations of H2A and LL-37, along with 5 μM SYTOX Green, and incubated at room temperature for three hours before imaging using fluorescence microscopy.

Fluorescence was uniform in *E. coli* treated with LL-37 alone, indicating a diffuse bacterial chromosome (Figure 6.3A). The addition of H2A to the LL-37-treated cells induced a webbed pattern in the chromosome, consistent with the induced reorganization of the chromosome by histones. Principal component analysis (PCA) was used analyze differences in the chromosomal structure in LL-37-treated cells and cells treated with both histones and LL-37. Raw images were analyzed using principal component analysis using image analysis tools developed previously[9] and modified in Matlab (Version R2017b). Briefly, individual cells were identified in phase contrast images using canny edge detection. Images of LL-37-treated cells and of cells treated with both LL-37 and H2A were pooled together, rotated such that the major axis of the cell was parallel to

the x-axis and resized to 30x100 pixels. The covariances between corresponding pixels of different cells were computed using the 16-bit intensity values from the rotated and resized fluorescence images and for the same images rotated by an additional 180 degrees. The orientation that gave the lower covariance was used for the analysis. Principal components for the covariance matrix was computed using approximately 100 cells and the principal components that gave the two largest eigenvalues were identified. This analysis, which transforms the data into fewer dimensions while retaining general trends and patterns, identified that the chromosomal patterns induced by the combined treatment of H2A and LL-37 was distinct from that of LL-37 alone (Figure 6.3B).

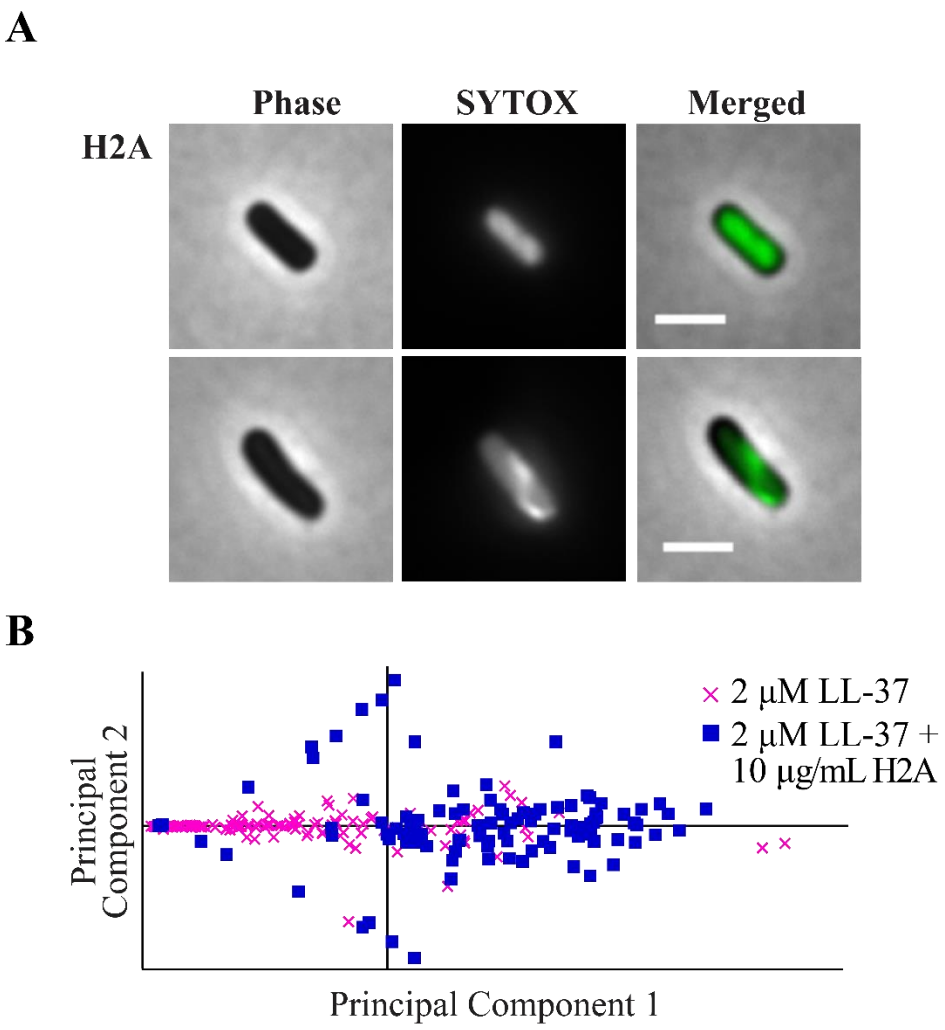

Figure 6.3. Histone H2A induces a webbed pattern in the bacterial chromosome. Mid-exponential *E. coli* were treated with 2 μM LL-37, with or without the addition of 10 μg/mL H2A, and stained with SYTOX Green, a nucleic acid stain which exhibits green fluorescence upon binding nucleic acids. (A) Merged images, containing phase contrast and SYTOX fluorescence, are shown for *E. coli* treated with LL-37 alone with LL-37 and H2A. (B) A principal component analysis (PCA) determined that the LL-37-treated cells and cells treated with both LL-37 and H2A form distinct chromosomal patterns. Each dot represents a single cell. Representative images are shown for both conditions. Scale bars represent 2 μm. Imaging and analysis performed by Henry Amir.

6.3 Histone H2A Suppresses Bacterial Transcription

Given that histones bind to *E. coli* DNA *in vitro* and perturb the chromosomal organization in live *E. coli*, the effects of histones on bacterial transcription were explored. To investigate how histone entry into the bacterial cell impacts transcription, expression of mCherry in an *E. coli* strain containing a tetracycline promoter transcriptionally fused to a gene encoding mCherry was measured. This *E. coli* strain (MG1655 attλ::[*cat tetR* ϕ(*tetA-mCherry)*]) contains the *tetR* and *tetA* genes integrated at the phage lambda attachment site and a transcriptional fusion of mCherry to the 3′ end of *tetA*.

E. coli was cultured to mid-exponential phase and pre-treated with 10 μg/mL Histone H2A, 2 μM LL-37, or a combinatorial treatment of both LL-37 and H2A. *E. coli* were incubated for one hour before the addition of 50 ng/mL of anhydrotetracycline (aTc) to induce transcription. *tetA-mCherry* fluorescence was measured after one hour using single-cell fluorescence microscopy. Pre-treatment of *E. coli* with LL-37 had little effect on *tetA-mCherry* fluorescence, indicating LL-37 does not inhibit the induction of transcription upon aTc treatment (Figure 6.4). However, in *E. coli* treated with both LL-37 and H2A, mCherry fluorescence was significantly decreased compared to untreated *E. coli* and *E. coli* treated with LL-37 alone, indicating H2A specifically inhibits transcription. Since treatment with 10 μg/mL Histone H2A alone did not inhibit transcription, suppression of bacterial transcription is dependent upon membrane permeabilization.

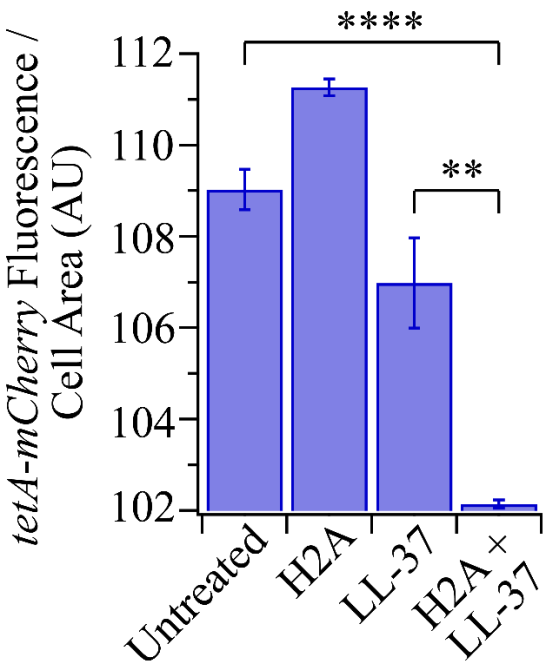

Figure 6.4. Histone H2A suppresses bacterial transcription. *E. coli*, containing a tetracycline promoter transcriptionally fused to a gene encoding mCherry, were pre-treated with 10 μg/mL H2A, 2 μM LL-37, or both for one hour before the addition of 50 ng/mL of anhydrotetracycline to induce transcription. mCherry fluorescence was measured after a 1-hour incubation. Bars indicate mean ± SEM for three independent experiments. ** $p \leq 0.01$, **** $p \leq 0.0001$.

Transcription of the mCherry reporter is controlled by the tetracycline promoter, which is activated by anhydrotetracycline. As such, this reporter measures the level of transcriptional activation. Similar constructs have been used to measure transcription in other studies[10–13]; however, inhibition of translation could also affect mCherry fluorescence. To further analyze whether H2A inhibits transcription, the effects of H2A on bacterial transcription were analyzed by quantifying RNA yields in *E. coli* treated with histones. *E. coli* were cultured to mid-exponential phase and treated with 10 μg/mL H2A, 1 μM LL-37, or 10 μg/mL H2A and 1 μM LL-37. An additional experiment was performed with increasing concentrations of H2A, from 0-100 μg/mL H2A. Bacterial cultures were harvested at 30 minutes, washed with H_2O, and resuspended in 600 μL Total Lysis Solution (TE 8.0 (10 mM Tris-HCl, 1 mM EDTA), 0.5 mg/mL lysozyme (Sigma), and 1% SDS). Nucleic acid extraction was performed with a hot phenol-chloroform extraction and ethanol precipitation[14], and RNA yield was measured using a Nanodrop 2000.

The addition of 10 μg/mL H2A caused no difference in RNA yields compared to untreated *E. coli* (Figure 6.5). However, a decrease in total RNA yield was observed after 30 minutes of treatment with 10 μg/mL H2A and 1 μM LL-37. Additionally, the total RNA yield was dramatically decreased after 30 minutes of treatment with 50 or 100 μg/mL H2A alone, which are concentrations that inhibited growth (Figure 6.6). The addition of 50 and 100 μg/mL H2A caused extended the lag time and slowed the growth rate of *E. coli* (Figure 6.6). Furthermore, *E. coli* treated with 100 μg/mL H2A reached a lower OD_{600} after a 24-hour growth period. These histone-mediated reductions in RNA yields are consistent with H2A inhibiting transcription across the population (Figure 6.4).

Although the majority of experiments thus far have included a dual-treatment with 10 μg/mL H2A histones and pore-forming antimicrobial agents, it is plausible that high concentrations of

histones, such as 50 and 100 μg/mL H2A, may occur locally in NETs or upon release from lipid droplets. Additionally, the goal of the transcriptional data was to understand the specific response of bacteria to H2A, which could only be achieved by using increasing concentrations of histones since transcriptional data for bacteria treated with H2A and AMPs would likely convolve the effects of H2A and interpretation would be unclear. Thus, increasing concentrations of H2A revealed general trends in upregulated genes without interference from LL-37 (see Section 6.4).

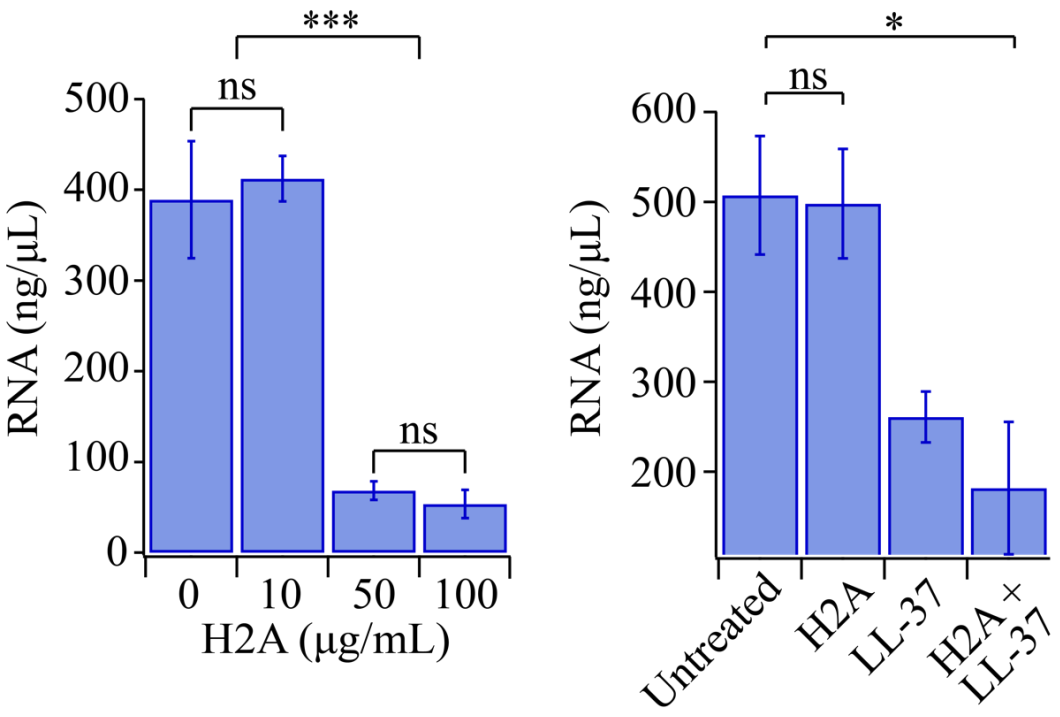

Figure 6.5. Histone H2A decreases RNA yields. Mid-exponential *E. coli* were treated with 10 µg/mL H2A, 1 µM LL-37, 10 µg/mL H2A and 1 µM LL-37, 50 µg/mL H2A, or 100 µg/mL H2A. Bacterial cultures were harvested at 30 minutes, washed with H_2O, and resuspended in 600 uL Total Lysis Solution (TE 8.0 (10 mM Tris-HCl, 1 mM EDTA), 0.5 mg/mL lysozyme (Sigma), and 1% SDS). Nucleic acid extraction was performed with a hot phenol-chloroform extraction and ethanol precipitation, and RNA yield was measured using a Nanodrop 2000. Bars indicate mean ± SEM for three independent experiments. *** $p \leq 0.001$, * $p \leq 0.05$, ns > 0.05.

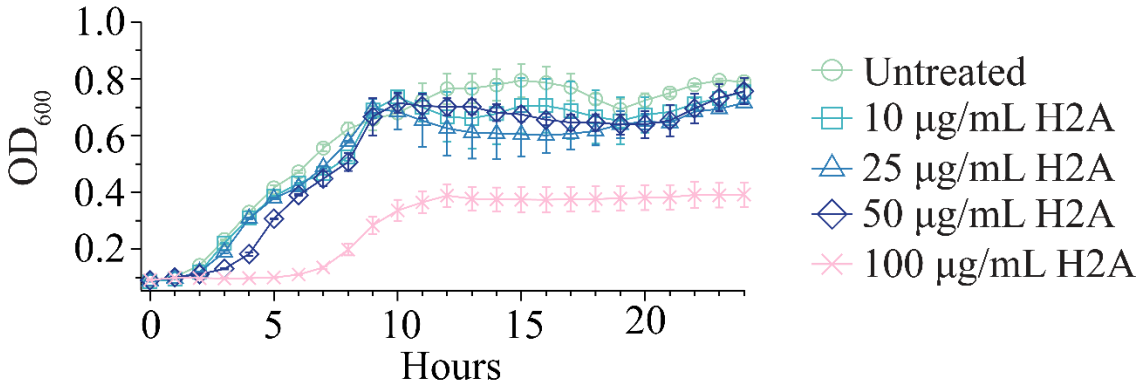

Figure 6.6. High concentrations of Histone H2A kill *E. coli*. Growth profiles of mid-exponential phase *E. coli* treated with increasing concentrations of H2A in media containing physiological (1 mM) magnesium over a 24-hour growth period. In physiological magnesium, 50 µg/mL H2A was required to see an effect on *E. coli* growth. Data points are the average of at least four independent experiments (n = 4) and error bars indicate SEM.

6.4 Histone H2A Selectively Upregulates Membrane Biogenesis Components

Little work has been done exploring transcriptome responses of bacteria to histones. Microarray analyses of *E. coli* that were histone-selected showed two plasmid inserts belonging to the colonic acid (CA) cluster: wcaI/cpsB/cpsG/wcaJ and wzc/wcaA, a 19-gene cluster that encodes genes required for exopolysaccharide and O-antigen production (which results in semi-smooth LPS)[15–17]. The gene cluster is tightly regulated by a signal transduction cascade governed by the *rcs* (regulator of capsule synthesis) phosphorelay system[18]. O-antigen and exopolysaccharide have been shown to provide histone resistance in *E. coli*, and O-antigen confers similar resistance against histones in other Gram-negative pathogens, including *Shigella flexneri* and *Klebsiella pneumoniae*[15].

K. pneumoniae mutants for bacterial capsule polysaccharide (CPS) show decreased resistance to antimicrobial peptides, including defensin 1, β-defensin 1, lactoferrin, protamine sulfate, and polymyxin B, whereas O-antigen did not have an effect in antimicrobial peptide resistance[19]. There was a correlation seen between CPS amounts and polymyxin B resistance, due to decreased polymyxin B binding, indicating CPS may protect Gram-negative bacteria by minimizing interactions between antimicrobial peptides and the bacterial membrane. *K. pneumoniae* also increased CPS amounts and upregulated *cps* transcription when grown in the presence of polymyxin B and lactoferrin. The CPS operon, present in both *E. coli* and *K. pneumoniae* contains the *wza, wzb, wzc*, *wzx,* and *wzy* genes and is regulated transcriptionally by the Rcs (regulation of capsule synthesis) proteins[20]. Wza is a lipoprotein thought to form channels in the outer membrane, Wzb is a cytoplasmic protein tyrosine phosphatase that dephosphorylates Wzx, Wzc is an inner membrane tyrosine kinase that polymerizes capsule

polysaccharides, Wzx is an inner membrane protein that transfers polysaccharide units across the inner membrane, and Wzy is an inner membrane protein that assembles longer polysaccharide chains from building blocks transported by Wzy. WzxC is a LPS biosynthesis protein.

To fully quantify the effects of histones on the transcriptome, an RNA sequencing pipeline was used. Following nucleic acid extraction with a hot phenol-chloroform extraction and ethanol precipitation, samples were DNase digested and treated with RiboZero to remove ribosomal RNA. A cDNA library was constructed from the RiboZero-treated samples and sequenced using the Princeton University Genomics Core Facility, with a depth of at least 10 M reads. Sequences were aligned to the MG1655 genome using Bowtie2. A heatmap of the top thirty upregulated genes was constructed using the R package pheatmap (Figure 6.7) and a table of the top 100 upregulated genes in shown in Table 6.1.

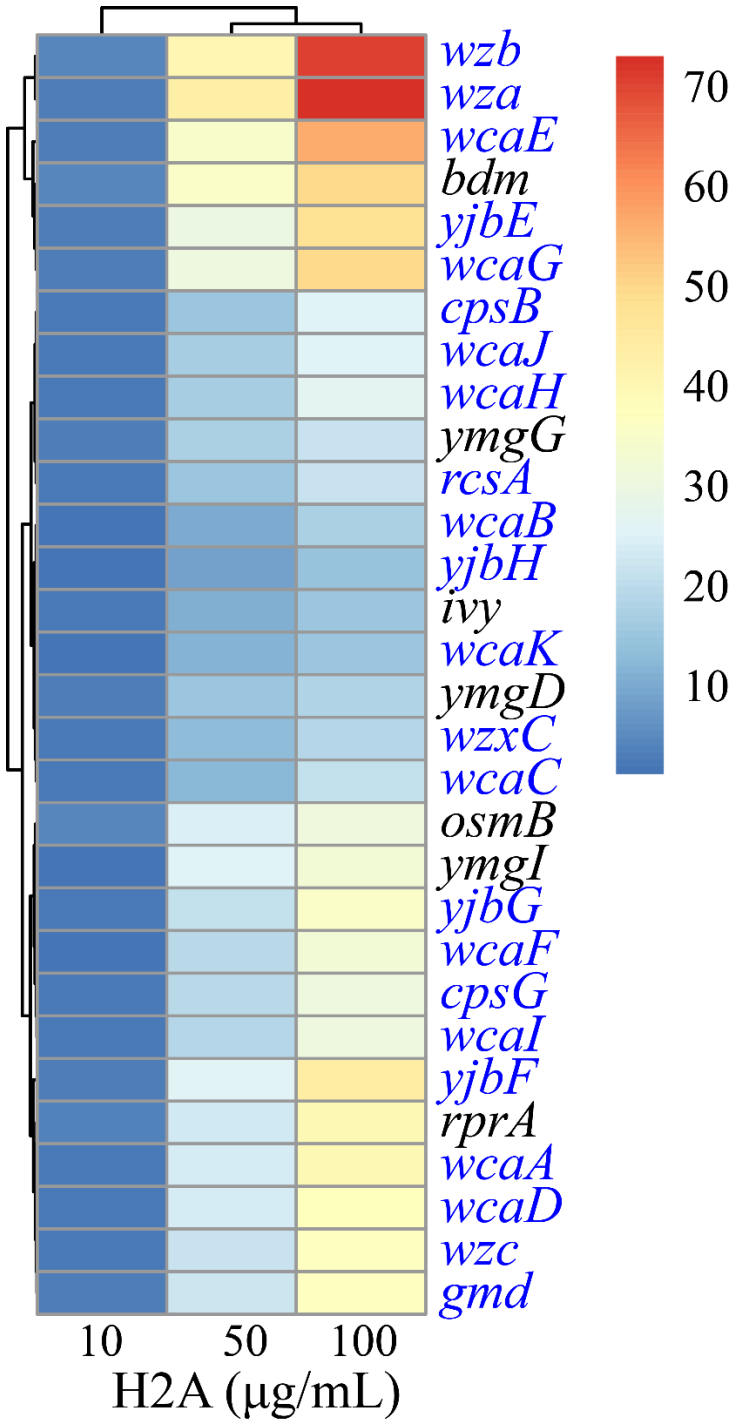

Figure 6.7. Histone H2A upregulates membrane biogenesis components. Mid-exponential *E. coli* were treated with 10, 50, or 100 µg/mL H2A and a cDNA library was constructed. The upregulation ratio for each condition was constructed by dividing the histone-treated value by the untreated value for each gene. The top 30 upregulated genes are shown. The majority of the genes (blue) are involved in the colonic acid/slime pathway, which synthesizes lipids and sugars that strengthen the outer membrane.

Table 6.1. Fold-change in mRNA transcripts in the top 100 genes upregulated in *E. coli* following a 30-minute treatment with H2A. The 10/0, 50/0, and 100/0 labels indicate comparison between 10, 50, or 100 μg/mL H2A and untreated cells. Values are the average of three independent experiments.

Gene	Function	10/0	50/0	100/0
wza	colanic acid export protein; outer membrane auxillary lipoprotein	2.9	43.3	72.8
wzb	colanic acid production protein-tyrosine-phosphatase; Wzc-P dephosphorylase	3.9	40.2	70.2
wcaE	putative glycosyl transferase	2.5	34.6	55.7
wcaG	bifunctional GDP-fucose synthetase: GDP-4-dehydro-6-deoxy-D-mannose epimerase/ GDP-4-dehydro-6-L-deoxygalactose reductase	3.1	29.8	49.8
bdm	biofilm-dependent modulation protein	4.0	35.3	49.6
yjbE	extracellular polysaccharide production threonine-rich protein	2.8	29.5	47.5
yjbF	extracellular polysaccharide production lipoprotein	2.9	25.8	44.0
wcaA	putative glycosyl transferase	2.1	23.3	39.7
rprA	Null	3.4	23.1	39.5
wcaD	putative colanic acid polymerase	2.2	23.3	37.6
gmd	GDP-D-mannose dehydratase, NAD(P)-binding	2.4	22.3	36.6
wzc	colanic acid production tyrosine-protein kinase; autokinase; Ugd phosphorylase	2.1	21.6	36.3
yjbG	extracellular polysaccharide export OMA protein	2.2	20.5	34.9
wcaF	putative acyl transferase	1.6	19.5	32.2
ymgI	uncharacterized protein	1.0	25.1	32.0
osmB	osmotically and stress inducible lipoprotein	4.2	24.5	30.6
wcaI	putative glycosyl transferase	2.3	18.5	30.2
cpsG	phosphomannomutase	1.9	19.4	30.2
wcaH	GDP-mannose mannosyl hydrolase	1.8	16.1	26.4
wcaJ	colanic biosynthesis UDP-glucose lipid carrier transferase	2.3	16.5	25.2
cpsB	mannose-1-phosphate guanyltransferase	2.1	15.2	24.7
rcsA	transcriptional regulator of colanic acid capsular biosynthesis	1.9	14.7	21.6
ymgG	UPF0757 family protein	2.9	17.2	21.6
wcaC	putative glycosyl transferase	1.8	12.4	20.4
wzxC	putative colanic acid exporter	2.0	12.8	18.5
ymgD	periplasmic protein, HdeA structural homolog	2.5	14.8	18.2
wcaB	putative acyl transferase	1.4	9.7	16.9
wcaK	colanic acid biosynthesis protein	1.6	11.3	14.8
ivy	inhibitor of c-type lysozyme, periplasmic	1.8	10.6	14.7
yjbH	DUF940 family extracellular polysaccharide protein	1.4	8.9	14.3
ygaC	uncharacterized protein	2.1	10.1	14.1

mliC	inhibitor of c-type lysozyme, membrane-bound; putative lipoprotein	1.5	7.0	10.2
osmY	salt-inducible putative ABC transporter periplasmic binding protein	1.6	6.6	9.4
ugd	UDP-glucose 6-dehydrogenase	1.2	6.6	8.9
ygdI	DUF903 family verified lipoprotein	1.6	6.0	8.2
ypeC	DUF2502 family putative periplasmic protein	1.5	5.3	8.2
ytjA	uncharacterized protein	1.4	5.5	8.1
ycfJ	uncharacterized protein	1.4	5.0	7.7
ybgS	putative periplasmic protein	1.2	5.2	7.2
wcaL	putative glycosyl transferase	1.3	5.4	7.1
yaiY	DUF2755 family inner membrane protein	1.4	4.8	7.0
iraM	RpoS stabilzer during Mg starvation, anti-RssB factor	1.1	5.1	6.8
ydeI	hydrogen peroxide resistance OB fold protein; putative periplasmic protein	0.9	5.6	6.6
ecpR	putative transcriptional regulator for the ecp operon	1.2	4.8	6.2
yghA	putative oxidoreductase	1.1	4.1	6.0
ycfT	inner membrane protein	1.1	3.7	5.9
katE	catalase HPII, heme d-containing	1.2	4.2	5.8
degP	serine endoprotease (protease Do), membrane-associated	1.2	3.6	5.3
osmC	lipoyl-dependent Cys-based peroxidase, hydroperoxide resistance; salt-shock inducible membrane protein; peroxiredoxin	1.4	3.9	5.1
yiaD	multicopy suppressor of bamB; outer membrane lipoprotein	1.5	4.3	5.1
yegS	phosphatidylglycerol kinase, metal-dependent	1.2	4.0	5.0
sra	stationary-phase-induced ribosome-associated protein	1.3	3.9	5.0
ecpB	ECP production pilus chaperone	1.2	2.9	4.8
ypfG	DUF1176 family protein	1.2	3.4	4.7
yohP	uncharacterized protein	2.0	3.1	4.7
yiaB	YiaAB family inner membrane protein	0.7	3.1	4.6
hslJ	heat-inducible lipoprotein involved in novobiocin resistance	1.3	3.9	4.6
ecpA	ECP pilin	1.1	3.3	4.6
yjdP	putative periplasmic protein	1.3	3.5	4.5
bax	putative glucosaminidase	1.5	3.9	4.5
yajI	putative lipoprotein	1.4	3.2	4.4
loiP	Phe-Phe periplasmic metalloprotease, OM lipoprotein; low salt-inducible; Era-binding heat shock protein	1.2	3.3	4.3
spy	periplasmic ATP-independent protein refolding chaperone, stress-induced	0.8	2.7	4.3
osmE	osmotically-inducible lipoprotein	1.4	3.3	4.2
yjbT	putative periplasmic protein	1.3	3.0	4.1
ybjP	lipoprotein	1.2	3.4	4.0
ytfK	DUF1107 family protein	1.1	2.8	3.9
ysaB	uncharacterized protein	1.3	3.6	3.9
galP	D-galactose transporter	1.2	3.0	3.8

rcnB	periplasmic modulator of Ni and Co efflux	1.3	3.4	3.7
ybaY	outer membrane lipoprotein	1.1	2.7	3.7
omrB	Null	1.1	2.4	3.7
omrA	Null	1.0	2.5	3.6
eco	ecotin, a serine protease inhibitor	1.2	2.8	3.5
stpA	DNA binding protein, nucleoid-associated	1.6	3.8	3.4
wcaM	colanic acid biosynthesis protein	1.2	3.1	3.4
ygdR	DUF903 family verified lipoprotein	1.1	2.7	3.3
ydeT'	pseudogene	0.8	3.0	3.3
ygaM	putative membrane-anchored DUF883 family ribosome-binding protein	1.1	2.2	3.3
glsA	glutaminase 1	1.5	2.0	3.2
yhbO	stress-resistance protein	1.0	2.3	3.2
yggE	oxidative stress defense protein	1.2	2.6	3.1
ybiH	DUF1956 domain-containing tetR family putative transcriptional regulator	1.3	2.0	3.1
yodB	cytochrome b561 homolog	1.2	2.6	3.1
ygiM	SH3 domain protein	1.1	2.4	3.0
ydeQ	putative fimbrial-like adhesin protein	1.3	2.1	3.0
ybhG	putative membrane fusion protein (MFP) component of efflux pump, membrane anchor	1.4	1.8	3.0
otsB	trehalose-6-phosphate phosphatase, biosynthetic	1.3	2.2	2.9
yjbJ	stress-induced protein, UPF0337 family	1.4	2.4	2.9
ybfA	DUF2517 family protein	1.2	1.5	2.9
ybdG	mechanosensitive channel protein, miniconductance	1.2	2.3	2.9
yehX	putative ABC transporter ATPase	1.4	1.7	2.8
fepA	ferrienterobactin outer membrane transporter	1.0	2.2	2.8
gmr	cyclic-di-GMP phosphodiesterase; csgD regulator; modulator of RNase II stability	1.0	2.2	2.8
ybdZ	stimulator of EntF adenylation activity, MbtH-like	1.0	2.2	2.7
entE	2,3-dihydroxybenzoate-AMP ligase component of enterobactin synthase multienzyme complex	1.0	2.0	2.7
yfeY	RpoE-regulated lipoprotein	1.1	2.0	2.7
yceB	lipoprotein, DUF1439 family	1.1	2.2	2.7
ydeS	putative fimbrial-like adhesin protein	1.2	1.8	2.6
caiD	carnitinyl-CoA dehydratase	1.4	2.3	2.6

The *E. coli* genes that exhibited the greatest upregulation in response to H2A treatment were determined through the RNA sequencing pipeline using triplicate experiments. The RNA sequencing analysis revealed that a majority of the upregulated genes are involved in the colonic acid/slime pathway, a 19-gene cluster encoding genes for exopolysaccharide and O-antigen production[16,17]. This pathway synthesizes lipids and sugars that strengthen the outer membrane. Evidence suggests colonic acid allows bacterial survival outside of the mammalian host or in conditions of desiccation, osmotic stress, or acid stress[21–23]. Additionally, colonic acid may be involved in virulence and biofilm formation[23,24].

In particular, the H2A-upregulated genes*: wcaI/cpsB/cpsG/wcaJ* and *wzc/wcaA* belong to the colonic acid (CA) cluster. These genes have been shown to be upregulated previously in a microarray analysis of a histone selected population of *E. coli*[15]. Overexpression of *wcaI, cpsB, and cpsG* in *E. coli* led to high resistance to histones, with *cpsB* as the main contributor to the phenotype[15]. The *wca/wca* cluster showed lower resistance to histones, corresponding to lower frequency of selection in the genetic screen. CpsB and CpsG are enzymes involved in the synthesis of sugar precursors, whereas WcaJ, WcaI, and WcaA are glycosyltransferases involved in the assembly of the sugar unit at the inner membrane[16,25]. Wzc is an inner membrane tyrosine kinase that polymerizes capsule polysaccharides and is involved in the export of the polysaccharide[26].

Notably, *wza* was upregulated 73-fold in cultures treated with 100 μg/mL H2A for 30 minutes (Table 6.1). The CA gene cluster is tightly regulated by a signal transduction cascade governed by the *rcs* (regulator of capsule synthesis) phosphorelay system[27]. The regulation of capsular synthesis (Rcs) phosphorelay allows Enterobacteriaceae to respond to membrane perturbations and damage[28]. The outer membrane lipoprotein RcsF receives a signal and activates the kinase

activity of the sensor kinase RcsC. RcsC autophosphorylates and the phosphoryl group is passed to the response regulator RcsB. Phosphorylated RcsB interacts with DNA and affects expression of numerous genes, including those related to virulence, biofilm formation, motility, and extracellular polysaccharide production[29]. Both motility and extracellular polysaccharide production require the unstable auxiliary protein RcsA, which is negatively regulated by the histone-like protein H-NS[30]. In the RNA sequencing experiments, transcription of the H-NS-regulated *rcsA* regulator increased 22-fold due to histone treatment (Figure 6.7, Table 6.1)

The Rcs proteins also transcriptionally regulate the capsule biosynthesis (CPS) operon, which regulates polysaccharide production[20]. RcsA has been found to form a heterodimer with phosphorylated RcsB, increasing affinity for Rcs-regulated promoters, including the *cps* operon[29,31]. This operon contains the *wza, wzb, wzc, wzx,* and *wzy* genes, most of which are upregulated following histone treatment[20]. Wza is a lipoprotein thought to form channels in the outer membrane, Wzb is a cytoplasmic protein tyrosine phosphatase that dephosphorylates Wzx, Wzc is an inner membrane tyrosine kinase that polymerizes capsule polysaccharides and is involved in the export of the polysaccharide, Wzx is an inner membrane protein that transfers polysaccharide units across the inner membrane, and Wzy is an inner membrane protein that assembles longer polysaccharide chains from building blocks transported by Wzy. These polysaccharides make up the bacterial capsule, which protects the bacteria.

Additional increases were seen for genes of the *wca* operon, including *wcaE*, *wcaG*, *wcaD*, *wcaH*, *wcaC*, *wcaB*, *wcaL*, and *wcaK*, which are associated with the slime biogenesis pathway[25]. WcaE is a putative glycosyl transferase, WcaG is a GDP-L-fucose synthase, WcaD is a colonic acid polymerase, WcaH hydrolyzes GDP-mannose, WcaC is a glycosyl transferase, WcaB is a

colonic acid acetyltransferase, WcaL is a glycosyltransferase, and WcaK is a colonic acid biosynthesis protein.

Furthermore, all the genes in the yjbEFGH operon are upregulated. This operon is involved in the production of extracellular polysaccharides distinct from colonic acid[32]. YjbE is is positively regulated by RcsC, which is also upregulated[33]. Additionally, Gmd, which catalyzes the conversion of GDP-D-mannose to GDP-4-dehydro-6-deoxy-D-mannose[34], and Ugd, which synthesizes UDP-alpha-D-glucuronate from UDP-alpha-D-glucose, are upregulated following histone treatment[16]. Wzc regulates phosphorylation of Ugd[35].

Apart from genes that upregulate membrane biogenesis components, there is a minor increase in DegP, a serine endoprotease that degrades transiently denatured/unfolded/misfolded proteins in the periplasm[36,37]. This serine protease has a preference for cleaving valine and isoleucine[38], both of which are prevalent amino acids in histone H2A. SufA, a subtilisin-like extracellular serine protease of *Finegoldia magna*, a Gram-positive, anaerobic bacterial strain that colonizes skin and mucous membranes and acts as an opportunistic pathogen,has been shown to degrade histones and LL-37[39,40]. In addition to the increase in DegP, there was a slight increase in the *eco*, a serine protease inhibitor that is thought to protect bacteria against neutrophil elastase, a key component of NETs[41,42]. Additionally, the upregulated genes *ivy* and *mliC* inhibit the antimicrobial enzyme lysozyme. Ivy has lysozyme inhibitor[43], and mliC specifically inhibits C-type lysozymes[44]. The Rcs regulon in *E. coli* encodes for *ivy* and *mliC*[45].

Rcs positively controls expression of ydeI, which encodes a 14 kDa periplasmic protein important for persistent infection of *S. enterica* serovar Typhimurium in mice[46]. Thus, activation of the Rcs phosphorlay may play a role in the regulation of virulence and drive a transition from localized to systemic bacterial infection. RprA, a sRNA that is highly upregulated, is positively

regulated by the Rcs phosphorelay in *E. coli*[47]. This sRNA base pairs with the 5' end of the *rpoS* mRNA (which encodes the alternative sigma factor σ^S) and increases translatability of this mRNA[48,49]. The general stress-responsive alternative sigma factor σ^s transcribes genes for bacterial survival during stationary phase and in conditions of environmental stress, such as hyperosomolarity and oxidative damage[50]. There is some evidence that σ^S represses expression of cps operon and yjbEFGH operon[51]. The Rcs phosphorelay and σ^S may enable the bacterial cell to modulate genetic expression to appropriate levels.

Genes involved in flagella biosynthesis, including EcpB, EcpA, and EcpR, are slightly upregulated. EcpB is a fimbrial, periplasmic chaperone protein that assembles the *E. coli* common pilus (ECP) and is involved in cell adherence and biofilm formation[52]. ECP is composed of the highly-upregulated EcpA and EcpR is a transcriptional regulator of the *ecp* operon[53]. Additionally, Bdm, a biofilm-dependent modulation protein, regulates flagella assembly[54]. However, the Rcs phosphorelay pathway is a key regulator of motility and phosphorylated RcsB represses expression of *flhDC*, the master regulator of flagella production[55].

The genes *osmB*, *osmY*, and *osmC*, which are involved in the osmotic stress response are upregulated following histone treatment. OsmB is an osmotically and stress inducible lipoprotein, responding either to σ^S or to the Rcs [56,57]. OsmY encodes a periplasmic protein and is involved in the uptake of osmoprotectants across the membrane[58,59]. OsmC is involved in the hyperosmotic response and oxidative stress response by metabolizing organic hydroperoxides[60].

Although PhoP and PhoQ are not upregulated in the RNA sequencing results, which were obtained in conditions of physiological magnesium, (see Chapter 3), a couple of genes involved in the PhoPQ magnesium starvation response are. The slightly upregulated IraM inhibits RpoS proteolysis by regulating RssB activity, thus increasing stability of the sigma stress factor RpoS

during magnesium starvation[61]. RcsC, part of the Rcs phosphorelay, is a sensor histidine kinase that has been linked to the PhoPQ system[62].

Finally, a couple of uncharacterized genes, including YmgG and YmgD are highly upregulated. Although YmgG is uncharacterized, this protein has a glycine-zipper-containing OmpA-like membrane domain. Although not upregulated in the RNAseq data, OmpA is a major protein in the *E. coli* outer membrane and is important for stress survival[63]. YmgD is also uncharacterized; however, it has homology to HdeA[64], an acid stress chaperone that is thought to cooperate with other periplasmic chaperones including the serine endoprotease DegP[65].

RNA sequencing results were validated by confirming upregulation of *rcsA*, a H-NS-regulated gene implicated in the regulation of the CA gene cluster[27]. Upregulation of *rcsA* by increasing concentrations of H2A was performed using a transcriptional fusion of YFP to the *rcsA* promoter in *E. coli* co-expressing CFP under control of the *ompA* promoter. Similar to the RNA sequencing conditions, mid-exponential phase bacteria were diluted into warmed MinA media with increasing concentrations of H2A. In addition, PI was added to the culture to specifically measure fluorescence intensities in membrane-permeabilized cells. After a 30-minute incubation period, YFP, CFP, and PI fluorescence were measured.

Membrane-permeabilized *E. coli* showed a significant increase in *rcsA-yfp* expression and decrease in *ompA-cfp* expression (Figure 6.8), supported a mechanism by which H2A induces selective upregulation of membrane biogenesis components while globally decreasing transcription. Treatment of *E. coli* with 100 μg/mL induced bacterial aggregation, as previously seen (Figure 4.20). Within the bacterial clump, there was high variability in PI fluorescence, indicating differential degrees of membrane permeabilization. Bacteria with lower levels of membrane permeabilization has relatively consistent *ompA-cfp* transcription and little to no *rcsA-*

yfp transcription (Figure 6.9). In contrast, membrane-permeabilized *E. coli* showed a prominent increase in *rcsA*-*yfp* transcription and a notable decrease in expression of *ompA*-*cfp*.

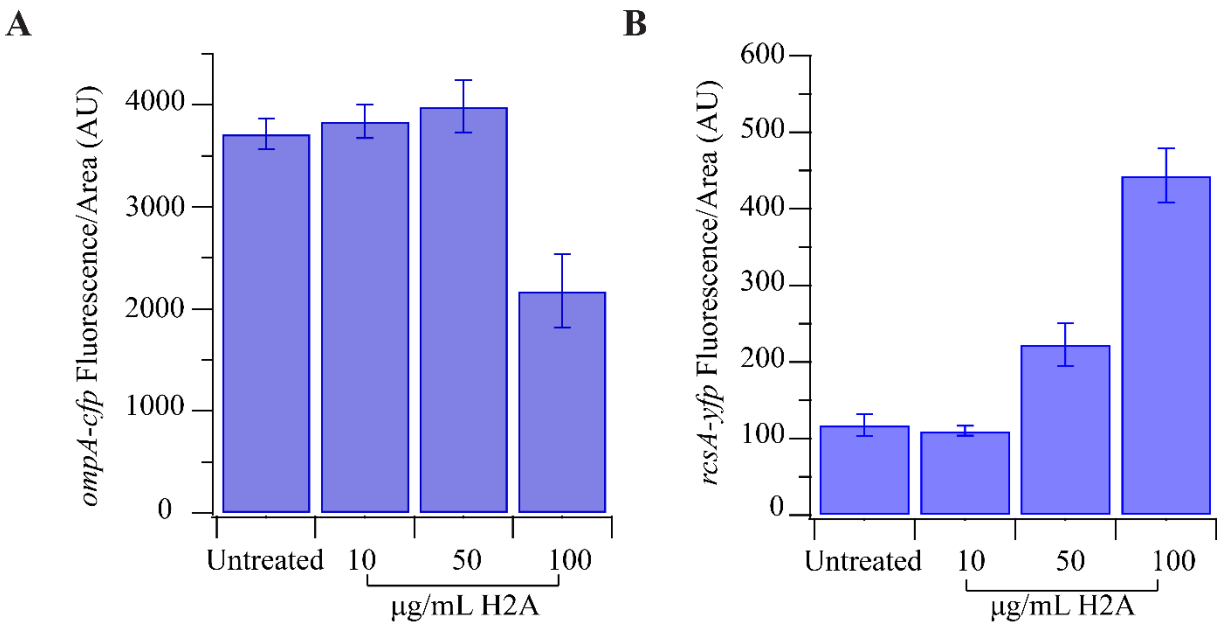

Figure 6.8. Histone H2A upregulates the Rcs phosphorelay pathway. A decrease in expression of *ompA-cfp* (A) and an increase in *rcsA-yfp* transcription (B) were observed in membrane-permeabilized *E. coli* in response to treatment with increasing concentrations of H2A. Mid-exponential *E. coli*, containing a transcriptional fusion of YFP to the *rcsA* promoter and a transcriptional fusion of CFP to the *ompA* promoter, were treated with 10, 50, or 100 µg/mL H2A for 30 minutes. 30 µM propidium iodide was added at the beginning of the incubation period to identify membrane permeabilization. Bars indicate mean ± SEM for three independent experiments.

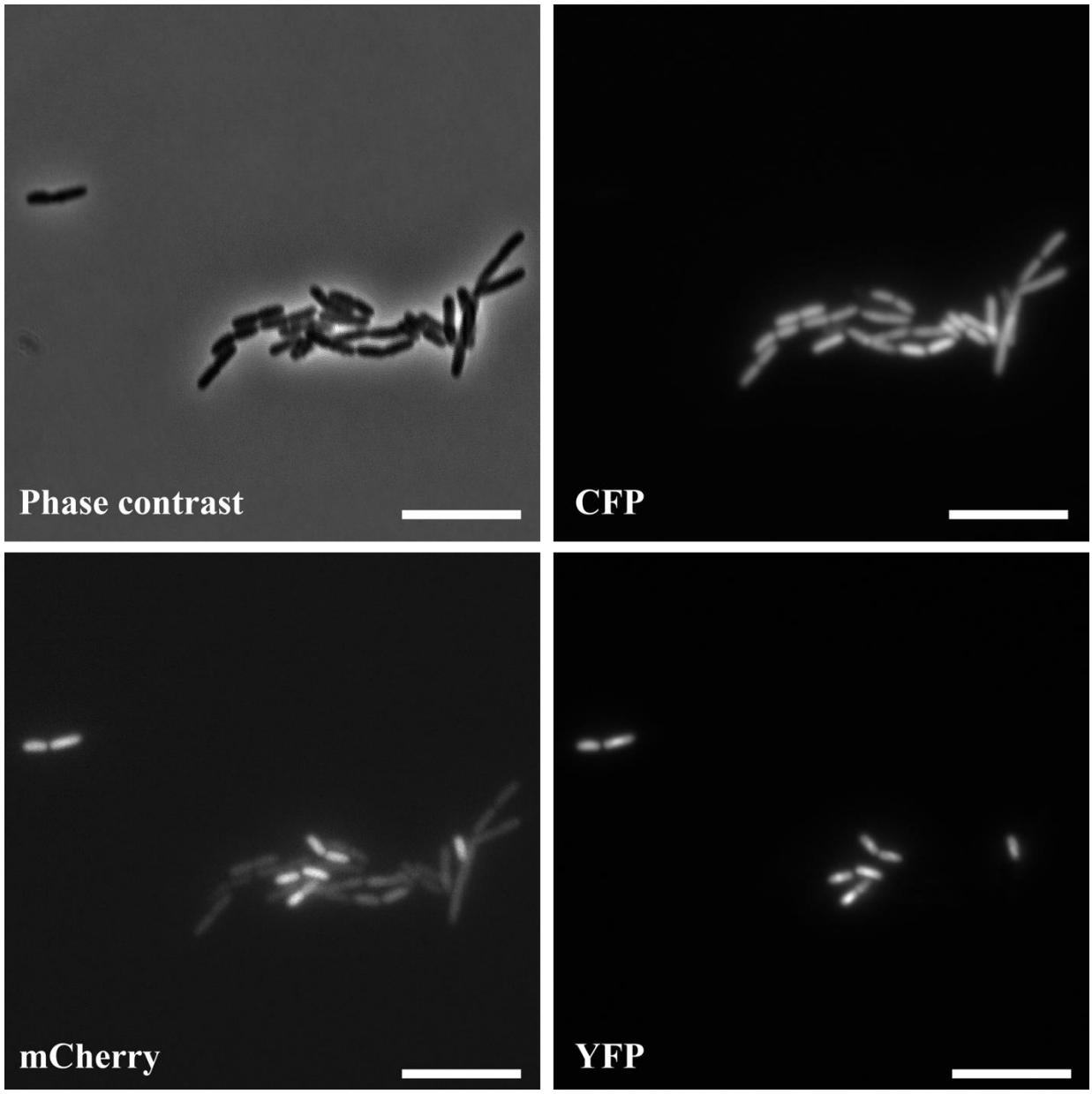

Figure 6.9. Membrane-permeabilized *E. coli* upregulate the Rcs phosphorelay pathway. Membrane-permeabilized *E. coli* (PI positive) showed the highest *rcsA-yfp* transcription and a notable decrease in expression of *ompA-cfp*. Mid-exponential *E. coli*, containing a transcriptional fusion of YFP to the *rcsA* promoter and a transcriptional fusion of CFP to the *ompA* promoter, were treated with 10, 50, or 100 μg/mL H2A for 30 minutes. 30 μM propidium iodide was added at the beginning of the experiment. Scale bars represent 10 μm.

To further understand the role that the *rcsA* gene plays in the *E. coli* response to histone treatment, an *rcsA* (Δ*rcsA*) mutant strain was constructed by P1 transduction of the D(*rcsA*)::kan allele from the Keio collection [66] strain JW1935, yielding AT14A. Treatment of mid-exponential phase Δ*rcsA* with the synergistic combination of histones and LL-37 inhibited growth and significantly increased the lag time compared to wild-type *E. coli* treated with histones and LL-37 (Figure 6.10). The *rcsA* mutant showed increased sensitivity to treatment with H2A and LL-37, indicating its key role in survival in response to H2A.

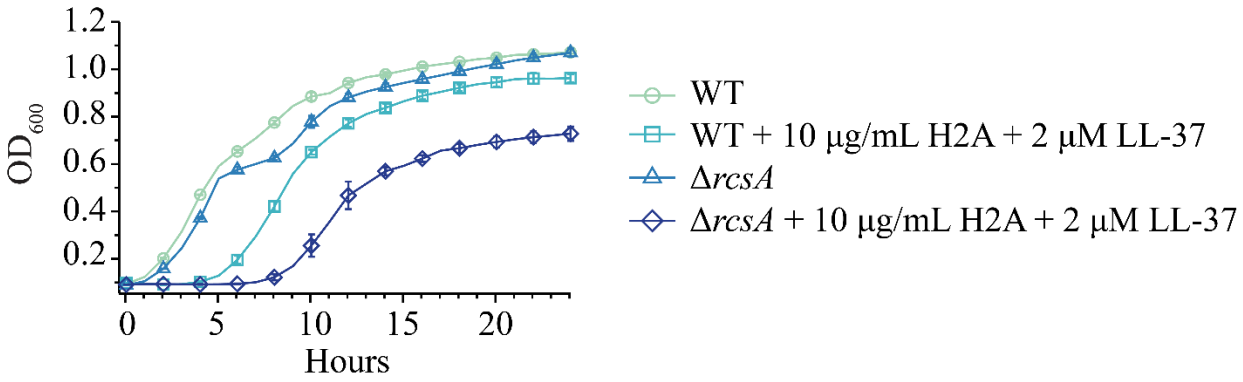

Figure 6.10. The Rcs phosphorelay pathway improves *E. coli* survival under dual treatment with H2A and LL-37. The absence of *rcsA* increases sensitivity of *E. coli* to the dual treatment of H2A and LL-37. Growth profiles of mid-exponential phase wild-type (WT) *E. coli* and Δ*rcsA* mutant *E. coli* treated with 10 μg/mL H2A, 2 μM LL-37, and the synergistic combination of both H2A and LL-37 in media containing physiological (1 mM) magnesium over a 48-hour growth period. There were few differences in growth between untreated WT and untreated Δ*rcsA E. coli*. Additionally, the addition of H2A alone had no effect on *E. coli* growth for either *E. coli* strain. The addition of LL-37 extended the lag phase for both *E. coli* strains; however, the delay in growth is more prominent for the Δ*rcsA* mutant *E. coli*. Treatment of Δ*rcsA* with LL-37 alone decreased the final OD_{600} over the 48-hour growth period. The synergistic combination of H2A and LL-37 significantly decreasing growth rates and extending lag times of Δ*rcsA* compared to synergy-treated WT *E. coli*. Data points are the average of four independent experiments (n = 4) and error bars indicate SEM.

6.5 Conclusion

Histone uptake into the bacterial cytoplasm is observed in histone treatment in low ionic conditions and in all cases of synergy between histones and pore-forming antimicrobial agents, including LL-37, MAG2, and PMB. This histone uptake supports an intracellular role for histones. Additionally, electroporation of *E. coli* in the presence of H2A led to significant inhibition of bacterial growth. Since electroporation does not lead to persistent membrane pores, this further supports a membrane-independent mechanism of histone killing. Since Histone H2A is well-characterized as a component of the histone core, I hypothesized that the positively charged histone subunit may complex with negatively charged microbial DNA, thereby perturbing replication and transcription.

In vitro, increasing levels of Histone H2A inhibited bacterial DNA migration through a PAGE gel, indicating significant interactions occur between histone H2A and *E. coli* DNA. In contrast, low levels of binding were observed between LL-37 and microbial DNA, support a mechanism by which the primary role of AMPs in NETs and on lipid droplets is membrane permeabilization and facilitation of histone entry into the bacterial cell.

In vivo experiments measuring the effect of H2A on *E. coli* chromosomes, using the nucleic acid stain SYTOX Green, revealed a diffuse bacterial chromosome in LL-37-treated cells and a webbed pattern in dual treated cells, consistent with the induced reorganization of the chromosome by histones. In addition to rearranging the bacterial chromosome, histones specifically inhibit transcription, as measured by transcription on an mCherry reporter and RNA yields following nucleic acid extraction.

Although global transcription is repressed, the bacterial cells highly upregulate genes involved in membrane biogenesis, including genes in the colonic acid/slime pathway, a 19-gene cluster

encoding genes for exopolysaccharide and O-antigen pathway. As this pathway synthesizes lipids and sugars that strengthen the outer membrane, this supports selective upregulation of membrane biogenesis genes while globally decreasing transcription. This CA gene cluster is tightly regulated by a signal transduction cascade governed by the *rcs* (regulator of capsule synthesis) phosphorelay system which allows Enterobacteriaceae to respond to membrane perturbations and damage. Transcription of the *rcsA* regulator increased 22-fold due to histone treatment. The RNA sequencing results were independently validated using a strain of *E. coli* containing transcriptional fusions of YFP and CFP to *rcsA* and the constitutively expressed *ompA*, respectively. In membrane-permeabilized *E. coli*, there was a prominent increase in *rcsA-yfp* transcription and a notable decrease in expression of *ompA-cfp*. Thus, these results validate a mechanism of histones inducing selective upregulation of membrane biogenesis components while globally decreasing transcription.

6.6 References

1. Haney, E. F. *et al.* Mechanism of action of puroindoline derived tryptophan-rich antimicrobial peptides. *Biochimica et Biophysica Acta (BBA) - Biomembranes* **1828**, 1802–1813 (2013).
2. Park, S.-C. *et al.* A plausible mode of action of pseudin-2, an antimicrobial peptide from Pseudis paradoxa. *Biochimica et Biophysica Acta (BBA) - Biomembranes* **1808**, 171–182 (2011).
3. Ma, L. *et al.* Effective antimicrobial activity of Cbf-14, derived from a cathelin-like domain, against penicillin-resistant bacteria. *Biomaterials* **87**, 32–45 (2016).
4. Hayden, R. M. *et al.* Complementary Effects of Host Defense Peptides Piscidin 1 and Piscidin 3 on DNA and Lipid Membranes: Biophysical Insights into Contrasting Biological Activities. *The Journal of Physical Chemistry B* **119**, 15235–15246 (2015).
5. TBE buffer. *Cold Spring Harbor Protocols* **2006**, pdb.rec8458 (2006).
6. Zhang, X. *et al.* Dual functions of the human antimicrobial peptide LL-37—Target membrane perturbation and host cell cargo delivery. *Biochimica et Biophysica Acta (BBA) - Biomembranes* **1798**, 2201–2208 (2010).
7. Lande, R. *et al.* Plasmacytoid dendritic cells sense self-DNA coupled with antimicrobial peptide. *Nature* **449**, 564–569 (2007).
8. Bakshi, S. *et al.* Nonperturbative Imaging of Nucleoid Morphology in Live Bacterial Cells during an Antimicrobial Peptide Attack. *Applied and Environmental Microbiology* **80**, 4977–4986 (2014).
9. Cowles, K. N. *et al.* The putative Poc complex controls two distinct *Pseudomonas aeruginosa* polar motility mechanisms: *tonB / exbB / exbD* homologues regulate polar motility. *Molecular Microbiology* **90**, 923–938 (2013).
10. Lasaro, M. *et al.* Escherichia coli Isolate for Studying Colonization of the Mouse Intestine and Its Application to Two-Component Signaling Knockouts. *Journal of Bacteriology* **196**, 1723–1732 (2014).
11. Libby, E. A., Roggiani, M. & Goulian, M. Membrane protein expression triggers chromosomal locus repositioning in bacteria. *Proceedings of the National Academy of Sciences* **109**, 7445–7450 (2012).
12. Roggiani, M. & Goulian, M. Oxygen-Dependent Cell-to-Cell Variability in the Output of the Escherichia coli Tor Phosphorelay. *J. Bacteriol.* **197**, 1976–1987 (2015).
13. Carey, J. N. *et al.* Regulated Stochasticity in a Bacterial Signaling Network Permits Tolerance to a Rapid Environmental Change. *Cell* **173**, 196-207.e14 (2018).
14. Siryaporn, A., Kuchma, S. L., O'Toole, G. A. & Gitai, Z. Surface attachment induces *Pseudomonas aeruginosa* virulence. *Proceedings of the National Academy of Sciences* **111**, 16860–16865 (2014).
15. Chaput, C., Spindler, E., Gill, R. T. & Zychlinsky, A. O-Antigen Protects Gram-Negative Bacteria from Histone Killing. *PLoS ONE* **8**, e71097 (2013).
16. Stevenson, G., Andrianopoulos, K., Hobbs, M. & Reeves, P. R. Organization of the Escherichia coli K-12 gene cluster responsible for production of the extracellular polysaccharide colanic acid. *J. Bacteriol.* **178**, 4885–4893 (1996).
17. Meredith, T. C. *et al.* Modification of Lipopolysaccharide with Colanic Acid (M-antigen) Repeats in *Escherichia coli*. *Journal of Biological Chemistry* **282**, 7790–7798 (2007).

18. Stout, V. Identification of the promoter region for the colanic acid polysaccharide biosynthetic genes in Escherichia coli K-12. *Journal of Bacteriology* **178**, 4273–4280 (1996).
19. Campos, M. A. *et al.* Capsule Polysaccharide Mediates Bacterial Resistance to Antimicrobial Peptides. *Infection and Immunity* **72**, 7107–7114 (2004).
20. Whitfield, C. Biosynthesis and Assembly of Capsular Polysaccharides in *Escherichia coli*. *Annual Review of Biochemistry* **75**, 39–68 (2006).
21. Mao, Y., Doyle, M. P. & Chen, J. Role of colanic acid exopolysaccharide in the survival of enterohaemorrhagic Escherichia coli O157:H7 in simulated gastrointestinal fluids. *Lett. Appl. Microbiol.* **42**, 642–647 (2006).
22. Mao, Y., Doyle, M. P. & Chen, J. Insertion Mutagenesis of wca Reduces Acid and Heat Tolerance of Enterohemorrhagic Escherichia coli O157:H7. *Journal of Bacteriology* **183**, 3811–3815 (2001).
23. Li, G., Laturnus, C., Ewers, C. & Wieler, L. H. Identification of Genes Required for Avian Escherichia coli Septicemia by Signature-Tagged Mutagenesis. *Infection and Immunity* **73**, 2818–2827 (2005).
24. Subashchandrabose, S., Smith, S. N., Spurbeck, R. R., Kole, M. M. & Mobley, H. L. T. Genome-wide detection of fitness genes in uropathogenic Escherichia coli during systemic infection. *PLoS Pathog.* **9**, e1003788 (2013).
25. Ren, G., Wang, Z., Li, Y., Hu, X. & Wang, X. Effects of Lipopolysaccharide Core Sugar Deficiency on Colanic Acid Biosynthesis in Escherichia coli. *J. Bacteriol.* **198**, 1576–1584 (2016).
26. Cuthbertson, L., Mainprize, I. L., Naismith, J. H. & Whitfield, C. Pivotal Roles of the Outer Membrane Polysaccharide Export and Polysaccharide Copolymerase Protein Families in Export of Extracellular Polysaccharides in Gram-Negative Bacteria. *Microbiology and Molecular Biology Reviews* **73**, 155–177 (2009).
27. Navasa, N., Rodríguez-Aparicio, L., Ferrero, M. Á., Monteagudo-Mera, A. & Martínez-Blanco, H. Polysialic and colanic acids metabolism in *Escherichia coli* K92 is regulated by RcsA and RcsB. *Biosci. Rep.* **33**, 405–415 (2013).
28. Laubacher, M. E. & Ades, S. E. The Rcs Phosphorelay Is a Cell Envelope Stress Response Activated by Peptidoglycan Stress and Contributes to Intrinsic Antibiotic Resistance. *Journal of Bacteriology* **190**, 2065–2074 (2008).
29. Majdalani, N. & Gottesman, S. THE RCS PHOSPHORELAY: A Complex Signal Transduction System. *Annual Review of Microbiology* **59**, 379–405 (2005).
30. Sledjeski, D. & Gottesman, S. A small RNA acts as an antisilencer of the H-NS-silenced rcsA gene of Escherichia coli. *Proceedings of the National Academy of Sciences* **92**, 2003–2007 (1995).
31. Wehland, M. & Bernhard, F. The RcsAB Box: CHARACTERIZATION OF A NEW OPERATOR ESSENTIAL FOR THE REGULATION OF EXOPOLYSACCHARIDE BIOSYNTHESIS IN ENTERIC BACTERIA. *J. Biol. Chem.* **275**, 7013–7020 (2000).
32. Ferrieres, L., Aslam, S. N., Cooper, R. M. & Clarke, D. J. The yjbEFGH locus in Escherichia coli K-12 is an operon encoding proteins involved in exopolysaccharide production. *Microbiology* **153**, 1070–1080 (2007).
33. Ferrières, L. & Clarke, D. J. The RcsC sensor kinase is required for normal biofilm formation in Escherichia coli K-12 and controls the expression of a regulon in response to growth on a solid surface: E. coli Rcs regulon. *Molecular Microbiology* **50**, 1665–1682 (2003).

34. Sturla, L. *et al.* Expression, purification and characterization of GDP- D -mannose 4,6-dehydratase from *Escherichia coli*. *FEBS Letters* **412**, 126–130 (1997).
35. Grangeasse, C. *et al.* Autophosphorylation of the *Escherichia coli* Protein Kinase Wzc Regulates Tyrosine Phosphorylation of Ugd, a UDP-glucose Dehydrogenase. *J. Biol. Chem.* **278**, 39323–39329 (2003).
36. Lipinska, B., Zylicz, M. & Georgopoulos, C. The HtrA (DegP) protein, essential for Escherichia coli survival at high temperatures, is an endopeptidase. *J. Bacteriol.* **172**, 1791–1797 (1990).
37. Isaac, D. D., Pinkner, J. S., Hultgren, S. J. & Silhavy, T. J. The extracytoplasmic adaptor protein CpxP is degraded with substrate by DegP. *Proc. Natl. Acad. Sci. U.S.A.* **102**, 17775–17779 (2005).
38. Kolmar, H., Waller, P. R. & Sauer, R. T. The DegP and DegQ periplasmic endoproteases of Escherichia coli: specificity for cleavage sites and substrate conformation. *J. Bacteriol.* **178**, 5925–5929 (1996).
39. Murphy, E. C., Mohanty, T. & Frick, I.-M. FAF and SufA: proteins of Finegoldia magna that modulate the antibacterial activity of histones. *J Innate Immun* **6**, 394–404 (2014).
40. Karlsson, C. *et al.* SufA--a novel subtilisin-like serine proteinase of Finegoldia magna. *Microbiology (Reading, Engl.)* **153**, 4208–4218 (2007).
41. Yang, S. Q., Wang, C.-I., Gillmor, S. A., Fletterick, R. J. & Craik, C. S. Ecotin: a serine protease inhibitor with two distinct and interacting binding sites. *Journal of Molecular Biology* **279**, 945–957 (1998).
42. Eggers, C. T., Murray, I. A., Delmar, V. A., Day, A. G. & Craik, C. S. The periplasmic serine protease inhibitor ecotin protects bacteria against neutrophil elastase. *Biochem. J.* **379**, 107–118 (2004).
43. Clarke, C. A., Scheurwater, E. M. & Clarke, A. J. The vertebrate lysozyme inhibitor Ivy functions to inhibit the activity of lytic transglycosylase. *J. Biol. Chem.* **285**, 14843–14847 (2010).
44. Callewaert, L. *et al.* A New Family of Lysozyme Inhibitors Contributing to Lysozyme Tolerance in Gram-Negative Bacteria. *PLoS Pathog* **4**, e1000019 (2008).
45. Callewaert, L., Vanoirbeek, K. G. A., Lurquin, I., Michiels, C. W. & Aertsen, A. The Rcs Two-Component System Regulates Expression of Lysozyme Inhibitors and Is Induced by Exposure to Lysozyme. *Journal of Bacteriology* **191**, 1979–1981 (2009).
46. Erickson, K. D. & Detweiler, C. S. The Rcs phosphorelay system is specific to enteric pathogens/commensals and activates *ydeI* , a gene important for persistent *Salmonella* infection of mice. *Molecular Microbiology* **62**, 883–894 (2006).
47. Guo, X.-P. & Sun, Y.-C. New Insights into the Non-orthodox Two Component Rcs Phosphorelay System. *Front. Microbiol.* **8**, 2014 (2017).
48. Majdalani, N., Hernandez, D. & Gottesman, S. Regulation and mode of action of the second small RNA activator of RpoS translation, RprA: RprA regulation and mode of action. *Molecular Microbiology* **46**, 813–826 (2002).
49. Majdalani, N., Chen, S., Murrow, J., St John, K. & Gottesman, S. Regulation of RpoS by a novel small RNA: the characterization of RprA: RprA, a small RNA regulator of RpoS. *Molecular Microbiology* **39**, 1382–1394 (2004).
50. Kazmierczak, M. J., Wiedmann, M. & Boor, K. J. Alternative Sigma Factors and Their Roles in Bacterial Virulence. *Microbiology and Molecular Biology Reviews* **69**, 527–543 (2005).

51. Ionescu, M. & Belkin, S. Overproduction of Exopolysaccharides by an Escherichia coli K-12 rpoS Mutant in Response to Osmotic Stress. *Applied and Environmental Microbiology* **75**, 483–492 (2009).
52. Garnett, J. A. *et al.* Structural insights into the biogenesis and biofilm formation by the Escherichia coli common pilus. *Proceedings of the National Academy of Sciences* **109**, 3950–3955 (2012).
53. Martínez-Santos, V. I., Medrano-López, A., Saldaña, Z., Girón, J. A. & Puente, J. L. Transcriptional Regulation of the *ecp* Operon by EcpR, IHF, and H-NS in Attaching and Effacing Escherichia coli. *J. Bacteriol.* **194**, 5020–5033 (2012).
54. Kim, J.-S., Kim, Y. J., Seo, S., Seong, M.-J. & Lee, K. Functional Role of bdm During Flagella Biogenesis in Escherichia coli. *Curr Microbiol* **70**, 369–373 (2015).
55. Francez-Charlot, A. *et al.* RcsCDB His-Asp phosphorelay system negatively regulates the flhDC operon in Escherichia coli: Regulation of flhDC by RcsB. *Molecular Microbiology* **49**, 823–832 (2004).
56. Boulanger, A. *et al.* Multistress Regulation in Escherichia coli: Expression of osmB Involves Two Independent Promoters Responding either to S or to the RcsCDB His-Asp Phosphorelay. *Journal of Bacteriology* **187**, 3282–3286 (2005).
57. Jung, J. U., Gutierrez, C. & Villarejo, M. R. Sequence of an osmotically inducible lipoprotein gene. *J. Bacteriol.* **171**, 511–520 (1989).
58. Yim, H. H. & Villarejo, M. osmY, a new hyperosmotically inducible gene, encodes a periplasmic protein in Escherichia coli. *J. Bacteriol.* **174**, 3637–3644 (1992).
59. Frossard, S. M. *et al.* Identification of a Third Osmoprotectant Transport System, the OsmU System, in Salmonella enterica. *Journal of Bacteriology* **194**, 3861–3871 (2012).
60. Lesniak, J., Barton, W. A. & Nikolov, D. B. Structural and functional features of the *Escherichia coli* hydroperoxide resistance protein OsmC. *Protein Sci.* **12**, 2838–2843 (2003).
61. Bougdour, A., Cunning, C., Baptiste, P. J., Elliott, T. & Gottesman, S. Multiple pathways for regulation of σS (RpoS) stability in Escherichia coli via the action of multiple anti-adaptors: IraM and IraD, new regulators of σS proteolysis. *Molecular Microbiology* **68**, 298–313 (2008).
62. Hagiwara, D. *et al.* Genome-Wide Analyses Revealing a Signaling Network of the RcsC-YojN-RcsB Phosphorelay System in *Escherichia coli*. *J. Bacteriol.* **185**, 5735–5746 (2003).
63. Wang, Y. The Function of OmpA in Escherichia coli. *Biochemical and Biophysical Research Communications* **292**, 396–401 (2002).
64. Socher, E. & Sticht, H. Probing the Structure of the *Escherichia coli* Periplasmic Proteins HdeA and YmgD by Molecular Dynamics Simulations. *J. Phys. Chem. B* **120**, 11845–11855 (2016).
65. Zhang, M. *et al.* A genetically incorporated crosslinker reveals chaperone cooperation in acid resistance. *Nat Chem Biol* **7**, 671–677 (2011).
66. Baba, T. *et al.* Construction of Escherichia coli K-12 in-frame, single-gene knockout mutants: the Keio collection. *Molecular Systems Biology* **2**, (2006).

Chapter 7: Conclusion and Future Directions

7.1 Histone H2A Provides Multiple Modes of Assault Against Bacteria

There is a pressing need to develop new therapeutic agents and approaches to combat the increasing issue of antibiotic resistance. Investigating natural host defense proteins and pathways may enable the development of effective, synthetic drugs, guided by the principles of nature. Of particular interest, histones proteins were shown to be antimicrobial in nature as early as 1942[1]. The antimicrobial activity of histones were further characterized in 1958 using *E. coli* as a model organism[2]. However, these small, alkaline histone proteins were later shown to play a key role in packaging the DNA into nucleosomes that condense chromatin, and this was seen as their primary function for many years. As such, minimal research was conducted on the antimicrobial role of histones and the possible mechanisms by which histones kill bacteria. The 2004 discovery that histones have a central role in NET-mediated killing of bacteria, an innate immune response for combating bacterial infections[3], shifted interest back towards histones as antimicrobial agents and has renewed interest into understanding the mechanism by which histones kill bacteria.

Histones are positively-charged, stemming from the large proportion of positively-charged amino acids lysine and arginine, which facilitate their interactions with negatively-charged DNA. Similar to antimicrobial peptides (AMPs), histones also contain a high proportion of hydrophobic amino acids and possess the ability to form alpha helices[4,5]. Additionally, AMPs and individual histone proteins are comparable in size[6,7] and both are present in NETs[8,9]. Given that AMPs and histones share key biochemical properties, their functions have been seen as redundant[10]; however, this has not been fully explored.

Histone-derived AMPs have been suggested to function via membrane permeabilization (See Chapter 1) and full-length histones show high affinities for LPS[11], supporting a mechanism where histones interact with the bacterial membrane to kill bacteria. Other work has suggested histones have a cytoplasmic target[12]. Thus, despite being originally proposed to function as antimicrobial agents [13,14], and having an essential role in mammalian innate immune responses[3], little was known about how histones function as antimicrobial agents. Additionally, the small body of work regarding the mechanism of histone-mediated killing was complicated by the usage of low-ionic solutions and buffers that are not physiologically relevant[3,15–29] and the high, unphysiological concentrations of histones (120 μg/mL), well in excess of the MIC [18,28,30]. Since histones are less effective at killing bacteria in physiologically relevant conditions[5,18], this has raised questions regarding whether histones are truly antimicrobial agents.

Although histones showed weak activity *in vivo*, I hypothesized that the antimicrobial activity of histones is dependent upon interactions with other immune system mechanisms or components, including AMPs. Synergy between antimicrobial peptides has been well-established and, within the immune system, histones are co-localized with antimicrobial peptides (AMPs). Thus, it seemed plausible that histones function as part of a larger antimicrobial mechanism *in vivo.* Within this particular work, the antimicrobial activity of histones has been characterized in the context of other aspects of the innate immune system, as opposed to a sole antimicrobial agent.

The work presented here reveals that, in physiological environments, the antimicrobial activity of histones are unmasked when histones combine with other pore-forming antimicrobial agents which cause bacterial membrane permeabilization. Membrane permeabilization can be achieved through electroporation, low ionic conditions, or the addition of membrane-permeabilizing agents, including the antibiotic polymyxin B, the AMP LL-37, or the AMP

magainin-2. This membrane permeabilization facilitates histone uptake into the cytoplasm. Given the colocalization of AMPs and histones in immune cells, it is plausible that a primary function of AMPs is the formation of pores in the bacterial membrane. This AMP-mediated pore formation enables histones to enter into the bacteria and stabilize the bacterial pores. Within the cytoplasm, H2A targets multiple processes in the cell and provides multiple modes of assault against bacteria. In particular, the ability of H2A to disrupt the protein motive force and block ATP production, combined with its rearrangement of the bacterial chromosome and inhibition of transcription, ensures that bacteria cannot mount a transcriptional response to repair membrane or cellular damage that is caused by antimicrobial peptides or histones. Interestingly, although the antimicrobial activity of histones appears partially dependent upon histone uptake into the cell, increasing concentrations of histones alone induced cellular aggregation. It is possible that this aggregation is beneficial from a host perspective, enabling the host to promote microbial clearance; however, future work will need to investigate the role of this aggregation *in vivo*.

The limited antimicrobial activity of histones alone shown in this work agree with previous findings under physiological conditions[3,15–29]. This work demonstrates that the antimicrobial effects of histones are fully revealed when the bacterial membrane is permeabilized and histones are able to stabilize the pores and enter the bacterial cell. Thus, an additional mechanism is required to permeabilize the membrane and facilitate pore stabilization and the entry of histones into the bacterial cytoplasm.

Host innate immune responses, such as release of NETs from neutrophils to trap and kill bacteria, require concerted action among multiple components and mechanisms. The synergistic antimicrobial activity of AMPs and histones described in this work represent such a mechanism. The individual effects of pore-forming AMPs, such as LL-37 and magainin-2, on bacterial

physiology have been investigated for decades. These studies have revealed that these antimicrobial agents have moderate inhibitory effects on bacterial growth when considered individually, but prior studies have not considered the combined effects AMPs and histones. The body of work discussed here considers the effects of dual treatment with both AMPs and histones. Alone, LL-37 induces permeation of the outer and inner bacterial membrane, causing a decrease in cellular size, whereas Histone H2A alone induces bacterial clumping and increased transcription of membrane-strengthening genes. When considering the functions of AMPs and histones in an innate immune response, the role of AMPs would appear to be the formation of membrane pores that facilitate pore stabilization and the entry of other antimicrobial molecules, such as histones, into bacteria. Likely this mechanism enables the entry of molecules that may have weak pore-forming ability into the cytoplasm of the bacteria. Once inside, such molecules may target different bacterial growth mechanisms, as seen in this work.

When supplied together, the AMP LL-37 and Histone H2A have a synergistic killing effect on Gram-negative and Gram-positive bacteria through a novel mechanism: AMPs enables the entry of histones into the cell, where histones can exert multiple modes of assault, including chromosome-altering effects, disruption of ion gradients, and inhibition of transcription and bacterial repair. Importantly, this work demonstrates that Histone H2A and the AMP LL-37 employ a multi-step mechanism to kill bacteria.

7.2 Histones and AMPs Form a Positive Feedback Loop

Together, the human AMP LL-37 induces permeation of the outer and inner bacterial membranes, enabling the entry of histones into the cell, where histones can bind to the bacterial chromosome, decreasing transcription and inducing chromosomal reorganization. The two antimicrobial agents synergize to compromise membrane integrity and facilitate uptake of both molecules into bacteria, where H2A reorganizes bacterial chromosomal DNA and represses transcription. Thus, AMPs and histones represent two complementary components of a multi-step innate immunity antimicrobial mechanism.

Together, histones and AMPs constitute a positive feedback loop: the entry of histones into bacteria facilitates the uptake of AMPs, which further increases histone uptake (Figure 7.1). Feedback loops, such as this, provide exponential amplification of small signals.

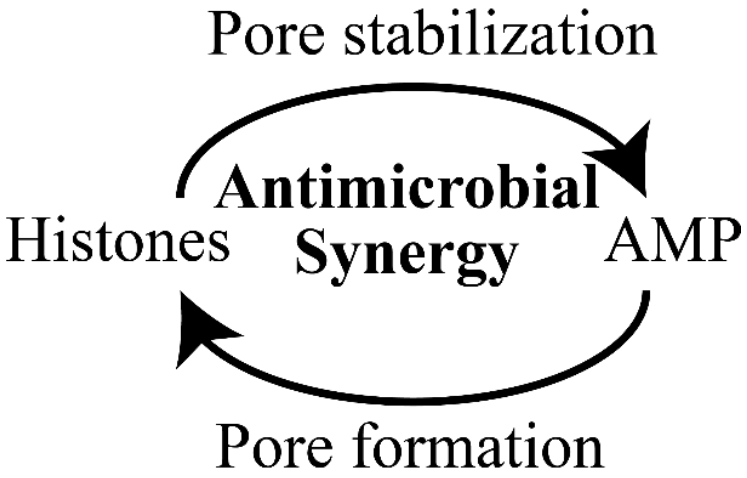

Figure 7.1. Histones and AMPs form a positive feedback loop that facilitates the uptake of antimicrobials into the cell. The interactions between histones and AMPs constitute a positive feedback loop in which AMP-induced pore formation increases the uptake of histones, which in turn, stabilizes the pore to facilitate uptake of additional AMPs.

A simple mathematical model can be derived to describe the dynamics of histone and AMP uptake into bacterial cells. Histones and AMPs enter passively using simple diffusion:

$$\frac{d[His_{in}]}{dt} = k_{His}[His_{out}]$$

$$\frac{d[AMP_{in}]}{dt} = k_{AMP}[AMP_{out}]$$

where [His_{in}] and [His_{out}] represent the concentrations of histones inside and outside of the cell, respectively, [AMP_{in}] and [AMP_{out}] represent the concentrations of AMP inside and outside of the cell, respectively, and $k_{Hisentry}$ and $k_{AMPentry}$ are the rate constants associated with the passive entry of histones and AMPs into the cell, respectively.

Molecules of histones and AMPs can leave the cell through a number of ways including cell division, shedding of cell components, and transport through drug efflux pumps. These combined effects on histones and AMPs are described using the rate constants $k_{Hisexit}$ and $k_{AMPexit}$, respectively. To encode the behaviors that histones increases the intracellular AMP concentration and that AMPs increase intracellular histone concentrations, potentially through pore-stabilization, the rate constants $k_{Hisstab}$ and $k_{AMPstab}$ were defined, arriving at the equations:

$$\frac{d[His_{in}]}{dt} = k_{Hisentry}[His_{out}] - k_{Hisexit}[His_{in}] + k_{Hisstab}[AMP_{in}] \quad (1)$$

$$\frac{d[AMP_{in}]}{dt} = k_{AMPentry}[AMP_{out}] - k_{AMPexit}[AMP_{in}] + k_{AMPstab}[His_{in}]. \quad (2)$$

In simulations, the initial histones and AMP concentrations inside the cell were set to 0. The concentration of histones and AMPs outside the cell remained constant, which describes an environment in which there is an excess of histones and AMPs. The permeation rates of $k_{Hisentry}$ and $k_{AMPentry}$ were set to 0.004 s^{-1} based on permeation measurements of the charged antibiotic tetracycline into bacterial cells[31]. The rate constants $k_{Hisexit}$ and $k_{AMPexit}$ were set to correspond to a

doubling time of 30 minutes, which is a conservative estimate of the rate of histone and AMP removal from the cell that does not require the existence of an export mechanism. The synergy condition was simulated by setting $k_{Hisstab}$ and $k_{AMPstab}$ to 0.1 s^{-1} and the non-synergistic condition was simulated by setting these rate constants to 0 s^{-1}.

To analyze uptake dynamics, the concentrations of histones and AMP outside of the cell were set to 1 and the total intracellular concentration of these molecules was computed as a function of time. Density plots were constructed by computing the total intracellular concentration of histones and AMPs following 60 minutes of exposure to a range of histones and AMPs concentrations outside of the cell.

In the histone-AMP positive feedback model described, the feedback between AMPs and histones exponentially amplifies the uptake of both molecules into the bacterial cell. Thus, the presence of low concentrations of both histones and AMPs, such as those concentrations used throughout this work, can trigger an exponential uptake of histone and AMP molecules into the bacterial cell (Figure 7.2, 7.3).

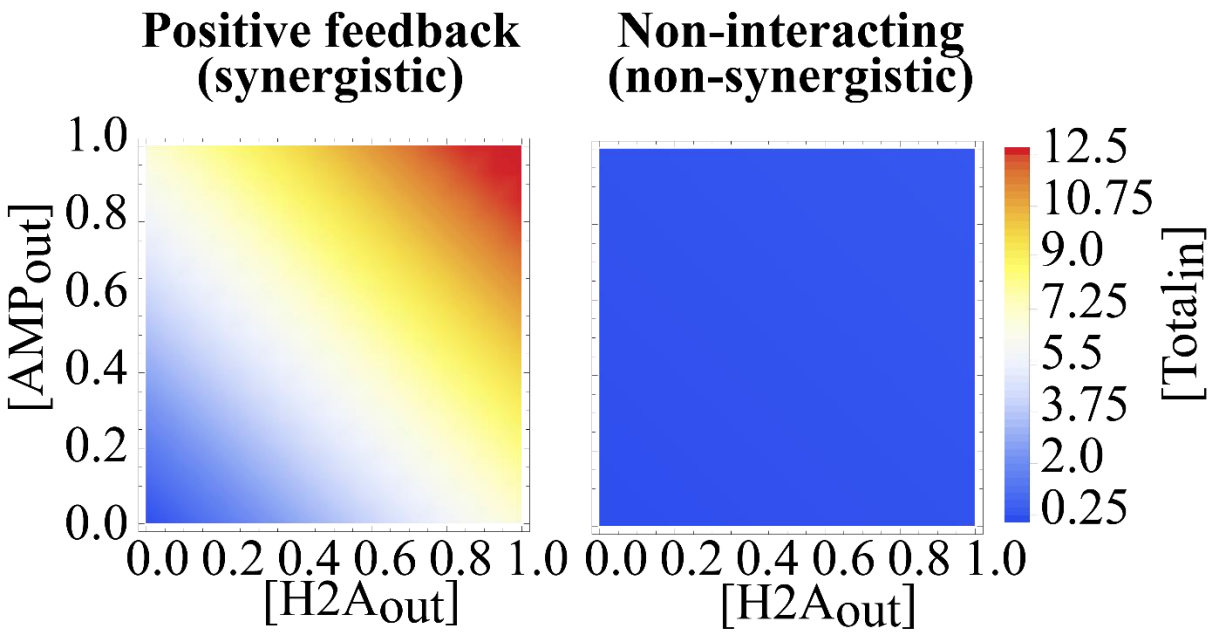

Figure 7.2. Low concentrations of AMPs and H2A trigger an exponential uptake of H2A and AMPs. Simulations indicating the total intracellular histone and AMP concentration for positive feedback and non-interacting relationships for a range of histone and AMP concentrations outside of the cell. Details of the simulations are described in the text.

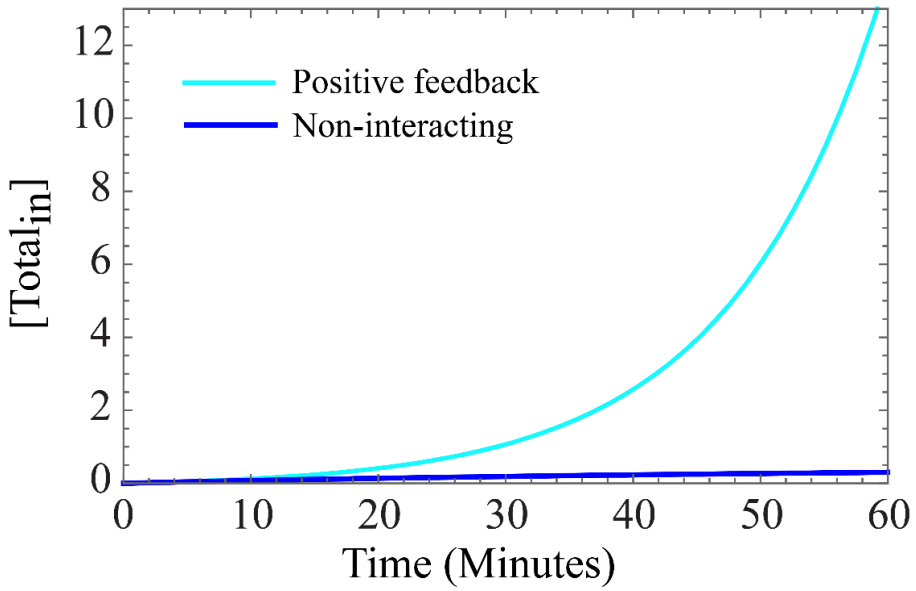

Figure 7.3. A positive feedback loop results in the exponential uptake of H2A and AMPs. The positive feedback loop underlying the H2A and AMP synergy results in exponential uptake of H2A and AMPs (light blue). Removal of the feedback loop (dark blue) results in uptake at a significantly lower rate. Simulations indicate the total intracellular concentration of H2A and AMP for positive feedback (light blue) and non-interacting (dark blue) relationships over a 60-minute time period.

This exponential uptake functions to effectively lower the MIC of these histones and AMPs, resulting in rapid bacterial killing. This is consistent with the all-or-none bimodal membrane permeabilization phenotype that is observed among dual-treated populations (Figure 7.4). If the interaction between the two molecules lacked positive feedback, cells would take up far less of each of these antimicrobial molecules and a continuous distribution of membrane permeabilization would be observed instead of a bimodal phenotype. In addition, while bacteria may respond to a dual histone/AMP attack by increasing the expression of outer membrane repairing machinery, as indicated in the RNA sequencing data, this response does not defeat the exponential nature of the positive feedback loop and only serves to elevate the threshold concentration required to activate it.

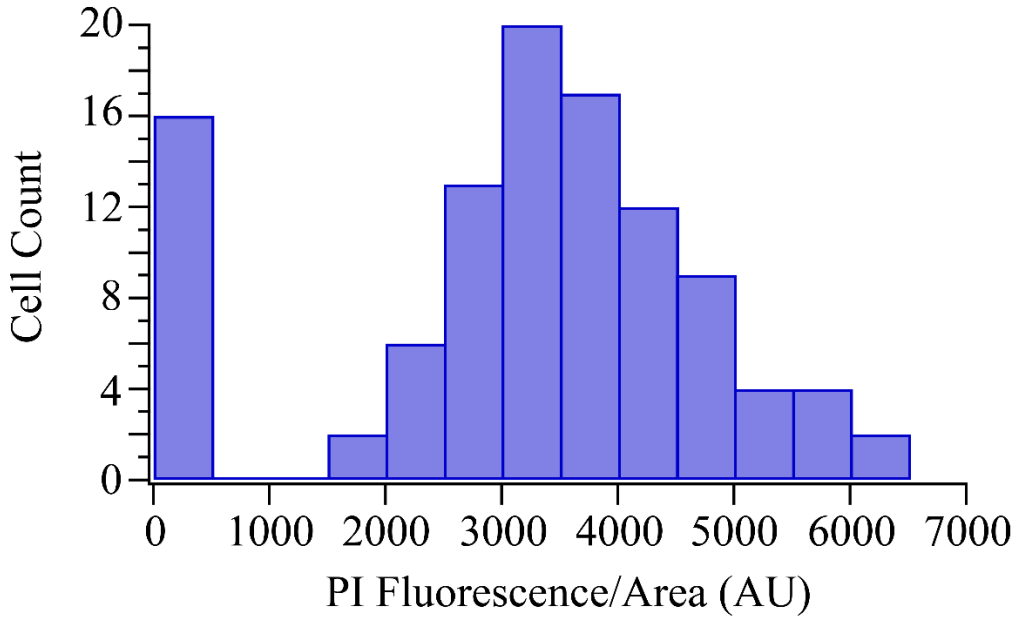

Figure 7.4. Dual-treated bacterial populations contain a bimodal distribution of uptake phenotypes. *E. coli* were treated with 10 μg/mL H2A and 1 μM LL-37 for a 1-hour period. 30 μM PI was added at the beginning of the treatment period to measure membrane permeability. A histogram of PI fluorescence intensities following treatment indicates a bimodal distribution of uptake phenotypes.

7.3 The Effect of Citrullination on the Antimicrobial Activity of Histones in NETs

The synergies observed between pore-forming agents and H2A are not exclusive to the H2A histone subunit. Although the different histone proteins share low levels of sequence similarity, each histone protein is composed of three helices, separated by loops. Since all histone subunits share a common fold, synergies were expected between pore-forming AMPs and any histone subunit[32]. Indeed, a similar synergistic killing response was seen with *E. coli* treated with a combinatorial treatment of LL-37 and H3. Similar to Histone H2A, calf thymus Histone H3 (Figure 7.5) or human H3 (Figure 7.6) alone had no effect on *E. coli* growth, and cultures treated with both H3 and LL-37 had decreased growth rates compared to untreated or LL-37-treated samples (Figure 7.5). Although identical concentrations of Histone H3 and LL-37 were used, as in previous synergy experiments with H2A, there was a decrease in the killing ability of H3 compared to H2A. However, the synergy is still apparent, suggesting synergy is a general property with pore-forming AMPs and histones.

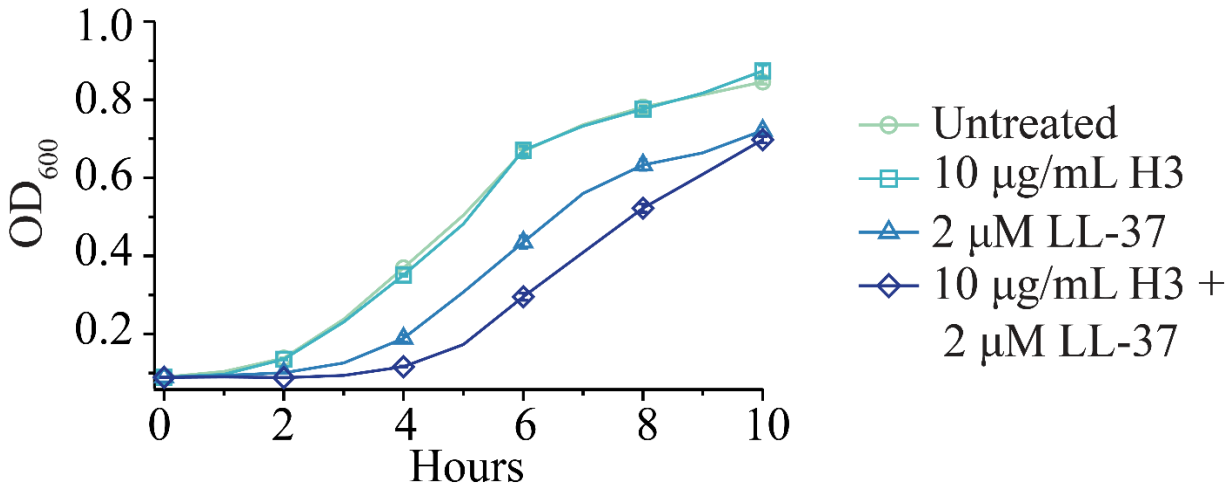

Figure 7.5. Histone H3 and LL-37 synergize to kill *E. coli*. Growth profiles of exponential phase *E. coli* treated with H3 and LL-37 in media containing physiological (1 mM) magnesium over a 10-hour growth period. The addition of H3 alone has no effect on *E. coli* growth in the physiological concentration of magnesium. The addition of LL-37 extends the lag phase and slows exponential growth. Histone H3 and LL-37 synergize to kill *E. coli*, significantly decreasing growth rates and extending lag times compared to untreated or LL-37-treated samples. Growth curves are presented for the first ten hours of growth to better visualize the effect of the dual treatment. Data points are the average of four independent experiments (n = 4) and error bars indicate SEM.

During the process of NETosis, histones are citrullinated by peptidylarginine deiminase 4 (PAD4), an enzyme which converts positively-charged arginine residues to neutral citrulline residues, decondensing the chromatin[33]. Since arginine residues in histone-derived antimicrobial peptides are associated with increased antimicrobial activity[34] and citrullination of histones during NETosis decreases histone potency[35], there may be differential roles for the different histone subunits in natural host defense responses. Although calf thymus H3 and human H3 showed moderate levels of synergy with LL-37 (Figure 7.5, 7.6), citrullination of human H3 eliminated this synergistic killing effect (Figure 7.6).

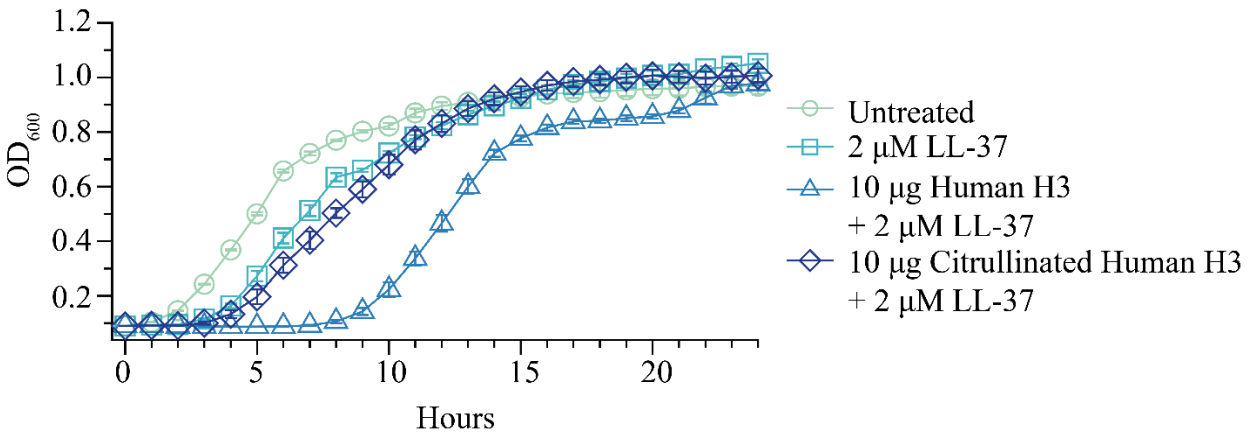

Figure 7.6. Citrullination of Histone H3 eliminates synergy with LL-37. Growth profiles of mid-exponential phase *E. coli* treated with 10 μg/mL human H3 or 10 μg/mL citrullinated human H3, with and without 2 μM LL-37 in media containing physiological (1 mM) magnesium over a 24-hour growth period. The addition of H3 or citrullinated H3 had no effect on *E. coli* growth. The addition of LL-37 extended the lag phase and slowed exponential growth. H3 and LL-37 synergized to kill *E. coli*, significantly decreasing growth rates and extending lag times compared to untreated or LL-37-treated samples. Citrullination of H3 eliminated this synergistic killing effect. Data points are the average of at least four independent experiments (n = 4) and error bars indicate SEM.

The extent of histone H2A citrullination during NETosis has not been well-documented. However, H2A is found in much higher concentrations than H3, which is extensively citrullinated in NETs[16]. The process of NETosis may involve a balance between decondensing DNA and retaining histone killing ability. The frequency of lysine to arginine residues within histones may reflect this balance. Given the human sequences of H2A and H3, H2A has 14 lysine residues (making up 10.8% of the total sequence) and 13 arginine residues (10%). In contrast, H3 has 13 lysine residues (11.5%) and 18 arginine residues (15.9%). Histone H3 is much more arginine rich compared to Histone H2A. It is possible that histone citrullination decreases histone potency of certain histones, such as H3, while leaving other histones, such as H2A, unaltered. In theory, this would provide a mechanism that balances antimicrobial activity and toxicity to the host, especially given that positively charged lysine residues are not converted to citrulline during citrullination.

On the other hand, the role of citrullination in NET formation is an area of active study and has recently come into question. Several reports indicate that NET formation can proceed through a citrullination-independent process, supporting the notion that histones may retain their full killing abilities within NETs[36,37]. Furthermore, histones localize to lipid droplets for targeted release to kill bacteria[18]. Lipid droplets are ubiquitous in the host and histones released from the lipid droplets do not undergo citrullination. Regardless, the impact of citrullination on histone killing is an interesting question. Future work will need to investigate the effects of citrullination on histone subunits, and the effects of this citrullination on the potency of histones within the context of the innate immune system.

7.4 The Usage of Histones and Histone-Derived Fragments as Future Therapeutic Agents

Although cleavage of histones is not known to occur in mammals, histone fragments have been extensively reported in non-mammalian species (Chapter 1). Most histone-derived fragments share homology with the N-terminal of the histone protein. These fragments are considered to be AMPs, with their antimicrobial activity stemming from their amphipathic secondary structure and cationic charge[4]. In certain environments, such as a lesion or NETs, proteases may cleave histones, producing histone-derived peptides[38]. Furthermore, as AMP antibacterial activity can be modulated, peptides may be designed in the future to increase membrane permeabilization, translocation, or synergy with other AMPs[34,39]. It is feasible that this self-amplifying mechanism described between AMPs and histones extends to histone fragments as well.

The combination of histones, or histone fragments, with a pore-forming agent could provide a new strategy to kill bacteria. Notably, histones synergize with the cationic antibiotic polymyxin B (PMB), a pore-forming antibiotic that is used only after all other antibiotics have failed. PMB permeabilizes the bacterial membrane and enables uptake of the peptide itself [40,29], a mechanism similar to LL-37. Recent reports show that polymyxin-resistant strains of *E. coli* have emerged[41]. The continued emergence of antibiotic resistance against last-line defenses represents a significant challenge in healthcare. In this work, treatment with low levels of PMB slightly inhibited growth, whereas the combinatorial treatment of low levels of histones and PMB completely eradicated the growth of *E. coli* over a 24-hour growth period (Figure 4.16). This is consistent with the model discussed above, whereby supplementing PMB treatment with H2A results in positive feedback and constitutes a multi-functional killing mechanism, ultimately giving rise to synergistic killing. Thus, this model demonstrates that incorporating a natural defense strategy can have a potent

impact on antibiotic efficacy. Identifying other synergies in natural host defenses is likely to yield important insights that can be incorporated into future antimicrobial designs.

With the exception of the dual treatment of H2A and PMB, *E. coli* treated with synergistic combination of AMPs and H2A recovered during the growth period measured. This is attributed to small fraction of resistant mutants or phenotypic variants that are persister cells, one possible mechanism of antibiotic tolerance and resistance[42–45]. Such recovery is typical following antibiotic treatments. This recovery was similarly observed upon treatment with the antibiotic chloramphenicol (Figure 4.6). Furthermore, recovery was observed with kanamycin treatment, both at concentrations near the MIC and concentrations well above (Figure 4.5, 4.8). This mechanism of resistance should be considered in the context of future antimicrobial designs involving histones.

The co-occurrence of histones and AMPs ubiquitously in the immune system suggests that this antimicrobial mechanism is present in a wide range of cell types. In addition to the formation of NETs by neutrophils, histone- and AMP-rich extracellular traps form in macrophages (METs) and in dendritic cells [46,47]. Extracellular traps (ETs) have been observed in other immune cells, including mast cells and eosinophils, suggesting a role for histones and AMPs in antimicrobial activity in these cells [48]. In addition, histones are recruited and bound to lipid droplets[49], which are lipid-rich organelles found in all eukaryotic organisms, that dynamically regulate the storage and breakdown of lipids[50]. In the presence of bacterial lipopolysaccharide (LPS) or lipoteichoic acid (LTA), these lipid droplet-bound histones are released from the lipid droplets and kill bacteria *in vivo*[51]. Future work will need investigate the general co-occurrence of histones and pore-forming agents within and beyond the innate immunity system, where they may function effectively as a two-component antimicrobial mechanism. Given the simple mechanism of synergy described here

between histones and AMPs, the co-occurrence of these molecules in other cell types would suggest their role as antimicrobial agents, establishing a positive feedback loop that enables effective antimicrobial activity at low concentrations.

Future work should test the model suggested by these initial studies, whereby AMPs and histones form a multi-step mechanism. Additional experiments will need to be conducted to further characterize this mechanism of the innate immune system which protects the host from bacterial proliferation and to characterize novel mechanisms developed by bacteria to combat this host response. These future experiments may enable the identification of new antimicrobial targets for drug design and may provide a basis for synthetic antimicrobials based on natural principles.

7.5 References

1. Miller, B. F., Abrams, R., Dorfman, A. & Klein, M. ANTIBACTERIAL PROPERTIES OF PROTAMINE AND HISTONE. *Science* **96**, 428–430 (1942).
2. Hirsch, J. G. BACTERICIDAL ACTION OF HISTONE. *Journal of Experimental Medicine* **108**, 925–944 (1958).
3. Brinkmann, V. Neutrophil Extracellular Traps Kill Bacteria. *Science* **303**, 1532–1535 (2004).
4. Hancock, R. E. W. & Lehrer, R. Cationic peptides: a new source of antibiotics. *Trends in Biotechnology* **16**, 82–88 (1998).
5. Hancock, R. E. W. & Sahl, H.-G. Antimicrobial and host-defense peptides as new anti-infective therapeutic strategies. *Nat. Biotechnol.* **24**, 1551–1557 (2006).
6. Dürr, U. H. N., Sudheendra, U. S. & Ramamoorthy, A. LL-37, the only human member of the cathelicidin family of antimicrobial peptides. *Biochimica et Biophysica Acta (BBA) - Biomembranes* **1758**, 1408–1425 (2006).
7. Chua, E. Y. D. *et al.* 3.9 Å structure of the nucleosome core particle determined by phase-plate cryo-EM. *Nucleic Acids Res.* **44**, 8013–8019 (2016).
8. Kawasaki, H. & Iwamuro, S. Potential roles of histones in host defense as antimicrobial agents. *Infect Disord Drug Targets* **8**, 195–205 (2008).
9. Ganz, T. Defensins: antimicrobial peptides of innate immunity. *Nature Reviews Immunology* **3**, 710–720 (2003).
10. Brinkmann, V. & Zychlinsky, A. Neutrophil extracellular traps: Is immunity the second function of chromatin? *The Journal of Cell Biology* **198**, 773–783 (2012).
11. Augusto, L. A. *et al.* Histones: A Novel Class of Lipopolysaccharide-Binding Molecules †. *Biochemistry* **42**, 3929–3938 (2003).
12. Kawasaki, H., Koyama, T., Conlon, J. M., Yamakura, F. & Iwamuro, S. Antimicrobial action of histone H2B in Escherichia coli: Evidence for membrane translocation and DNA-binding of a histone H2B fragment after proteolytic cleavage by outer membrane proteinase T. *Biochimie* **90**, 1693–1702 (2008).
13. Miller, B. F., Abrams, R., Dorfman, A. & Klein, M. ANTIBACTERIAL PROPERTIES OF PROTAMINE AND HISTONE. *Science* **96**, 428–430 (1942).
14. Hirsch, J. G. BACTERICIDAL ACTION OF HISTONE. *Journal of Experimental Medicine* **108**, 925–944 (1958).
15. Brinkmann, V. *et al.* Neutrophil extracellular traps kill bacteria. *Science* **303**, 1532–1535 (2004).
16. Urban, C. F. *et al.* Neutrophil Extracellular Traps Contain Calprotectin, a Cytosolic Protein Complex Involved in Host Defense against Candida albicans. *PLoS Pathogens* **5**, e1000639 (2009).
17. Cermelli, S., Guo, Y., Gross, S. P. & Welte, M. A. The Lipid-Droplet Proteome Reveals that Droplets Are a Protein-Storage Depot. *Current Biology* **16**, 1783–1795 (2006).
18. Anand, P. *et al.* A novel role for lipid droplets in the organismal antibacterial response. *eLife* **1**, (2012).
19. Kahlenberg, J. M., Carmona-Rivera, C., Smith, C. K. & Kaplan, M. J. Neutrophil Extracellular Trap-Associated Protein Activation of the NLRP3 Inflammasome Is Enhanced in Lupus Macrophages. *The Journal of Immunology* **190**, 1217–1226 (2013).
20. Park, I. Y., Park, C. B., Kim, M. S. & Kim, S. C. Parasin I, an antimicrobial peptide derived from histone H2A in the catfish, *Parasilurus asotus*. *FEBS Letters* **437**, 258–262 (1998).

21. Birkemo, G. A., Lüders, T., Andersen, Ø., Nes, I. F. & Nissen-Meyer, J. Hipposin, a histone-derived antimicrobial peptide in Atlantic halibut (Hippoglossus hippoglossus L.). *Biochimica et Biophysica Acta (BBA) - Proteins and Proteomics* **1646**, 207–215 (2003).
22. Patat, S. A. *et al.* Antimicrobial activity of histones from hemocytes of the Pacific white shrimp. *European Journal of Biochemistry* **271**, 4825–4833 (2004).
23. Luders, T., Birkemo, G. A., Nissen-Meyer, J., Andersen, O. & Nes, I. F. Proline Conformation-Dependent Antimicrobial Activity of a Proline-Rich Histone H1 N-Terminal Peptide Fragment Isolated from the Skin Mucus of Atlantic Salmon. *Antimicrobial Agents and Chemotherapy* **49**, 2399–2406 (2005).
24. Kawasaki, H., Koyama, T., Conlon, J. M., Yamakura, F. & Iwamuro, S. Antimicrobial action of histone H2B in Escherichia coli: Evidence for membrane translocation and DNA-binding of a histone H2B fragment after proteolytic cleavage by outer membrane proteinase T. *Biochimie* **90**, 1693–1702 (2008).
25. Cho, J. H., Sung, B. H. & Kim, S. C. Buforins: Histone H2A-derived antimicrobial peptides from toad stomach. *Biochimica et Biophysica Acta (BBA) - Biomembranes* **1788**, 1564–1569 (2009).
26. Dorrington, T., Villamil, L. & Gómez-chiarri, M. Upregulation in response to infection and antibacterial activity of oyster histone H4. *Fish & Shellfish Immunology* **30**, 94–101 (2011).
27. Morita, S., Tagai, C., Shiraishi, T., Miyaji, K. & Iwamuro, S. Differential mode of antimicrobial actions of arginine-rich and lysine-rich histones against Gram-positive Staphylococcus aureus. *Peptides* **48**, 75–82 (2013).
28. Tagai, C., Morita, S., Shiraishi, T., Miyaji, K. & Iwamuro, S. Antimicrobial properties of arginine- and lysine-rich histones and involvement of bacterial outer membrane protease T in their differential mode of actions. *Peptides* **32**, 2003–2009 (2011).
29. Hancock, R. E. W. & Sahl, H.-G. Antimicrobial and host-defense peptides as new anti-infective therapeutic strategies. *Nat. Biotechnol.* **24**, 1551–1557 (2006).
30. Morita, S., Tagai, C., Shiraishi, T., Miyaji, K. & Iwamuro, S. Differential mode of antimicrobial actions of arginine-rich and lysine-rich histones against Gram-positive Staphylococcus aureus. *Peptides* **48**, 75–82 (2013).
31. Sigler, A., Schubert, P., Hillen, W. & Niederweis, M. Permeation of tetracyclines through membranes of liposomes and Escherichia coli. *Eur. J. Biochem.* **267**, 527–534 (2000).
32. Arents, G., Burlingame, R. W., Wang, B. C., Love, W. E. & Moudrianakis, E. N. The nucleosomal core histone octamer at 3.1 A resolution: a tripartite protein assembly and a left-handed superhelix. *Proceedings of the National Academy of Sciences* **88**, 10148–10152 (1991).
33. Lewis, H. D. *et al.* Inhibition of PAD4 activity is sufficient to disrupt mouse and human NET formation. *Nat. Chem. Biol.* **11**, 189–191 (2015).
34. Cutrona, K. J., Kaufman, B. A., Figueroa, D. M. & Elmore, D. E. Role of arginine and lysine in the antimicrobial mechanism of histone-derived antimicrobial peptides. *FEBS Letters* **589**, 3915–3920 (2015).
35. Li, P. *et al.* PAD4 is essential for antibacterial innate immunity mediated by neutrophil extracellular traps. *J. Exp. Med.* **207**, 1853–1862 (2010).
36. Konig, M. F. & Andrade, F. A Critical Reappraisal of Neutrophil Extracellular Traps and NETosis Mimics Based on Differential Requirements for Protein Citrullination. *Frontiers in Immunology* **7**, (2016).

37. Neeli, I. & Radic, M. Opposition between PKC isoforms regulates histone deimination and neutrophil extracellular chromatin release. *Front. Immun.* **4**, (2013).
38. Higuchi, K. *et al.* Proteases released in organ culture by acute dermal inflammatory lesions produced in vivo in rabbit skin by sulfur mustard: hydrolysis of synthetic peptide substrates for trypsin-like and chymotrypsin-like enzymes. *Inflammation* **12**, 311–334 (1988).
39. Lim, C. H. *et al.* Thrombin and Plasmin Alter the Proteome of Neutrophil Extracellular Traps. *Front Immunol* **9**, 1554 (2018).
40. Moore, R. A., Bates, N. C. & Hancock, R. E. Interaction of polycationic antibiotics with Pseudomonas aeruginosa lipopolysaccharide and lipid A studied by using dansyl-polymyxin. *Antimicrobial Agents and Chemotherapy* **29**, 496–500 (1986).
41. Liu, Y.-Y. *et al.* Emergence of plasmid-mediated colistin resistance mechanism MCR-1 in animals and human beings in China: a microbiological and molecular biological study. *The Lancet Infectious Diseases* **16**, 161–168 (2016).
42. Lewis, K. Persister Cells. *Annu. Rev. Microbiol.* **64**, 357–372 (2010).
43. Lewis, K. Persister Cells: Molecular Mechanisms Related to Antibiotic Tolerance. in *Antibiotic Resistance* (ed. Coates, A. R. M.) vol. 211 121–133 (Springer Berlin Heidelberg, 2012).
44. Wood, T. K., Knabel, S. J. & Kwan, B. W. Bacterial Persister Cell Formation and Dormancy. *Appl. Environ. Microbiol.* **79**, 7116–7121 (2013).
45. Fisher, R. A., Gollan, B. & Helaine, S. Persistent bacterial infections and persister cells. *Nat Rev Microbiol* **15**, 453–464 (2017).
46. Doster, R. S., Rogers, L. M., Gaddy, J. A. & Aronoff, D. M. Macrophage Extracellular Traps: A Scoping Review. *Journal of Innate Immunity* **10**, 3–13 (2018).
47. Loures, F. V. *et al.* Recognition of Aspergillus fumigatus Hyphae by Human Plasmacytoid Dendritic Cells Is Mediated by Dectin-2 and Results in Formation of Extracellular Traps. *PLOS Pathogens* **11**, e1004643 (2015).
48. Goldmann, O. & Medina, E. The expanding world of extracellular traps: not only neutrophils but much more. *Frontiers in Immunology* **3**, (2013).
49. Cermelli, S., Guo, Y., Gross, S. P. & Welte, M. A. The Lipid-Droplet Proteome Reveals that Droplets Are a Protein-Storage Depot. *Current Biology* **16**, 1783–1795 (2006).
50. Li, Z. *et al.* Lipid Droplets Control the Maternal Histone Supply of Drosophila Embryos. *Current Biology* **22**, 2104–2113 (2012).
51. Anand, P. *et al.* A novel role for lipid droplets in the organismal antibacterial response. *eLife* **1**, (2012).

Appendix A: Effect Size and Power Analyses for ANOVA Tests

Figure	Eta Squared	Power
Figure 3.2 – *E. coli*	0.8696353	0.8337105
Figure 3.2 – *S. aureus*	0.9144234	0.8718639
Figure 3.5	0.8723718	0.4932418
Figure 3.7	0.8897267	0.9999999
Figure 4.4	0.9054198	0.8647214
Figure 4.11A	0.9891974	0.741925
Figure 4.11B	0.715802	0.4356387
Figure 4.14	0.9299618	0.5490211
Figure 4.17	0.9017738	0.521746
Figure 4.20	0.8381097	0.5210979
Figure 4.21	0.9861355	0.6758675
Figure 4.22	0.9402953	0.5589799
Figure 5.3A	0.9721602	0.6619887
Figure 5.9	0.9885205	0.6049317
Figure 5.12	0.7906787	0.4150216
Figure 5.14	0.9665282	0.8546667
Figure 5.15	0.8573485	0.6003948
Figure 5.16	0.9608449	0.8497897
Figure 5.17	0.7461094	0.4706037
Figure 5.18	0.7998084	0.4236251
Figure 5.19	0.7236337	0.5672634

Figure	Eta Squared	Power
Figure 6.4	0.9493115	0.5676435
Figure 6.5 – Increasing H2A	0.9189575	0.5383881
Figure 6.5 – Synergy Conditions	0.4843935	0.6213774

Appendix B: Effect Size and Power Analyses for Welsh t-tests

Figure	**Cohen's d**	**Power**
Figure 5.3B	9.348578	1
Figure 5.5	7.49286	0.9999951
Figure 5.7 – *E. coli*	6.517468	0.9998731
Figure 5.7 – *S. aureus*	4.66885	0.9852364
Figure 5.11	24.83243	1